DOKUZ EYLÜL UNIVERSITY
GRADUATE SCHOOL OF NATURAL AND APPLIED SCIENCES

PRODUCTION, CHARACTERIZATION AND ELECTROCHEMICAL SENSOR APPLICATIONS OF METAL OXIDE NANOSTRUCTURES

by

Tülay KOÇ DELİCE

October, 2024

İZMİR

PRODUCTION, CHARACTERIZATION AND ELECTROCHEMICAL SENSOR APPLICATIONS OF METAL OXIDE NANOSTRUCTURES

A Thesis Submitted to the
Graduate School of Natural and Applied Sciences of Dokuz Eylül University
In Partial Fulfillment of the Requirements for the Degree of Doctor of Philosophy in Department of Nanoscience and Nanoengineering, Nanoscience and Nanoengineering Program

by

Tülay KOÇ DELİCE

October, 2024

İZMİR

Ph.D. THESIS EXAMINATION RESULT FORM

We have read the thesis entitled **"PRODUCTION, CHARACTERIZATION AND ELECTROCHEMICAL SENSOR APPLICATIONS OF METAL OXIDE NANOSTRUCTURES"** completed by **Tülay KOÇ DELİCE** under supervision of **ASSOC.PROF.DR.N. Funda AK AZEM** and we certify that inour opinion it is fully adequate, in scope and in quality, as a thesis for the degree of Doctor of Philosophy.

Assoc.Prof.Dr.N. Funda AK AZEM

Supervisor

Prof. Dr. Şenol ALPAT	Assoc. Prof. Dr. Işıl BİRLİK
ThesisCommitteeMember	Thesis Committee Member
Prof. Dr. Emre YALAMAÇ	Prof. Dr. Süleyman KOÇAK
ExaminingCommitteeMember	Examining Committee Member

Prof. Dr. Okan FISTIKOĞLU

Director

Graduate School of Natural and Applied Sciences

ACKNOWLEDGEMENT

After many years of dedicated work, I am nearing the end of my long and arduous PhD journey. I believe that this achievement would not have been possible without the help, support, guidance and encouragement of many people in my life. Therefore, I would like to express my sincere gratitude to everyone who contributed to the successful completion of my PhD study.

Above all, I would like to express my gratitude to my supervisor, Assoc. Prof. Dr. N. Funda AK AZEM, for her support and guidance not only during this research but also in all of the research I have undertaken during my five years of association. Her friendly demeanor, keen insight, and incredible strength in the face of adversity continue to inspire her students and colleagues alike.

In addition, I would like to express my sincere gratitude to Assoc. Prof. Dr. Işıl BİRLİK for her helpful discussions in the thesis and her priceless advice, direction, and support. She has always been a light to me.

Special thanks to Prof. Dr. Şenol ALPAT, who were more than willing to help out and for their support in helping me to understand the basics of electrochemical sensor on short notice.

I am grateful to Kazım ÖZDEMİR for his cooperation in electrochemical sensor studies and evaluation of the corresponding results obtained. I would also like to thank my lab group: Dr. Ramazan DALMIŞ, Özgür Yasin KESKİN, Dr. Çağrı KILINÇ and Dr. Serhan KÖKTAŞ for their help in the lab.

I am grateful to my precious friend Dr. Oylum ÇOLPANKAN GÜNEŞ for her effort, help and every moment we shared together.

I would specially like to acknowledge with gratitude the support and love of my family, without their support I would not have been able to complete my doctoral studies. My profound appreciation to my cherished spouse, Kılıç DELİCE, for his everlasting love, support, and prayers. Without you, I could never have been this successful. You patiently sacrificed your time while being steadfast in order to support

me at each and every trying period. Last but not least, it's time to give thanks for my children, Baki Musab Ömer and İnci Amine.

Even though I did not spend much time with them, their sweet grins and kisses lifted my spirits, and their innocent antics made me feel better. By helping me let go of all my anxieties and tiredness, they gave me the energy I needed to face the difficulties of the next day. Without them, this thesis would not have been possible. I always need them by my side. I sincerely apologize to everyone else whose names I overlooked.

I would like to thank the Turkish Council of Higher Education for providing me with funding under the PhD 100/2000 scholarship program.

Tülay KOÇ DELİCE

PRODUCTION, CHARACTERIZATION AND ELECTROCHEMICAL SENSOR APPLICATIONS OF METAL OXIDE NANOSTRUCTURES

ABSTRACT

The thesis study aims to use metal oxide nanostructures in the detection of salbutamol sulphate analyte and to develop materials for electrochemical sensor applications. The study consists of two main parts. In the first part, we conducted the synthesis and characterization of copper oxide (CuO) and tin oxide (SnO_2) nanoparticles doped with transition metal, manganese (Mn), and rare earth element, cerium (Ce), using the sol-gel method. The effects of sol-gel parameters on nanoparticle structure, size, and morphology were investigated. In the second part, a carbon paste electrode for salbutamol (SAL) detection was prepared and modified with synthesized nanoparticles. The undoped and doped CuO nanoparticles with Mn or Ce dopants showed the highest sensitivity and lowest detection limits. The sensor developed with Mn doped CuO nanoparticles (CuO-Mn2) detected SAL from 2 µM to 200 µM, and the limit of detection (LOD) was 58.25 nM. The correlation value of the sensor generated with Ce-doped CuO was 0.9929, the LOD was 34.18 nM, and the LOQ was 113.95 nM. The sensor, which was built using undoped SnO_2 nanoparticles, was found to be ineffective in detecting SAL. In this case, the sensor properties were improved by doping SnO_2 nanoparticles with transition metals and rare earth elements. Mn and Ce doped SnO_2 sensors showed LOD values of 56.84 nM and 3.16 nM, respectively, and the correlation values for SAL were calculated as 0.9995 between 5 µM and 100 µM and 0.9905 between 2 µM and 100 µM. These findings indicate that using additives in carbon paste electrodes improved sensitivity and lower detection limits for analyte detection. It was determined that the amount and type of additives used, as well as the nanostructured metal oxide component, significantly affected the sensor's electrochemical performance.

Keywords: Nanostructures, Copper oxide, Tin oxide, Doping, Electrochemical sensor

METAL OKSİT NANOYAPILARIN ÜRETİMİ, KARAKTERİZASYONU VE ELEKTROKİMYASAL SENSÖR UYGULAMALARI

ÖZ

Tez çalışması salbutamol sülfat analitinin tespitinde metal oksit nanoyapıların kullanılması ve elektrokimyasal sensor uygulamaları için malzeme geliştirmesini amaçlamaktadır. Çalışma iki ana bölümden oluşmaktadır. İlk bölümde, sol-jel yöntemi kullanılarak geçiş metali, mangan (Mn), ve nadir toprak elementi, seryum (Ce), katkılı bakır oksit (CuO) ve kalay oksit (SnO_2) nanopartiküllerinin sentezini ve karakterizasyonunu gerçekleştirilmiştir. Sol-jel parametrelerinin nanopartikül yapısı, boyutu ve morfolojisi üzerindeki etkileri araştırılmıştır. İkinci bölümde, salbutamol (SAL) tespiti için bir karbon pasta elektrot hazırlanmış ve sentezlenen nanopartiküller ile modifiye edilmiştir. Mn veya Ce katkılı katkısız ve katkılı CuO nanopartikülleri en yüksek hassasiyeti ve en düşük algılama limitlerini göstermiştir. Mn katkılı CuO nanopartikül (CuO-Mn2) ile geliştirilen sensör SAL'ı 2 µM ila 200 µM arasında tespit etmiş ve tespit limiti (LOD) 58,25 nM olmuştur. Ce katkılı CuO ile üretilen sensörün korelasyon değeri 0,9929, LOD 34,18 nM ve LOQ 113,95 nM olmuştur. Katkısız SnO_2 nanopartikülleri kullanılarak oluşturulan sensörün SAL'ı tespit etmede etkisiz olduğu görülmüştür. Bu durumda, SnO_2 nanopartikülleri geçiş metalleri ve nadir toprak elementleri ile katkılanarak sensör özellikleri geliştirilmiştir. Mn ve Ce katkılı SnO_2 sensörleri sırasıyla 56,84 nM ve 3,16 nM LOD değerleri göstermiş ve SAL için korelasyon değerleri 5 µM ile 100 µM arasında 0,9995 ve 2 µM ile 100 µM arasında 0,9905 olarak hesaplanmıştır. Bu bulgular, karbon pasta elektrotlarda katkı maddelerinin kullanımının analit tespiti için gelişmiş hassasiyet ve daha düşük tespit limitleri ile sonuçlandığını göstermektedir. Kullanılan katkı maddelerinin miktarı ve türü ile nanoyapılı metal oksit bileşeninin sensörün elektrokimyasal performansını önemli ölçüde etkilediği belirlenmiştir.

Anahtar kelimeler: Nano yapılar, Bakır oksit, Kalay oksit, katkılama, Elektrokimyasal sensör

CONTENTS

Page

LIST OF FIGURES

Page

LISTOF TABLES

Page

ABBREVIATIONS

SAL	: Salbutamol
WADA	: World Anti-Doping Agency
IOC	: International Olympic Committee
CPE	: Carbon Paste Electrodes
CV	: Cyclic Voltammetry
DPV	: Differential Pulse Voltammetry
XRD	: X-Ray Diffraction
DLS	: Dynamic Light Scattering
FTIR	: Fourier İnfrared Spectroscopy
XPS	: X-Ray Photoelectron Spectroscopy
LOD	: Limit Of Detection
WE	: Working Electrode
RE	: Reference Electrode
CE	: Counter Electrode
CuO_2	: Copper Oxide
SnO_2	: Tin Oxide
CPE	: Carbon Paste Electrode
PBS	: Phosphate Buffer Solution
LOD	: Limit Of Detection
LOQ	: Limit Of Quantification
RSD	: Relative Standard Deviation

CHAPTER ONE
INTRODUCTION

Materials at the intersection of materials science and nanotechnology are called nanomaterials, and they have unique properties compared to traditional materials. The most important feature of these materials is their extraordinary surface area due to their nanoscale dimensions. Hence, their surface reactivity and functionality far exceed those of bulk materials. Nanomaterials attract attention with their mechanical, optical, thermal, and electrical properties that vary depending on the structure and size of the material. Nanomaterials have impressive physicochemical properties and provide increased sensitivity for evaluating single molecules. Their adsorption and reactive qualities, high surface-to-volume ratios, and other properties not present in bulk materials account for this. These properties make them suitable for an analytical approach that improves sensitivity and represents a significant advancement. Over the past few decades, electrochemical structures and biosensors with nanostructured materials have become widely accepted as an analytical method due to their ease of administration, cost-effectiveness, high sensitivity, selectivity, fast reaction times, smooth manufacturing, and portability. In addition, nanoparticles can be equipped with various functional groups through surface modification, which makes it possible to optimize them for specific tasks. Nanomaterials are divided into four categories based on their sizes: 0D, 1D, 2D, and 3D. Nanoparticles in the zero-dimensional material group offer significant advantages in characteristics like chemical reactivity and biocompatibility owing to their elevated ratios of surface area to volume. Because of their unique characteristics, nanoparticles can play a variety of functions in different electrochemical sensing systems. These roles can be classified into essential functions: immobilizing biomolecules, catalyzing electrochemical reactions serving as reactants, improving electron transport, and labeling biomolecules. These particles are widely used in targeted drug delivery, medical imaging, environmental cleaning, and advanced material production.

Electrochemical sensors offer significant advantages over other types of sensors due to their sensitivity, selectivity, and fast response time. These sensors can measure target analytes with high accuracy, even in low-cost and portable devices, by using the

electroactive properties of target analytes and are widely used in various applications such as biosensors, gas sensors, and environmental monitoring. Other advantages of electrochemical sensors include low energy consumption, wide dynamic range, high repeatability, and the ability to detect analytes in various matrices. These features make electrochemical sensors a preferred technology in critical areas such as medical diagnosis, environmental analysis, and food safety. The application of nanoparticles in electrochemical sensor design has seen a surge in attention in recent years, with notable progress made in detecting various analytes. Both the sensitivity and selectivity of electrochemical sensors are improved due to the extensive surface area and high conductivity of nanoparticles. A variety of nanoparticle compositions and sizes have found widespread application as sensitive and adaptable tracers for electrical, optic, and microgravimetric transmission of various biomolecular recognition processes in recent years. In particular, metal oxide nanoparticles, graphene, and carbon nanotubes are frequently utilized to enhance sensor performance.

Non-enzymatic sensors form a subgroup of biosensors and stand out as technologies that directly measure chemical, physical, or electrical changes instead of enzymes. These sensors often contain active components, including metal oxides, carbon based compounds, or other semiconductors, and are used to measure chemical or electrical responses. Non-enzymatic sensors offer faster response times because they do not depend on enzymatic reactions and are more resistant to environmental factors. These properties make them particularly suitable for applications with aggressive chemicals or high temperatures. For example, metal oxide-based sensors can be used effectively in gas detection or electrochemical analyses. Salbutamol (SAL) is a commonly used medication active component that can be inhaled or used orally to treat respiratory conditions that cause bronchoconstriction, such as emphysema, bronchitis, and asthma. Premature births throughout pregnancy are also prevented with its help. While there is no benefit for asthmatic patients using SAL-containing medications over non-asthmatic athletes, some non-asthmatic athletes use SAL-containing medications to improve their performance (power or duration of exercise) due to strong adrenergic stimulation and possible anabolic-like effects. In other words, SAL is abused by bad-intentioned athletes due to its doping effect. In other words, because SAL has anti doping properties, it is misused by well-meaning sportsmen. Due to misuse as a

stimulant and anabolic agent, excessive dosages of salbutamol are not allowed in sports. To use this class of medications for medicinal purposes, athletes must receive approval from the World Anti-Doping Agency (WADA) and the International Olympic Committee (IOC) and demonstrate medical necessity. Its inhalation usage has been restricted to athletes who suffer from asthma or asthma brought on by exertion. WADA and the IOC consider a doping test positive if there is a salbutamol (MW=337.39 g/mol) concentration of more than 1000 ng/mL (2.96 μM) in the urine. Although concerns have been raised about the abuse of salbutamol, given its importance in the treatment and control of asthma, the use of salbutamol by athletes is permitted up to the prescribed dose. Still, it has been decided that it should be monitored. The potential for SAL to be abused as a doping agent has led to the emergence of sensitive and reliable detection techniques.

Currently, several analytical techniques, including high-performance liquid chromatography, immunoassay, spectrophotometry, capillary electrophoresis, colorimetry, electrochemiluminescence, and electrochemical determination, have been developed to measure salbutamol. Unfortunately, most of these methods require more complex procedures, such as several derivatization steps and effective extraction purification before final analysis or a combination of several detection methods, which require time-consuming, expensive, and heavy instrumentation. At the same time, some of them may not show sufficient detection limits or satisfactory selectivity. Compared with other approaches, electroanalytical techniques' cheap cost, ease of use, low background current, broad potential range, high sensitivity and selectivity, speed and accuracy, and quick surface renewal have all shown them attractive alternative methods. Despite all of these benefits, a more effective technique for high-sensitivity and selectivity SAL identification still has to be developed. Due to its high sensitivity, superior signal-to-noise ratio, simplicity, and adaptability, the voltammetric approach has been regarded as the most widely used method in electrochemical analysis in several studies. When a voltage is applied, voltammetric sensors functioning as working electrodes offer information about the redox processes in the solution and help create voltammograms that display the redox processes associated with the chosen electroactive material. Because of their high aspect ratio, low background current, high specific surface area, chemical stability andinertia, low background

current, ease of interchangeability based on the target analyte, and suitability for a variety of sensing and detection applications, carbon electrodes have been found a wide range of applications. They are also inexpensive to manufacture. Because of their distinct chemical stability, simplicity and rapidity of preparation, affordability, ability to mix various components during paste preparation, porous surface, shallow background current (in comparison to graphite electrode), high aspect ratio, and high specific surface area, carbon paste electrodes (CPEs) have garnered attention from all over the world. Furthermore, the relevance of CPE is increased when they are used at both positive and negative potentials, depending on the supporting electrolytes. At the same time, it is simple to alter an electrode to create a novel sensor with the required characteristics. Notwithstanding these encouraging characteristics, sluggish electron transfer response issues and electrode contamination can occur with bare CPE. These factors make it very interesting to modify the electrode by adding compounds with the required characteristics. Simultaneously, several investigations into electrode modification have been carried out recently in an effort to increase the sensitivity, speed, and selectivity of electrochemical measurements. Because nanomaterials have fundamental characteristics including reduced size and superior optical, magnetic, and mechanical capabilities, they are employed in biomedical and sensor applications. These materials include carbon nanotubes, fullerenes, nanoparticles, and nanodiamonds. The improved peak current and reduced positive oxidation potential are the results of the electrochemical process catalyzed by electrodes enhanced with nanoparticles. Recently, metal oxide nanoparticles have garnered much attention from nanoparticle researchers. Nanoparticles on modified carbon paste electrodes (CPE) exhibit high sensitivity and selectivity in the electrochemical detection of SAL. These sensors enable the analysis of SAL using electrochemical methods like differential pulse voltammetry (DPV) across a broad range of concentrations. Therefore, electrochemical sensors equipped with nanoparticles are a unique and valuable instrument for pharmacological analysis of SAL and doping controls.

Several reports have been published on nanoparticle-based materials for determining Salbutamol through electrochemical methods using nanoparticle-modified CPE with various metal oxide nanostructures. However, this thesis study aims to provide detailed and comparative results on different types and amounts of

additives in an electrochemical sensor structure developed using various metal oxide nanostructures. The strategic impact of the study lies in obtaining results that simulate realistic conditions by using Ventolin syrup, where Salbutamol is the active ingredient. Therefore, the investigation of the effect of the types and concentrations of doped elements on the determination of SAL increases the potential contribution of the thesis study. This gap in the literature has been tried to be filled with the studies conducted within the scope of the thesis and the sensors developed. In addition to all these, the study contributes significantly to the literature on sensor technologies by providing comparative results of the effect of both n-type and p-type semiconductor metal oxide nanostructures on electrochemical sensor performances.

This thesis aims to produce metal oxide nanoparticles and develop electrochemical sensors by modifying carbon paste electrodes to detect pharmaceuticals that contain SAL. The modified carbon paste electrode is developed using undoped and doped CuO and SnO_2 metal oxide nanoparticles for electrochemical sensors. This work also evaluated the relationship between as-prepared undoped/doped metal oxide nanoparticles and their electrochemical sensor performance. In addition, determining biomolecules and pharmaceuticals is an important thrust area in future work related to developing electrochemical sensors based on metal oxide nanoparticles modified CPE electrodes since it provides insight into a wide array of electrochemical processes.

This thesis essentially consists of five chapters. Each investigation includes sections on introduction, theoretical background, experimental procedures, results, discussion, and conclusion. In the introduction and theoretical background section, literature on the properties of selected nanoparticles, sensors, and electrochemical sensors, an overview of some recent studies, and the aim of the study are presented. The experimental part contains descriptions of the materials used, the experimental procedures, and the characterization methods. The results and discussion section assess the findings, and the conclusion section at the end of the thesis compares the results and the achievement of the study's goal.

Chapter 1 provides a brief introduction to nanoparticles and electrochemical sensors and an overview of the thesis's main aims and objectives and the methods used in it.

Chapter 2 includes information on the applications of sensors and biosensors while providing detailed background information on the approach, properties, and fabrication methods of nanostructures in these sensors. It also focuses on electrochemistry and theories of sensor types and parameters affecting measurement.

Chapter 3 outlines the processes for producing and characterizing nanoparticles to modify carbon paste electrodes and the experimental approach for evaluating electrochemical SAL. The synthesis of undoped and doped metal oxide nanoparticles for use in the design of electrochemical sensors involves a sol-gel technique. X-ray diffraction (XRD), Dynamic light scattering (DLS), X-ray photoelectron spectroscopy (XPS) and Fourier infrared spectroscopy (FTIR) have all been used to explain the structural and chemical structures of the synthesized nanoparticles. The morphology of the synthesized metal oxide structures was investigated using scanning electron microscopy (SEM). The procedures for measuring SAL using cyclic voltammetry (CV) and differential pulse voltammetry (DPV) are given.

Chapter 4 focuses on the advancement of CPE through nanoparticle modification, specifically for their application in electrochemical sensors. CPE was modified by undoped and doped CuO and SnO_2 metal oxides nanoparticles, and the electrochemical performance of CPE was investigated as a detecting candidate material for the detection of SAL analyte. The electrochemical sensor performance of the optimized nanoparticles in SAL determination was examined using CV and DP techniques. Optimum parameters for SAL determination were determined through optimization studies.

Chapter 5 summarizes the results obtained within the scope of the thesis and presents the discussions and conclusions of th e studies. Based on the obtained results, future research aims to significantly improve sensitivity and selectivity for a wide range of analytes using metal oxide nanostructures.

CHAPTER TWO
THEORETICAL BACKGROUND

2.1 Sensors and Biosensors

A sensor is defined as "a device that monitors physical and chemical qualities and turns those measurements into a signal that may be detected by an observer or an instrument" (Y. Li et al., 2015; Thévenot et al., 2001). The use of sensors and biosensors in detecting and monitoring analytes has gained more popularity in recent years, particularly in clinical analysis, medical diagnosis, environmental monitoring, and food safety. In contrast to conventional methods such as immunoassays, spectroscopy, and chromatography techniques, they are associated with high sensitivity, a short analysis time, and lower costs (Justino et al., 2016; D. Zhu et al., 2016). A further advantage is that the general public may use them to analyze complex samples without preparing complex procedures. These sensors include potent tools such as glucose biosensors, cholesterol tests, pregnancy tests, and blood analyzers (Gooding, 2008).

There are six types of sensors in terms of transduction techniques: optical sensors, gravimetric sensors, heat sensors, gas sensors, electrochemical sensors, and biosensors (Stetter et al., 2003). Optic sensors are one of the new sensitive technologies. Typically, optical sensors track how one or more light beams change in strength or phase as they come into contact with physical systems (Rai, 2007). Gravimetric sensors, which exploit the piezoelectric effect, are beneficialas gas sensors. They include devices like the surface acoustic wave sensor. They are based on a movement in mass on the surface of an oscillating crystal that causes a shift in oscillation frequency. The amount of substance absorbed on the surface determines how much frequency shift occurs (Kuchmenko & Lvova, 2019). Transducers like thermistors or platinum thermometers are used to measure the heat of a chemical reaction involving the analyte. They frequently referred to as calorimetric sensors. Gas sensors are commonly referred to as calorimetric sensors. They are primarily used to detect the presence of hazardous gases in the air. Sensors for CO, CO_2, and SO_2 are the most frequently used gas sensors. Depending on the permeability of the gas membrane, these sensors' selectivity changes. Real-time data on a system's composition is

obtained by the combination of an electrochemical transducer and a chemically selective layer, or recognition element, in electrochemical sensors (Bekmezci et al., 2022). Due to their superior detectability, simplicity of testing, and low cost, electrochemical sensors are more desirable than optical, mass, and thermal sensors. They are among the most advanced sensors being released into the commercial market right now, and they have a wide range of critical applications in clinical, industrial, agricultural, and environmental research. The definition of a biosensor is an analytical instrument that combines a sensor and a physicochemical translator. The presence or concentration of a biomolecule, a biological structure, a bacterium, etc., may be determined using a biosensor (Thévenot et al., 2001). A signal, a signal converter, and a reading device are the three components of a biosensor that identify the analyte.

The four fundamental types of sensors and biosensors are calorimetric, optical, piezoelectric, and electrochemical, and there are several approaches to a transduction electrical signal (Mittal et al., 2017). These sensors are designed to create an electrical signal proportional to the targeted analyte to be detected. They consist of electronic and electrical parts that produce inverters. Sensors consist of a system that combines the signal generated by the interaction of a bioactive component with the material under examination, along with a method for monitoring these signals.

Many researchers are interested in electrochemical sensors and biosensors because of their uncomplicated experimental design, low cost, and exceptional detection limits. It is increasingly utilized, particularly in the clinical, industrial, environmental, agricultural, and healthcare sectors(Canbaz, Şimşek and Sezgintürk, 2014; Oliveira *et al.*, 2013). One of the most obvious reasons for the growing interest in biosensors is the capability of electrochemical devices to continually monitor the levels of a drug or therapeutic metabolite (Basabe-Desmonts, Müller and Crego-Calama, 2007).

A traditional biosensor is a combination of biological and physiochemical components (Figure 2.1) (Grieshaber et al., 2008). The term "biological components" refers to biological molecules, such as antibodies, enzymes, nucleic acids, and others, that may recognize and interact with a particular analyte. Transducers are identified as physiochemical components because they transform the bioreceptor-analyte interplay

into signals. At the electrode interface, the signal generated by a particular biological event is captured, amplified, analyzed, and displayed (Eggins, 2008).

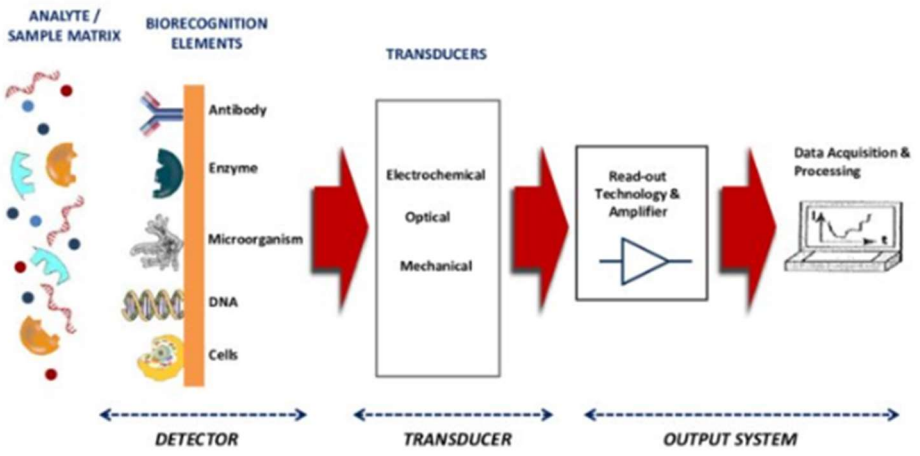

Figure 2.1 Three-component biosensor schematic diagram: output system, transducer, and detector (Grieshaber et al., 2008)

To build a highly effective and competent biosensor, selectivity, sensitivity, limit of detection, linearity, response time, reproducibility, and stability are various dynamic and static attributes that need to be improved (Daniel R Thévenot et al., 2001; Bhalla et al., 2016). A biosensor's selectivity is the most important feature. The ability to distinguish one analyte from multiple additional admixtures and undesirable contaminants in a sample is known as selectivity. Sensitivity is the ratio of a sensor's change in the output signal to variations in the measured quantity. The lowest amount or concentration of a substance that can be consistently and reliably identified by a given analytical technique is known as the limit of detection or (LOD). Comparably, the lowest concentration in a compound-containing sample (LOD) is the concentration that allows us to differentiate it from the concentration in a blank sample (a sample that does not include the component) (Desimoni & Brunetti, 2015). The lowest concentration of an analyte is at which it is possible to quantify it with sufficient precision about a blank sample. Most biosensors require LOD, as the analyte concentration in the sample is often as low as ng/ml or even fg/ml for various medical and environmental monitoring applications. Mathematically, linearity is described as $y=mc$, where y represents the output signal, m is the biosensor sensitivity, and, c

denotes the analyte concentration. Linearity represents the precision of the observed response to a straight line for a group of tests with varying analyte concentrations. Response time measures how long it takes for a system query to receive a response. In other words, response time is when the sensor changes its output signal from its initial baseline state to a certain percentage of the final value (A. K. Sharma & Mahajan, 2023). The time following a measurand measurement is when a sensor's output signal stabilizes within a certain tolerance. It is also described in specific applications as the time needed to receive 95% of the total signal. The degree of agreement between measurements made under different conditions is defined as reproducibility, the degree of agreement between measurements made in other circumstances. The biosensor must consistently yield the same results when analyzing the sample multiple times. Stability is the ability of a measurement system to generate the same values repeatedly while testing the same sample. The application, which necessitates ongoing target analyte monitoring, places a high priority on this. This is crucial for the application, as it requires continual target analyte monitoring.

The scientific community is interested in biosensors because they have several advantages. As shown below, the top benefits of biosensors include (Kara, 2012).

i) Biosensors can detect target molecules at concentrations as low as picomolar, demonstrating their remarkable sensitivity.

ii) Biosensor detection methods are particular because of the interaction between the bioreceptor and analyte.

iii) Biosensors provide continuous, actual timedetection of the target molecules, giving information on the mechanisms of binding and dissociation as affinities.

iv) Biosensors have a fast response time.

v) The compact size of miniature biosensors enables on-site testing.

Because of their benefits, biosensors have several uses in the medical industry, including drug development, illness detection, pharmaceutical usage, and more. They can also be used for quality control, pollution monitoring, and product monitoring in

the food and environmental fields. Biosensors may also be used in the military and for research.

Biosensors can be categorized according to the physiochemical signal transduction mechanism or the biological mechanism that provides specificity. Biosensors can be classified into six main types: gravimetric, optical, thermal, acoustic, electronic, and electrochemical, depending on the physiochemical and electrochemical, depending on the physiochemical signal transduction method. Electrochemical biosensors are the most prolific, widespread, and effectively marketed biomolecular electronics devices among these different biosensors. The reason is that electrochemical biosensors tend to be more portable, work in turbid conditions (in contrast to optical ones), have a quick reaction time (in comparisonto bioluminescent ones), attain lower detection limits, and be less expensive than the other biosensors. Environmental pollutants such as fertilizers, pesticides, estrogenic compounds, CO, and CO_2 are effectively monitored using electrochemical biosensors, making it crucial to address these factors. They are also used to detect industrial bioprocess products like amino acids, yeast, lactic acid, and ethanol, as well as clinical diagnostics-relevant substances like glucose, alcohol, DNA, and hormones, as well as forensics-related substances such as cocaine, anthrax, and nerve agents (Daniel R. Thévenotet al, 2001b).

Over the last 50 years, biosensor development has improved. Only a small number of these biosensors have achieved widespread success. Electrochemical glucose biosensors and lateral flow pregnancy test biosensors are two biosensors that have been effectively utilized in the commercial market. Because it is challenging for businesses to translate academic scientific research into prototypes that can be used commercially, several constraints restrict the production of biosensors for commercial application. Scientists experienced in biosensors face the challenge of collaborating with scientists from other fields, such as engineering, to develop biosensors. It's challenging to find organizations willing to support academic research that has been peer-reviewed and proposed for commercialization. Additionally, there are conflicts of interest caused by scientific politics. The goal of biosensors research should be to create biosensors that can be tested and measured. It takes a while after academic research to provide the proof of concept before a biosensor can be produced commercially. Another issue that

impacts them is finding a market for biosensors. It is strongly advised to verify the biosensor's functioning over an extended period of time, and the minimum storage period needed for commercial usage is six months. Academic and engineering scientists are very motivated to find solutions to these problems, and the production of commercial biosensors is increasing (Bhalla et al., 2016).

2.2 Electrochemical Biosensors

Electrochemical biosensors are molecular sensors that connect electrochemical transducers to biological recognition components. The biological recognition event is converted by the biosensors into an electrical signal that is proportionate to the analyte concentration. Since its inception, electrochemical devices have dominated the field of biosensor development, becoming the most widely utilized biosensors for clinical analytical monitoring and diagnosis testing.

Electrochemical biosensors require surface features that allow for sufficiently high sensitivity and unique identification of the response with the targeted biological event. For instance, biofluids can vary greatly in pH and ionic strength, which can impact how crucial biosensors like immunosensors respond. Because of this, there has been a recent push to use nanotechnology to reduce the size of electrochemical sensor elements to sizes that can increase the signal-to-noise ratio for processes intended to occur at the device interface, as well as to find ways to use multiple enzymatic tags to improve the signal per event. Developing novel micro(bio)chemical sensors and sensor arrays that are specific, sensitive, reliable, and selective will be made possible by combining expertise in the fields of biochemistry and electrochemistry, bioengineering, solid state and surface physics, data processing, and integrated circuit silicon technology. This will address the remaining issues. Thus, it is appropriate to review recent developments in this broad sector and talk about the potential for further advancement (Grieshaber et al., 2008) .

The cell design includes an electrolyte, one or more electroactive materials, and other reagents that will react with the electrolytic products and the electrochemical apparatus. The electrochemical cell with three electrodes is shown in Figure 2.2.

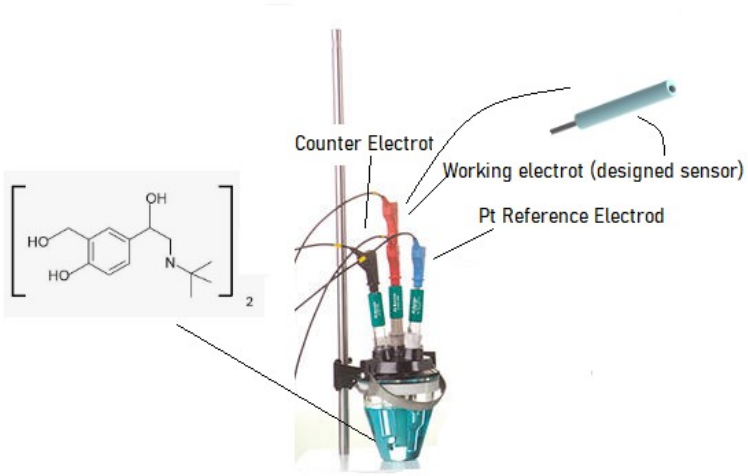

Figure 2.2 Electrochemical-sensor electrode set.
(https://www.metrohm.com/tr_tr/products/accessories/)

Electrochemical biosensors can be classified into 3 groups according to their signal transduction types: potentiometric, amperometric and conductometric, and 2 groups according to their biological recognition mechanisms: biocatalytic sensors and affinity sensors (Švancara et al., 2009). Various electrochemical techniques can be used to analyze electrochemical reactions. An electroanalytical method is classified into three categories (Brett, 1998): (i) conductimetric (impedimetric), in which the response is determined based on the solution's conductance;(ii) potentiometric in which a current is applied to two electrodes (working and reference electrode) to determine the potential difference between the electrodes, and (iii) amperometric (voltammetric), in which the current is measured by applying a set voltage between the working and reference electrodes. Every technique offers advantages for a particular purpose for a specific range of applications, so it is important to choose the most appropriate method.

Due to their detection sensitivity, this study utilized cyclic voltammetry and differential pulse voltammetry, both amperometric techniques.

2.2.1 Potentiometric sensors

Potentiometric sensors measure the potential difference between a reference solution and a sample solution using indication and reference electrodes. A membrane with an ionophore specific for a certain ion separates the two solutions. The Nernst

equation (Eq 2.1) provides the relationship between potential difference and target ion activity.

$$E = E_0 + \frac{RT}{zF} \ln \frac{a^s}{a^m} \qquad \text{Eq 2.1}$$

E refers to the potential, and the oxidized and reduced species have an activity of a_{Ox} and a_{Red}. The universal gas constant (R), temperature (T), Faraday constant (F), electric potential (E0), and the number of transferred electrons per molecule (z) are the additional factors in the equation. (Y. Wang et al., 2008). Potentiometric sensors have been widely used since the 1930s due to their simplicity and versatility. Ion-selective electrodes (ISE), coated wire electrodes (CWES), and field effect transistors are the three primary categories of potentiometric devices (FETS) (Stradiotto et al., 2003). The activity of certain ionic substances in the surrounding solution is measured by the ion-selective electrod. The ion-conducting, permselective membrane that divides the electrode from the external solution forms the basis of the operation of the ISE devices. The membrane's composition is crucial when creating the ISE for a specific ionic species. The potential of the reference electrode remains constant, whereas the working electrode's potential is determined by its surroundings. The change in the potential difference or working electrode potential determines the target ion concentration (Bobacka, Ivaska and Lewenstam, 2008). The pH electrode is the most effective and popular type of potentiometric sensor. Its success is due to its stability, simplicity of handling, reproducibility, widevariety of applications, and cost (Stradiotto *et al.*, 2003). The revolutionary advancements in detection limit, nanoscale potentiometry and, sensor stability are described in detail by Bakker and Pretsch (Bakker & Pretsch, 2008).

2.2.2 Conductometric sensors

The idea behind conductometric sensors is to utilize changes in the material's electrical conductivity (used to build the detection device) that interact with the analyte to provide sensory information. Conductometric sensors are typically non-selective. However, selectivity can be increased through more exact miniaturization and surface modification. Conductometric sensors do not require a reference electrode to operate, reducing both their price and complexity of use. There are reports in the literature of

various thin film modifications primarily for gas sensing. These thin-film modified conductometric sensors comprise, for example, the detection of H_2S using copper-doped oxides (Rumyantseva et al., 1997). In contrast, the detection of CH_4 is carried out using semiconductor films made of Ga_2O_3. Modifications were performed to conductive polymers, such as polypyrole, to detect volatile amines; CdS films were modified to detect oxygen; and $MnWO_4$ films were modified to serve as humidity sensors (Sun et al., 1997).

2.2.3 Amperometric sensors

A potentiostat manages the potential in amperometric sensing while the electron transfer reaction monitors the current. In biological processes, the current that is produced when electroactive molecules are reduced or oxidized is continuously observed. The term "amperometry" refers to this method of measuring current at a voltage that is constant. Voltammetry is the measurement of current under carefully regulated potential variations. Furthermore, the concentration of the investigated electroactive species is exactly correlated with the current's peak value as measured throughout a linear potential range.. The potential can be swept between two possible values (potentiodynamic sensing) or kept constant (potentiostatic detection). Electron conduction between the analyte and the working electrode forms the basis of the theory. Studies have indicated that amperometric devices have better sensitivity than potentiometric devices despite the drawbacks of this technique, which is often an indirect detection approach (Grieshaber et al., 2008). Amperometric measurements are an analytical method in which the applied voltage promotes electrocatalytic redox reactions that generate electric currents proportional to the analyte concentration, and this method is often preferred for its high accuracy and sensitivity (Baranwal et al., 2022). Amperometric sensors work by measuring changes in electric current. Amperometry monitors increases or decreases in signal due to oxidation or reduction reactions of analytes, and these changes provide a current response corresponding to the analyte concentration. The signal is detected through an electrode at a specific potential that facilitates electron transfer (Matthews et al., 2021). A potentiostat, three electrodes -a working electrode, a reference electrode, and a counter electrode soaked in the proper electrolyte to form an electrochemical cell- are the essential components

of amperometric sensing apparatus. Graphite, platinum, stainless steel, and other inert conducting materials are utilized to provide the counter electrode or auxiliary electrode. In amperometric sensing, the electron transfer occurs at the working electrode's surface. A reference potential is applied to the working and counter electrodes through the reference electrodes (Figure 2.3). Figure 2.4 illustrates a typical amperometric sensing system (Murray, 1983a).

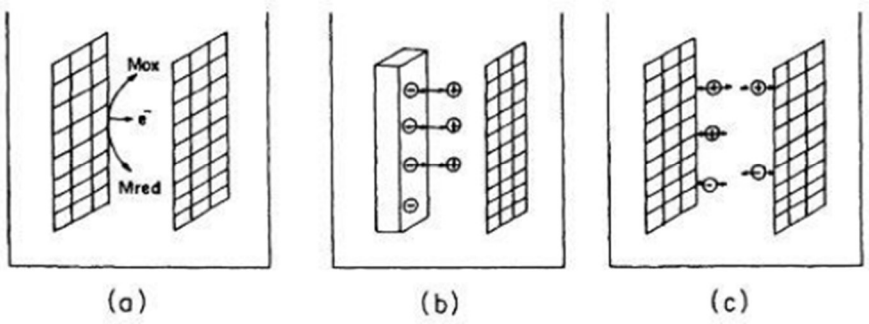

Figure 2.3 The schematic illustrates the potential of three types of biosensors: (a) amperometric, (b) potentiometric, and (c) conductimetric (Malhotra & Turner, 2003)

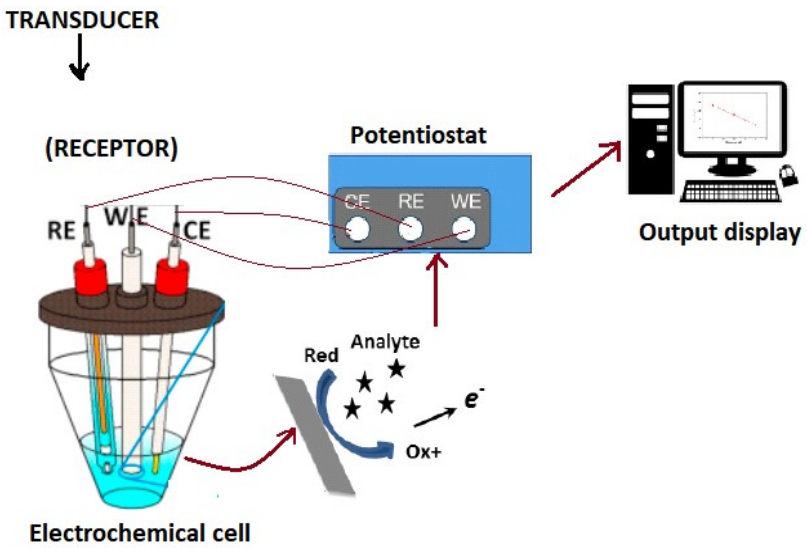

Figure 2.4 A typical amperometric sensor system illustration revised from (Miranda-Castro et al., 2020)

2.3 Electrode Surface Modification

Electrochemical sensors are advantageous because their design is simple, their electroactive surface area is lage, they perform well in voltammetry tests, and their electrochemical activity increases (Svancara et al., 2012). Despite the sufficiency of traditional electrode materials, there is an ongoing necessity for the research and development of material platforms as electrode substrates for effective and dependable electrochemical sensors for various applications. Given the importance of analyzing and comprehending pharmaceuticals and biologically significant chemicals, simple analytical methods based on sophisticated electrochemical sensors with high efficiency and selectivity are still desired.

One of the most essential techniques for sensor development is electrode surface modification. Modifying the electrode surface can improve the limits on electron or mass transport across an electrode surface. This can be accomplished by employing substances or functional groups that enhance electron transport and by creating or immobilizing electroactive species or reactants at or close to the electrode-solution interface (Svancara et al., 2012). The surface of an electrochemical biosensor electrode is modified according to the specific requirements for particular detection purposes. Significant overpotentials are frequently required for direct oxidation on unmodified electrode surfaces (Lorenzo et al., 1998). Additionally, electrode surface modification could be required to meet fundamental criteria for selectivity, electron transfer, or the catalysis of slow electrode processes (Baldwin & Thomsen, 1991). Therefore, there are two approaches to accomplish this target: intrinsic and extrinsic modifications.

2.3.1 Intrinsic Modification

In this instance, the functional groups that change the electrode are its constituent parts. When highly oxidizing chemicals, like nitric acid, oxidize carbon, oxygen-containing groups are formed on the surface. This is an excellent place to start since it will lead to the formation of phenols and quinone structures. Consequently, carbonyl groups may be chemically reduced to phenols and alcohols, which can be employed directly or as anchoring groups for the natural modifier. Depending on the chemical structure, the natural modifier can then be attached directly or indirectly.

2.3.2 Extrinsic Modification

Extrinsic modification refers to adding extra components and modifiers to the electrode material. It is often classified based on the location of the modifiers within the electrode. Extrinsic modification may be achieved by utilizing particles or paste. In this scenario; reactive groups are typically bonded covalently to the particles.

2.3.3 Surface Modification

The modifier can be present in membranes, thin layers, coatings, or electrode surfaces.

Submonolayers: A quantity of the modifying agent that is less than required to generate a monolayer is randomly applied to the electrode surface.

Monolayers: The modifier typically forms a single layer over the electrode surface as self-assembled monolayers or Langmuir-Blodgett films. Inconsistencies in the monolayers, or "pinholes" in the layer structure, may cause issues.

It has been noted that molecules with functionalized alkyl chains that adsorb strongly to the surface spontaneously form self-assembled monolayers. Another functional group at the opposite end, often hydrophilic, interacts with the adsorbed molecules to create a stable structure. Van der Waals interactions could influence the development of stable bonds between alkyl chains.

Polylayers: These structures can be homogenous or heterogeneous and comprise several modifier layers. In the latter scenario, modifiers are incorporated into a three-dimensional polymeric network. Such layers can be created via electrodeposition, such as using electropolymerized organic polymers, applying solutions after the solvent has evaporated (generally polymeric solutions), or directly applying a membrane (also commonly made of polymers). The deposited layer may operate directly on the target analyte, acting as the actualmodifier's trap or anchoring backbone or through its size-exclusion properties (Svancara et al., 2012).

2.3.4 Bulk Modification

Although surface modifications can also be carried out on solid electrodes made of homogeneous materials, heterogeneous materials offer the advantage of allowing the modification of the electrode material as a whole under normalconditions. An electrode can be modified by adding the modifier directly to the carbon paste (the term "direct mixing" for this procedure was coined by Baldwin et al.), which is the most straight forward and feasible method. Alternatively, the modifier may also be mixed with or adsorbed in the carbon powder during the paste preparation (Ravichandran & Baldwin, 1981). The modifier can also be dissolved in the liquid for making the paste. To achieve a high degree of uniformity in the particulate component modification, it is essential to consider the size and uniformity of the modifier particle (Svancara et al., 2012). To be effective for their intended uses, modifiers must meet specific requirements. They must, for instance, significantly adsorb on the carbon particles or be insoluble in the liquids to which they will be exposed. If not, the electrode may "bleed," producing results that are difficult to reproduce. Making modifying molecules more lipophilic can lead to improvements. Strong background currents may otherwise deteriorate or impair electrochemical responses. Hence, the modifier should not be electroactive at the potential of interest unless electrocatalytic effects are to be used. The modifier is usually present in bulk modification at concentrations of 5% to 10% (wt/wt) of the paste. Excessively high concentrations can adversely alter the physicochemical and physical properties of the electrode material by increasing the background current and ohmic resistance, while insufficient concentrations do not have the desired effect. On the other hand, some paste compositions contain 50% (w/w) or more modifiers and the resulting CPEs are said to work well (Svancara et al., 2012).

As was previously indicated, there may be significant differences in the chemical composition of the many modifiers that can support the functions. The most commonly used mediators include metals, metal complexes and salts, redox-capable polymers, and newly created nanosized materials, including nanoparticles (NPs), nanorods, and nanotubes. One type of electrocatalytically active alteration that can occur when a

robust positive potential is applied is the electrochemical creation of functional groups on the surface of carbon particles.

Redox polymers could be a highly sophisticated method of connecting redox enzymes. Reagentless biosensors allow for the direct electrochemical conversion of the enzyme's active core without reagents. These polymers might be osmium, toluidine blue, phthalocyanines, or ferrocenes (Yuan & Minteer, 2019).

Metals: Compact metallic components such as Pt, Pd, Ru, or Rh are commonly used to increase the catalytic activity of carbon paste electrodes. They can be employed to catalytically oxidize substances like hydrazines and hydrogen peroxide. . The metals can be applied in a dispersed form or coated on the carbon particles. Less noble electrochemical metals, like nickel, can also be used for specific tasks, such as oxidizing methanol. The usage of nanomaterials in applications has become increasingly common in recent times.

Metal complexes and salts: Metal complexes or salts are responsible for producing the majority of electrocatalytically active modifiers. To reduce the overpotential for intermediates or co-factors, CoII, FeII, NiII, and MoVI are most typically utilized while building oxalic acid, pesticides, peroxides, phenols, ephedrine, and vitamin B1 biosensors. Hexacyanoferrates and analogs containing nickel or platinum metals are also coupled synergistically with carbon nanotubes and ferrocenes (primarily as electron transfer mediators in biosensors) to detect peroxides.

Metal oxides:MnO_2, FeO, Fe_2O_3, SnO_2, CuO, and similar compounds are helpful because they are effective catalytic mediators when they exist in different oxidation states, which helps find the corresponding substrates. As modifiers, oxides in nanoparticles form attract more attention due to their outstanding properties compared to macro- or micro-sized powders. The significance of these nanosized materials catalyticallyactive modifiers has increased overthe last 20 years. Nanosized particles have a large surface area, which allows them to perform catalytic processes that are not evident in macrosized form. Additionally, they might enhance the macro- or micro powder's already-existing catalytic activity (Svancara et al., 2012).

2.4 Nanomaterials and Their Effects

The size and composition of an electrode, which can be customized to improve the analytical output, significantly impact its electrochemical performance. Nanomaterials can modify electrode surfaces, facilitating electron transport and enhancing the electrochemical response. Recent years have seen a significant increase in interest in nanomaterials because of their unique and unusual qualities, making them practical across various fields. Nanomaterial refers to a material with nanoscale dimensions (1-100nm). Their size and the ratio of atoms on the material's surface affect its physical and chemical properties. This situation becomes more critical as the size decreases and the chemical reactivity increases. Surface area (SA)/volume (V) and/or unit weight are important contributing variables. Most atoms in the atomic lattice are found at or close to the surface when the SA/V ratio rises (Findik, 2021).

In particular, nanomaterials, such as nanoparticles, carbon-based nanomaterials, and nanocomposites are utilized to develophighly sensitive biosensors, enhance the functionality of existing ones, and offer new methods for electrochemical signal transduction (L. Li et al., 2024). In other words, each nanomaterial has a greater surface area to volume ratio than the bulk material. This provide s ahigh surface area for immobilizing biomaterials in biosensor applications (Banerjee et al., 2021).

These unique qualities make them highly regarded for usage in various fields, including biomedical healthcare, agriculture, catalysis, chemistry, business, electronics, environmental sectors, food industry, and physics (Ealias & Saravanakumar, 2017). Nanotechnology focuses on developing different nanomaterials for typical applications in photonics, electronics, and pharmaceuticals. Numerous nanoplatforms, particularly in medicine, have been extensively studied for biosensing, bioimaging, drug delivery, gene therapy, tissue engineering, and nanomedicine (Qu et al., 2015).

Nanomaterial applications in electrochemical biosensing can be categorized based on their primary uses: labels or modifications to electrotransducing surfaces. Both strategies require the exceptional qualities of nanomaterials, particularly nanoparticles, to improve the electron transfer rate when used as modifiers of electrochemical

transducers or enhance the electrochemical signal when employed as labels (L. Li et al., 2024).

Nanomaterials are available in various shapes, such as spherical, tubular, irregular, fused, aggregated, and agglomerated. Based on their dimensions, they are divided into four categories. Zero-dimensional (0-D), in which most objects in all three dimensions (x, y, and z) are atomic clusters and are less than 100 nm. In a one-dimensional system (1-D), two of the dimensions (x, y) are at the nanoscale but dimension (z) is not. Nanowires, nanotubes, nanorods, ceramic crystals, and polymer nanofibers are one-dimensional (1-D) materials. At the same time, nanoparticles, quantum dots, nanodots, core-shell quantum dots, and nanoparticles are zero-dimensional (0-D) materials. Graphene, nanofilms, nanoplates, and nanocoatings are two-dimensional (2-D) materials. In all dimensions, three-dimensional (3-D) materials are not limited to the nanoscale level (e.g., polycrystals and spherical particles) (Tiwari et al., 2012). This classification is not limited to the 1-100 nm nanoscale range. There are several different types of nanomaterials, such assingle- and multi-walled (carbon) nanotubes, single-walled and multi-walled nanoparticles, nanoclusters, nanoparticles, nanocomposites, nanocapsules, nanowires, and nanoporous materials, among others (Pokropivny and Skorokhod, 2007). The typical dimensional properties of nanomaterials are depicted in Figure 2.5.

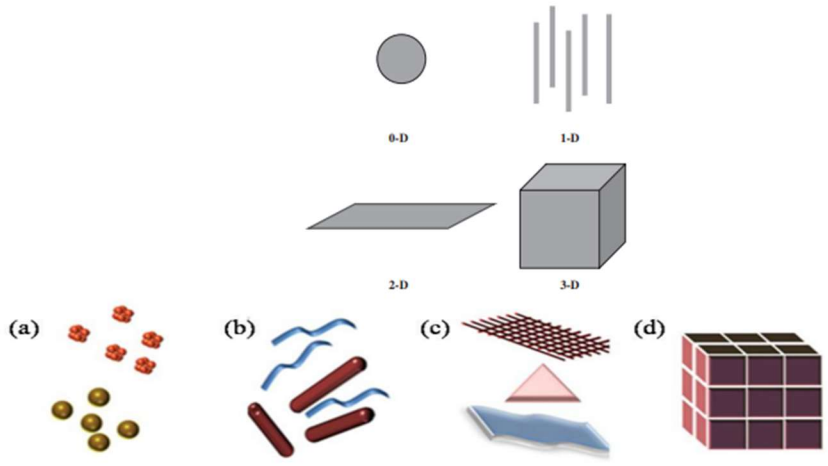

Figure 2.5 Diagrammatic representation of the nanomaterials categorization 0D spheres and clusters, 1D nanofibers, wires, and rods, 2D nanofilms, nanoplates, and networks, and 3D nanomaterials (Banerjee et al., 2021)

In addition to being classified by size, nanostructures are also divided into four groups depending on their chemical properties: oxide (e.g., titanium dioxide, zinc oxide), polymeric (e.g., graphene), metallic (e.g., gold, silver) and carbon based (e.g., graphene, carbon nanotubes). Metallic nanostructures are often employed in biological imaging and treatment due to their plasmonic characteristics, whereas metal oxide nanostructures are frequently utilizedin catalysis and UV protection applications. Carbon-based and polymeric nanostructures, which constitute an essential class of nanostructures, play an important role in electrical and energy storage applications and drug delivery systems, respectively, thanks to their properties. In addition, hybrid/composite nanoparticles formed by fusing various materials can be used in more complex and advanced applications by offering multifunctional and qualified properties (Dinda, 2019).

2.5 Zero Dimensional Nanomaterials: Structure and Properties

In recent decades, the field of nanotechnology has experienced rapid growth. Many nanoparticles with altered physical and physicochemical properties can be created by changing nanomaterials' atomic organization, chemical composition, or dimensions (Carneiro et al., 2019). Since the word "nanotechnology" was first coined in 1974 by Norio Taniguchi, zero-dimensional (0-D) nanomaterials have been considered the precursors of nanotechnology (Z. Wang et al., 2020). Because of the intrinsic structural features of 0-D nanomaterials, such as their very tiny diameters and high surface-to-volume ratios, contain more active edge sites per unit mass. The edge and quantum confinement effects enable 0-D nanomaterials to gain new or improved properties, such as excellent quantum efficiency. According to Wu et al. (2020), 0-D nanomaterials include carbon quantum dots (CQDs), graphene quantum dots (GQDs), inorganic quantum dots (QDs), magnetic nanoparticles (MNPs), fullerenes, polymer dots (Pdot), upconversion nanoparticles (UCNPs) and noble metal nanoparticles. These materials may be used in materials science, sensing, biomedicine, photovoltaic science, energy, catalysis, and nanodevices. Since their surface to volume ratio is so high, nanoparticles offer superior characteristics than bulk materials. Two different effects can explain this phenomenon. First, quantum effects, which are describedas discontinuities in behavior due to the confined delocalized electrons on the surface of

NPs due to their small size; second, surface effects, which are explained as weakly bound and more reactive, since most of the atoms are on or near the surface (Roduner, 2006).

The rise in the ratio of surface area to volume as a material's size decreases significantly increases the number of unsaturated atoms with highly reactive, open atomic orbitals, superficially for surface enhancement. Nanoparticles display unique material behavior because of this characteristic (Huang et al., 2021; Narayanan & El-Sayed, 2005).

2.5.1 Metal Oxides

Metal oxide nanostructures have potential as electrode materials for sensor applications and energy conversion. As a result of their large volume to surface area ratio, they can carry many membrane molecules and expose numerous surfaces for the analyte molecules to oxidize. The modified electrode surface allows for immobilizing enzymes to facilitate biological activity, coating various membranes, and catalyzing slow electrode processes for swift electron transfer (redox-active). Sensor technology uses metals and semiconductor metal oxides for accurate and reliable performance. Metals such as Pd, Pt, Rh, and Ir are frequently utilized as active catalysts due to their incomplete d-shells, enabling the detection of free electrons. A different detection method is employed in metal oxide sensing systems. The electrical conductivity of metal oxides can change when specific lattice point defects are present. Although the conductivity of metals can also change, this transformation is relatively subtle and challenging to observe (Mandelis and Christofides 1993).

Furthermore, precise processing and integration of metal oxide nanomaterials into biosensor designs results in exceptional target analyte detection sensitivity, specificity, and efficiency. Because of their diverse range of electrical, chemical, and physical properties, oxides like copper oxide (CuO), tin oxide (SnO_2), nickel oxide (NiO), manganese oxide (MnO_2), iron oxide (Fe_2O_3), cobalt oxide (Co_3O_4), zinc oxide (ZnO), titanium oxide (TiO_2), and cadmium oxide (CdO) have been extensively utilized in various biosensor applications over the past 20 years. Copper, zinc, iron, and manganese oxides are the best magnetic nanomaterials with high electron mobility

among the metals indicated above; hence, they are used to produce electrochemical biosensors (Malik et al., 2023). A third of the market for consumer items using nanotechnology is formed of metal oxide NPs used in many fields. These substances are employed as paint pigments (TiO_2), sunscreen and cosmetic ingredients (TiO_2, ZnO), antibacterial agents (CuO, MgO), in industrial processes (MnO_2, Al_2O_3), and in the medical field (Fe_3O_4, Al_2O_3, Fe_2O_3). Drug distribution is facilitated by aluminum nanoparticles, which encapsulate medications to increase their solubility, evade detection processes, and enable site-specific targeting of drugs to cells. TiO_2, CdO_2, C60, and carbon nanotubes were the only nanomaterials used in prior toxicity research. Even though iron oxide nanoparticles are the only metal oxide nanoparticles that have been given clinical approval, only a few studies have looked into the toxicity of these particles (Szalay et al., 2012). Zinc oxide (ZnO) nanoparticles are extensively employed in glucose sensor applications thanks to their superior biocompatibility and large surface area. The glucose level can be precisely measured by dispersing these nanoparticles and the glucose oxidase enzyme (Malik et al., 2023). The use of titanium dioxide (TiO_2) nanoparticles in optical biosensors for DNA and protein residues is significant. Chemical stability and high photocatalytic activity of TiO_2 are vital in identifying these biomolecules (Khaliq et al., 2021). Iron oxide (Fe_3O_4) nanoparticles are also used in targeted medication delivery systems and magnetic resonance imaging (MRI) in biomedical applications because of their magnetic properties. Biomolecules are functionalized onto Fe_3O_4 nanoparticles to enable targeted classification or enhanced sensitivity in pathogen detection (Lee et al., 2016). Utilizing nickel oxide (NiO) nanoparticles to catalyze substrate conversion in enzymatic biosensors, metabolites can be electrochemically stained (Kailasa et al., 2020). These particular instances of diverse metal oxide nanoparticles in distinct biosensor applications demonstrate the adaptability of nanomaterials and their essential part in the advancement of biosensor technologies. Semiconductor materials of the metal oxide class employed in sensor design can be generically categorized as intrinsic and extrinsic semiconductors based on their energy gap, as demonstrated in the flow chart below (Figure 2.6).

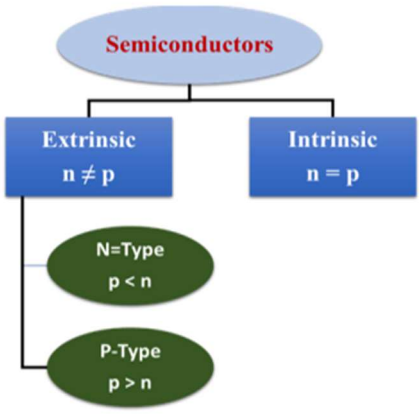

Figure 2.6 Various types of semiconductor (Albarakati & Matter, 2023)

The number of holes in an intrinsic semiconductor's conduction band is equal to the number of electrons in the semiconductor's pure, impurity-free material. These semiconductors include silicon and pure germanium, which have "forbidden energy gaps" relatively small (0.72 and 1.1 eV, respectively). Even at average temperature, the valence electrons in an intrinsic semiconductor might "jump out of the conduction band" due to an abundance of accessible energy. These semiconductors are used in relatively limited applications because of their electrical conductivity at room temperature and higher.

Minimal concentrations of impurities referred to as "dopant(s)" or "doping agent(s)" are added to produce extrinsic semiconductors (the ratio does not exceed 0.01 ppm). Pentavalent or trivalent doping materials are chosen because they have three or five electrons in the valence band, respectively. Simultaneously, the dopant atoms and semiconductor should have the same size, and the semiconductor's "lattice structure" should not be altered by the dopant concentration. The two types of extrinsic semiconductors are n-type and p-type, depending on the doping material's valence (Behera, 2022; Boshta et al., 2022).

Doping semiconductor materials like Si and Ge with pentavalent elements results in the formation of the n-type semiconductor. In this case, the doping atoms are from the fifth group of the periodic table. In contrast, the semiconductor atoms (Si and Ge) are from the fourth group, guaranteeing a closely matched size between the atoms. When a pentavalent atom is doped into Si atoms, four electrons form bonds with four

Si atoms, and the fifth electron is only weakly connected to the dopant atom. This loose electron can only be liberated and moved at ambient temperature with little ionization energy "Majority current carriers" are the free electrons in the n-type that are doped and have a negative charge on them. Nonetheless, the thermal generation of a small number of "holes" (alsoknown as minoritycarriers) results from thes ynthesis in electron-hole pairs (Figure 2.7). Arsenic, phosphorus, antimony, and bismuth are among the pentavalent elements that are employed to dope semiconductors (Behera, 2022; Boshta et al., 2022; Dixon et al., 2016; Gurylev, 2021; Albarakati and Matter 2023).

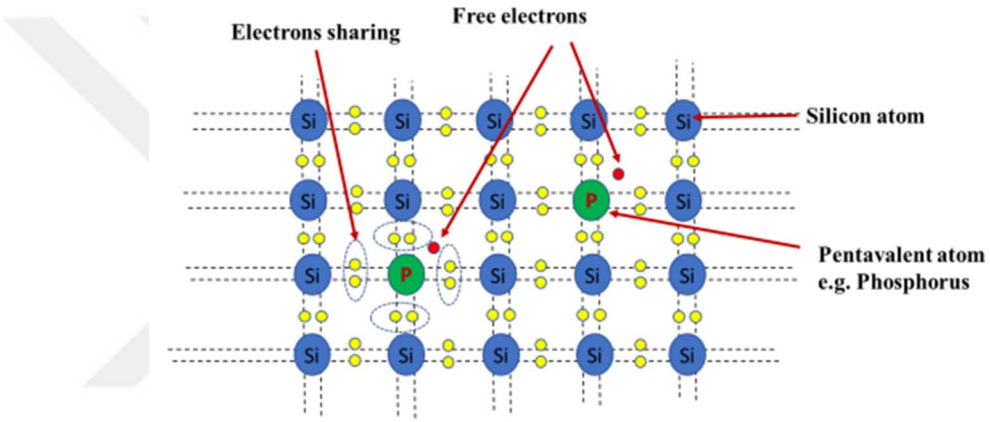

Figure 2.7 N-type semiconductor (Albarakati & Matter, 2023)

P-type describes the "positive charge" from impurity atoms added to trivalent silicon. In this instance, one hole (positively charged) is created for each trivalent dopant atom because four adjacent silicon atoms and the trivalent atom generate a connection. Because a trivalent atom may accept one electron, it is also known as an acceptor atom. The quantity of trivalent atoms incorporated into silicon results in an equal amount of "holes"; these holes are referred to as majority carriers. Nevertheless, the thermal creation of electron-hole pairs (minoritycarriers) forms multiple conduction band electrons in addition to the holes (Figure 2.8).

Gallium, indium, and boron are the trivalent dopants most frequently used in p-type semiconductors (Behera, 2022; Albarakati & Matter, 2023). However, p-type metal oxide semiconductors are still limited compared with their n-type counterparts because, for oxide semiconductors, the VB is mainly derived from the strongly

localized O 2p orbitals, which leads to deep acceptor levels and large hole effective mass (Albarakati & Matter, 2023).

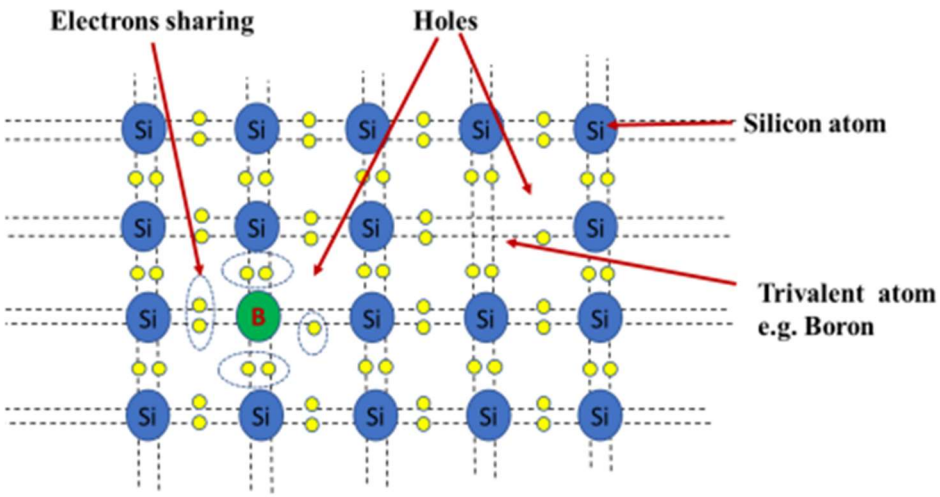

Figure 2.8 P-type semiconductors (Albarakati & Matter, 2023)

Copper is a member of the transition metals. The electron configuration of copper is [Ar] 3d10 4s1, and two oxides correspond to Cu^{+} and Cu^{2+}: Cu_2O (Cuprous Oxide) and CuO (copper oxide or cupric oxide), respectively. In Cu_2O, copper oxide crystalline forms a simple cubic structure, whereas in CuO, copper oxide crystalline forms monoclinic tenorite structures (Figure 2.9) (B. K. Meyer et al., 2012).

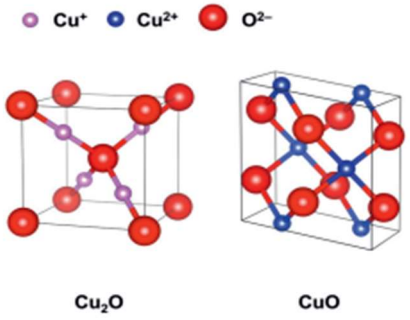

Figure 2.9 CuO and Cu_2O unit cell (Pike et al., 2006)

Copper oxide (CuO) nanoparticles have been used in many applications, especially in biomedical applications, because they exhibit potent antibacterial, catalytic, and anticarcinogenic properties and are used as coating agents. CuO is abundant in natural resources and is low-cost. These nanoparticles can also exist in Cu 0, Cu I, Cu II, and

Cu III oxidation states, and they have interesting physicochemical characteristics.CuO is a semiconducting metal oxide that crystallizes in the C2/c space group. CuO has a molecular mass of 79.685 g/mol and a 6.32 g/cm^3 density. It has a monoclinic crystal structure, melts at 1326 °C, and is insoluble in water. The lattice parameters are as follows: a = 4.6837Å, b = 3.4226 Å, c = 5.1288 Å, α = 90°, β = 99.54°and γ = 90°. Copper (II) oxide is a perfect p-type semiconductor owing to its narrow band gap of 1.2 eV. CuO has a refractive index of 2.63 (Tran & Nguyen, 2014). CuO's p-type semiconductor status has been developed due to Cu atom vacancies. Instead of free electrons, holes in the valence shells of p-type semiconductors are often responsible for conductivity. The conductivity of CuO, which ranges from 1.59 x 10^{-3} to 0.11 (Ω cm)$^{-1}$, is caused by defects in the Cu atoms, which provide too many holes in the valence shells, allowing for conductivity. The CuO material's electrical conductivity may be changed by adding more components. Copper oxide nanoparticles (CuO NPs) have potential uses in optics, electronics, catalysts, water purifiers, pharmaceuticals, lubricants, nano-fluids, nano-fertilizers, conductive coatings, as well as antifungal and antibacterial agents (W. Meyer et al., 2008). CuO possesses a high band gap, exceptional catalytic activity, and superior optical qualities, making it a significant compound for enhancing its applications in industry, pharmaceuticals, and environmental solutions (Gao et al., 2010). The aforementioned superior properties depend on these materials' size, shape, and environment; however, compared to their bulk condition, nanoparticles have a high surface-to-volume ratio; these properties differ from materials of the same type and are often more advanced.

In sensor applications, copper nanoparticles are favored over alternatives due to their cost-effectiveness, excellent physical and chemical stability, good conductivity qualities, good catalyst performance, and ability to be easily separated and converted into new products. CuO nanoparticles are very sensitive and respond quickly in biosensors, especially when detecting glucose and other biomolecules. Analytes at low concentrations can be detected using electrochemical sensors thanks to their broad band gap and good electrical conductivity. They possess strong conductivity qualities, are efficient catalysts, and are readily separated and repurposed. They also exhibit physical and chemical stability. CuO nanoparticles are very sensitive and respond quickly in biosensors, especially when detecting glucose and other biomolecules.

Additionally, the stable structures and low cost of CuO nanoparticles provide practical advantages, making them stand out in sensor technologies. These attributes offer significant potential for applications in environmental monitoring, medical diagnostics, and industrial analysis (Sahin & Kaya, 2019).

The physical characteristics of CuO nanostructures, which directly impact the sensitivity and response/recovery time of glucose analytes, have been controlled using various techniques to develop CuO-based glucose sensing. For non-enzymatic glucose sensing, Li and colleagues created flower-like CuO nanostructures. These nanostructures have a sensitivity of approximately 5,000 $\mu A.mM^{-1}\ cm^{-2}$, much greater than that of conventional NMO glucose sensors. Using nanostructured CuO wires, platelets, and spindles, an enzymatic CuO glucose sensor with low sensitivity values was created (Y. Li et al., 2011). Li and co-workers fabricated crystalline leaf-like CuO nanostructures for an amperometric glucose sensor with a 246 $\mu A\ mM^{-1}\ cm^{-2}$ sensitivity, responding well to human serum levels and remaining stable for 90 days. Wang and co-workers achieved a wide linear detection range and sensitivity values of up to 709.52 $\mu A\ mM^{-1}\ cm^{-2}$ (X. Wang et al., 2010). Kim and co-workers investigated CuO nanostructures that are morphologically similar to the rose structure and have excellent glucose detection range and good sensitivity (Kim et al., 2015).

Among semiconductor metal oxides, tin oxide based materials, especially SnO_2 (tin oxide), are widely used in sensor applications due to their thermally and chemically most stable oxidation state. Tin oxide has anadaptable position in metal oxides due to their variable valence state and oxygen vacancy defects. Tin (IV) oxide, also known as stannic oxide (SnO_2), and tin (II) monoxide, also known as stannous oxide (SnO), are the two forms of tin oxide compounds. In the case of SnO, oxygen atoms are tetrahedrally bound to tin atoms, giving the material a structure similar to Sn-O-Sn stacked pyramids. Sn atoms are at the apex of regular square-based pyramids based on O atoms in this pyramid-like structure. Because of the Sn vacancies and O gaps in the structure, SnO is a p-type semiconductor with a direct band gap of 2.5–3.0 eV and an indirect band gap of 0.5–0.7 eV. SnO_2 is an n-type semiconductor with an energy band gap of around 3.6 eV, which is more comprehensive than SnO. With an asymmetric tetragonal structure (a = b = 0.4737 nm and c = 0.3186 nm), SnO_2 resembles a rutile

structure. Its unit cell comprises two metal atoms and four oxygen atoms. Six O atoms surround each Sn atom, creating the vertices of a reasonably regular octahedron. Three Sn atoms are approaching the vertices of an equilateral triangle and encircling the oxygen atoms. The unit cells of tetragonal SnO_2 and SnO are shown in Figure 2.10. The oxygen deficiency that causes the n-type behavior of SnO_2 is assigned to donors that can be single or double oxygen deficiency. These properties have increased their adaptability and applications in various fields, including photonics, catalysis, semiconductors, optical devices, transparent conductive electrodes, low-emissivity window coatings, microelectronics, and rechargeable lithium-ion batteries. Furthermore, due to their intrinsic redox nature, SnO_2-based nanomaterials can be very useful in catalysis. These nanoparticles, which have excellent sensitivity, good stability, and inexpensive manufacturing costs, are the most widely used sensing materials for solid-state chemical sensors. Their vast surface area, durability, high adsorption capacity, and distinctive electrochemical activity make them a significant class in the production of electrochemical sensors (A. Sharma et al., 2021).

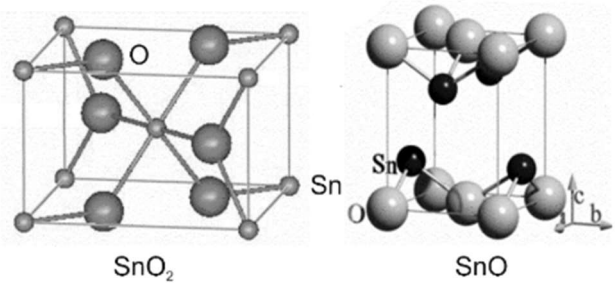

Figure 2.10 SnO_2 and SnO unit cell (Nunes et al., 2019).

The literature contains several studies showcasing SnO_2 nanoparticles and nanostructures in chemical biosensor applications. In a study by Dong and Zheng, SnO_2 nanoparticles with a 4 nm diameter, synthesized using the precipitation method, exhibited potential for detecting L-cysteine. Coating these nanoparticles with multi-walled carbon nanotubes achieved a low limit of detection (LOD) of 0.03 μM (Dong & Zheng, 2014). Yang et al. reported using acetylcholinesterase enzyme to functionalize SnO_2 nanoparticles produced by the sonication process for pesticide detection. Using cyclic voltammetry (CV), they found LOD values of 5×10^{-14} for methyl parathion and 5×10^{-13} for carbofuran (Yang et al., 2013). For H_2O_2 detection,

Lavanya et al. employed SnO_2 nanoparticles produced by microwave irradiation technique; the surface functionalized with HPOx allowed for a LOD value of 43 nM to be achieved by differential pulse voltammetry (DPV) (Lavanya et al., 2012). Furthermore, Li et al.'s thermal evaporation method-synthesized SnO_2 nanowires were employed for H_2O_2 detection, and CV reported a 0.8 μM LOD value (L. Li et al., 2010). Alim et al. used SnO_2 nanowires obtained by the electrospinning method for glucose detection and obtained a 1.8 μM LOD value by functionalizing with HPOx and GOx (Alim et al., 2019). Cheng et al. synthesized SnO_2 nanobelts by physical vapor deposition method. Using D-biotin molecules, they functionalized them and reported a 100 pM LOD value for detecting troponin I, a protein marker associated with myocardial infarction (Cheng et al., 2011). SnO_2 nanoplates were produced by Wang et al. using a hydrothermal process. They functionalized them with an anti-Aβ antibodies and reported a 0.17 pg/mL LOD value by photo charge measurement for the determination of amyloid β-protein (Aβ) (Y. Wang et al., 2018). These examples demonstrate the vast potentialand versatility of SnO_2 in various biosensor applications (Şerban & Enesca, 2020).

2.6 Modification Techniques of Nanoparticles

Nanostructures stand out as especially intriguing sensor materials when it comes to sensitivity. This is due to a few factors: (1) Higher surface area makes nanoparticles and analytes more comparable in size, which enhances the sensitivity of tiny analytes; (2) High direct electron transfer raises the sensitivity and raises the detection limit; (3) The particle size of the nanostructure, similar to the Debye length, effectively increases the sensor sensitivity. Metal oxide nanostructures have been used in biosensor research and offer far-reaching advantages. Copper, tin, iron, zinc, nickel, cerium, titanium, zirconium, and magnesium are metal oxide nanostructures with excellent catalytic qualities and exceptional nanomorphological, biocompatible, functional, and non-toxic characteristics. The remarkable electron characteristics of nanostructured metal oxides are caused by the high charge level on their surfaces (Keles et al., 2024). In electrochemical biosensors, metal oxides improve sensitivity by increasing the receptor’s surface area. Furthermore, the electrocatalytic activity of metal oxides increases electron transfer. Biosensors' reaction times are shortened, and their

efficiency is increased by the quicker transport of electrons (P. Kumar et al., 2024). Although metal oxide structures have superior catalytic properties in the presence of sufficient stimuli and are widely used in catalysis, some associated problems hinder their practical use.

Since metal oxides often have wide band gaps, electron-hole pairs must occur under high-energy radiation. This property renders them inactive catalysts in the visible range, which covers a significant section of the solar spectrum. Moreover, the products can cover the catalyst surface in some catalytic processes, which deactivates the catalyst by stopping charges from interacting with the target molecule. Numerous methods have been employed to mitigate the adverse impacts of metal oxide, such as the creation of heterojunctions with other semiconductors to improve charge transfer and separation, doping with metal and nonmetal elements to enhance optical absorption and prevent charges from building up, metal deposition, and surface modification using inorganic acid.

Thanks to advancements in semiconductor material technology, the area of biosensors has seen significant growth in recent years. One of the sensor technologies that is evolving the quickest is semiconductor-based biosensors. The invention of FET (field effect transistor) sensors, based on the direct interaction of chemical or biological constituents with an electric field, marked the beginning of this trend in the 1970s. These semiconductor methods can make compassionate and efficient use of potential differences where the forces between charges are spread in the electric field. For example, in ion-sensitive field-effect transistors (ISFETs), the amount of free electrons flowing through the sensitive material is related to the potential difference across the element.

The measured current is increased when going at the same speed. By altering the potential difference across the sensitive material of the sensor, doping components can regulate the current flowing through transistors, taking into account biological influences. The creation of susceptible biological sensors has been made possible by fundamental advancements in semiconductor materials. Additionally, the proliferation of bioengineering applications has dramatically enhanced because of these advancements in semiconductor technology (Pohanka & Leuchter, 2017). One of the

basic techniques for modifying host materials' electrical, chemical, optical, and magnetic characteristics is doping, which is the intentional introduction of impurities into the structure (Shenoy et al., 2022). Doping is a process that allows substitutional ions to be incorporated into a material's crystalline structure, producing interesting features (Bharat et al., 2019). Doping is frequently used as an essential strategy for regulating the characteristics of nanomaterials. Incorporating impurities can give doping nanoparticles unique features, but controlling morphology, crystallinity, dopant concentration, and dispersion at the nanoscale scale simultaneously can be difficult (Erwin et al., 2005; Koshkin & Slezov, 2004). Therefore, choosing an appropriate dopant for the desired characteristic change is essential in doping. To establish the doping approach, one must specify, optimize, and control the desired modification of the materials by adding impurities. Identifying atoms or ions is the first and most important phase in the doping process. The most common doping technique includes adding dopant ions with identical radii and valence (homovalence) to the nanostructure to replace the existing ions (Figure 2.11 A,D,E) (He et al., 2015). Lattice contraction and a reduction in the nanostructure size will arise if the homovalence dopant ion is replaced with an ion with a smaller radius than the host lattice ions. Alternatively, substituting the host lattice ion with a homovalence dopant ion with a higher radius will cause the lattice to expand and the size of the nanostructures to increase (Hu et al., 2015). If the dopant is heterovalent (has a different valence than the host ion in the nanostructure), the additional valency will acquire ions in the vacant spaces (Figure 2.11 B, C). Furthermore, ions may be taken up by the host nanostructure's interstitial space into the lattice during material nucleation and growth in the reaction media (Figure 2.11 F). The heterovalence ion dopants have a significantly more enormous effect on the nanostructures' size, shape, phase structure, and composition than homovalence ions. Additionally, impurities can be introduced into interstitial regions of the lattice structure where dopants do not fit but can still influence the chemical and physical characteristics of the nanomaterials. The choice of dopant directly impacts the crystal lattice of nanostructures during the doping process. Controlling the nanostructure's structural, optical, electrical, and magnetic characteristics requires choosing the appropriate additives and adjusting their concentrations (Norris et al., 2008; Pradhan et al., 2017).

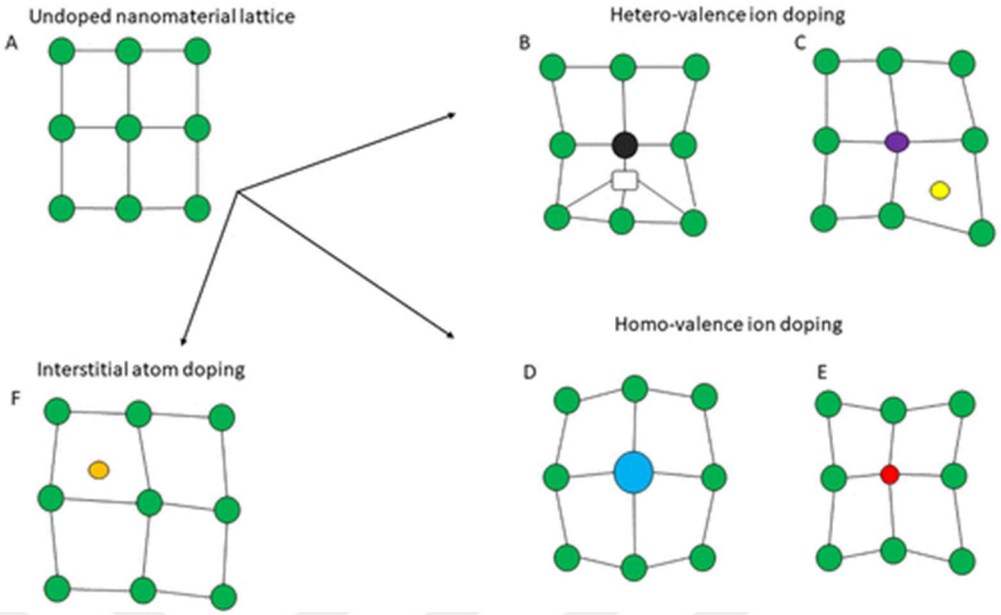

Figure 2.11 The techniques for doping nanoparticles into the lattice are schematically represented in (A) Host ion-containing nanomaterial lattice (green). (B) Lattice tempering is done by substituting a heterovalence ion dopant (black), and indemnification is charged via vacancy possession (white). (C) Interstitial ownership of an extra ion and charge indemnification by replacing a heterovalence ion dopant (purple) in the lattice (light yellow). (D) Lattice modification caused by large radii replacing a homovalence ion dopant (blue). (E) Lattice modification by smaller radii replacement of a homovalence ion dopant (red). (F) Lattice tempering caused on by the presence of a small dopant interstitially (dark yellow) (Sharma et al., 2022).

Dopants are incorporated into materials during growth through solid-state mixing, hydrothermal, sputtering, solution combustion, sol-gel. Traditional synthesis procedures involve controlling temperature, pH, and reaction environment to accurately control experimental parameters (Hu & McClements, 2014). The most important reasons for choosing the appropriate method are variable additive selection, simple control over additive precursor concentrations, and simplicity due to the absence of extra doping steps. On the other hand, dopants spontaneously modify nanoparticles' anisotropic growth and nucleation processes, leading to changes in their shape and crystallinity or the absence of NP formation. Therefore, choosing an appropriate dopant for the desired characteristic change is essential in doping (Norris et al., 2008). For this reason, different dopant materials are used in n-type and p-type semiconductors.

Different doping procedures modify n and p-type semiconductors to maximize their performance and functionality in electrical devices. Donor atoms like phosphorus (P), arsenic (As), or antimony (Sb) are frequently utilized in N-type semiconductors to raise the electron density. By adding extra electrons to the semiconductor matrix, these donor atoms encourage electron mobility and boost conductivity. In contrast, acceptor atoms like boron (B), gallium (Ga), or aluminum (Al) are used in p-type semiconductors to raise the density of holes. These acceptor atoms improve the mobility of vacancies and conductivity in the semiconductor matrix by causing electron deficits. Altering the electrical characteristics of semiconductors makes these doping techniques suitable for various optoelectronic and electronic applications (M. A. Rahman, 2014).

The doping of transition metals into metal oxides is a technique capable of significantly changing these products' electronic and optical properties. Transition metals such as iron (Fe), chromium (Cr), nickel (Ni), manganese (Mn), and cobalt (Co)can affect band gaps, change the density of electron and vacancy carriers, and even impart new magnetic properties to the metal oxide matrix. This doping process improvesmetal oxides' semiconductor, ceramic, and catalytic properties. Transition metal atoms are integrated into the crystal structure of metal oxides to form specialized electronic levels, which is particularly critical for developing spintronics and sensor technology. This makes it possible to create useful and higher-performing materials for various industrial and sensor applications (Fang et al., 2013; Pinto et al., 2022a; Haider & Haider, 2021).

In the study, a high-performance voltammetric sensor for urea detection using iron-doped nickel oxide (NiO) nanoparticles was developed, which was able to precisely measure low concentrations of urea and provide reliable results with high electrochemical signals (Mohammadzadeh Jahani et al., 2021). Alvin et al. created an electrochemical device based on paper that was altered using graphene oxide and Ni-doped TiO_2 nanocrystals. This apparatus demonstrated the promise of paper-based sensors by enabling the detection of ascorbic acid with great sensitivity and low detection limits (Alvin et al., 2024). In another study, an extremely sensitive biosensor for dopamine identification using iron-doped cobalt oxide (CoO) nanostructures was

developed, which was able to detect low concentrations of dopamine with high accuracy and a significant improvement in electrochemical signals (Tahira et al., 2016). Doping metal oxides with rare earth elements can significantly change the physical and chemical properties of these materials and enable these properties to be optimized. When rare earth elements such as lanthanum (La), cerium (Ce), neodymium (Nd), praseodymium (Pr), and ytterbium (Yb) are integrated into the crystal structure of metal oxides, they often improve the electrical, optical, and magnetic properties of the oxide. The doping of these elements can narrow the band gaps of metal oxides, enhance photocatalytic activity, and change the magnetic properties of materials. In addition, rare earth elements can increase the ionic conductivity of metal oxides, leading to performance improvements in applications such as fuel cells, sensors, and optoelectronic devices. Doping with rare earth elements can also increase the thermal stability and mechanical strength of materials, leading to the development of industrial and therapeutic applications (Mehtab et al., 2022; H. Xu et al., 2022; S. Zhao et al., 2021; Zheng et al., 2022).

Yıldız et al. studied a sensor that used zinc oxide (ZnO) nanoparticles doped with thulium (Tm) to detect dopamine with good sensitivity and selectivity. This sensor detected low dopamine concentrations accurately and proved its efficiency by providing high voltammetric signals (Yıldız et al., 2024). Mijajlovic et al. demonstrated that carbon paste electrodes modified with Eu_2O_3 and Cr_2O_3 nanoparticles are effective in the sensitive and efficient detection of L-DOPA. These electrodes provided low detection limits, outstanding repeatability, and excellent selectivity and sensitivity for detecting L-DOPA (Mijajlovic et al., 2023). In another study, a high-performance sensor for the detection of venlafaxine was developed using Europium-doped NiO nanocomposites. This sensor exhibited a broad dynamic range and accurately detected low venlafaxine concentrations, making it a good fit for prospective uses (Mohammadzadeh Jahani et al., 2021).

The potential of these elements to enhance significantly the electrical, optical and catalytic characteristics of metal oxides is the primary rationale for choosing Mn (manganese) and Ce (cerium) doping to CuO and SnO_2 compounds in this thesis. Although CuO and SnO_2 metal oxides have many uses in their pure form, doping is

often employed to enhance their capabilities. As a transition metal, Mn can change the electron transport properties and magnetic behavior of CuO and SnO_2. This can improve performance, especially for sensors and catalysts. On the other hand, Ce, a rare earth element, can increase photocatalytic activity and thermal stability by changing the oxidation-reduction (redox) properties of CuO and SnO_2. Moreover, the ability of Ce to narrow the energy band gaps and change the electronegativity of the materials can increase their efficiency in various applications. In this context, the effects of Mn and Ce doping on CuO and SnO_2 were selected to expand the properties of these compounds and optimize their performance.

2.7 Synthesis Methods of Nanoparticles

There are two types of approaches for nanoparticle synthesis: top-down and bottom-up. These two methods are essentially considered biological, chemical, and physical methods. Chemical and biological approaches are collectively called bottom-up approaches, while physical approaches are also known as top-down approaches. A biological approach is also known as "green systems of nanoparticles". Bottom-up synthesis entails creating nanomaterials of smaller sizes to produce the desired nanoparticle shapes. At the same time, top-down approaches focus on breaking down bulk nanomaterials to obtain the desired nanoparticle structures (hence top-down). These approaches are categorized into different types based on the method used (Negrescu et al., 2022.; Nam et al. 2019; Altammar 2023). The procedures outlined for each approach to NP synthesis are shown in Figure 2.12.

2.7.1 Top-down approaches

Nanoparticles are physically produced by mechanically breaking down a considerable metal framework using the top-down approach. It is a time-consuming, expensive, and energy-intensive process. The capacity to control NP morphologies and size distribution is its main advantage. The bulk counterpart is where the top-down method starts, which gradually leaches away bit by bit to produce fine NPs. For the mass manufacture of NPs, a variety of physical processes are used, including mechanical milling, photolithography, anodization, electron beam lithography, sputtering, and plasma and ion etching (O'Regan & Grätzel, 1991; Baig et al., 2021).

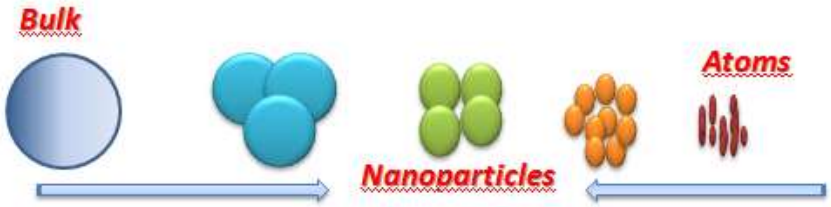

Figure 2.12 Symbolic representation of the many approaches used in nanoparticles creation (Wang, H., & Lu, J.; 2020)

The Mechanical Milling method involves obtaining nanoparticles by physically abrading a large block of material. Milling, grinding, and micronization techniques are used. While it has advantages such as high productivity and the capacity to process large quantities of material, it can be difficultto achieve complete control over particle sizes and requires significant energy consumption.

Another most commonly used top-down technique is lithography. In this method, high-energy laser beams vaporize the target material, which is then cooled and converted into nanoparticles. While this approach can provide very pure and uniform nanoparticles, its drawbacks include the need for expensive apparatus and unsuitability for industrial manufacturing (Namakka et al., 2023).

2.7.2 Bottom-up approaches

The bottom-up method involves assembling atoms and molecules to produce a range of NPs. This method uses physical, chemical, and biological processes (plant, biological products, microorganisms, etc.) to generate NPs. Among the bottom-up methods are chemical vapor deposition (CVD), self-assembly of monomer/polymer molecules, green synthesis, plasma or flame spraying synthesis, electrochemical or chemical nanostructural precipitation, and sol-gel processing (Altammar, 2023; Baig et al., 2021; Srinivasan & Rana, 2024).

In Chemical Vapor Deposition (CVD), reactive components in the gas phase undergo chemical reactions on the surface to form thin films or nanoparticles. The process permits the deposition of a wide range of materials while offering excellent purity and regulated growth. The major disadvantage of the method is that it requires high temperature and pressure and high-cost equipment. The electrospinning

technique draws a polymer solution into thin fibers under high voltage and uses these fibers to form nanoparticles or nanofibers. High surface area and a variety of nanomorphologies can be achieved, which is the primary benefit of the approach, but it requires high-cost equipment and process complexity (Namakka et al., 2023).

The synthesis of different materials and nanoparticles is a common use of the sol-gel process. This method provides energy efficiency and produces high purity products thanks to its ability to synthesize at low temperatures. The excellent manufacturing efficiency makes it possible to create intricately shaped optical components. In addition, it offers a homogenous composition with the chemical composition design and permits the production of homogeneous compounds in the form of compound oxides. Products having unique forms, such as fibers, aerogels, and surface coatings, can be produced using this approach. Amorphous materials can have altered physical features such as a low thermal expansion coefficient, low UV absorption, and high optical transparency by being synthesized and applied in thin layers. Furthermore, creating porous materials enhanced with organic and polymeric components is possible. Because the precursors have a high chemical reactivity, the procedures carried out in the solution phase enable fine control of the material structure. With the capacity to modify the variables at the beginning, these strategies yield high-quality goods with a cheap initial expenditure (Bokov et al., 2021; Thiagarajan et al., 2017).

2.7.2.1 Sol-gel Technique

One popular wet chemical procedure for creating nanomaterials is the sol-gel method. This method produces a variety of superior metal-oxide-based nanomaterials. The procedure is called the "sol-gel method" because, in the process of creating the metal-oxide nanoparticles, the liquid precursor becomes a sol, and the sol subsequently becomes a network structure called a gel (Danks et al., 2016).

The usual precursors utilized in the sol-gel method to produce nanomaterials are metal alkoxides. The sol-gel approach involves several steps in the production of nanoparticles. To make a sol, the metal oxide is first hydrolyzed in water or with alcohol. The next step is condensation, which causes the solvent to become more viscous and forms porous structures that are then allowed to age (Tseng et al., 2010).

Hydrolysis and condensation, two concomitant events required for forming a three-dimensional polymeric structure, can greatly affect the final product's quality. In hydrolysis, hydroxyl groups (OH) replace alkoxide groups (OR) (2.1).

$$M(OR)n + H_2O \rightarrow M(OR)_{n-1}(OH) + ROH \quad (2.1)$$

The M-O-M network is formed in condensation reactions

$$M(OR)_{n-1}(OH) + M(OR)_n \rightarrow (RO)_{n-1}M\text{-}O\text{-}M\ (OR)_{n-1} + ROH \quad (2.2)$$

$$M(OR)_{n-1}(OH) + M(OR)_{n-1}(OH) \rightarrow (RO)_{n-1}M\text{-}O\text{-}M(OR)_{n-1} + H_2O \quad (2.3)$$

Nucleophilic substitution is the process used in both alkoxylation (2.2) and oxolation (2.3). The production of hydroxo- (M–OH–M) or oxo– (M–O–M) bridges during the condensation or polycondensation process leads to the development of metal–hydroxo– or metal–oxo–polymer formation in solution. Polycondensation associated with aging leads to composition, properties, and porosity changes. Porosity decreases, and the distance between colloidal particles increases with age. The gel is dried after aging to eliminate any traces of organic solvents and water. The final stage in creating nanoparticles is the calcination process (Bokov et al., 2021; Parashar et al., 2020). Figure 2.13 depicts the nanostructures that can be produced with the sol-gel approach and their formation processes.

The final product obtained through the sol-gel process relies on a number of factors, such as the concentration of precursor, the nature of the precursors and solvent, pH, aging period, rate of hydrolysis, and molar ratio of the precursor to H_2O, pre and post-heat treatment of the materials, type of additives added and their concentration (Namakka et al. 2023; Shrividhya Thiagarajan, Sanmugam, and Vikraman 2017). Materials with a range of surface chemistry and microstructures can be created by varying these processing controls. Different ceramic materials can be produced by further processing of the "sol". Producing thin films on a substrate by spin or dip coating is simple. This will cause the "Sol" to become a wet "gel" when it is poured into the mold. The "gel" becomes even thicker glass or ceramic particles by drying and heating it.

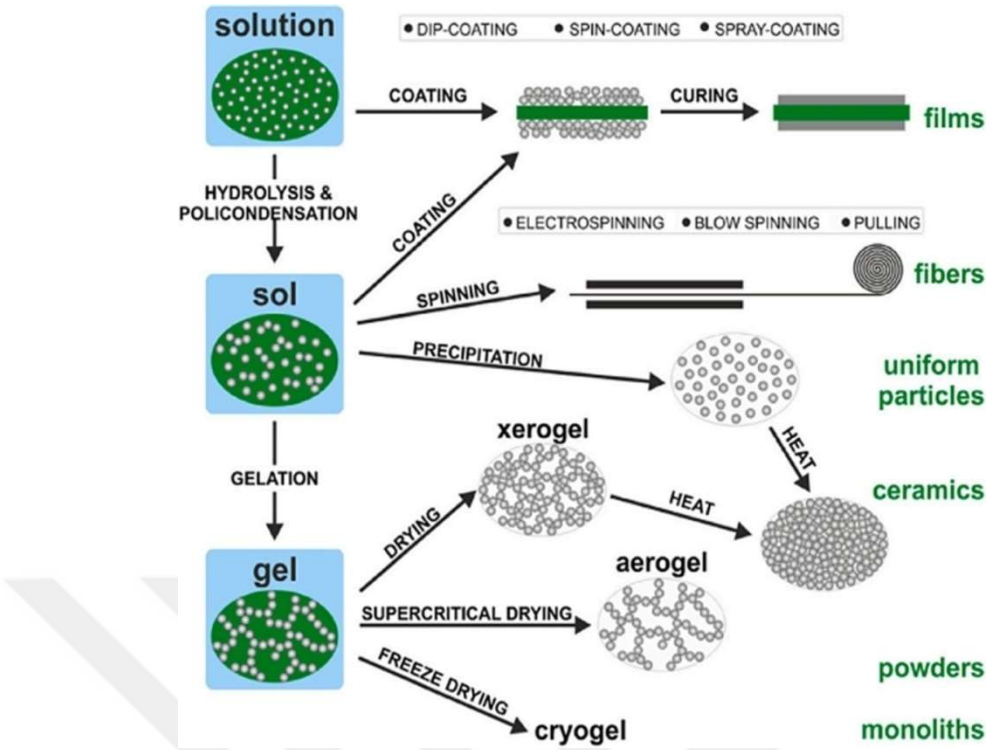

Figure 2.13 Steps in the sol-gel process from hydrolysis to the creation of gel via various routes and their respective product applications (Namakka et al., 2023)

The liquid in a wet "gel" can be extracted in supercritical states to create a very low-density, highly porous material called an "aerogel." There is evidence of silicate hydrolysis and condensation to generate polysilicate gels and particles in a variety of natural systems, including opals and agates (Bokov et al., 2021). The sol-gel method stands out with its simple process procedure and high purity product production capacity. Production efficiency is relativelyhigh and enables the production of optical components with complex geometry. In addition, it provides the ability to design and control the chemical composition in the homogeneous formation of compound oxides. Obtaining homogeneous compositions is possible by producing products with particularmorphologies like fibers and aerogels.

Additionally, it works well in synthesizing thin-layered amorphous materials and surface coating procedures. Creating materials with altered physical characteristics, such as a low thermal expansion coefficient, less UV absorption, and great optical transparency, is possible. Furthermore, organic and polymeric chemicals can create porous and rich materials. Because of the strong chemical reactivity of the precursors

and the early stage changeable tunability, processes performed in the solution phase allow for fine control of the material structure. Products produced with the sol-gel technique can be made as dense or porous materials in thin layers or powder form (Bokov et al., 2021).

2.8 Electrochemical Sensors, Types, Advantages, and Principles of Operation

2.8.1 Voltammetric Techniques

Voltammetry is an electroanalytical method built on the fundamental studies of oxidation, reduction, current-voltage, and concentration processes in various environments, using a polarized electrode called a working electrode. It is an analysis technique that evaluates the properties of current curves obtained from solutions of different concentrations of inorganic and organic substances that can be oxidized or reduced (Skoog, Holler, and Nieman, 1998).

The non-destructive method, electrochemical impedance spectroscopy (EIS), offers comprehensive details on the activities at the solid-liquid interface (charge and mass transfer, adsorption, charging of the double layer, etc.). In EIS studies, the AC sinusoidal signal is a small excitation signal applied to the electrode at a specified frequency. This signal measures the electrochemical cell's impedance (resistance and reactance). At the same time, this AC signal is held at a specified DC potential, i.e., a fixed direct current potential is applied on to the AC signal. This is done to simulate or study a specific electrochemical state of the cell (Figure 2.14).

The signal getting measured is an AC and phase angle (Barbezat, 1955). Impedance is the measurement of a circuit's resistance to electric current and can be calculated for various processes due to differences in time constant. The system is scanned over a wide frequency range to obtain the response of differenttime constants. The electrode/electrolyte interface and associated processes are modeled using an electrical equivalent circuit (EEC) consisting of resistors and capacitors. This provides information on the mass transport, kinetic, and electric/dielectric properties (Randviir & Banks, 2013).

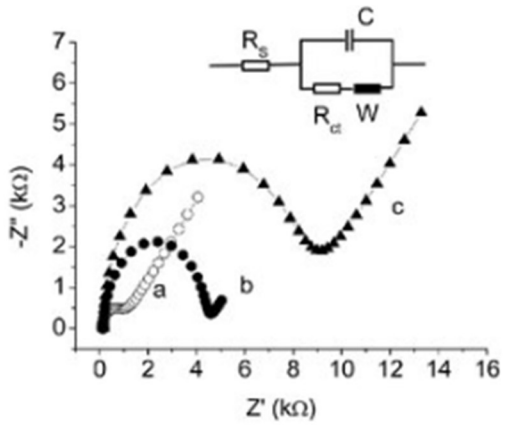

Figure 2.14 Electrochemical impedance spectroscopy schematic illustration (Jaskova, Pavlovicova, and Jurkovicova, 2014)

2.8.2 Square Wave Voltammetry (SWV)

A symmetrical square waveform is superimposed over a base staircase potential that is delivered to the working electrode in the square wave method, which is a broad amplitude differential technique. The measured current is sampled twice during each square wave cycle: once at the end of the forward pulse and once at the end of the reverse pulse. The difference between them is displayed against the base staircase potential. The reverse pulse causes the reverse reaction of the pulse because the square wave amplitude modulation is substantial. The resulting voltammogram exhibits symmetry (Figure 2.15). With a half-wave potential, the peak current is directly compared to the concentration. Due to the high sensitivity of this approach, the net current exceeds both the forward and reverse components. This approach is more sensitive than the differential pulse technique, which does not employ reverse current. The approach can detect analyte concentrations as low as 1 x 10^{-8} M. Compared to differential pulse voltammetry, square wave currents for reversible and irreversible processes are approximately 4 times more important than the differential pulse response. This approach offers a significant benefit in terms of speed (Electrochemistry, 2001a).

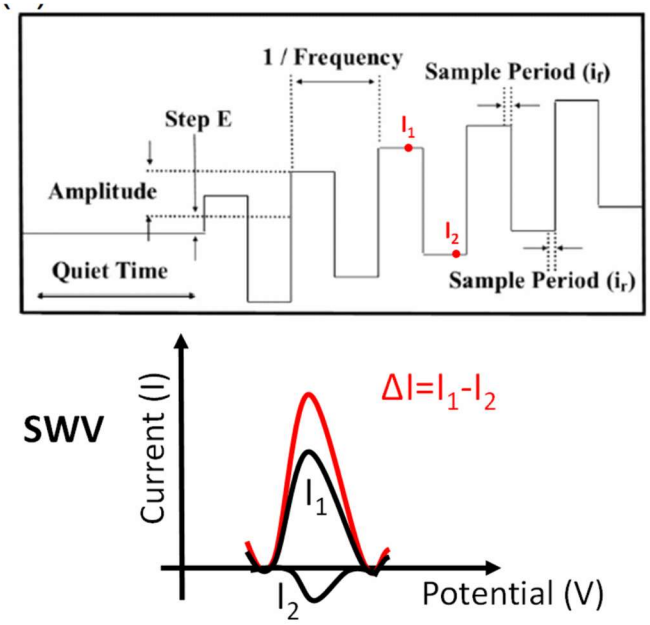

Figure 2.15 Square Wave Voltammetry schematic illustration (Mills, 2017).

2.8.3 Linear Sweep Voltammetry (LSV)

Linear sweep voltammetry is a standard method for examining the efficiency of mass transport and electron transfer in electrochemical systems (Figure 2.16) (Nicholson 1965;Albrecht et al. 2022). In linear sweep voltammetry, the potential is scanned at a constant scan rate between two values, E_1 and E_2:

$$E(t) = E_1 - v_s t \qquad \text{Eq 2.2}$$

Where v_s is the potential sweep's scan rate.

In the case of a reversible reaction, mass transfer in solution controls current behavior while the electron transfer rate exhibits a high magnitude. The concentration of O (oxidized form) and R (reduced form) close to the electrode is preserved in balance as the voltage is swept in a negative direction.

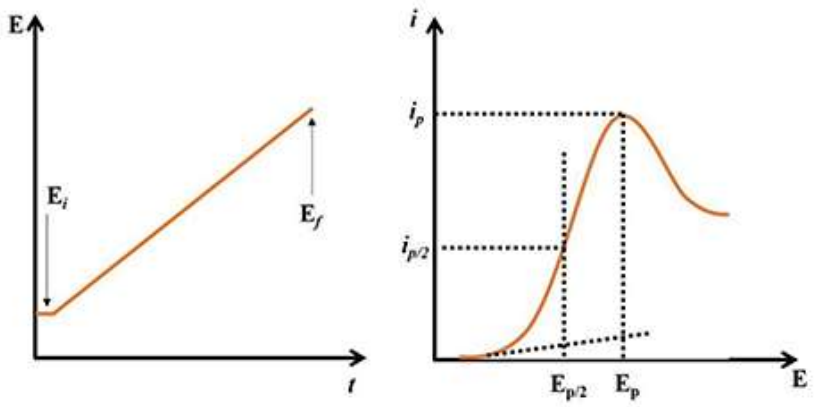

Figure 2.16 Linear sweep voltammogram staring at E_i and resulting i–E curve (Albrecht et al., 2022)

According to the Nernst equation, peak current I_p arises when new O flux cannot rapidly reach the electrode surface due to the diffusion layer's growing thickness. When the voltage approaches the oxidation-reduction point, the oxygen level on the electrode surface is considerably reduced. The reversible reaction's peak potential is constant.

$$\left|E_p - E_{\frac{p}{2}}\right| = 2.2\frac{RT}{F} \qquad \text{Eq 2.3}$$

The scan rate (v_s) and reactant concentration in solution both affect peak current (I_p):

$$|I_P| = 0.4463nAFC_{bulk}\left(\frac{nFvsD_A}{RT}\right)^{\frac{1}{2}} \qquad \text{Eq 2.4}$$

This equation, known as the Randles-Sevcik equation, is frequently utilized in research (Kissinger & Heineman, 1983). Peak current value and square root of scan rate change linearly as a function of each other. A thinner diffusion layer and a larger flow of species to the electrode surface are the results of the increased scan rate.

2.8.4 Cyclic Voltammetry (CV)

The CV approach is the most popular technique for gathering qualitative information about electrochemical processes (Figure 2.17). This method provides

information on the thermodynamics of redox processes, linked chemical reactions, adsorption processes, and the kinetics of heterogeneous electron-transfer events. The technique enables the rapid examination and calculation of the electroactive species' redox potentials. Additionally, it offers a practical approach to assessing the impact of the environment on the redox process. Using a triangle waveform, the technique applies a linear potential to a static working electrode in an undisturbed solution. The performed potential during a potential scan is what the potentiostat uses to measure the current. The measurement information is exhibited as a cyclic voltammogram, which plots the potential against current (Electrochemistry, 2001a).

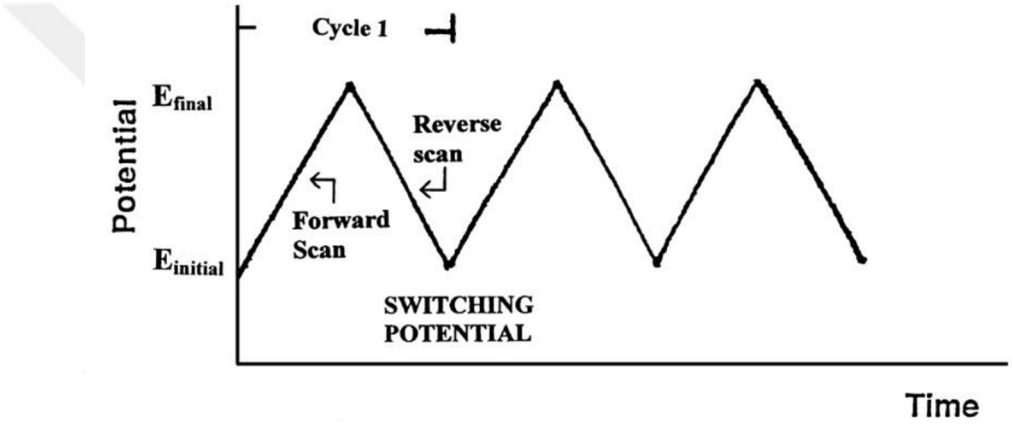

Figure 2.17 Cyclic voltammetry plotted with potential-versus-time (Albrecht et al., 2022)

Depending on the required data, one or more scans may be carried out during the tests. The cyclic voltammetric technique is shown in Figure 2.18. Because the CV rapidly and comprehensively offers information on redox processes and the kinetics of heterogeneous electron transfer reactions, it is the first experiment in an electroanalytical study (Electrochemistry, 2001a; Kissinger and Heineman, 1983). The potential cycling reveals the linked redox reactions' reversibility, showing whether a system is based on reversible, irreversible processes, or quasi-reversible (Ferrari et al., 2018). For an essential reversible couple, the ip anodic and ip cathodic values should be the same, signifying a rapid process. However, the reactions connected to the electrode process can impact the ratio between those values.

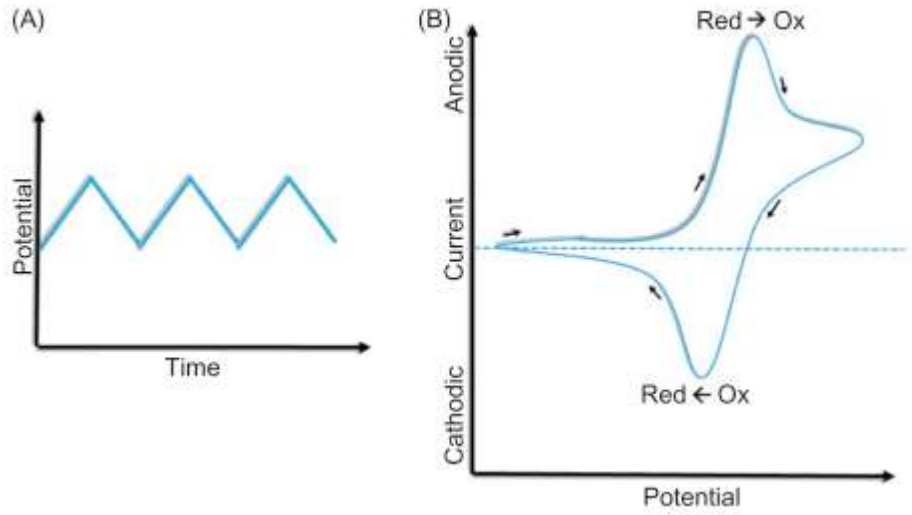

Figure 2.18 (a) Potential–time excitation signal in a CV experiment, and (b) a cyclic voltammogram for a reversible Ox+ne^-⇌Red reaction (Albrecht et al., 2022)

Further information can be extracted by measuring the formal potential of the redox process, called the peak potential (E_p) (Kissinger and Heineman, 1983). You may use voltammetric peak-to-peak analysis to determine whether a process is reversible. For a reversible process, the peak-to-peak spacing is 57 mV, independent of the scan rate. On the other hand, in electrochemical quasi-reversible or irreversible processes, the peak-to-peak separation is more extensive and is dependent on the scan rate for potential sweep (Kissinger and Heineman, 1983;Ferrari et al., 2018; Electrochemistry, 2001a). Furthermore, the individual peaks in this instance are smaller and farther apart. A shift in the E_p with the scan rate, which results from a sluggish electron exchange between the electroactive species and the WE, is a characteristic of completely irreversible systems (Kissinger and Heineman, 1983).

2.8.5 Pulse Voltammetry

The pulse voltammetry method was created to replace the linear scanning voltammetry due to its low sensitivity and slowness. This method was initially developed for the dripping mercury electrode and applied to other electrodes. An essential part of this procedure is measuring the current after the applied pulse.

Normal pulse voltammetry applies a sequence of pulses with increasing amplitude potentials at a predefined interval following the completion of each falling life. The electrode's surface is kept at a constant voltage between pulses. The analyte exhibits no response at this voltage. With every drop, the data show a linear amplitude increase (Figure 2.19). The charging current's contribution to the current measurement is essentially nonexistent forty minutes after the pulse was delivered. This technique yields a sigmoidal voltammogram with a limited current (Electrochemistry, 2001a).

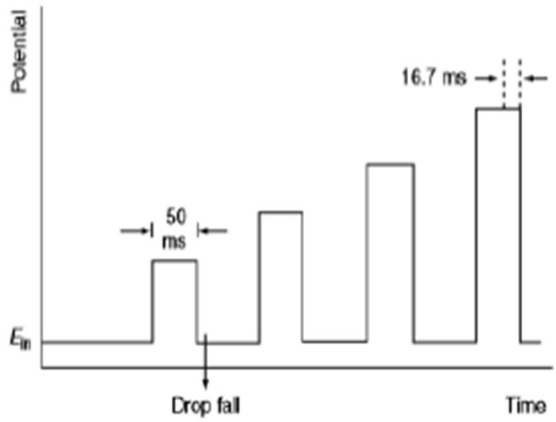

Figure 2.19 Excitation signal plot for normal pulse voltammetry (Albrecht et al., 2022)

2.8.6 Differential Pulse Voltammetry (DPV)

This technique is used to quantify minimal amounts of inorganic and organic compounds. The working electrode in the DPV approach receives a linear potential. This potential is applied just before a drop arrives on the electrode. This stage involves adding short-term pulses (pulse-shaped signals) during a linear increase or decrease in the potential. The current is measured at two distinct times during the application of a pulse: The instant the pulse is administered, the initial current sample is carried out. When the charging current starts to decline after the pulse is delivered, that is when the second current sample is carried out. The transitory current produced by the charges that build up on the electrode surface is known as the charging current, which gradually drops. On a graph (voltammogram), the net current, which results from calculating the difference between these two current samplings, is displayed as a function of voltage. The voltammogram plots the current against the applied potential

(Figure 2.20). This voltammogram is used to ascertain the substance's concentration and electrochemical characteristics. For DPV measurements, the concentration level is 10^{-8} M, or around 1 mgL^{-1}. Differential pulse measurements provide a distinctive peak-shaped response that makes it much easier to distinguish between two species with the same redox potential.

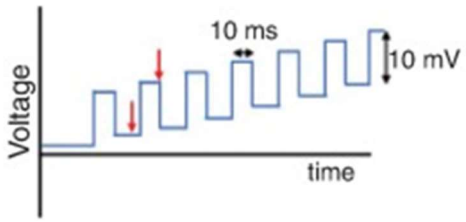

Figure 2.20 Illustration of applied potential versus time in Differential Pulse Voltammetry (Albrecht et al., 2022)

The observed peaks rely on both peak potentials and widths, and are spaced 50 mV apart. The stoichiometry of the electrons determines the peak's breadth. Irreversible redox reactions, which result in peak currents that are broader and lower than peak currents, are what define reversible systems. The DPV method details the analyte's chemical appearance, such as its oxidation states or complexion (Electrochemistry, 2001a).

2.9 Sensor Parameters

2.9.1 Sensitivity

Sensitivity, the ratio of change in the output signal to the input signal, is a critical sensor performance parameter. The slope of a sensor's response curve, which plots its output signal against its input signal, is another way to define sensitivity (Bănică, 2012; P. Li et al., 2017). Sensitivity refers to the slope of the current-versus-analyte concentrations curve in the context of electrochemical sensors. The wide surface area and widely accessible recognition sites for analyte-active site interaction are credited with the high sensitivity to analytes in 2D materials-based sensors. Introducing

recognition elements that successfully bind the target analytes is one of many methods used to increase sensitivity (Meng et al., 2019).

2.9.2 Limit of Detection

The limit of detection (LOD) or detection limit is another critical feature of sensor performance. It is the minimum analyte concentration that the sensor can detect, and it can be easily distinguished from the blank sample or baseline signal (Vig and Walls, 2000; Loock and Wentzell, 2012).

A blank sample indicates an absence of analyte in the sample's solution. The limit of detection (LOD) may be found using one of two methods: computed LOD or experimental LOD. Sensor response data at the analyte's lowest standard solution are used to calculate the experimental LOD. The formula for calculating LOD is $LOD = 3\sigma/s$, where σ is the blank sample's standard deviation, and s is the sample's sensitivity.

Sensitivity (s) is calculated by determining the slope of the response curve, which compares concentrations of the analyte to sensor response. As the LOD and sensitivity are interrelated, the LOD decreases and sensitivity increases. The LOD and sensitivity are interconnected, as the LOD decreases with increasing sensitivity. The sensitivity and LOD can be enhanced by the conductivity of the electrode materials, comprehensive coverage, availability of active sites, wide accessible surface area, and strong interactions between the analyte and the material (Püntener et al., 2004).

2.9.3 Linear Detection Range

A sensor's maximum and minimum measurable concentrations (LOD) are called the detection range, and the analyte concentration range corresponding to these values is known as the detection range. A wide detection range is ideal to meet the detection requirement. The detection range over which the sensor response is linear over a range of analyte concentration is known as the linear detection range (LDR). A fitted response curve's LDR is the region where the detection range is linear, and the correlation coefficient is $R^2 \geq 0.95$. A broad LDR is recommended to exceed the sensing requirements and calibrate a sensor. A wide LDR is crucial for determining

the range of concentrations at which a sensor can operate reliably and produce precise and accurate results. On the contrary, a non-linear sensor needs higher-order equations or mathematical manipulations to create a connection between analyte concentration and response. Significant measurement errors or sensor damage may result from an output value outside the detection range. Various LDRs can be obtained by considering appropriate electrode materials, analyte-material interaction, and accessible surface area (Meng et al., 2019).

2.9.4 Selectivity

The capacity of a sensor to distinguish between the target analytes and a range of possible interferents without experiencing any cross-interference is known as selectivity or specificity. The strength of the analytical signals from the target analytes is compared to that of the interferents to evaluate the selectivity of an analytical device. Furthermore, the selective detection of the target analytes over possible interferents is made possible by the application of recognition components in analytical equipment. In a similar vein, modifying experimental variables like temperature and pressure may help improve an analytical device's selectivity (Z. Meng et al., 2019). High selectivity in detecting a mixture of different analytes is always a desirable trait for sensors (Baranwal et al., 2022).

2.9.5 Stability

A sensor's stability is determined by its ability to consistently generate the same result for a given analyte concentration across time. The stability of a sensor may be verified by monitoring its reaction over time (Vig and Walls, 2000). Stability is essential for ongoing and routine measurements of environmental samples. A sensor should withstand high chemical, environmental, mechanical, or physical stress (Meng et al., 2019).

2.9.6 Repeatability

The ability of a sensor to yield the same result for the same analytes in two successive tests under reliable measurement settings is referred to as "repeatability" (Kalantar-Zadeh, 2013). Repeatability assesses a sensor's accuracy. The relative

standard deviation (RSD) of multiple measurements conducted with a sensor is typically used to determine repeatability. A low RSD indicates high repeatability of the sensor (Baranwal et al., 2022).

2.9.7 Reproducibility

The ability of a sensor to produce consistent output signals in different measurement scenarios is known as repeatability (Kalantar-Zadeh, 2013). A sensor's repeatability determines its quality, and this repeatability may be evaluated by determining the RSD of the output signals from several different sensor. In electrochemical sensor applications, RSD is an important statistical parameter used to assess the reliability and repeatability of a measurement series. RSD is calculated as the ratio of the standard deviation of the measured data to the mean expressed as a percentage and is defined by the formula (Ma et al., 2016);

$$RSD(\%) = \frac{\text{standard deviation (s)}}{\text{mean } (\overline{x})} x\ 100 \qquad \text{Eq 2.5}$$

In this formula, the standard deviation (s) represents the dispersion of the measured values around the mean, while the mean ($\bar{x}$) represents the overall trend of the measurements. RSD is used to understand the variability in measurement results when evaluating sensor performance. A low RSD indicates consistency of measurements and high repeatability of the sensor.

2.9.8 Recovery

The recovery is the ratio of analyte concentrations added to a test sample to its measured concentrations and evaluates the sensitivity of a sensor. The recovery rate is expressed as a percentage. The outstanding precision of a sensor is evidenced by achieving a recovery percentage close to 100% (Ma et al., 2016).

2.10 Electrodes

2.10.1 Reference Electrodes Used in Voltammetry

The steady and well-known potential of the reference electrode makes it a valuable point of reference for measurements and potential control in an electrochemical

system. The current passing through the reference electrode is kept at or close to zero (ideally zero) thanks to the high input impedance of the electrometer and the counter electrode's capacity to terminate the current circuit (Autolab Application Note EC08, 2011; Lomae et al., 2022). The reference electrode provides control over the working electrode's potential. A reference electrode should, in theory, have only a few features, such as (i) having the Nernst equation as its primary source of control for potential (should be electrochemically and chemically reversible), (ii) Potential should return to its previous value following a minor current flow and should remain constant when no current is flowing,(iii) The thermal coefficient of potential has to be low (Scholz, 2010).

According to their chemical connection to standard potential (E°), the most often used reference electrodes are as follows: Saturated Calomel Electrode (SCE) (2.4)

$$Hg_2Cl_2 + 2e \rightleftarrows 2Hg + 2Cl - \quad (E° = 0.268V \text{ vs. NHE}) \tag{2.4}$$

Silver/Silver chloride electrode (Ag/AgCl) (2.5)

$$AgCl + e^- \rightleftarrows Ag + Cl^- \quad (E° = 0.222V \text{ vs. NHE}) \tag{2.5}$$

Normal hydrogen electrode (NHE) (2.6)

$$2H^+ + 2e^- \rightleftarrows H_2 \quad (E° = 0.000V) \tag{2.6}$$

2.10.2 Auxiliary Electrode

In an electrochemical cell, the counter electrode, also known as the auxiliary electrode (source and sink of electrons), closes the current circuit but typically stays out of the electrochemical processes. To prevent restricting the kinetics of the reaction being studied, the total surface area of the counter electrode in an electrochemical responseshould be greater than that of the working electrode as current flows between the two electrodes. Ideally, the counter electrode comprises an inert material such as graphite, stainless steel, glassy carbon, Au, or Pt (Delahay & Mattax, 1954).

2.10.3 Working Electrodes Used in Voltammetry

The working electrode experiences reduction-oxidation reactions, charge transfer, and linear time-dependent voltage variations. Due to the wide variety of working electrodes and their suitability for modification processes, they can be used for numerous applications and paired with various materials.

The performance of the voltammetric method depends significantly on the material for the working electrode. It is crucial that the selected exhibit high signal-to-noise characteristics and deliver a consistent response. The materials used as working electrodes must be chosen based on how the target analyte behaves in a redox reaction and the background current seen over the potential range. The materials also have availability, toxicity, cost, mechanical properties, surface repeatability, electrical conductivity, and other qualities. The most commonly utilized working electrodes are carbon, nickel, gold, mercury, silver, copper, and platinum (Electrochemistry, 2001; Smith & Stevenson, 2007; Westbroek, 2005).

2.10.4 Mercury Based Electrodes

Mercury-based electrodes are typically the preferred electrodes in voltammetric experiments. Their smooth, highly repeatable, and readily renewable surface, together with their high hydrogen overvoltage that significantly expands the cathodic potential window, make them very desirable.

There are several varieties of mercury electrodes, including regularly used mercury film electrodes, hanging mercury drop electrodes (MFE), and dropping mercury electrodes (DME). These electrodes are specified based on the properties of the substance to be analyzed, the test settings, and the procedures. The DME device for electrocapillary research is the most frequently used in polarography. The HDME is mainly used for cyclic voltammetry and stripping analysis. The mercury electrodes' drawbacks include their toxicity and narrow anodic range (Electrochemistry, 2001; Smith & Stevenson, 2007; Westbroek, 2005).

2.10.5 Solid Electrodes

Solid electrodes can be categorized as platinum, gold, and carbon electrodes. Nickel, silver, and copper can also be used in various applications. Metal electrodes have excellent conductivity but are not frequently used due to their high cost compared to other solid electrodes. Due to their high conductivity, platinum electrodes are utilized in voltammetric measurements. The electrode has the disadvantage of quick oxidation, limiting its long-term use in analysis. The gold electrode is a highly conductive material and is less oxidized than the platinum electrode. Since reproducible results can be obtained in experiments, the gold electrode is preferred to a platinum electrode in voltammetric analysis.

The electrode's surface condition is a crucial consideration when employing solid electrodes. The major drawback of solid electrodes is that they need to produce a smooth, uniform surface for each new analysis. As a result, using such electrodes requires careful cleaning and polishing to get repeatable results (Electrochemistry, 2001; Smith & Stevenson, 2007; Westbroek, 2005).

2.10.6 Carbon Electrodes

Carbon electrodes are frequently employed in electroanalysis because of their rich surface chemistry, cheap cost, chemical inertness, low background noise, and appropriateness for sensing and detecting applications. Carbon electrode surfaces tend to exhibit slower electron transport rates than metal electrodes. Carbon electrodes are fundamentally made up of an aromatic ring with six members and sp^2 bonding. The densities of the edge and basal planes at the surfaces of these electrodes vary. Furthermore, carbon-based electrodes are also suitable for application in portable systems. Due to its natural conductivity, carbon can be easily modified in various systems, allowing it to be used as an electrode substrate. Specific analyses obtain outstanding reproducible results. Nowadays, carbon-based electrodes are the subject of numerous studies. The most common forms of carbon materials include carbon paste electrodes, glassy carbon, pencil electrodes, screen-printed carbon electrodes, carbon films, and carbon composites such as graphite-epoxy, wax-impregnated

graphite, and kelgraf, as shown in Figure 2.21 (Electrochemistry, 2001; Smith & Stevenson, 2007; Westbroek, 2005).

2.10.7 Glassy-Carbon Electrodes

The extraordinary mechanical and electrical properties, wide potential window, chemical inertness (solvent resistance), and typically reproducible performance of glassy (or "vitreous") carbon have made it more and more attractive. An inert environment simulates a polymeric resin body (phenol-formaldehyde) and then precisely manages the heating process to create the substance. To confirm that oxygen, nitrogen, and hydrogen are removed, the carbonization process is performed carefully over 300–1200°C. Glassy carbon comprises thin ribbons of cross-linked sheets that resemble graphite. No impregnating process is necessary due to its high density and small pore size.

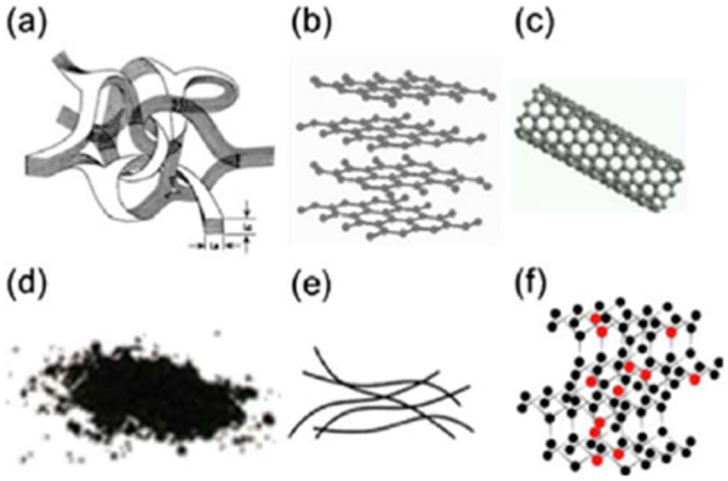

Figure 2.21 Structures of (a) glassy carbon, (b) graphite, (c) carbon nanotubes, (d)graphite powder, (e) carbon fibers, and (f) boron-doped diamond (Brett et al., 1994)

To create glassy-carbon electrodes that are both reproducible and active, as well as to enhance their analytical performance, surface pretreatment is usually necessary. To make a bright, "mirror-like" surface, this pretreatment is often accomplished by polishing with tiny alumina particles (down to 0.05 m) using a polishing clothThe electrode has to be cleaned with deionized water before use. The performance has also been improved by other activation techniques such as electrochemical, chemical, laser

heat, or laser treatments. The enhanced electron-transfer reactivity (which functions as an interfacial surface mediator) has been attributed to the removal of surface contaminants, the exposure of new carbon edges, and an increase in the density of surface oxygen groups (Electrochemistry, 2001b).

2.10.8 Carbon-Fiber Electrodes

The widespread usage of carbon fibers in electroanalysis results from the rising interest in ultramicroelectrodes. These materials are produced via catalytic chemical vapor depositionor by polymer textiles' high-temperature pyrolysis, primarily used in creating high-strength composites. Different carbon fiber microstructures are available based on the manufacturing technique. Three general categories may be used to classify them: low-, medium-, and high-modulus types. The final variety has a low porosity and a well-ordered structure similar to graphite, making it the most appropriate for electrochemical research. Different electrode pretreatments, notably weak and high electrochemical activations or heat treatment, can improve electron transfer performance. Most electroanalytical applications depend on fibers with the requisite radial diffusion and a 5 to 20 μm diameter. These fibers are commonly employed in cylindrical or disk forms and mounted with epoxy adhesive at the tip of a drawn glass capillary. Taking precautions to prevent the epoxy from contaminating the carbon surface is essential. The primary advantage of carbon-fiber working electrodes is their small size (5–30 μm diameter for commercial productfibers). This characteristic makes them especially useful for anodic measurements in various microenvironments, like the extracellular brain region where neurotransmitter release is observed. It is possible to create nanometer-sized carbon fibers by etching them in a flame or under an ion beam (Electrochemistry, 2001b).

2.10.9 Screen Printed Electrodes

Screen-printed electrodes are produced from inks containing carbon, silver, platinum, gold, or carbon nanotubes. Novel strips are made for environmental, agricultural, and medicinal electrochemical analysis. Rapid, simple, cheap, and disposable biosensors in industries like environmental, clinical, and industrial analysis have gained popularity in recent years. The disposable biosensors created with thick-

film technology are the most popular. A thick-film biosensor setup typically consists of layers of specific inks (or pastes) that are successively deposited onto an insulating support or substrate (Figure 2.22). Screen printing, one of the oldest techniques of graphic art reproduction, is a crucial characteristic that identifies a thick-film technique. Due to benefits such as miniaturization, adaptability, low cost, and, notably, the ability to mass produce, screen printing is one of the most important candidates for enabling the large-scale introduction of biosensors soon. The development of sensors and biosensors using thick-film technology is a new field. The sensing or active membrane and its adherence to the transducer layer are the most crucial components in producing thick-film biosensors (Albareda-Sirvent, Merkoçi, and Alegret, 2000).

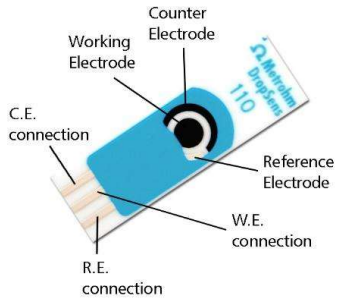

Figure 2.22 Screen-printed electrode (Albrecht et al., 2022)

2.10.10 Carbon Paste Electrodes

Adams first developed carbon paste electrodes (CPE) in 1958, and the uses for this type of electrode have greatly expanded throughout the years. At first, it was created by mixing mineral oil and graphite powder, but the number of heterogeneous electrodes significantly increased over time. The simplicity of preparing carbon pastes, the ability to renew the electrode surface, the adaptability for adding new additives to the paste, and the extremely low costs of fundamental materials (mineral oil and carbon powder) to make CPE are the key strengths of this spectacular expansion. Nowadays, studies using unmodified paste electrodes are less common. This is mainlybecause scientists now have access to various modifications that can enhance the CPE signal. Many studies published in recent years have focused on the use of CPE in the electroanalysis of organic molecules (Sawkar et al., 2022; Stojanović et al., 2023; Svancara et al., 2001; Xin et al., 2020).

2.11 Modified Electrodes

The development of electrochemical sensors based on electrodes modified with nanostructured materials has garnered much attention in recent years. These sensors offer significant advantages such as simple operating procedures, long-term physical and chemical stability, low energy consumption, economical cost, compact design, and high sensitivity and selectivity. Modifying the electrode surface with nanomaterials not only expands the active surface area but also selectively lowers the potential of target redox reactions, increasing the sensitivity and selectivity of the analyses. Significant advancements in developing sensors and biosensors based on electrodes modified with metal oxides have occurred within the past 20 years (Sabbaghan et al., 2021). In recent years, solid electrodes in electrochemistry have grown significantly and found numerous applications. Since the surfaces of solid electrodes may be altered, they are preferred to mercury electrodes. Undesirable events and reactions on a solid electrode surface can be prevented by surface modification, or some reactions can occur (Murray, 1983). Chemically modified electrodes (CMEs) are utilized in various electrochemical processes, including sensing, energy conversion, optics, and electronics. The most popular techniques for altering electrode materials include creating a modifier layer via covalent attachment or adsorption, which endows the underlying electrode surface with desired properties (Durst et al., 1997). Various techniques are utilizedto chemically alterelectrode surfaces, including:

Chemisorption: The adsorption mechanism on the electrode surface is the foundation for these modifications. Using this technique, monolayers can self-assemble.

Covalent bonding: To establish a strong connection, organosilane is bonded to the electrode surface. These modifications can be made using the electrografting technique. These covalently bound silane molecules can then be employed as a binder to form a thin film containing solid adhesion modifiers with the required characteristics in the following stage. Composite: A chemical modification directly modifies the electrode matrix to give it the appropriate properties. For instance, modified carbon paste electrodes use a modifier, graphite, and binder to produce the electrode.

Polymer films: Electrode surfaces are covered with coatings of organic, inorganic, or organometallic polymers that are deposited via chemical or physical adhesion. There are two types of polymer films: conductive and non-conductive. Chemical modifiers may already be present when they are deposited onto the surface of an electrode, or they may subsequently be acquired through a procedure known as functionalization (Durst et al., 1997). Polymer films can be produced by electrochemical deposition, spin coating, polymerization, and dip coating with a film thickness of 0.1 to 10 nm (Murray, 1983).

In recent years, the topic of modifying electrode surfaces for electroanalytical applications has gained attention. Improving control over the behavior of the electrode surface and resolving various electroanalytical issues associated with unmodified surfaces has opened up new routes in the sensing field. Many electrochemical sensing applications offer much easier ways to increase sensitivity, reproducibility, stability, and selectivity. Preconcentration, or selecting the kind of modification such that the target analyte and modifier combine to produce a more incredible analytical result, improves selectivity and sensitivity (Uslu & Ozkan, 2007).

The electrode modification aims to achieve several goals, such as mass transit of species control, selective permeation and exclusion capabilities, efficient electron transfer, and possible chemical reactions to improve the electrochemical response (Electrochemistry, 2001b). The redesigned electrode should be robust, easy to use, and provide a repeatable, sensitive analytical result for voltammetric sensing (Stradiotto et al., 2003). Essential elements that may affect how successful electrode modification is in terms of sensitivity and selectivity include the shape of the electrode, the modifier's content, and the quantity of surface covered by films. The modifiers' chemical characteristics and composition can impair the target analyte's sensitivity and selectivity. Organic ligands, ion exchangers, clays, zeolites, silicon-based materials, and nanoparticles can all be used to modify electrodes (Murray et al., 1987; Navrátilová & Kula, 2003).

2.12 Previous Work and Motivation of Research

Chronic obstructive pulmonary disease (COPD) and asthma are typically treated with salbutamol (SAL), which is a bronchodilator and belongs to the ß2-adrenergic agonist class (D. Chen et al., 2016). SAL is also widely used in veterinary medicine due to its ability to relax smooth muscles and lower systemic vascular resistance (Blanca et al., 2005; (Bourdillon et al., 1980). Athletes may be tempted to use SAL illegally to enhance strength and muscle growth, as it can yield anabolic-like effects when consumed in high quantities. A SAL concentration in urine of more than 1000 ng/mL (about 3 M), according to the World Anti-Doping Agency (WADA), is direct evidence of doping activity (Ventura et al. 2009; Karuwan et al. 2009). The most popular ß2-agonist for promoting growth in animal feed is SAL, which also enhances the transformation of nutritious body fat into greater muscle mass (M. Y. Wang et al. 2016; Blanca et al. 2005). Nevertheless, SAL used to stimulate development may readily build up in animal tissues and organs, which might have an adverse effect on humans by passing through the food chain and being consumed in the form of animal products. This can lead to serious health effects, including various symptoms such as palpitations, tremors, and nervousness (Guo et al., 2017). Most nations, notably China and the European Union, forbid using SAL as a growth booster (Lian et al., 2017).

Therefore, developing an analytical method and tool that can accurately and sensitively determine SAL for rapid identification and verification in controlling growth promotion and sports doping is crucial. Various analytical techniques, including spectrophotometry, gas chromatography, capillary electrophoresis, potentiometry, high-performance liquid chromatography (HPLC), and flow injection analysis, have been described to detect SAL in biological samples or pharmaceutical formulations in recent times (Lomae et al., 2022). According to Dol and Knochen, they conducted research on the determination of salbutamol using flow injection spectrophotometric methods with 4-aminoantipyrine. Using a sequential one-way procedure, they optimized the values of four variables: two reactor lengths and two reactant concentrations.

After the method was validated, it was compared with a High- Precision Liquid Chromatography (HPLC) method specified by the United States Pharmacopoeia

(USP). The method's linearity extends from 0 to 74.1 mg/L for salbutamol sulfate, ensuring accurate and reliable results ($R^2 = 0.9999$). The outcomes demonstrated that the technique may be used forstandard laboratory testing without costly and time-consuming processes like HPLC (Dol & Knochen, 2004). Basavaiah et al. used N-bromosuccinimide (NBS) and two dyes, methylene blue and rhodamine-B, to present a straightforward, sensitive, and quick titrimetric and two spectrophotometric techniques for the detection of salbutamol sulfate (SBS). The quantity that reacted with NBS matches the concentration of SBS. The reaction stoichiometry is 1:6 (SBS), and the titrimetric technique is suitable in the range 1.74×10^{-4} - 8.68×10^{-4} mol L^{-1}. The absorbance was observed to rise linearly with SBS concentration in spectrophotometric techniques; correlation values of 0.9993 and 0.9988 for method A and method B, respectively, supported this finding (Basavaiah et al., 2007). Bernal et al. compared HPLC and Scanning Flow Cell (SFC) methods for determining salbutamol sulfateand its impurities in pharmaceuticals. This study proved that the HPLC method is more flexible than the supercritical fluid chromatography (SFC) method in analyzing tablets and cough syrups. When using the SFC method, the excipient made it difficult to identify and quantify various chemicals in cough syrup samples (Bernal et al., 2006). Chen et al. devised a method utilizing non-contact conductivity detection and capillary electrophoresis to identify the presence of salbutamol sulfate in medications. Several significant factors were examined, including pH, separation voltage, injection time of the sample, aqueous and non-aqueous solvents, basic electrolytes and their concentrations, and excitation voltage and frequency. The mass concentration of salbutamol sulfate and the peak area response were linearly related ($R^2 = 0.995$) in the 9.60 to 48.0 mg/L range. The detection limits (S/N = 3) were 1.92 mg/L (C. Chen et al., 2011). A flow-injection device for the flow-channel electrochemical detection of salbutamol has been developed by Karuwan et al. The system comprises the electrochemical electrodes on a glass substrate and the PDMS (polydimethylsiloxane) microchannel. Following SU-8 molding, casting, and chemical nanomaterials (CNTs) fabrication, PDMS microchannels were constructed on the glass substrate using oxygen plasma treatment. Flow injection and ECD of SAL were carried out for in-channel detection using the amperometric detection mode. Evaluations were conducted on analytical

characteristics, sensitivity, reproducibility, and dynamic range. Their results showed that the CNTs electrode showed high consistency for amperometric detection and strong stability in a flowing environment (Karuwan et al., 2009). Although these methods are sensitive and efficient, they have drawbacks such as lengthy processes, complex procedures, expensive instrumentation, and difficulty to be used for in situ applications or rapid screening tests (Lomae et al., 2022). On the other hand, electrochemical techniques are sensitive, accurate, simple, rapid, inexpensive, and useful for the identification and detection of SAL. The sensitivity of electrochemical analysis may be influenced by the interaction of the analyte with the bare electrode. As a result, creating a sensitive modified electrode is crucial for using electroanalytical methods to identify pharmaceutical samples that contain SAL (Toghan, Am, and Hm 2019; Yinfeng Li et al. 2014). Studies concentrating on the electrochemical approaches of Salbutamol determination have increased in the last several years (Pinar et al., 2018; Thanh Nhi et al., 2024; Toghan, Abo-Bakr, et al., 2019). Toghan and colleagues conducted measurements for SAL determination by cyclic and differential pulse voltammetry on graphene oxide and polymer-modified glass surface carbon electrodes using electrochemical techniques. An analysis of the impacts of SAL concentration, pH, and scan rate revealed a considerable shift in the acidic peak current. Apart from ascorbic acid and p-nitrophenol, there was no other interference in the detection of SAL. The limits of detection and quantification were defined at 56 and 188 nM, respectively. Furthermore, a RSD of 6.2% was computed based on six parallel determinations of 89.55 μM SAL in GO/poly(O-NBA)/GCE in PBS (pH = 7.6) to verify the reproducibility of the data (Toghan, Am, et al., 2019). To build an electrochemical sensor for salbutamol based on MIP, Dechtrirat et al. studied the co-electropolymerization of amino-phenylboronic acid and o-phenylenediamine in the presence of the template molecule. This MIP layer was constructed on top of the screen-printed carbon electrode SPCE and modified with graphene/PEDOT: PSS. Here, the sensor's sensitivity was raised using the graphene nano-composite to enhance current responsiveness. Additionally, the sensor demonstrated outstanding selectivity, extraordinary repeatability, and exceptional stability. Reusability might be achieved without significantly losing electrochemical responsiveness with at least ten additional measurements. The recommended sensor showed good recovery results for sample

analysis without necessitating time-consuming and arduous preparation procedures (Dechtrirat et al., 2018). Nagle et al. suggested using a nanoporous gold (NPG) electrochemical sensor, which can provide a unique fingerprint signal from inhalable drugs, to study the electrooxidation of salbutamol, the primary bronchodilator in Ventolin^{TM} formulations. Salbutamol was detected amperometrically and different from the chloride excipient at 0.0154 M using NPG-modified microdisc electrode arrays. Bare gold microdisk electrode arrays cannot afford to make this difference because of the overlap in the potential for salbutamol oxidation and chloride adsorption processes. The nanoconfinement effect is the source of NPG's discriminative ability. The nanoconfinement effect for chloride in its interior pores, which positively affects the electron transfer kinetics of this slower process compared to the quicker, diffusion-controlled oxidation of salbutamol, gives NPG its capacity to differentiate between distinct compounds. Pt was employed as a quasi-reference electrode while sensing at a completely integrated three-electrode cell-on-chip (Nagle et al., 2021). An electrochemical sensor incorporating an immunoassay was created by Han et al. to quantify salbutamol precisely. Polyamide amine-Au nanoparticle (PMA-Au) nanocomposites and horseradish oxidase-graphene antibodies (HRP-G-Abs) were used to boost the signal. While PMA-Au was utilized to stabilize the biomolecules' immobilization, graphene was utilized to increase the amount of HRP that was loaded. A competitive immune method was used to construct electrochemical sensors. Additionally, salbutamol was successfully detected in actual samples using the proposed immunosensor (Han, 2020).

Apart from the research mentioned above, most techniques in the literature necessitate diverse derivatization phases and efficient extraction, purification, or amalgamation of diverse detection techniques before the ultimate examination. These methods are time-consuming, expensive, and dependent on sophisticated equipment. Furthermore, specifictechniques might not have enough selectivity or detection limitations. Due to its benefits, which include cheap cost, ease of use, low background current, broad potential range, high sensitivity and selectivity, accuracy and speed, sensitivity, and quick surface renewal, electrochemical techniques are a helpfulsubstitute for other approaches. Despite these benefits, a more effective technique for high-sensitivity and selectivity SAL identification must still be

developed. Because of its excellent signal-to-noise ratio, simplicity, adaptability, and high sensitivity, the voltammetric methodology has been acknowledged as the most often employed electrochemical analytical method in several research. When a voltage is provided, voltammetric sensors function as working electrodes, gather information on redox activities in the solution, and produce voltammograms that depict the redox reactions associated with the chosen electroactive chemical (Koc Delice et al., 2024).

Various sensing and detecting applications can benefit from the high aspect ratio and specific surface area of carbon electrodes, as well as their chemical stability, chemical inertness, low background current, cheap manufacturing cost, ease of customization based on target analyte, and affordability. Among carbon electrodes, carbon paste electrodes (CPEs) are exceptional due to their distinct chemical stability, ease of preparation and speed, affordability, adaptability in combining different materials during paste preparation, porous surface, shallow background current (in contrast to graphite electrodes), high specific surface area, and high aspect ratio. They are becoming increasingly significant because CPEs may be employed at both positive and negative potentials, depending on the electrolytes used. Furthermore, altering an electrode to create a novel, high-quality sensor with the required characteristics is easy (Ben Brahim et al., 2023; Svancara et al., 2001). Despite all these favorable properties, bare CPEs can be susceptible to electrode difficulties, electrode contamination, and problems related to discontinuous electron transfer reactions. For these reasons, modifying electrodes with chemicals to achieve desired properties has attracted significant attention. In recent years, many studies have been published on electrode modification to increase the speed, selectivity, and sensitivity of electrochemical determinations (Tiwari et al., 2012; C. Y. Wang et al., 2000).

Due to their exceptional qualities, including their small size and outstanding optical, magnetic, and mechanical capabilities, nanoparticles, fullerenes, and carbon nanotubes are employed in biomedical and sensing applications. It has been demonstrated that electrodes enhanced with nanoparticles speed up electrochemical reactions, resulting in larger peak current and lower positive oxidation potential (F. Meng et al., 2017; Sivanesan & Abraham John, 2009; Yao, 2019). Metal oxides are very advantageous due to their low cost and structural stability, which have led to a wide range of

applications in the chemical, catalytic, and technical sectors. Metal oxides have recently distinguished themselves from other semiconductor materials due to their catalytic capabilities for sensing and biosensor applications. Metal oxide nanostructures have demonstrated desirable traits such as efficient biocompatibility, non-toxicity, and catalytic activity due to their excellent performance capabilities and huge specific surface area. Furthermore, these nanostructured materials are suited for microenvironments due to their improved electron transfer kinetics and excellent adsorption capacity. The controlled synthesis of metal oxides could be used to enhance biosensing physiologies.

Numerous transition series metal oxides, including ZnO, TiO_2, Fe_2O_3, and Mn_2O_3, are employed in investigations on the detection of SAL using electrochemical sensors to enhance sensor characteristics (Koc Delice et al., 2024). Based on our literature research, it's evident that, unlike other metal oxides in the transition series, there exists a notable absence of comparative studies on the synthesis, characterization, and electrochemical performance techniques utilized for CuO and SnO_2 nanoparticles. P-type semiconductors, such as copper oxide (CuO), have exceptional features such as high conductivity, good stability, vigorous catalytic activity, and an effective electrode in photovoltaics. Its 1.2 eV small band gap is another feature. CuO has a wide range of applications in gas sensors, field effect transistors, semiconductors, catalysts, and biosensors due to its unique features (Abutaleb & Imran, 2021; Jang et al., 2016). SnO_2 is unquestionably another well-known metal oxide nanostructure. SnO_2 is a well-known n-type metal oxide semiconductor that has a high carrier concentration, a broad optical band gap spanning 3.6 to 4.0 eV, and good transmittance in the visible range. With a comprehensive band gap energy of 3.67 eV, SnO_2 thin films are extremely conductive and transparent in the visible spectrum. They have been an auspicious material for spin tronics devices because of their great optical transparency and electrical conductivity. SnO_2 is one of the most effective semiconductors utilized in various applications, including transparent conductive electrodes, solar cells, biosensors, gas sensors, and transparent conductive electrodes (H. Xu et al., 2022).

Numerous research works described the production of SnO_2 and CuO nanoparticles using physical, chemical, and biological methods, including solvothermal (Karan et

al., 2016), microwave irradiation (Ponnar et al., 2018a), co-precipitation (Hilary et al., 2015), laser ablation (Khashan et al., 2018) and sol-gel method (Mohammed et al., 2018). The sol-gel technique is an interesting synthesis since it is cost-effective and environmentally friendly. Furthermore, by adjusting several parameters, including the pH level, precursor concentrations, and reaction temperature, this method can control the shape and particle size of nanoparticles produced. Furthermore, doping in the sol-gel process enables the modification of several material characteristics. Within the scope of the thesis, Mn and Ce doped CuO, and SnO_2 nanostructures were used to modify CPE to detect SAL. Manganese (Mn) possesses chemical and physical qualities that set it apart from other transition metals in electrochemical sensor applications, which is why it was chosen as a doping elment. There are many oxidation states for manganese (Mn), such as Mn^{2+}, Mn^{3+}, Mn^{4+}, and Mn^{7+}. These multiple oxidation states allow Mn to operate over a wide range of redox potentials, which offers the advantage of detecting various target molecules in electrochemical sensors. Mn exhibits high catalytic activity in electrochemical reactions, increasing sensors' sensitivity and reaction rate. Furthermore, Mn and its components are resistant to various environmental conditions and support long-term, reliable operation of sensors. Mn frequently exhibits excellent performance in electrochemical sensors and is crucial for detecting biomolecules like hydrogen peroxide and glucose. Mn-based sensors have numerous applications, including water quality monitoring, gas detection, environmental sensors, and biosensors. Furthermore, Mn-based materials offer good electron transfer and conductivity properties, which increases the speed and efficiency of sensors. For these reasons, Mn offers many advantages over other transition metals in electrochemical sensor applications and has a wide range of applications. Sabbaghan et al. found that sensors made using Mn doped ZnS nanoparticles successfully detect is oprenaline. In this study, the 10 wt% Mn-doped ZnS sensor showed a high signal strength against isoprenaline, with a signal of approximately 3.5 µA at a concentration of 1 µM. According to reports, the sensor's detection limit is 0.5 µM (Sabbaghan et al., 2021). Shukla et al. developed glucose biosensors using Mn-doped ZnO nanoparticles. Mn doped ZnO sensors demonstrated strong signals while detecting glucose. Specifically, at a glucose concentration of 0.5 µM, a current response of around 2.8 µA was recorded, and the sensor's detection limit was found to be 0.1 µM

(Shukla et al., 2018). Al Fatease et al. demonstrated that sensors developed with Mn-doped TiO_2 nanoparticles provide high performance for myoglobin detection. Despite this sensor's incredible sensitivity and selectivity for myoglobin detection, at 0.5 μM myoglobin concentration, a signal intensity of around 4.2 μA was achieved. The sensor's detection limit was reported to be 0.2 μM (Al Fatease et al., 2021).

Another contributing element is the rare earth element cerium (Ce) in the +3 and +4 oxidation states. Its several oxidation states benefit from detecting different analytes and enable it to function over a broad range of redox potentials. Cerium exhibits high catalytic activity, accelerating chemical reactions and increasing electrochemical sensors' reaction rate and efficiency. Highly chemically stable, cerium and its components ensure long life and reliable performance of sensors in harsh environmental conditions. Ce offers good electron transfer and conductivity properties, increasing the speed and sensitivity of sensors. Furthermore, its high surface reactivity and good adsorption ability enable efficient detection of analytes in gas and liquid phases. Cerium is a versatile and flexible material with many uses, including biosensors, environmental sensors, and water quality monitoring. Because cerium is abundant in nature and economical compared to rare earth elements, cerium-based sensors offer cost-effective solutions. Furthermore, Ce and its components generally have low toxicity, ensuring safe use in biosensors and medical applications. In Matt et al., cerium-doped zirconia nanoparticles were used to modify a carbon paste electrode for dopamine detection. The study showed that electrodes modified with 0.8 wt% Ce-doped zirconia nanoparticles provided a signal strength of 5.0 μA at 1 μM dopamine detection and offered high selectivity and sensitivity (Bullapura Matt et al., 2019). Dar et al. realized the detection of various hazardous chemicals using Ce-doped ZnO nanorods. These sensors showed high sensitivity with a signal strength of 2.3 μA at 0.5 μM level, enabling the effective detection of hazardous chemicals (Dar et al., 2012). Muthukumaran et al. used Ce-doped nickel oxide nanostructures for riboflavin and antibacterial applications. For riboflavin detection, 2 wt% Ce doped nickel oxide nanostructures were used to achieve a signal strength of 3.2 μA at a riboflavin concentration of 10 nM. These sensors provided high sensitivity and reliability in riboflavin detection (Muthukumaran et al., 2016). Consequently, these advantages of cerium make it stand out among other rare earth metals in electrochemical sensor

applications. Their properties include high oxygen storage capacity, catalytic activity, and chemical stability, and multiple oxidation states make Ce-based sensors more sensitive, reliable, and versatile.

The scientific investigations and methodologies used to detect salbutamol have been thoroughly evaluated. Based on the literature review, electrochemical detection was preferred in biosensor applications in this thesis due to its ease of use, cost-effectiveness, excellent sensor properties, and potential for widespread use. Furthermore, this thesis highlights undoped and doped metal oxide nanostructures' production, characterization, and properties. These nanostructures offer unique potential as candidate materials for sensor development.

The use of Ventolin for the detection of Salbutamol (SAL) offers a practical approach, mainly because this drug is available over the counter. Ventolin is a widely used medication for treating asthma and other respiratory diseases and is easily accessible to patients as it is available overthecounter. Ventolin is also a commercial formulation of salbutamol and is therefore used as a standard reference material in SAL assays. In addition to serving as a control and comparison tool to increase the accuracy of the analytical results, Ventolin usage offers a dependable foundation for detecting SAL. In the literature, specific studies on salbutamol detection using Ventolin are known to be limited. Most existing studies have focused on detecting SAL directly or with other formulations, and specific studies investigating commercial preparations such as Ventolin in this context still need to be included. Therefore, using Ventolin as a method for SAL detection could fill the gaps in the literature and offer a potential solution in practical applications.

The motivation for this thesis study is that CuO and SnO_2 nanostructures are potential candidate materials for use in electrochemical sensor applications. However, there is currently no comprehensive study in the literature on sensor performance related to the determination of SAL analyte, explicitly examining the contribution of Mn and Ce elements to these nanostructures.

CHAPTER THREE
EXPERIMENTAL PROCEDURES

In this study, the electrochemical detection of SAL analyte with metal oxide was used to modify the carbon paste electrode (CPE). In this context, metal oxide CuO and SnO_2 nanoparticles were initially synthesized via the sol-gel method, and the resulting nanoparticles modified the CPE electrode. Transition and rare earth elements were doped into metal oxide structures to investigate the electrochemical performance of CPE.

Carbon paste electrodes were prepared using graphite powder and binders. Modified CPEs were prepared by adding synthesized nanoparticles. The prepared pastes were placed in glass tubes to form electrodes, which were ready for use in electrochemical measurements.

The synthesized nanoparticles were characterized using a variety of methods, including Fourier transform infrared spectroscopy (FTIR), X-ray photoelectron spectroscopy (XPS), dynamic light scattering (DLS), scanning electron microscopy (SEM), and X-ray diffraction (XRD).. These methods evaluated the nanoparticles' morphology, size distribution, and chemical composition. Electrolytes and analyses were prepared using SAL solution and supporting electrolytes. Prepared solutions were analyzed by voltammetric techniques using modified CPEs. Electrochemical characterization was performed using cyclic voltammetry (CV) and differential pulse voltammetry (DPV) techniques. These techniques were used to determine the sensitivity, selectivity, and reproducibility of electrodes to determine SAL.

This study assessed the effectiveness of CPEs modified with CuO and SnO_2 nanoparticles, with or without Ce and Mn doping, in detecting SAL. It also included results on how these electrodes affect crucial sensor parameters like sensitivity, selectivity, and practicality.

3.1 Synthesis of Undoped and Doped Metal Oxide Nanoparticles by Sol-gel Method

3.1.1 Materials

Tin (IV) chloride pentahydrate and copper acetate dihydrate ($Cu(CH_3COO)_2.H_2O$) were purchased from Sigma Aldrich to create nanoparticles using the sol-gel method. The 99.5% pure monoethanolamine (C_2H_7NO) (EA), 2-propanol ($CH_3CH(OH)CH_3$), Ammonia solution 25%, Cerium (III) chloride hexahydrate ($CeCl_3H_{12}O_6$) and Manganese (II) chloride tetrahydrate ($MnCl_2.4H_2O$) are all purchased from Merck. Ethanol Absolute >99.9% was purchased from Tekkim. Using all chemicals requires no extra purification, and they are all of reagent grade. The Purelab Option-Q equipment was utilized to acquire ultra pure water for the research.

3.1.2 Synthesis of Nanoparticles

The pH of the solution and calcination temperature are crucial parameters that impact the nanoparticle's size and the electrochemical properties of the resulting nanostructures. Different solutions with variable starting sol pH values and calcination temperatures were created to optimize the nanoparticle characteristics. Copper acetate monohydrate was utilized as the copper precursor to obtain a sol solution to prepare undoped CuO nanoparticles. Copper acetate solution (1 M) and isopropyl alcohol is homogenized using magnetic stirring. While achieving homogeneity and keeping the solution's required level as pH 7, 8, and 9, EA is added to the mixture drop by drop. After mixing for an hour, a clear, homogenous solution resulted. The final products were dried overnight at 80 °C in an oil bath. Ultimately, calcination was carried out for an hour at different temperatures (between 500 and 600 °C) to produce CuO nanoparticles. Eq. (3.1) and (3.2) give formation mechanism of CuO nanoparticles.

$$Cu(CH_3COO)_2 \cdot H_2O + 2H_2O \rightarrow Cu(OH)_2 + 2CH_3COOH \quad (3.1)$$

$$Cu(OH)_2 \rightarrow CuO + H_2O \quad (3.2)$$

Doped particles were synthesized similarly to undoped CuO, and the CuO sol solution was prepared using copper acetate monohydrate as the copper precursor. 1 M copper acetate solution and isopropyl alcohol were homogenized via magnetic

stirring. To achieve homogeneity and maintain a pH of 7, an appropriate quantity of EA was added to the mixture drop by drop. After 1 hour of mixing, a homogenous and clear solution was obtained. Different molar ratios of manganese (II) chloride tetrahydrate were dissolved in isopropyl alcohol, with the molar ratio of Mn to CuO ranging from 0% to 2% (0, 0.25, 0.5, 1, and 2%). After adding the Mn solution to the copper sol, one hour of stirring was performed. The resulting sol was then dried in an oil bath overnight at 80 °C. A calcination procedure was used to produce the nanoparticles. The samples were designated CuO-Mn0.25, CuO-Mn0.5, CuO-Mn1, and CuO-Mn2, respectively, according to the amount of Mn addition.

Ce-doped CuO nanoparticles were synthesized utilizing the same process as Mn-doped CuO nanoparticles. Magnetic stirring was used to obtaina solution containing 1 M copper acetate and isopropyl alcohol. Ethylamine (EA) was added dropwise to the mixture while stirring for one hour to achieve homogeneity and maintain a pH of 7, producing a clear and homogenous solution. Then, Cerium(III) Chloride Anhydrous, dissolved in isopropyl at various molar ratios, was dropped into the Cu solution. The Ce/CuO ratio was established using molar ratios ranging from 0% to 2%. The mixture was agitated for another hour after adding the Ce solution, and the resultant sol was dried in an oil bath at 80°C overnight. The calcination step that followed the drying procedure resulted in the formation of nanoparticles. The samples are labeled by the Ce contribution rate: CuO-Ce0.25, CuO-Ce0.5, CuO-Ce1, and CuO-Ce2. The crystal structure of undoped and Mn and Ce doped CuO is shown in Figure 3.1.

To produce undoped SnO_2 nanoparticles, tin (IV) chloride pentahydrate ($SnCl_4.5H_2O$) was used as a tin precursor to prepare the SnO_2 sol solution. Ethanol (C_3H_2O) and distilled water were used in equal amounts to create a 0.1 M stannous chloride solution, which was then stirred for 60 minutes at room temperature. The solution's pH was raised to the necessary pH 2, 4, and 6 values, while homogeneity was maintained by gradually adding ammonia to the mixture. A homogenous, white solution was achieved after two more hours of mixing. After being subjected to an aging process at room temperature for 24 hours, the resulting structure was repeatedly cleaned with ethanol and water, and the resulting solution was dried in a 100 °C oil bath overnight.

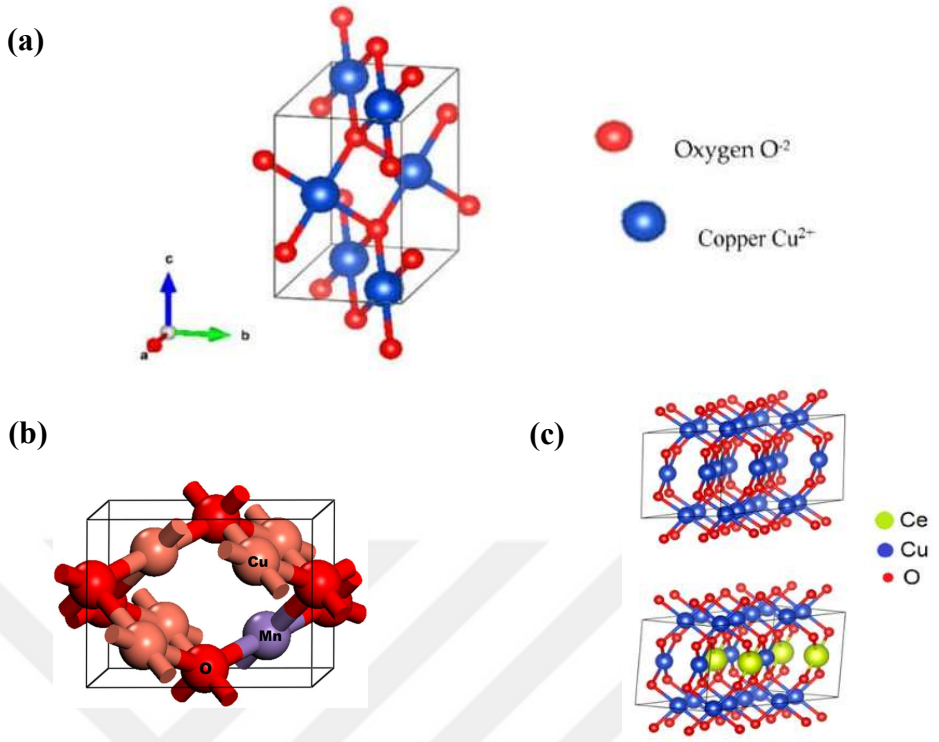

Figure 3.1 Crystal structure of (a) CuO (García Suárez et al., 2022), (b) Mn doped CuO (Sajid et al., 2018) and (c) Ce doped CuO (S. J. Singh et al., 2022)

The powdered structure was then calcined in an oven for 2 hours at 400 and 500 °C to synthesize nanoparticles. The synthesized SnO_2 nanoparticles were then used for characterization to examine the effect of pH and calcination parameters. Eq. (3.3) and (3.4) give SnO_2 nanoparticles formation mechanism.

$$SnCl_4 \cdot 5H_2O + H_2O \rightarrow Sn(OH)_4 + 4HCl + 5H_2O \quad (3.3)$$

$$Sn(OH)_4 \rightarrow SnO_2 + 2H_2O \quad (3.4)$$

The SnO_2 sol solution was formed using a tin precursor, tin (IV) chloride pentahydrate ($SnCl_4.5H_2O$). 0.16 M stannous chloride solution was prepared using an equal volume of distilled water and ethanol (C_3H_2O), and it was agitated at room temperature for 60 minutes. Ammonia was added to the mixture drop by drop while preserving homogeneity to raise the pH to the necessary value 2. Manganese (II) chloride tetrahydrate was dissolved in ethanol in several molar ratios, independent of one another. Mn to SnO_2 has a molar ratio from 0% to 2%. Stirring was continued for a further hour after the Mn solution was added dropwise to the tin sol, and another two

hours of mixing resulted in a uniform, white solution. The resulting sol was aged at room temperature for 24 hours before being periodically washed with water and ethanol. It was then allowed to dry overnight at 100 °C in an oil bath. The powdered bulk was calcinated for two hours at 400 °C to produce nanoparticles. Based on the increase of the molar ratio of Sn: Mn (0.25, 0.5, 1, and 2%), the samples were named SnO_2-Mn0.25, SnO_2-Mn0.5, SnO_2-Mn1, and SnO_2-Mn2, respectively.

To prepare Ce doped SnO_2, the SnO_2 sol solution was first made using tin (IV) chloride pentahydrate ($SnCl_4.5H_2O$), a tin precursor. A 0.16 M stannous chloride solution was made using an equal volume of distilled water and ethanol (C_3H_2O) and agitated at ambient temperature for 60 minutes. Ammonia was added drop by drop to the mixture to raise the pH to the necessary value of 2 while preserving homogeneity. Cerium (III) Chloride Anhydrous was dissolved in varying molar ratios relative to other substances in ethanol. The molar ratio range of Ce to SnO_2 is 0% to 2%. Stirring was continued for a further hour after the Ce solution was added dropwise to the tin sol. Another two hours of mixing resulted in a uniform, white solution. The resulting sol was aged at room temperature for 24 hours before being periodically washed with water and ethanol mixture It was then allowed to dry overnight at 100 °C in an oil bath. The powdered material was calcined in an oven for two hours at 400 °C to form nanoparticles. Based on the molar ratio of Sn: Ce of 0.25%,0.5%, 1% and 2%, the samples were named as SnO_2-Ce0.25, SnO_2-Ce0.5, SnO_2-Ce1, and SnO_2-Ce2, respectively. The crystal structure of undoped and Mn and Ce doped SnO_2 is shown in Figure 3.2.

3.1.3 Characterization of Synthesized Undoped and Doped Metal Nanoparticles

Many methods and approaches have been devised to acquire comprehensive data on nanostructure morphology and other characteristics, and they are extensively utilized for characterization. Scanning electron microscopy, dynamic light scattering, Fourier transform infrared spectroscopy, X-ray diffraction , and X-ray photoelectron spectroscopy are among the techniques employed in this investigation. A brief overview of how each is used and what data it provides is presented in this section.

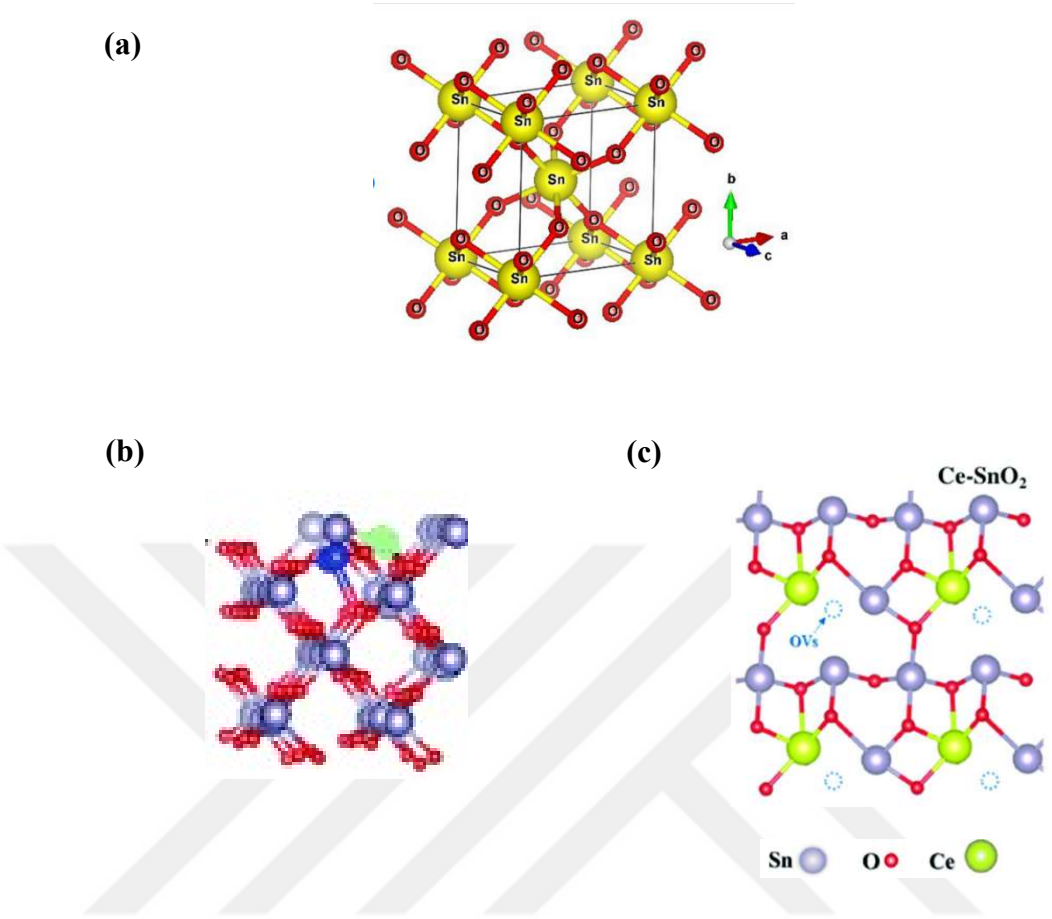

Figure 3.2 Crystal structure of (a) SnO_2 (A. Kumar et al., 2022), (b) Mn doped SnO_2 (Manikandan et al., 2018), and (c) Ce doped SnO_2 (Pinto et al., 2022 b)

3.1.3.1 X-ray Diffraction

The primary method of obtaining comprehensive data on the crystal structure of materials is X-ray diffraction (XRD). The qualitative and quantitative information that XRD may disclose are crystal planes, lattice parameters, phase of a material, and crystallinity degree (single crystal, polycrystalline, or amorphous). When an X-ray beam hits the crystal planes of the sample, the atoms of the material scatter and refract the X-rays. This diffraction occurs depending on the material's crystal structure. The strength of the diffraction pattern depends on the type and position of the diffraction peak formed by interference in the crystal structure of the atoms. Debye-Scherrer equation analysis of the diffraction peaks may be used to determine the average crystal size of nanoparticles (Holzwarth & Gibson, 2011):

$$D = \frac{k_{Sch}\lambda}{\beta_d cos\theta} \quad \text{Eq 3.1}$$

where: D = crystalline size (Å), The highest intensity peak's full width at half maximum (FWHM) is indicated by β, the diffraction angle is θ, the incident X-ray beam's wavelength is λ, and the Scherrer constant, k_{Sch}, is equal to 0.9.

X-ray diffraction (XRD, Rigaku, D / Max-2200 / PC) technique was used to examine the structure of the nanoparticles produced. With an incidence angle of 1° and a scanning rate of 4°, the nanoparticles were examined within the 2θ range of 3 to 90°.

3.1.3.2 Dynamic Light Scattering

The ability to measure the light scattering of small sized particles makes dynamic light scattering, or DLS, one of the most used techniques. This method is used in various applications such as emulsions, micelles, proteins, nanoparticles, colloids, polymers, and proteins. The basic principle is that a laser beam illuminates the sample and a fast photon detector operating at a specific scattering angle detects changes in the scattered light. Traditional DLS sensors measure at a specific angle to determine the average particle size over a narrow size range, but more advanced multi-angle instruments can determine the entire particle size distribution. Dynamic light scattering analysis (DLS) was performed using the Zeta Sizer Nano ZS90 to measure the particle size distribution.

3.1.3.3 Scanning Electron Microscopy

The scanning electron microscope (SEM) is a crucial instrument for examining the overall appearance of the generated nanostructures. SEM allows the evaluation of various properties of nanostructures, such as quality, shape, diameter, thickness, length, and orientation. An electron beam that has passed through electromagnetic lenses and reached the sample's surface creates the image used in SEM. The detector captures secondary or backscattered electrons released from the sample surface and transforms them into signals. This signal then focuses on a screen, providing detailed information about the sample morphology. The SEM has a magnification capacity of 20X to 30,000X and a spatial resolution of 50 to 100 nanometers. The study investigated the morphology of the synthesized nanostructures using a ZEISS EVO-

15 model SEM. At high magnifications, SEM images were also used to determine the average diameter of the particles and the grain morphology.

3.1.3.4 Fourier Transform Infrared Spectroscopy

FTIR spectroscopy is a vibrational spectroscopic method used to study optically molecular changes caused by chemical interactions. The method allows for the precise and thorough identification of functional groups, bond types, and molecular conformations. A substance's chemical structure may be immediately revealed by the spectral bands in vibrational spectra, which are exclusive to each molecule. The vibration of a particular chemical bond or functional group in the molecule is usually associated with distinct, narrow pixels in the FTIR spectrum.

Thermo Scientific Nicolet iS50 indicated the chemical composition of the nanoparticles with the FT-IR spectrometer in transmission mode. The measurements were conducted at a resolution of 4 cm^{-1} within the range of 500-4000 cm^{-1}.

3.1.3.5 X-Ray Photoelectron Spectroscopy

One of the most popular techniques in chemistry, materials science, and chemical engineering for assessing the composition, bond structure, and surface chemistry of surfaces and interfaces is X-ray photoelectron spectroscopy (XPS). The principle of X-ray photoelectron spectroscopy (XPS) is that the chemical environment of an atom influences the binding energies (BE) of electrons at the nuclear level; this phenomenon is often known as a chemical shift. This characteristic allows one to ascertain the bond structure and assess if processing conditions or surface treatments impact it. The measured BE values are compared with literature data to obtain information about the bonds present (Greczynski & Hultman, 2020).

In this study, an XPS device with monochromatic Al Kα from Thermo Scientific/K-Alpha Brand was used to analyze bond structure and surface chemistry.

3.2 Development of Bare and Metal Oxide Nanoparticle Modified Carbon Paste Electrode (CPE)

Sigma Aldrich supplies the chemicals required to produce electrochemical biosensors, including graphite powder (99.5% pure) and mineral oil. The standard procedure for preparing the bare CP electrode involves combining 15% (wt/wt) mineral oil and 85% (wt/wt) graphite powder in an agate mortar for 20 minutes. Next, the paste is placedin a glass rod 4 cm long and 3.3 mm in diameter. Different weights of graphite powder and various nanoparticles concentrations (2%, 5%, 10%, 15%, and 20% wt) were mixed with 0.15 g of mineral oil in an agate mortar to prepare the modified electrodes. The mixture is then stirred for 15 minutes until it becomes homogenous (Figure 3.3). Preparing nanoparticles modified CPE is identical to that of raw CPE. The sanded copper wire is used to provi deelectrical connections. Before each measurement, the surfaces of both electrodes are carefully cleaned and smoothed.

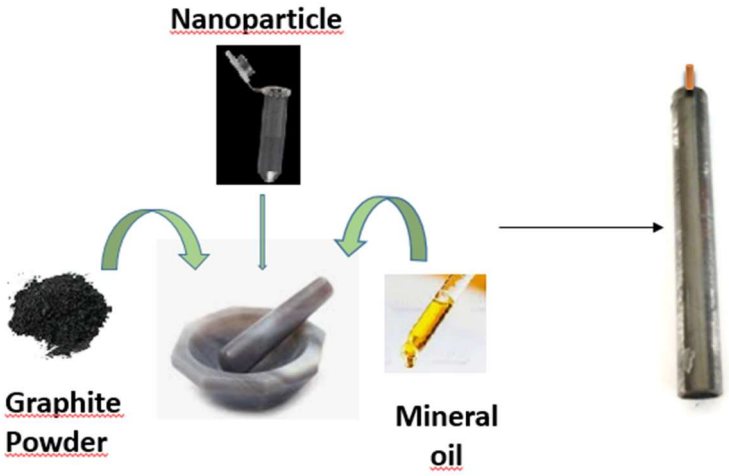

Figure 3.3 Design of carbon paste electrode

3.2.1 Preparation of Electrolytes and Analytes

Potassium dihydrogen phosphate (KH_2PO_4) was dissolved in distilled water, and the volume was added to one liter of distilled water for the buffer solution preparation. The pH was then adjusted using a NaOH solution. Following complete dissolution, the

liquid was supplemented with 0.1 M potassium nitrate. Consequently, a PBS with a pH of 7.5 in 0.1 M KNO_3 was produced.

To investigate the effect of electrolyte pH value, an electrolyte solution was prepared using potassium nitrate (KNO_3), sodium hydroxide (NaOH), acetic acid (CH_3COOH) and glycine ($C_2H_5NO_2$) at various pH values. In addition, 0.1 M NaCl, $NaNO_3$, and KCl electrolytes were formed to test the effect of different buffer solutions.

3.2.2 Electrochemical Characterization

To check the developed sensor's electrochemical capabilities against SAL, quantitative cyclic voltammetry (CV) measurements were first performed. Cyclic voltammetry was carried out after deposition in pH 7.5 phosphate buffer solution (PBS) comprising 0.1 M (KNO_3) and 8.5 x 10^{-5} M Ventolin syrup, applied at - 0.3 V under continuous stirring for 240 s. The measurements were performed within a potential range of ±1 V, at a scan rate of 40 $mV.s^{-1}$. Differential pulse (DP) measurements were carried out using various deposition times and deposition potential in a 0.1 M pH 7.5 PBS containing 0.1 M (KNO_3).

Many electrochemical experiments were conducted to investigate the effects of electrolyte pH, scan rate, carbon paste composition, and types of supporting electrolytes. After completing all electrochemical characterization experiments, calibration curves and detection limit measurements were used to assess the developed sensor's repeatability, stability, and selectivity.

3.2.3 Electrochemical Measurement Procedures

Electrochemical tests were conducted using an AutoLab PGstat-30 potentiostat/galvanostat instrument controlled by a PC running NOVA software (Metrohm Autolab). A typical three-electrode electrochemical cell was used for these studies (Figure 3.4). Ag/AgCl/KCl is a device that uses three electrodes: Pt serves as the counter electrode, 3 M serves as the reference electrode, and our custom-designed carbon paste electrode (CPE) serves as the working electrode. All studies were conducted at room temperature (25±1 °C), and a pH meter (WTW, Germany) was

utilized for the readings. A typical three-electrode cell's working, counter, and reference electrodes are all placed in the electrolyte solution. In three-electrode tests, the majority of the charge flow (current) is experienced by the working electrode and counter electrode, while the working electrode's potential is evaluated using the reference electrode. To drive current between the working and counter electrodes, the working electrode driver (red lead), counter electrode driver (black lead), and reference electrode sense (blue lead) are linked one to the other. Figure 3.4 depicts a standard three-electrode electrochemical cell arrangement.

Cyclic voltammetry (CV) and differential pulse (DP) methods were used for electrochemical measurements. Unmodified and nanoparticles modified electrodes were tested for their applicability in determining SAL using the quantitative Cyclic Voltammetry (CV) technique. Cyclic voltammetry was performed after deposition in 0.1 M pH 7.5 PBS containing 0.1 M (KNO_3) and 8.5 x 10^{-5} M Ventolin syrup, applied at -0.3 V under continuous stirring for 240 seconds. The measurements took place within a potential range of ± 1 V, at a scan rate of 40 $mV.s^{-1}$. Differential pulse (DP) measurements were then performed using different deposition time and deposition potential values in 0.1 M pH 7.5 PBS containing 0.1 M (KNO_3).

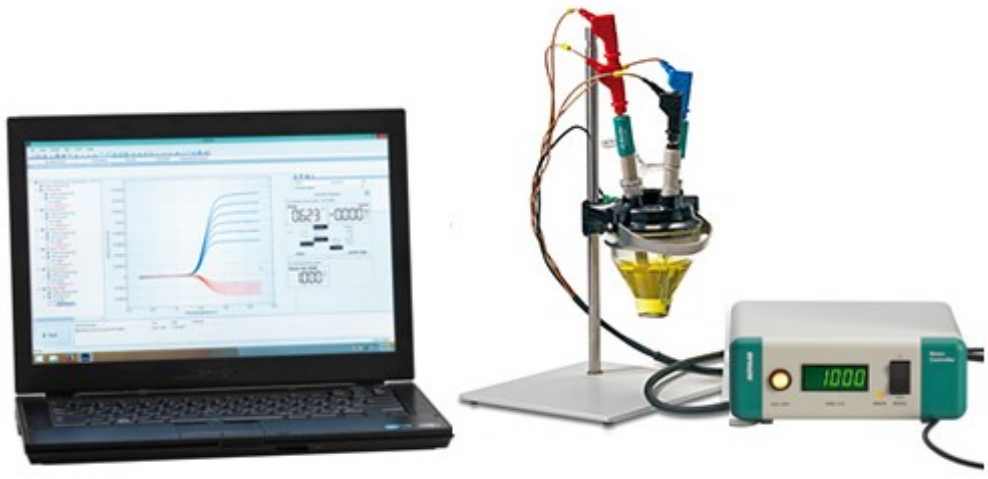

Figure 3.4 Typical setup for a three-electrode cell

CHAPTER FOUR
RESULTS AND CONCLUSIONS

4.1 Introduction

Metal oxide nanoparticles provide enormous surface areas, biocompatibility, high chemical stability, and unique electrical characteristics, making them excellent choices for diverse sensor applications, including gas sensors, biosensors, and optical sensors. Transition metals, in particular, are widely used invarious research and technology fields. Metal oxide semiconductor nanoparticles, including CuO, SnO_2, Fe_2O_3, TiO_2, and ZnO, are frequently used in different applications due to their large surface area, non-toxicity, sensitivity, biocompatibility, unique electronic properties, high chemical stability, and versatile surface chemistry. These substances actively contribute to the recognition of target molecules and the immobilization of biological molecules. The present study aims to explore the potential of undoped and doped CuO and SnO_2 nanoparticles (Mn and Ce) for electrochemical biosensor applications. These substances are thought to have significant potential for use in creating electrochemical sensors, particularly those used to identify medications like salbutamol. Salbutamol is a frequently prescribed bronchodilator for treating respiratory conditions, including chronic obstructive pulmonary disease (COPD) and asthma. Monitoring salbutamol levels in biological samples like blood or urine is critical to determine the drug's appropriate dose and evaluate the treatment's effectiveness. Some athletes can also abuse Salbutamol as a performance enhancer. According to WADA regulations, salbutamol usage is allowed up to a specific amount; nevertheless, going beyond these limits is regarded as doping. As a result, determining the presence of salbutamol in the bodily fluids of athletes is crucial for anti-doping measures. Salbutamol can also be used illegally in some countries to increase the growth rate of animals. Therefore, detecting salbutamol residues in food products (e.g. meat products) is critical for food safety. Furthermore, in the veterinary field, it may be necessary to monitor the levels of salbutamol used in the treatment of animals.

Electrochemical sensors direct salbutamol, offering direct response time and real-time analysis without requiring complex sample preparation in the laboratory. Furthermore, different dopants can be added to these sensors to boost performance.

Research on various nanomaterials, such as metal oxide, carbon nanotubes, and graphene oxide, has shown promise in improving the selectivity and sensitivity of electrochemical sensors for salbutamol detection.

Electrochemical detection using CuO and SnO_2 nanoparticles is more cost-effective and straightforward than other advanced techniques because it does not require complex and expensive equipment. CuO and SnO_2 nanoparticles enable the detection of analyses such as salbutamol even at low concentrations due to their excellent electrocatalytic properties. This, especially when added to the active surface properties of CuO and SnO_2, ensures high sensitivity in the determination of electrochemical methods. Furthermore, the specific surface chemistry of CuO and SnO_2 nanoparticles provides high selectivity towards particular analytes such as salbutamol. This property helps to minimize interferences caused by matrix effects and makes the detection process more reliable. However, in contrast to other metal oxides in the transition group, including ZnO (Jara-Ulloa et al., 2019), TiO_2 (B. Kumar et al., 2022), and Fe_2O_3 (R. Liu et al., 2023), Mn_2O_3 (Lu et al., 2024), there are, to the best of our knowledge, comparatively fewer investigations on the synthesis, characterization, and electrochemical performance technique utilized for CuO and SnO_2 nanoparticles.

Incorporating rare earth and transition metals into the metal oxide structure contributes significantly to the sensor performance of these materials. While transition metal doping can increase electrochemical activities by accelerating electron transfer kinetics and improving sensor sensitivity, it can also expedite adsorption-desorption processes by increasing the surface activity of oxide structures and improving sensor response times and sensitivity. The doping of rare earth elements improves the redox activity of the sensors by enabling the generation of more coherent and focused signals. Thanks to adding such elements to the metal oxide structure, metal oxide nanoparticles in electrochemical biosensors can now offer improved sensitivity, a more comprehensive dynamic range, and lower detection limits. This opens up new possibilities for advanced applications in food safety, environmental monitoring, and clinical diagnostics. Consequently, the contributions encourage using metal oxide nanoparticles in innovative sensor technology applications.

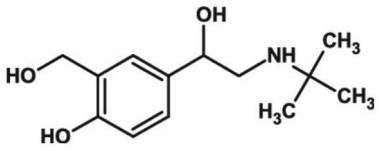

Figure 4.1 Illustration of the presence of hydroxyl groups in the salbutamol ring (Dicpinigaitis, 2014)

The electrochemical oxidation in solution that determines salbutamol's structure most likely occurs via $1H^+$ separation from the hydroxyl group indicated in red, and the C-O bond and chemical bonding follow. Literature reviews further support our theory since such compounds are readily oxidized, mainly through the B ring. The -OH group is then oxidized, and afterward, it remains a radical, making it easier for the molecule to form chemical bonds (Mülazımoğlu, 2008).

In this thesis, synthesis and characterization of undoped and Mn and Ce doped CuO and SnO_2 nanoparticles were carried out. The investigation focused on the synthesized nanoparticles' morphological and crystal structure and the impact of synthesis factors, such as solution pH value, calcination temperature, doping type, and concentration. An electrochemical sensor was also developed by modifying the CPE using produced nanoparticles. The electrochemical response of the salbutamol compound to a developed carbon-based electrode, as well as bare and metal oxide nanoparticle-modified CPE, was investigated using cyclic voltammetry (CV) and differential pulse voltammetry (DPV) methodologies. Differential pulse measurements were taken using different accumulation times and accumulation potential values in 0.1 M pH 7.5 PBS containing 0.1 M (KNO_3). The 0.1 M pH 7.5 PBS containing 0.1 M (KNO_3) and 8.5 x 10^{-5} M Ventolin syrup was used for the cyclic voltammeter investigation. After applying accumulation at -0,3 V for 240 s while continuously stirring, the mixture was held for 15 s. At a scan rate of 40 $mV.s^{-1}$, the potential range was within ± 1 V.

Accordingly, salbutamol was detected using electrochemical biosensors based on undoped and (Mn-Ce) doped CuO and SnO_2 nanoparticles. The performance of developed biosensors was assessed in terms of sensitivity, selectivity, response time, and detection limit.

4.2 Characterization Results of CuO Nanoparticles

4.2.1 Characterization Results of Undoped CuO Nanoparticles

This section of the thesis describes the synthesis of CuO nanoparticles using the sol-gel method. In this section, we examined the impact of calcination temperatures and solution pH, two crucial sol-gel technique factors, on the structural characteristics of the generated copper oxide (CuO) nanoparticles.

Figure 4.2 displays the CuO nanoparticle XRD pattern, which examines the phase and crystallite size. The JCPDS card number 45-0937 indicates that the diffraction peaks at 2θ values 32.48°, 35.52°, 48.72°, 53.45°, 58.33°, 61.54°, 66.23°, and 68.05°, respectively, correspond to (110), (002), (111), (202), (020), (202), (113), (311) and (220) planes. The XRD patterns of the samples made at various pH levels demonstrate that each sample has a flawless lattice and phase purity. Moreover, the XRD pattern's strong peak edges imply that the nanoparticles have a high degree of crystallinity (Hilary et al., 2015). Using the Debye-Scherrer equation, the average crystallite size of the CuO nanoparticles was determined to be 21.79, 22.24, and 25.15 nm for pH values of 7, 8, and 9, respectively.

CuO nanoparticles synthesized at low pH values (acidic environment) showed smaller sizes and homogeneous structures. The low pH led to rapid nucleation and slow growth of the particles, promoting the formation of more uniform and smaller crystals, resulting in sharper and higher intensity peaks in X-ray diffraction (XRD) analyses (Chithra et al., 2015a; Holzwarth & Gibson, 2011). The pH of the precursor solution is significantly influenced by the concentration of H^+ or OH^- ions in the original solution. Raising the pH of the solution under alkaline conditions causes the solution to produce more OH^-, which encourages the development of the crystal and nucleus. The pH change also impacts the solution's behavior throughout the hydrolysis and condensation phases of the gel formation process (Chithra et al., 2015a; Hussen et al., 2019). Similar findings have been documented in the literature, and it has been noted that the more outstanding crystal quality of CuO nanoparticles synthesized at low pH improves the strength of XRD peaks (Chithra et al., 2015a; Sivakumar et al., 2012). According to Chithra et al., the estimated crystal size changedfrom 13.8 nm to

33 nm when the pH value changed from 6 to 13 (Chithra et al., 2015b). In contrast, nanoparticles synthesized at high pH values (basic medium) generally tend to have a more oversized and irregular structure. This is due to the higher conversion rate of $Cu(OH)_2$ to CuO. This rapid conversion can form particles with larger and lower crystal structures (Zayyoun et al., 2016). As a result, it is seen that pH value directly affects the crystal structure and XRD peak intensity in CuO nanoparticles synthesis usingthe sol-gel method. While a low pH environment provides higher peak intensity and better crystal quality, a high pH environment can lead to larger, irregular particles and, thus, lower peak intensity. It was determined that the obtained results were consistent with the findings in the literature and that as the solution pH value increased, the nucleation rate slowed down, and the crystallite size increased.

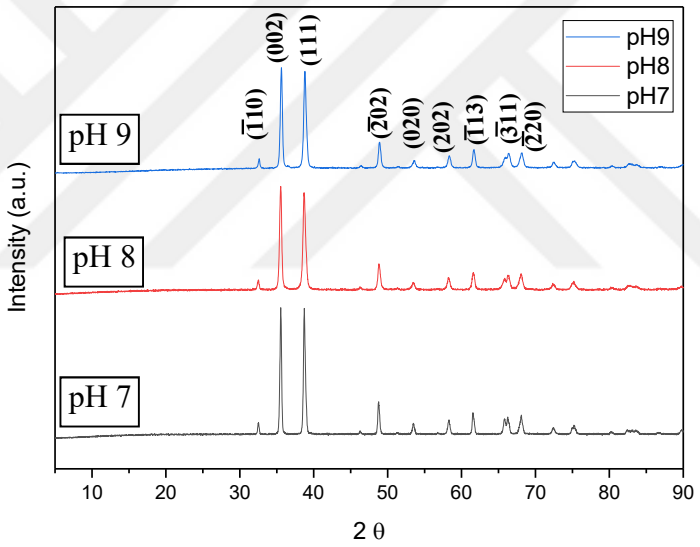

Figure 4.2 XRD pattern of CuO nanoparticles produced at different pH values

The DLS technique has been used to determine the particle size distribution of the CuO nanoparticles. The crystallite and particle size variations of CuO nanoparticles produced at varying pH values are depicted in Figure 4.3. The particle sizes measured for pH 7, 8, and 9 were 73.87, 90, and 132 nm, respectively. Results show that the pH of the precursor solution influences the hydrolytic and condensing behavior of the solution during gel formation. Thus, the pH of the solution affects the gel's capacity to form its polymeric three-dimensional structure. Basic pH values have more OH^- ions in solution, and hydrolysis is encouraged by alkaline circumstances.

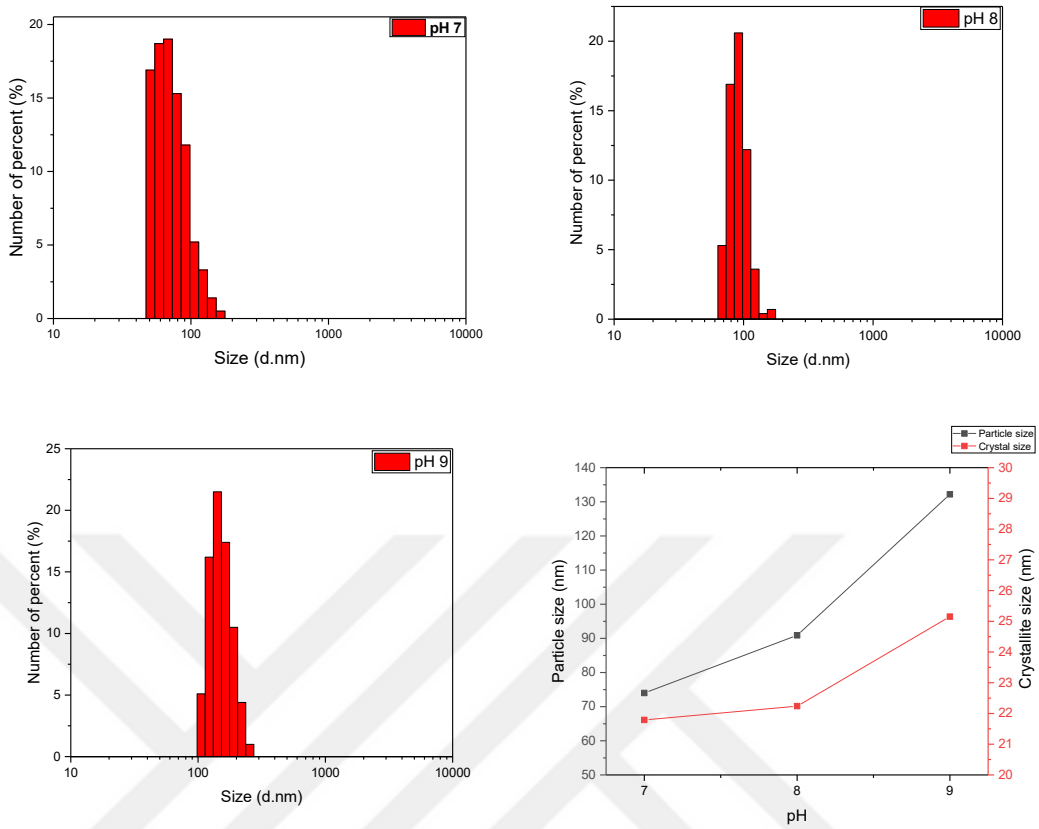

Figure 4.3 Crystallite and particle size characteristics of CuO nanoparticles produced at different pH levels

Under these conditions, there is an increase in particle size. Particle size was dependent on pH, and OH^- ions were found to promote CuO nucleation, growth, and particle generation. This discovery is consistent with findings reported in the literature, which indicate that an increase in pH causes a particle's size to grow (Sivakumar et al., 2012; Chithra, Sathya and Pushpanathan, 2015b, 2015a; Munir et al., 2017). A scanning electron microscope (SEM) was used to investigate the morphological characteristics of the CuO nanoparticles, as seen in Figure 4.4. The particles are spherical in form and range in size from 70 to 140 nm, according to SEM photographs. At the same time, it is observed that with increasing pH, the spherical forms of the particles deteriorate, and agglomerated structures are formed. The results obtained from the SEM analysis were consistent with the DLS measurement. When the effect of pH change on particle size was analyzed, it was observed that the nucleation rate decreased with pH increase in line with XRD results, which led to an increase in

particle size. In addition, it was determined that this increase also increased agglomerations.

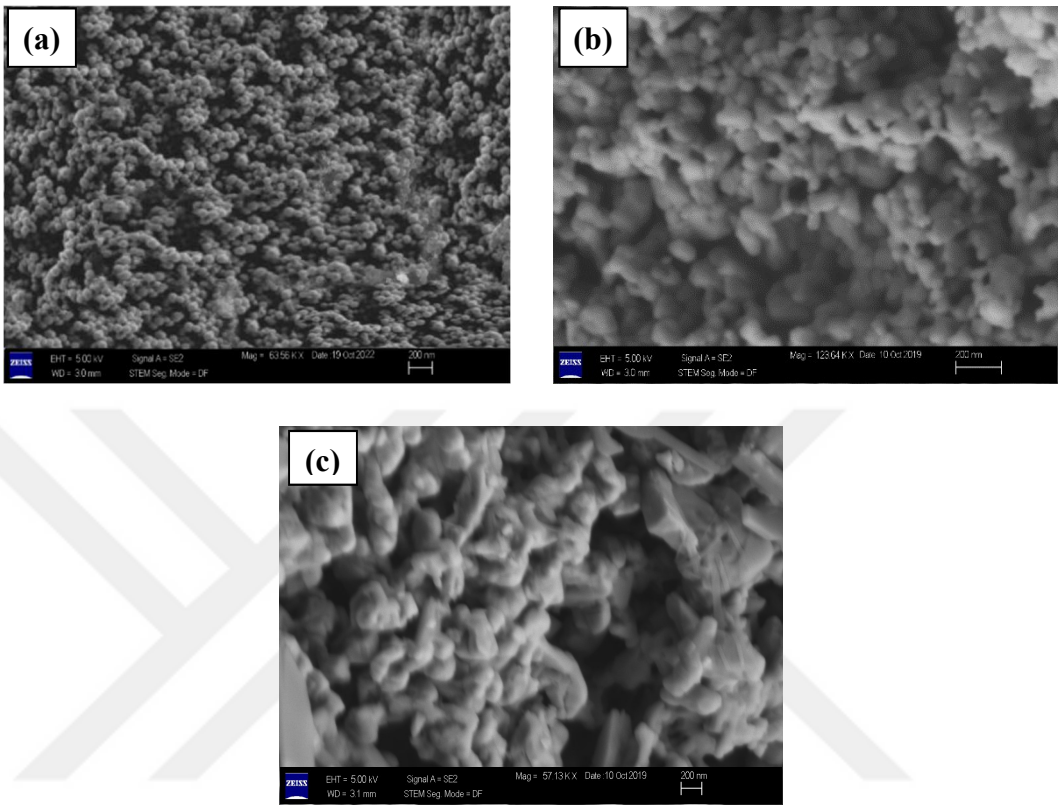

Figure 4.4 SEM images of CuO nanoparticles synthesised at different pH values (a) pH7, (b) pH8 and (c) pH9

FTIR spectra of synthesized CuO nanoparticles at different pH values (7, 8 and 9) are depictedin Figure 4.5. The slight vibrations observed in the 3600-3800 cm^{-1} range in the spectrum are attributed to O-H stretching vibrations (Momeni et al., 2014). In addition, vibrations in the 1400-2200 cm^{-1} range are assigned to be caused by moisture and CO_2 in the air (Naktiyok & Özer, 2019; P. K. Singh et al., 2016). The adsorption peak observed at 537 cm^{-1} in the spectrum is considered evidence of the characteristic stretching vibrations of the Cu-O bond in monocylindrical CuO (Attou et al., 2018; Sahu et al., 2021). The FTIR analysis results agree with the X-ray diffraction (XRD) analysis results.

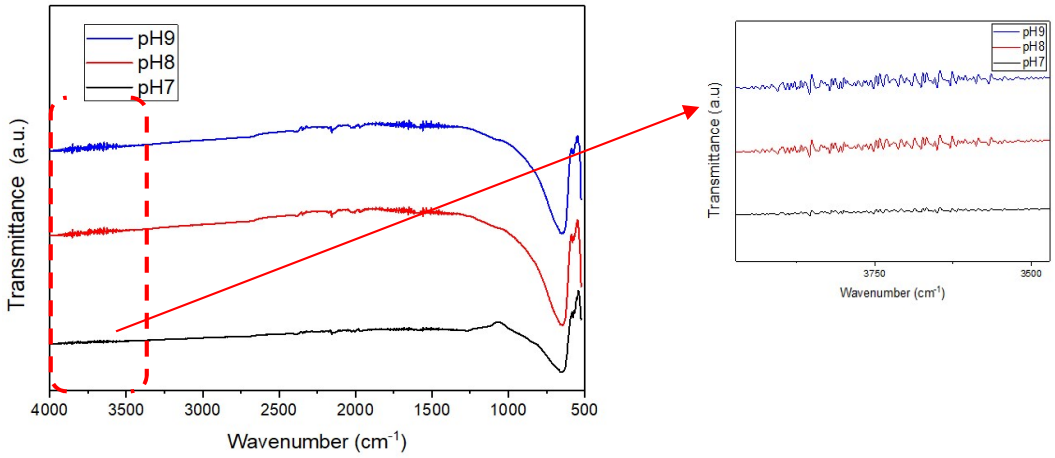

Figure 4.5 FTIR spectra of CuO nanoparticles synthesized at different pH levels

Particle size, crystallinity, and phase structure are among the structural characteristics of sol-gel produced particles that are significantly impacted by calcination temperature (S. A. Ibrahim & Sreekantan, 2011). According to the particle size measurement findings, pH 7 was used to synthesize CuO nanostructures with the smallest particle sizes. Therefore, we studied the synthesis at pH 7 to investigate the effect of calcination temperature. XRD patterns of synthesised CuO nanoparticles calcined at 500 °C and 600 °C are displayed in Figure 4.6. The XRD patterns represent two notable peaks at 2θ = 35.5° and 38°; they correspond to the (002) and (111) plane reflections, respectively. Monoclinic CuO crystals are supported by the obtained XRD pattern (JCPD card number: 45-0937). According to the XRD diffraction pattern, no additional peak was observed as the calcination temperature increased. It is observed that the peak intensity and peak width increase in XRD analysis with increasing calcination temperature during synthesis. This is evidence that increasing temperature promotes the regularity of the crystal structure and crystal growth. At higher calcination temperatures, the energy barriers of the crystal nuclei are overcome, leading to grain growth and increased crystallite size. In addition, the increasing diffusion rate with increasing temperature promotes grain growth. As a result, larger crystallites are characterized by narrower and more intense signals in XRD peaks. This indicates that the crystal has fewer defects and a more regular structure. This phenomenon indicates the maturation of the crystal phases and the reduction of crystal defects (Delice & Azem, 2022; Shah & Rather, 2021; Y. Zhao et al., 2022).

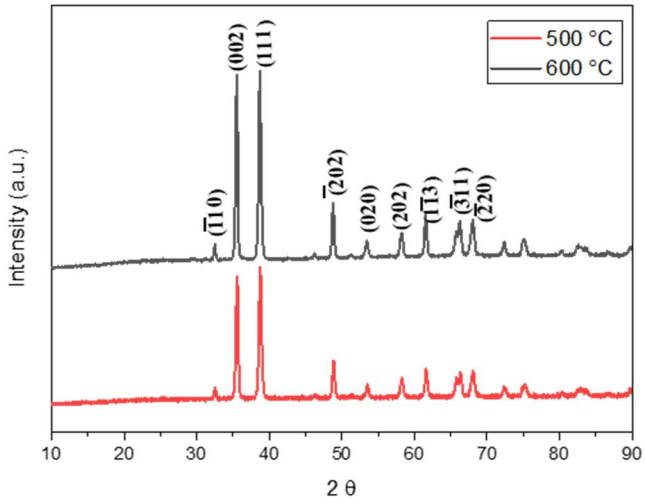

Figure 4.6 XRD patterns of CuO nanoparticles synthesized at different calcination temperatures

DLS measurement results of copper oxide nanostructures are presented in Figure 4.7. According to the literature high agglomeration causes copper oxide nanoparticles' average particle and crystallite size to increasewith increasing calcination temperature. Using the Debye Scherrer formula, the average crystallite size of CuO nanoparticles was around 21.79 nm and 25.63 nm at calcination temperatures of 500 °C and 600 °C, respectively. According to the results of the particle size analysis, the size of the CuO nanostructures rose from 73.87 nm to 238 nm when the calcination temperature was raised from 500 °C to 600 °C. The thermally induced crystallite development process is accelerated by raising the calcination temperature, which results in larger crystallites. At high temperatures, the increase in the crystal's internal energy increases the atoms' mobility and allows the energy barriers between crystal structures to be overcome. This leads to the coalescence of small crystallites to form larger crystallites. Crystallite growth results from the tendency of atoms to createa more stable and low-energy structure. Consequently, the crystal might have a more prominentand regular structure due to the increased calcination temperature, which causes the crystal structure to mature and the grain size to rise (Phromma et al., 2020). These results support the hypothesis that raising the calcination temperature causes the crystallite size of CuO particles to rise.

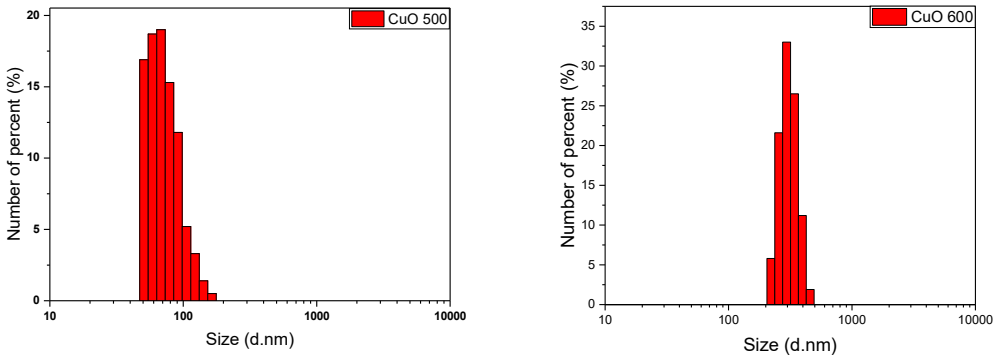

Figure 4.7 Particle size distribution of CuO nanoparticles calcinated at different temperatures.

Figure 4.8 displays the morphology of CuO nanoparticles, which were synthesized under different calcination temperatures. The dispersion of CuO nanoparticles, which are spherical particles with a size of around 73.87 nm and are generated at pH 7 and calcined at 500 °C, is specifically depicted in Figure 4.8(a) and Figure 4.8(b), on the other hand, displays the morphology of the nanoparticles that were calcined at 600 °C and prepared at the same pH value.

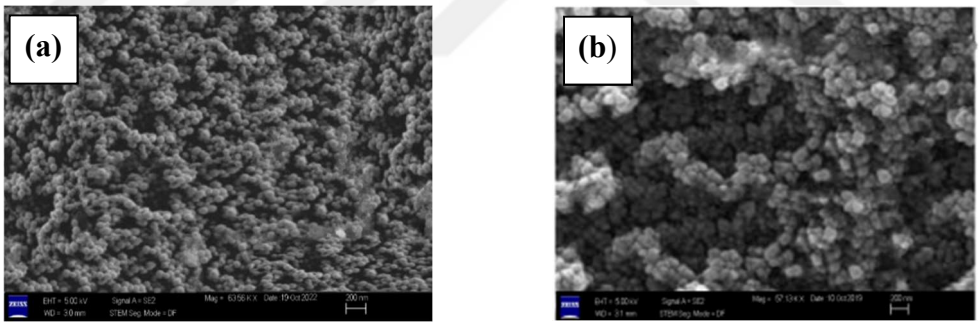

Figure 4.8 SEM image of CuO nanoparticles pH 7 calcinated at (a) 500 °C and (b) 600 °C

As observed from the SEM image, the particle size of the CuO nanoparticles increases with increasing temperature. These results align with those of the DLS study, which provides valuable information on how pH and calcination temperature affect the shape of CuO nanoparticles. Overall, the obtained data provides useful information for understanding the morphology of CuO nanoparticles and the role of calcination temperature and pH in their formation.

The FTIR spectra of CuO nanoparticles that were calcined at various temperatures are shown in Figure 4.9. The acquired spectrum's band vibrations resemble those of the spectrum derived from the pH effect research.

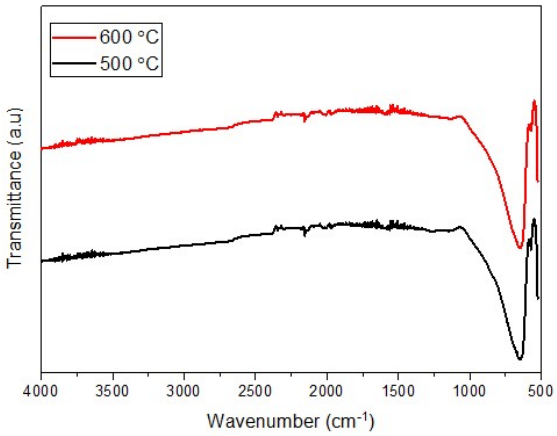

Figure 4.9 FTIR spectra of CuO nanoparticles calcined at different temperatures

For instance, the hydroxyl group's O-H stretching mode is responsible for the broad band around 3600 cm^{-1} (Momeni et al., 2014), moisture and CO_2 in the air are the cause of the band in the 1400–2200 cm^{-1} range (Singh et al., 2016; Naktiyok and Özer, 2019), and the stretching vibrations of CuO are responsible for the adsorption band observed at 537 cm^{-1} (Attou, Jaber and Ez-Zahraouy, 2018; Sahu *et al.*, 2021). These results are indicative of success in the production of CuO nanoparticles.

XPS analysis is utilized to determine the different oxidative states of elements and to investigate the chemical constituents present on the nanostructural surface and their binding energies. Figure 4.10 shows the chemical states of CuO nanoparticles by XPS analysis. Figure 4.10 (a) shows the full spectrum of CuO nanoparticles, including Cu2p and O1s spectra. As a result of expansive spectrum analysis, it was determined that only Cu, O, and C elements were present in the sample. The presence of element C was attributed to incidental carbon formed by exposure of the sample to air. A characteristic spin-orbit splitting peak attributed to the Cu^{2+} ion is found at around 20 eV. The Cu $2p_{3/2}$ and Cu $2p_{1/2}$ peaks are located at about 934 eV and 954 eV, respectively, indicating the presence of Cu ions in the synthesized nanoparticles.

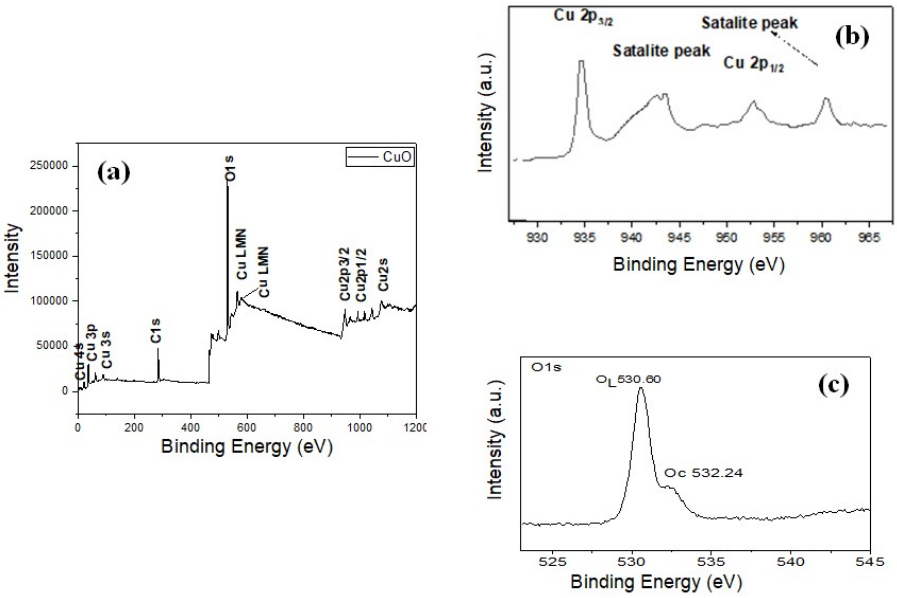

Figure 4.10 XPS spectra of CuO nanoparticles (a) survey spectra, (b) Core level spectra of copper, (c) Core level spectra of oxygen

Furthermore, the presence of Cu^{2+} and the $3d^9$ electronic configuration of the partially filled d-block is indicated by two short peaks observed at approximately 945 eV and 960 eV (Figure 4.10 (b)). The O(1s) core level spectrum of CuO is presented in Figure 4.10 (c). Both peaks, which show the O(1s) core level of CuO, are at about 530.6 and 532.24 eV. Moreover, the other peak, at 530.6 eV, is caused by the O^{2-} ion, but the peak at 532.15 eV indicates the presence of hydroxyl groups or chemically absorbed water molecules on the surface of CuO. The values of the binding energies for Cu and O coincide with the findings reported in the literature (Güldüren et al., 2023; Nagaveni et al., 2004; B. P. Singh et al., 2020; Vindhya & Kavitha, 2023).

4.2.2 Characterization Results of (Mn; Ce) doped CuO nanoparticles

The X-ray diffraction (XRD) patterns of undoped, 0.25%, 0.5%, 1%, and 2% of Mn doped CuO nanoparticles are depicted in Figure 4.11. The findings demonstrated that the diffraction peaks align with the reflections of CuO's monoclinic structure. Peaks were found at 32.48°, 35.43°, 38.66°, 48.84°, 53.39°, 61.57°, 66.48°, 67.82°, 72.33°, 75.26°, and 82.92°, respectively (JCPDS card no. 45-0937). These correspond to (hkl) values of (110), (002), (111), (202), (020), (202), (113), (310), (113), (311), (222) and (313). Sharp peaks suggest a high degree of crystallinity in the nanoparticles. It is

evident from the XRD spectra that the Mn-doped sample exhibits no additional peaks associated with secondary phase development, indicating that the addition of Mn ions to the CuO lattice has no negative effect on the monoclinic structure. It was found that the undoped nanoparticles had the highest peak intensity, which started to decline with Mn doping. The peak locations of Mn-doped CuO nanoparticles exhibit a slight shift towards larger angles in the XRD pattern, suggesting a minor distortion in the system's symmetry due to the formation of vacancies and defects. Manoharan and Mariammal et al. also came to similar conclusions (Albert manoharan et al., 2018; Mariammal et al., 2013). Additionally, Khan et al. showed that Mn doping of the copper oxide lattice (i.e., using Mn^{2+} rather than Cu^{2+}) causes a charge imbalance, which lowers peak intensity (Khan et al., 2013).

Furthermore, Bitra et al., discovered a minor shift towards the higher sides of the angle (2θ) values at the XRD patterns' peak positions. This shift suggests a slight deterioration in the CuO structure's symmetry due to the formation of holes and defects linked to Cu^{2+} being displaced by $Mn^{2+/3+}$ (Rao Bitra et al., 2021). Mn^{2+} has a larger ionic radius (0.83 Å) than Cu^{2+} (0.73 Å), resulting in a greater concentration of Mn doping, which leads to larger crystallites as evidenced by the reduced full width at half maximum (FWHM) value. In doping with elements with a larger radius, the distance in the d plane decreases. This leads to decreased peak intensity, peak broadening, and a shift to larger angles (T. Iqbal et al., 2022). Similarly, Manoharan's study found a tiny change in the peak locations of Mn-doped CuO nanoparticles towards higher angles. This shift was explained by the system's symmetry being slightly distorted due to voids and defects forming (Albert Manoharan et al., 2018). The replacement of Cu^{2+} ions by Mn^{2+} ions can cause expansions in the copper oxide lattice structure. Mn^{2+} ions have a larger ionic radius, which promotes mechanical stresses and expansions within the lattice.

These expansions create a structural change in the lattice that allows the formation of larger crystallites. Singh et al. stated that the stress induced by Mn doping in CuO crystals can increase crystal size (B. P. Singh et al., 2020). The rise of Mn doping may affect the mechanisms involved in the growth processes of crystallites. The doping element can integrate into the growth surfaces of crystallites and increase the growth

rate of these surfaces. In the study of Mariammal et al., it was stated that integrating Mn doping into CuO structures promotes the growth of crystallites and thus increases the average crystallite size (Mariammal et al., 2013).

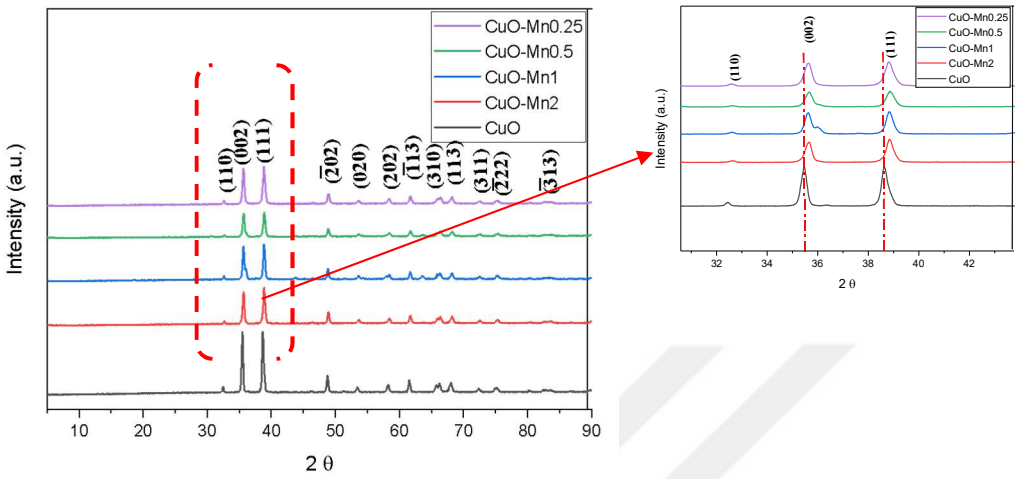

Figure 4.11 XRD pattern of undoped and Mn doped CuO nanoparticles

According to the investigations, the average crystallite size of undoped CuO nanoparticles is 21.79 nm; with Mn doping, this value rises to 22.51, 22.72, 23.16, and 23.12 nm, respectively. This shows that all Mn-doped CuO samples have larger average crystallite sizes than undoped CuO samples, in accordance with the literature.

Substituting Mn^{2+} ions with Cu^{2+} ions can cause stresses and voids in the lattice structure. These voids and stresses prevent the crystallites from growing correctly and thus may cause grain size reduction. In the literature, studies on the effect of Mn doping on grain size reduction have indicated that the displacements of Mn in the lattice and voids are the mechanisms that reduce grain size. For instance, according to Khan et al., Mn^{2+} doping reduces grain size because it causes stresses and defects during crystallite formation (Khan et al., 2018). In addition, it has been reported that Mn doping promotes nucleation in the crystallite growth process and supports the formation of smaller grains. Khlifi et al. reported that Mn^{2+} ions form new nucleation centers in the crystal structure, and these centers reduce the grain size, resulting in the formation of finer particles (Khlifi et al., 2022). As a result, the effect of increasing the amount of Mn dope on the grain size reduction of CuO nanoparticles can be explained by the nucleation centers, vacancies, and stresses created by Mn^{2+} ions in the lattice

structure. These mechanisms restrict the growth process of crystallites and hence result in smaller grain sizes.

Figure 4.12 depicts the Mn doped CuO nanoparticles' particle size analysis results and SEM images. The findings align with the literature, demonstrating that adding Mn reduces particle size. Furthermore, the spherical form of the particles remained unaltered by Mn doping. The particle sizes of 73.87, 73.10, 76.59, 68.27, and 68.67 nm for CuO, CuO-Mn0.25, CuO-Mn0.5, CuO-Mn1 and CuO-Mn2 samples, respectively, depending on the Mn doping ratio, were measured using the dynamic light scattering method.

The FTIR spectra of undoped and Mn-doped CuO nanoparticles, which were produced with varying Mn dopant concentrations, are shown in Figure 4.13. Mn doping has no effect on the chemical bond structures, while the vibrations in the 3600–3800 cm^{-1} range are attributed to O-H stretching vibration (Momeni et al., 2014). The air's CO_2 content and humidity are believed to be the cause of the vibrations at 1400-2200 cm^{-1} (Singh et al., 2016; Naktiyok and Özer, 2019). The absorption band at 1107cm^{-1} corresponds to the C–O stretching (Varughese et al., 2020). The characteristic stretching vibrations of the Cu-O bond seen in monoclinic CuO are linked to the adsorption at 537 cm^{-1}. The band located at about 530 cm^{-1} is associated with the stretching of CuO, and with Mn doping, the peak centered around 530 cm^{-1} shows a shift to higher band values (~ 600 cm^{-1}). The results from FTIR and XRD analyses exhibit remarkable alignment (Attou, Jaber, and Ez-Zahraouy, 2018; Sahu et al., 2021).

The valence electrons, charge characteristics, and chemical states of both undoped and Mn-doped CuO nanoparticles were analyzed using XPS. The XPS spectra of these nanoparticles exhibit the presence of Cu2p, Mn2p, and O1s elements, as illustrated in Figure 4.14(a). The absence of additional components confirms the purity of the samples. Figure 4.14(b) presents the Cu2p spectra, where the binding energies for $Cu2p_{3/2}$ and $Cu2p_{1/2}$ are approximately 933.27 eV and 953.36 eV, respectively.

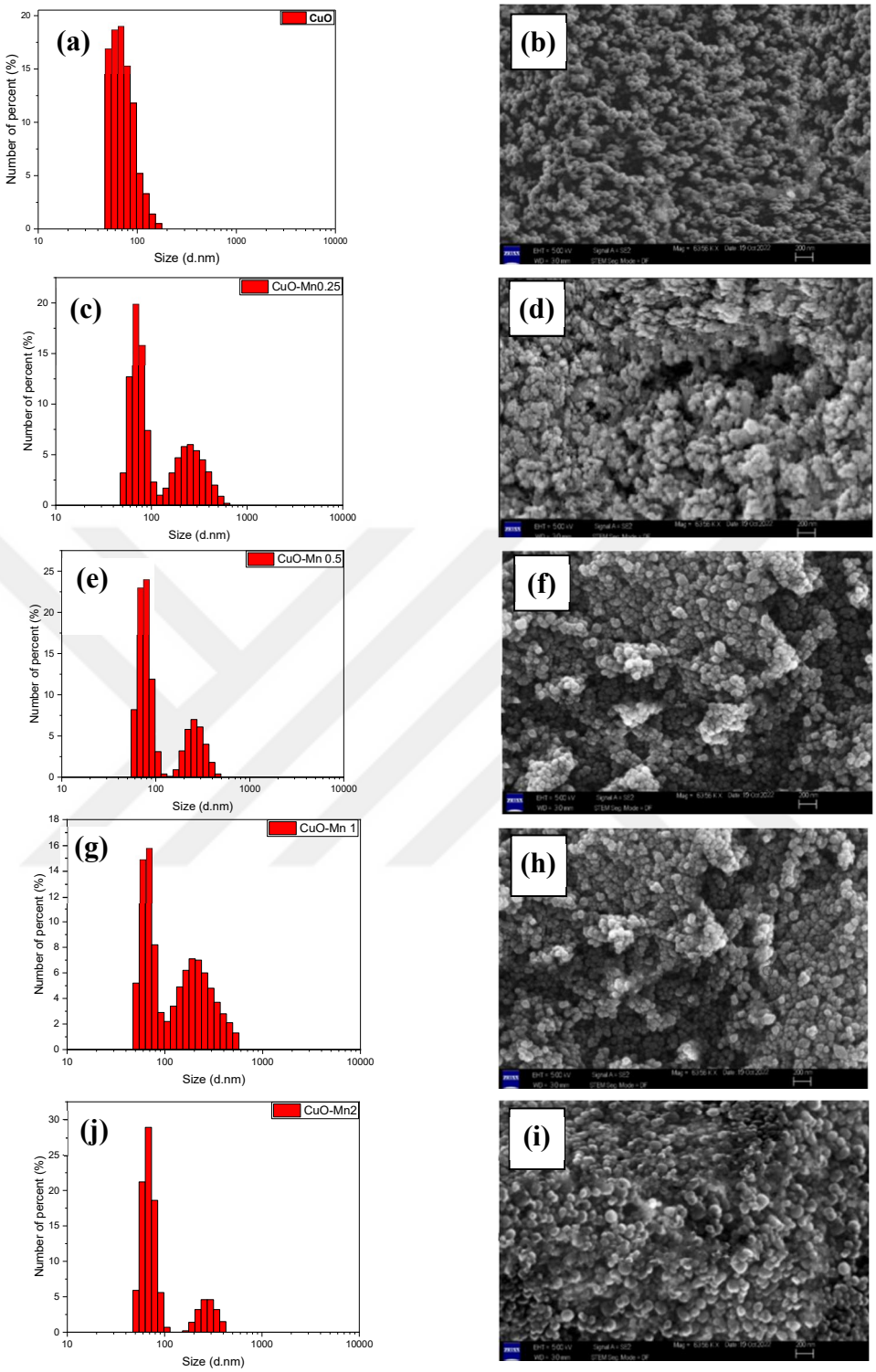

Figure 4.12 Particle sizedistribution histograms and SEM images (a), (b) undoped CuO and (c), (d) 0.25%, (e), (f) 0. 5%, (g), (h) 1%, (i), (j) 2% Mn doped CuO nanoparticles

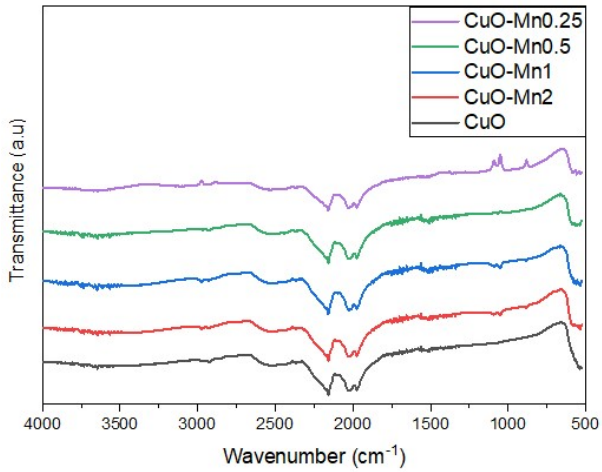

Figure 4.13 FTIR spectra of undoped and Mn doped CuO nanoparticles at different concentrations

These values, consistent with those reported by Nagajyothi et al. (2017), reflect a spin-orbit splitting of 20.1 eV, characteristic of the Cu^{2+} oxidation state. A slight shift in the $Cu2p_{3/2}$ binding energy was observed upon Mn doping, attributed to the interaction between Mn and Cu. (Nagajyothi et al., 2017; Benhadria et al., 2022). The Mn2p spectra, depicted in Figure 4.14(c), display binding energy peaks at 641.9 eV and 653.5 eV, corresponding to $Mn2p_{3/2}$ and $Mn2p_{1/2}$, respectively. These peaks show a spin-orbit splitting of 11.6 eV, indicative of Mn^{2+}. The satellite peak at 648.09 eV, located near $Mn2p_{3/2}$ but absent from $Mn2p_{1/2}$, points to an unfilled Mn 2p shell. This satellite feature, specific to Mn^{2+}, is lacking in higher oxidation states like Mn_2O_3 or MnO_2 and is attributed to satellite excitations (Ganesan et al., 2020; Kadam et al., 2022).

The rightward shift observed in the O1s spectra with Mn doping is due to changes in the chemical environment and bond structures due to the addition of Mn to the material. This shift can be attributed to the influence of the local electronic environment of oxygen atoms and the increase in bond energies with the addition of Mn in the CuO structure. Mn doping changes the electron density around the oxygen atoms in the CuO structure, causing an increase in the binding energy and a corresponding shift to the right. This shift generally reflects the role of Mn in the oxidation state and bond structure (Espitia et al., 2020).

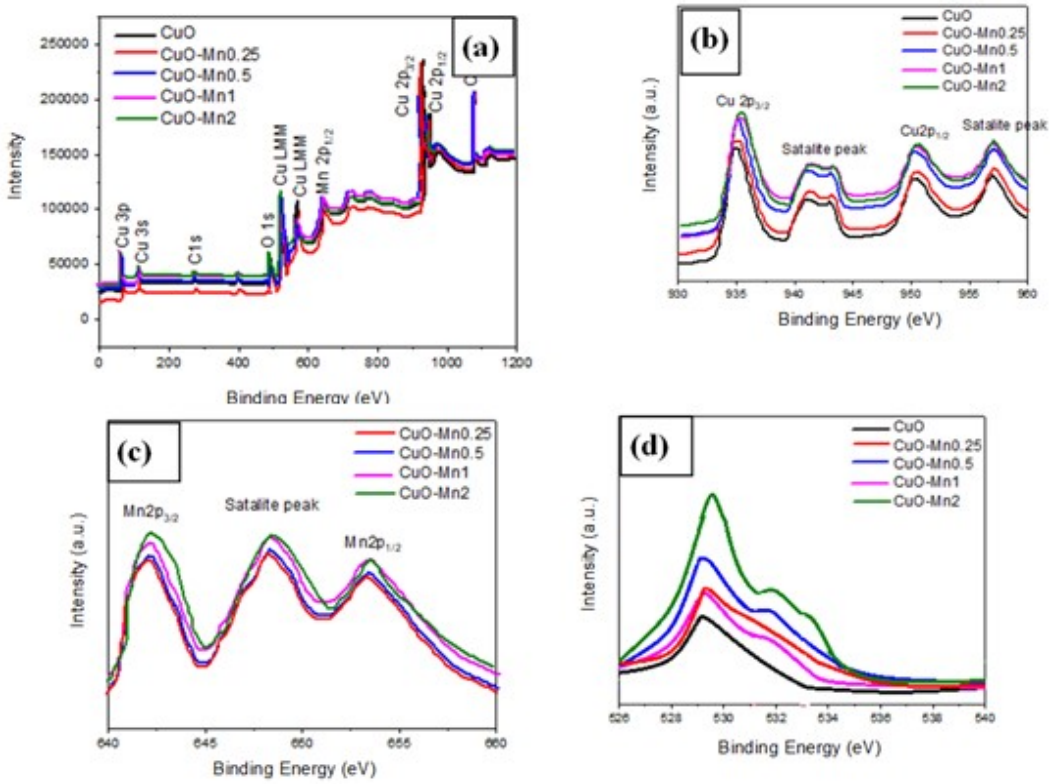

Figure 4.14 XPS spectra of undoped and Mn doped CuO nanoparticles (a) survey spectra (b) Core level spectra of copper, (c) Core level spectra of manganese, (d) Core level spectra of oxygen

Sharma et al. claim that the absence of a distinct satellite peak is caused by the heterogeneous oxidation states of Mn (A. Sharma et al., 2017). The lattice oxygen atom's binding energy is 529.5 eV, and the shoulder peak is situated at 531.2 eV, according to the O1 spectra displayed in Figure 4.14(d) (B. P. Singh et al., 2020). The hydroxyl group, which may be attributed to either the production process of the nanoparticles or their absorption of ambient moisture, is shown by the peak at 532.3 eV (P. Kumar et al., 2021). Mn ions were successfully doped into the CuO crystal lattice, causing modifications to the chemical state, surface energy, and structure. XPS results confirmed these changes, which were consistent with the XRD result.

The X-ray diffraction patterns for undoped and Ce-doped CuO nanoparticles with varying Ce concentrations (0.25%, 0.5%, 1%, and 2%) are presented in Figure 4.15. The detected XRD peaks at 32.48°, 35.43°, 38.66°, 48.84°, 53.39°, 61.57°, 66.48°, 67.82°, 72.33°, 75.26°, and 82.92° correspond to the (110), (002), (111), ($\bar{2}$02), (020), (202), ($\bar{1}$13), (310), (113), (311), ($\bar{2}$22), and ($\bar{3}$13) planes, respectively, which are

characteristic of the CuO phase (JCPDS No. 45-0937). The presence of Ce atoms is confirmed by peak position and intensity variations, indicative of structural modifications such as defects and vacancies in the lattice. These changes, resulting from Ce doping at Cu lattice sites, cause charge imbalances (Arfan et al., 2019). When the doping amount increased 2%, the (110) and (002) planes noticeably shifted towards higher angles, suggesting changes in interplanar spacing.

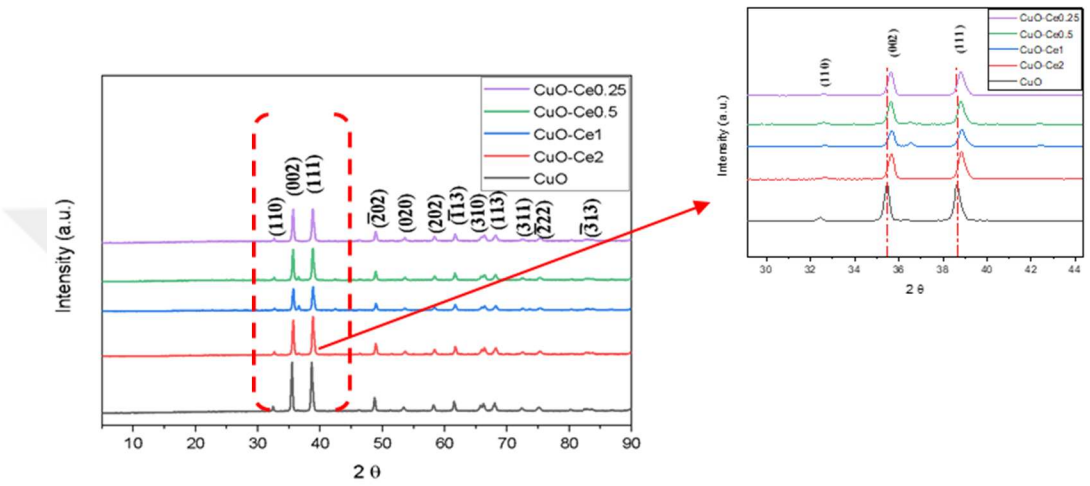

Figure 4.15 XRD pattern of CuO nanoparticles produced with different Ce dopant concentration

The reason for this change is that the bigger Ce atoms that were incorporated into the Cu lattice caused lattice expansion, as seen by the greater ionic radii of Ce^{3+} (1.143 Å) and Ce^{4+} (0.97 Å) than that of Cu^{2+} (0.73 Å) (Lv et al., 2020; F. Meng et al., 2017). The addition of dopant atoms, the stress, and defects created by Ce atoms in the crystal structure in the interstitial arrangement; increase the disorder of the crystal; and reduce the peak intensity. However, above a particular concentration, the formation of new nucleation centers can improve the crystal quality, and hence, an increase in the peak intensity can be observed. The decrease in peak intensity with increasing Ce content suggests a deterioration in crystallinity, likely due to disorder and defects introduced by Ce ions in the CuO lattice. At higher dopant levels, the deposition of additional Ce atoms within the grain is hindered, and the creation of new nucleation sites improves the crystallite quality, resulting in a subsequent increase in peak intensity (Kayani et al., 2018). These data confirm the successful doping of Ce into the CuO host matrix. The strong peaks show that the produced nanoparticles have substantial crystallinity. Using the Debye-Scherrer equation, the crystallite size of both undoped and Ce doped

CuO nanoparticles was determined. The findings show that crystallite size gradually decreases with increasing Ce content: for undoped CuO, it is 21.79 nm; for CuO-Ce0.25, CuO-Ce0.5, CuO-Ce1, and CuO-Ce2, it is 21.03 nm, 21.05 nm, 20.75 nm, and 20.67 nm, respectively. This suggests that Ce doping leads to a reduction in crystallite size compared to undoped CuO.

The nanoparticles were morphologically examined using SEM and DLS was used to analyze the size distribution. Figure 4.16 shows SEM images and particle size distribution histograms. It was discovered that Ce doping significantly alters the shape and structural characteristics of CuO nanoparticles. The undoped CuO sample has a large concentration of uniformly shaped, almost spherical nanoparticles (Figure 4.16(b)). A marked change in morphology was observed from 0.5% Ce onwards. Careful inspection testifies to the formation of nanoscales. The effective integration of Ce ions into the CuO matrix is responsible for this morphological change. The unique interaction between the Ce ion and the different crystallographic planes of CuO is the mechanism underlying the morphology change from sphere-like to nanoscale-like structure. This interaction can cause grain growth and morphological transformation because it increases the growth rate in the (111) direction (Jan et al. 2014; Ponnar et al. 2018a; Chu et al. 2022).

The particle size measurement results of undoped and Ce doped CuO nanoparticles with increasing Ce content of 0.25%, 0.5%, 1%, and 2% are 79.58, 86.10, 136.5, and 59.09 nm, respectively. Ce doping markedly altered the dispersion and size of CuO nanoparticles. The decrease in grain size when Ce doping reached 2% was attributed to the increase in nucleation with the rise of Ce to a certain level, as mentioned in XRD findings. Consequently, a structural disorder is caused by Ce doping into the CuO host matrix, and the microstrain shift impacted the form and size of the nanoparticles.

The results of FTIR spectra of undoped and Ce doped CuO nanoparticles prepared by introducing Ce with different concentrations are shown in Figure 4.17. Although Ce doping has been shown to have no appreciable effect on chemical bond structures, it was found that O-H stretching vibration was the source of the minor vibrations seen in the 3600-3800 cm^{-1} range (Momeni et al., 2014).

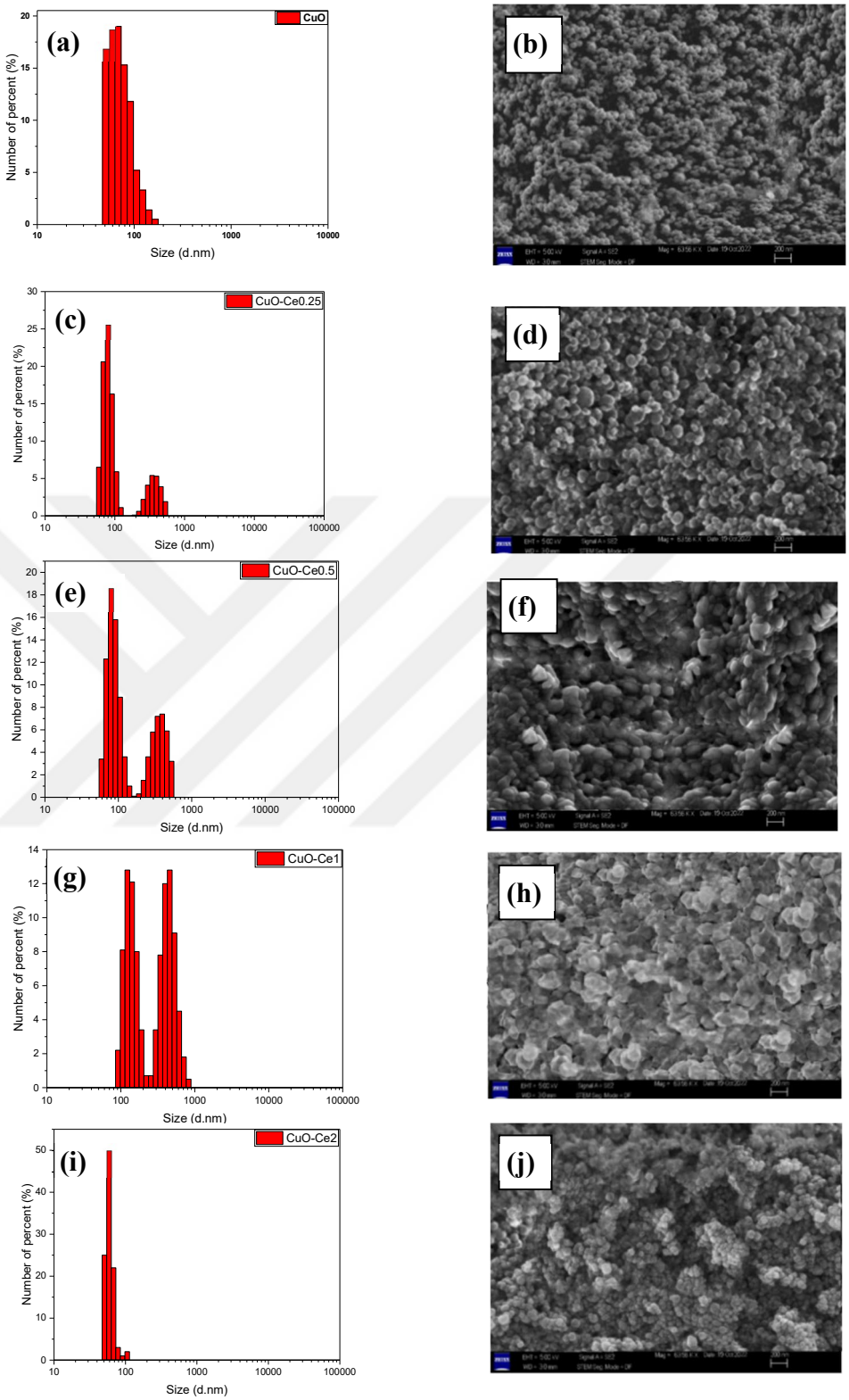

Figure 4.16 Particle size distribution histograms and SEM images (a), (b) undoped CuO and (c), (d) 0.25%, (e), (f) 0. 5%, (g), (h) 1%, (i), (j) 2% Ce doped CuO nanoparticles

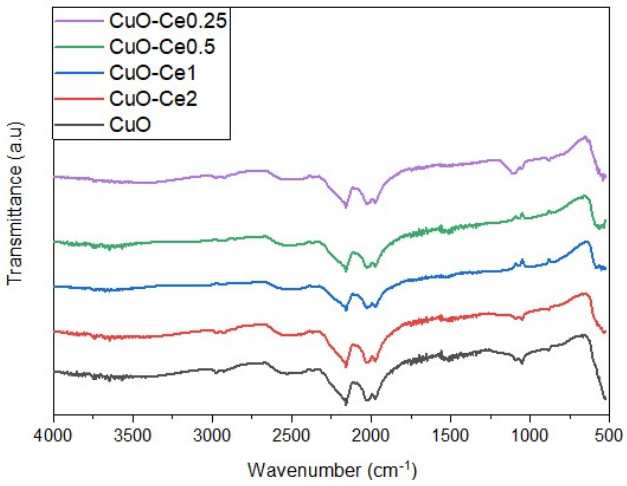

Figure 4.17 FTIR spectra of undoped and Ce doped CuO nanoparticles at different concentrations

Similar to the findings of undopedand Mn-doped CuO, it is believed that the vibrations in the 1400-2200 cm^{-1} range are generated by CO_2 and air humidity (Naktiyok and Özer, 2019; Singh and Sachan, 2022). The adsorption band at 537 cm^{-1} is associated with the usual stretching vibrations of the Cu–O bond seen in monoclinic CuO (Attou, Jaber, and Ez-Zahraouy, 2018; Sahu et al., 2021). In both undoped and doped samples, the stretching vibration at 537 cm^{-1} indicates the presence of CuO. No additional functional group in cerium or cerium oxides has been confirmed. Additionally, there is a good agreement between the results of the FTIR and XRD analyses. This agreement indicates that the crystal structure of the resulting nanoparticles is retained and that Ce doping has no discernible effect on the structural characteristics of CuO nanoparticles.

X-ray photoelectron spectroscopy (XPS) was used to examine cerium valence states and oxygen vacancies for undoped CuO and CuO-Ce0.25, as shown in Figure 4.18 (a). The high-resolution spectra of O 1s, Ce 3d, and Cu 2p are shown in Figure 4.18 (a). The peaks of Cu $2p_{1/2}$ and Cu $2p_{3/2}$, which are located at 953.5 eV and 933.7 eV, respectively, are what define Cu^{2+} ions (W. Lv et al., 2020; Y. Lv et al., 2020(b)). Additionally, satellite peaks were associated with slightly full Cu 3d at 941.6 eV, 944.1 eV, and 962.5 eV. The peaks of Cu $2p_{1/2}$ and Cu $2p_{3/2}$ for Ce-doped CuO nanoparticles showed a modest shift to higher binding energies at 953.8 eV and 933.8 eV, respectively, as shown in Figure 4.18 (b). This slight shift might result from bond length variations brought about by Ce ions entering the CuO lattice. ZnO

nanostructures doped with Ce have also been found to have a similar effect (Cervantes-López et al., 2017). The peaks in Figure 4.18 (c) at 883 eV and 898.7 eV are comparable to the previously discovered peaks at 883.4 eV and 901.6 eV, which represent the spin-orbit coupling of Ce $3d_{5/2}$ and Ce $3d_{3/2}$. Cerium exists in two frequent oxidation states: Ce^{4+} and Ce^{3+} (Aashima et al., 2019; Cervantes-López et al., 2017). The peaks at 883 eV, 889.4 eV, 901.2 eV, 907.8 eV, and 917 eV reflect the oxidation state of Ce^{4+}, whereas the peaks at 885.7 eV, 898.7 eV, and 903.4 eV represent the oxidation state of Ce^{3+}(Aashima et al., 2019).

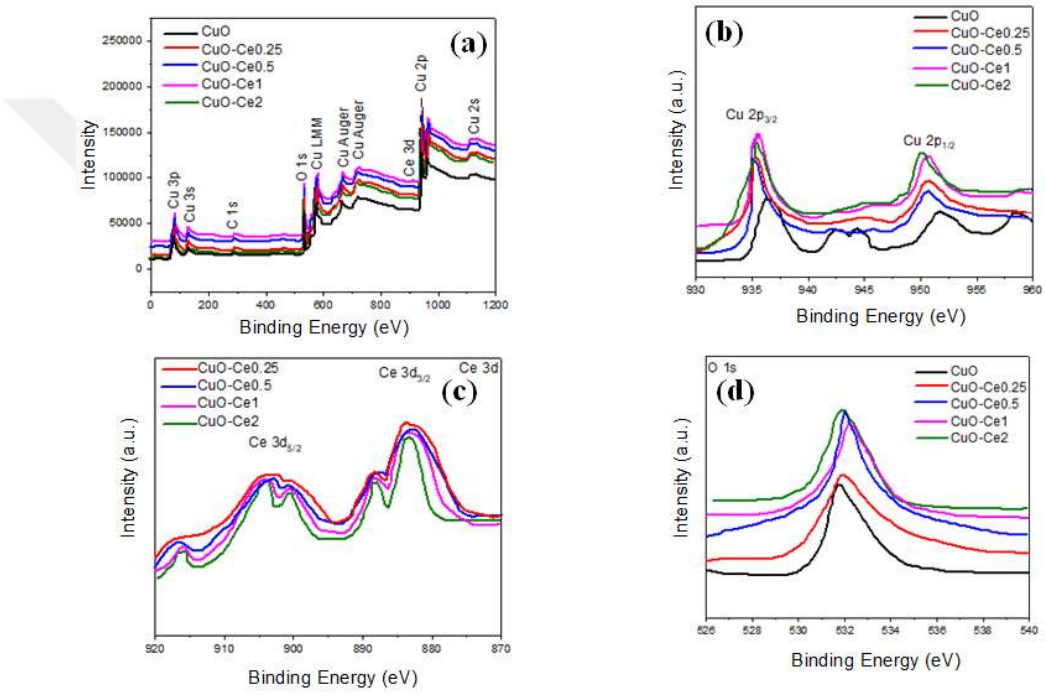

Figure 4.18 XPS spectra of undoped and Ce doped CuO nanoparticles (a) survey spectra (b) core level spectra of copper, (c) core level spectra of cerium, (d) core level spectra of oxygen.

According to Hu et al., the two peaks in the high-resolution spectra of O 1s shown in Figure 4.18(d) at 529.5 eV and 531.6 eV are typical peaks of the low-energy component at 529.5 eV connected to Cu-O binding (Hu et al., 2020). Moreover, the deconvoluted peaks of the O 1s spectra suggest that the more prominent binding energy peak is related with the surface oxygen vacancies caused by Ce^{3+} and Ce^{4+} doping in the CuO lattice (I. Singh et al., 2018).

The leftward shift observed in the spectra with Ce doping is due to changes in the chemical environment and bond structures caused by the incorporation of Ce into the material. This shift is related to the reorganisation of the local electronic environment of oxygen atoms as a result of Ce doping into CuO or other structure. Ce doping can cause the binding energy to decrease by reducing the electron density around the oxygen atoms, which manifests as a leftward shift in the spectrum. This leftward shift reflects the effect of Ce on the low oxidation state or bond structure within the material and reveals changes in the material's chemical structure (I. Singh et al., 2018; Singh et al. 2022).

4.3 Characterization Results of SnO_2 Nanoparticles

4.3.1 Characterization Results of Undoped SnO_2 Nanoparticles

The chemical, physical, and morphological features of the final product formed during the sol-gel technique are substantially determined by the sol composition, reaction temperature, pH, catalyst type, and drying conditions. One of these variables, the pH of sol-gel solutions, substantially impacts the formation of the three-dimensional structural network and the final physical shape. The pH value directly affects the speed of hydrolysis and condensation reactions, which are crucial for achieving the appropriate nanostructure characteristics. During the sol-gel reaction, hydrolysis and condensation reactionsoccur concurrently and at varying rates, and the rates of these reactions can be adjusted to proper pH levels, resulting in changes in the kinetics of the process (Koç et al., 2020). This variable determines the microstructure of sol-gel gels. Therefore, it is a crucial parameter forpH control. The acidity of the reaction medium has a significant impact on the rate of condensation and hydrolysis processes.

The characterisation results of SnO_2 nanoparticles, whose synthesis method is given in detail in section 3.1.2, are given below. XRD pattern of SnO_2 nanoparticles synthesized with different pH values is given in Figure 4.19. All diffraction peaks are ascribed to the tetragonal crystalline phase of tin oxide with a reference JCPDS cardno: 41-1445. Strong diffraction peaks appear at 26.61°, 33.89°, 37.95°, 51.78°, 69.23°, 71.77° and 78.71° correspond to the (110), (101), (200), (211), (221), (301), and (321)

planes and are in good agreement with the rutile (tetragonal) structure of the SnO_2 crystal. XRD results indicate that the diffraction maxima become sharper and more distinct as the pH increases.

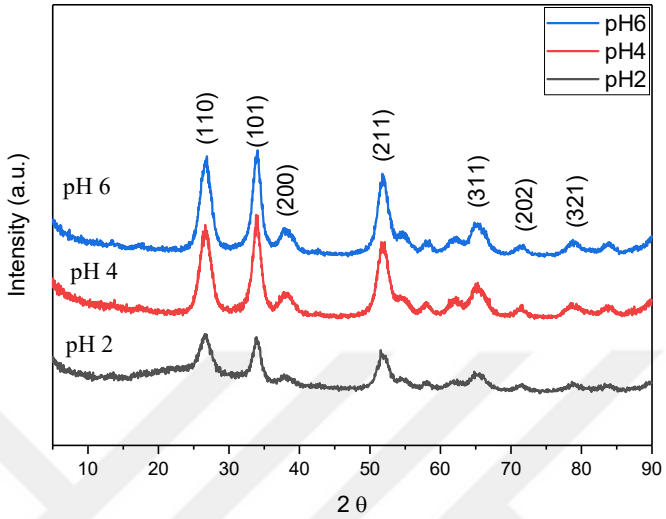

Figure 4.19 XRD pattern of SnO_2 nanoparticles synthesized with different pH values (calcination temperature 400 °C)

According to the XRD data, the diffraction peaks sharpen and become more noticeable as the pH level rises, suggesting that a higher pH level promotes crystallization and average crystallite size. The Debye-Scherrer equation determined that SnO_2 nanoparticles synthesized at pH 2, 4, and 6 have crystallite sizes of 6.24 nm, 6.29 nm, and 6.52 nm, respectively (Holzwarth & Gibson, 2011). These results validate the impact of pH variation on the size and crystal structure of SnO_2 nanoparticles. Rapid nucleation at low pH levels results in small crystallites and low crystallinity. In contrast, more controlled nucleation and a slow growth process at higher pH levels produce more prominent crystalline structures, as reported in the literature by Lwin et al and Richa et al. (Lwin et al., 2015; Richa et al., 2017).

Enhanced crystal stabilization and the generation of larger crystallites are achieved through heightened hydrolysis and condensation processes at elevated pH levels (Lwin et al., 2015; Richa et al., 2017). As a result, increasing pH level emerges as a fundamental mechanism that significantly affects the crystal size and crystallinity of SnO_2 nanoparticles. Figure 4.20 shows the size distribution histogram and SEM images of the synthesized particles at various pH levels. The measurements prove that

all particles are at the nanoscale. The measured mean particle size values are 66.42 nm, 115.2 nm, and 256.8 nm, depending on the pH increase. The investigations show that particle size increases as the pH rises.

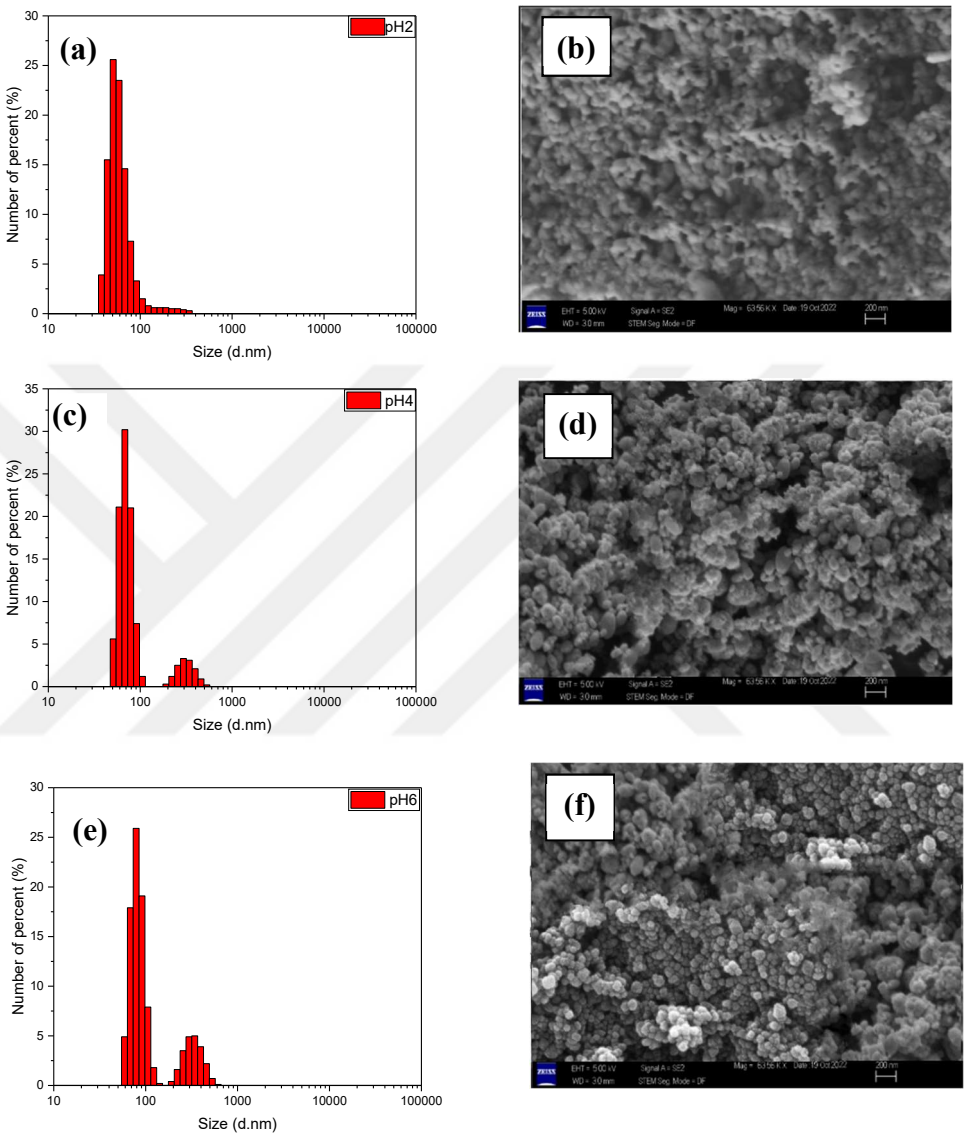

Figure 4.20 Particle size distribution histograms and SEM images SnO_2 nanoparticles synthesized at different pH values (a), (b) pH2 and (c), (d) pH4, (e), (f) pH6

Figure 4.21 demonstrates FTIR analyzes for SnO_2 nanoparticles synthesized at pH values of 2, 4, and 6, FTIR spectra were obtained from 4000 to 450 cm^{-1}. The spectra shows a wide range between 3400 and 3550 cm^{-1}, equivalent to the free hydrogen-bonded hydroxyl groups' OH- stretching vibrations (Krishnakumar et al., 2009). Another peak at 1637 cm^{-1} is presumably due to moisture absorption from the air

during measurement (Rajesh et al., 2014).It is hypothesized that large surface areas of these nanostructured materials cause water from the atmosphere to adsorb quickly (Horti et al., 2018). The low intensity and weak peaks observed in the 2923 cm-^{1}, 2854 cm-^{1}, and 1468 cm-^{1} regions of the spectrum are attributed to C-H vibrations (Shaalan et al., 2016). These C-H bonds can be attributed to organic residues left in the sample after calcination.

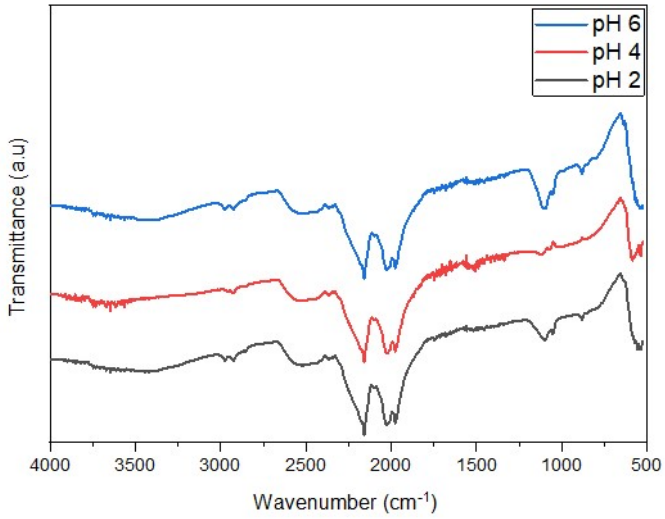

Figure 4.21 FTIR spectrum of SnO_2 nanoparticles synthesized with different pH values

The peak at 1200 cm^{-1} indicates vibrations of the hydroxyl tin (Sn-OH) bond (Horti et al., 2018). The most prominent and sharpest peak was observed at 624 cm^{-1}, representing the Sn-O functional groups of SnO_2 (Elci et al., 2018).This finding confirms that our FTIR study confirms the creation of SnO_2 metal oxide, indicating successful nanoparticle synthesis and characterization. The process of calcination modifies the crystal structures and physical characteristics of nanomaterials, significantly impacting particle size and morphology (G. Zhang & Liu, 1999). Temperatures of 400°C and 500°C were selected for the calcination process, which was conducted at these temperatures while maintaining a constant pH to explore further the impact of calcination temperature in the second part of this investigation. Reducing the calcination temperature restrains particle growth, resulting in more controlled crystal growth and more diminutive, uniform nanoparticles. These findings suggest that optimizing the calcination temperature is critical to ensure that the nanomaterials have the desired properties. Figure 4.22 depicts the XRD patterns of

synthesized SnO_2 nanoparticles calcined at different calcination temperature conditions. The crystallite size was calculatedusing the Scherrer Formula based on the XRD pattern (Holzwarth and Gibson, 2011). The crystal structure of SnO_2 nanoparticles is shown to be significantly influenced by the calcination temperature. The patterns revealed significant peaks at 26.61°, 33.89°, 37.95°, 51.78°, 69.23°, 71.77°, and 78.71° 2θ angles in the (110), (101), (200), (211), (221), (301), and (321) planes. These peaks confirm that the tin oxide phase is rutile (tetragonal) in accordance with JCPDS File No. 41-1445. The Scherrer formula yielded crystallite size values of 6.24 nm for SnO_2 nanostructures calculated at 400°C and 7.02 nm for those calcined at 500°C (Wu et al. 2007; Subramaniam et al. 2018). These results suggest that when the calcination temperature rises, the size of the crystallites increases. Additionally, it was discovered that a rise in peak density and an expansion in crystal size correspond with an increase in calcination temperature. These changes observed in Figure 4.22 reveal a densification trend that becomes more pronounced in the grain expansion and crystal structure with increasing calcination temperature.

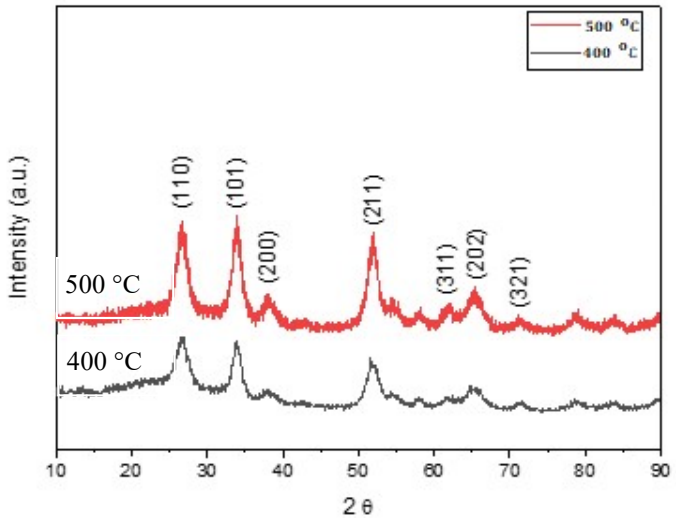

Figure 4.22 XRD pattern of SnO_2 nanoparticles calcined at different calcination temperatures (pH2)

Furthermore, the absence of any second phase or imperfections in the structure suggests that all samples belong to the high purity phase of SnO_2. The literature has revealed findings that are similar to our findings. Lwin et al. and Verma et al. stated that increasing calcination temperature promotes crystal growth, which leads to a decrease in peak width and an increase in crystalline density observed in XRD patterns(Lwin et al., 2015; Verma et al., 2022). As a result, determining the optimal

calcination temperature is critical for achieving desired particle sizes and increasing nanoparticle performance. Thus, this investigation and findings from the literature corroborate the crucial significance of calcination temperature for the crystal structure and size distribution of SnO_2 nanoparticles.

Figure 4.23 shows particle size distribution and SEM images of SnO_2 nanoparticles calcined at 400 and 500°C. Grain formation was seen at high temperatures since it was discovered that the diffusion rate increased with temperature. SnO_2 nanostructures are created by the thermal breakdown of their predecessors during calcination.

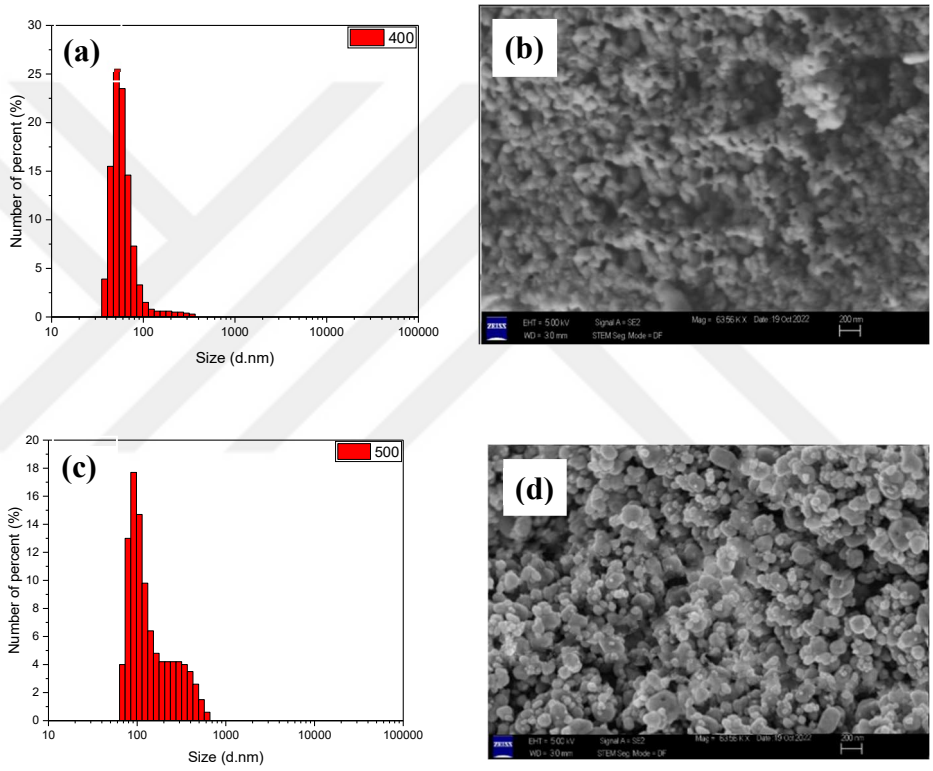

Figure 4.23 Particle size analysis and SEM images of SnO_2 nanoparticles calcined at different temperatures: (a), (b) 400 °C; (c), (d) 500 °C

Particle sliding and diffusion then contribute to these nanostructures' structural arrangement and densification. The capacity of the particles to diffuse rises with increasing calcination temperature, and the slow development of crystalline particles facilitates more precise crystal structure correction. Due to the high surface energy between the interfaces of small and large particles, the particles in the crystal can diffuse through the interface to the interior of the crystal structure, leading to the

movement of grain boundaries and crystal growth. High calcination temperatures lead to a significant increase in the degree of sintering and a marked decrease in the voids between the particles, which reduces the degree of lattice distortion, resulting in a more regular crystal structure (Song et al., 2010). The spherical shape, homogeneous distribution, and nano size of the nanoparticles produced are significant discoveries in assessing the morphological impacts of pH and calcination temperature.

This evaluation provides support for particle size analyses. Morphological investigation of produced SnO_2 nanoparticles demonstrates that the size of nanoparticles increases significantly with increasing calcination temperature. The difference between particles calcined at 400°C and 500°C can be explained by an increase in diffusion rate at higher temperatures, resulting in faster grain development. Consequently, obtained results reveal that the synthesis conditions of SnO_2 nanoparticles, particularly parameters of the calcination temperature and pH, have significant impact onthe morphological characteristics and final product's particle size.

Figure 4.24 presents the FTIR spectrum of the SnO_2 nanoparticles calcined at 400 and 500 °C temperature. The stretching vibration of the -OH groups of $Sn(OH)_2$ and adsorbed water molecules on the surface of SnO_2 nanoparticles are related to the broad spectrum at about 3400 cm^{-1}.

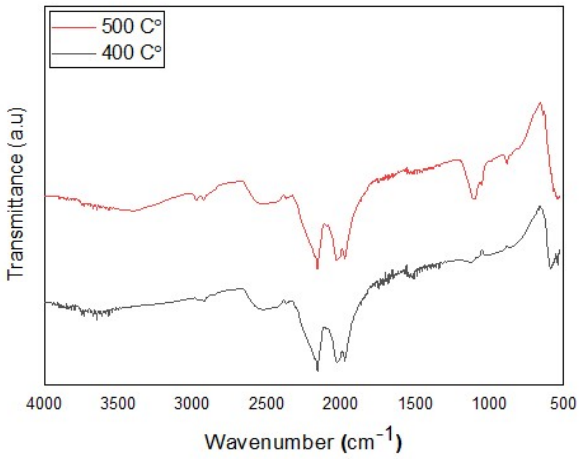

Figure 4.24 FTIR spectrum of SnO_2 nanoparticles calcined at different temperatures

Peak intensity reduce suggests that high temperature evaporation removes -OH groups from the sample. The lowest band in the 500–600 cm^{-1} range was identified as the SnO_2 O–Sn–O or Sn–O stretching vibration band. (Dangi et al., 2023). The signal at 1634 cm^{-1} is correlated with the stretching and bending bonds of adsorbed water molecules. The strong band at 3639 cm^{-1} is connected to the vibration of the hydroxyl group, whereas the peak at 2875 cm^{-1} is linked to C-H stretching (Saranya & Selladurai, 2018). When the calcination temperature is lowered, a decrease or disappearance of some spectral peaks is observed in FTIR analysis. This indicates that the calcination process changes the molecular structure and surface chemistry. In particular, organic residues and hydroxyl groups can provide high activity on the surface but can cause the weakening of O-Sn-O bridging bonds. On the other hand, some peaks exhibit a decline in strength or disappearance when the calcination temperature is lowered, suggesting that the calcination process has altered the molecular structure and surface chemistry(Gaber et al., 2014).

The compositions and surface chemical states of SnO_2 nanoparticleswere determined by XPS (Figure 4.25).

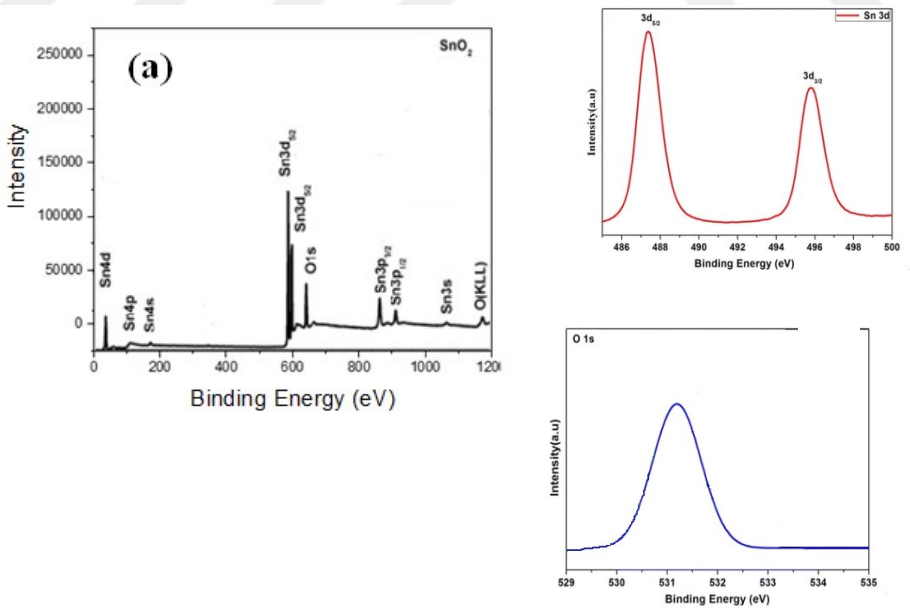

Figure 4.25 XPS spectra of SnO_2 nanoparticles (a) survey spectra (b) core level spectra of Sn, (c) core level spectra of oxygen

The survey scan of SnO_2 nanoparticles is shown in Figure 4.25(a), where the appearance of O 1s and Sn 3d peaks confirm the presence of Sn and O. The existence of Sn and O components in the products is confirmed by the XPS spectra shown in Figure 4.25(b). The Sn^{4+} oxidation state in the produced SnO_2 is confirmed by the binding energies of Sn, which are 486.4 eV and 494.9 eV (Collins et al., 2013). In Figure 4.25(c), the prominent O1s peaks corresponding to lattice oxygen are concentrated at 531.4 eV. According to previous research findings, chemisorbed oxygen plays an essential role in the reactions occurring on the surface of the synthesized particles (Gu et al., 2017).

4.3.2 Characterization Results of (Mn; Ce) doped SnO_2 Nanoparticles

The X-ray diffraction pattern of synthesized undoped and with varying Mn doping molar concentrations (0.25%, 0.5%, 1% and 2%) tin oxide nanoparticles is shown in Figure 4.26. The tin oxide phase structure is consistent with JCPDS File No. 41-1445 and rutile (tetragonal) in nature, as indicated by all diffraction peaks. The XRD study verified that the undoped and Mn doped SnO_2 nanoparticles have the same crystal structure. No additional contamination or second phase was found in the SnO_2 structures. Figure 4.26 shows that the XRD peaks are short and broad. The small crystallite sizes are the cause of the diffraction peaks' width. The Scherrer formula was used to determine the crystallite size of the synthesized SnO_2 nanoparticles. The average crystallite size of undoped SnO_2 nanoparticles was 6.24, 6.78, 5.94, 5.83, and 5.11 nm, while the average crystallite size increased with increasing Mn doping concentration (Holzwarth and Gibson, 2011). The results show that Mn ions prevent crystal grains in the SnO_2 matrix from growing. It was discovered that when the quantity of Mn ions increased, the unit cell volume values and lattice characteristics dropped. This could be due to substituting larger Sn^{3+} ions (0.71 Å) with smaller Mn^{3+} ions (0.53 Å), reducing lattice parameters and unit cell volume. When Mn^{4+} ions substitute the place of Sn^{4+} ions, unit cell volume, and lattice characteristics decrease, which is in line with findings reported in the literature (Ragupathy et al., 2023; Rajeshwaran & Sivarajan, 2015; Venugopal et al., 2014).

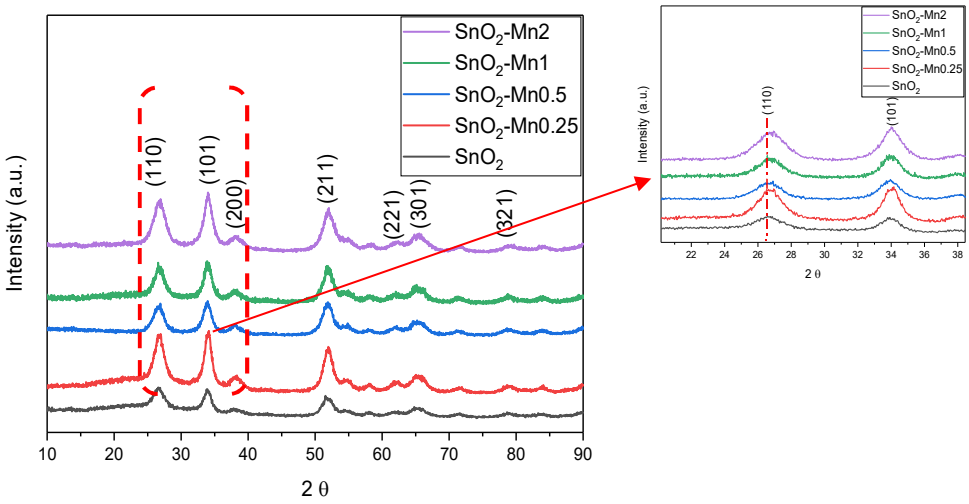

Figure 4.26 XRD pattern of undoped and Mn doped SnO_2 nanoparticles.

Figure 4.27 shows SEM pictures and a particle size measurement histogram of the undoped and Mn doped SnO_2 nanoparticles. As the Mn doping amount increased, the particle size values of SnO_2, SnO_2-Mn0.25, SnO_2-Mn0.5, SnO_2-Mn1, and SnO_2-Mn2 nanoparticles were measured as 66.42, 64.81, 53.63, 52.54 and 40.66 nm, respectively.

It can be seen that the increase in Mn doping rate visibly leads to a reduction in particle size. The literature has published comparable outcomes (Salah, Habib, & Azam, 2016; Salah, Habib, Azam, et al., 2016). This size reduction can be explained by the fact that Mn^{3+} ions have a smaller ionic radius than Sn^{4+} ions and the resulting distortion in the lattice structure (Williams et al., 2021).

Figure 4.28 displays the FTIR spectrum of SnO_2 nanoparticles doped with varying Mn concentrations. According to Choi et al., the oxide bridge functional group is responsible for the emergence of the new wide band centered at 624 cm^{-1}, which shows that SnO has transformed into SnO_2 (Choi et al., 1994). According to Z. Li et al., the band seen at 1366 cm^{-1} can be attributed to the bending modes of various surface hydroxyl group types (Li et al., 2005).

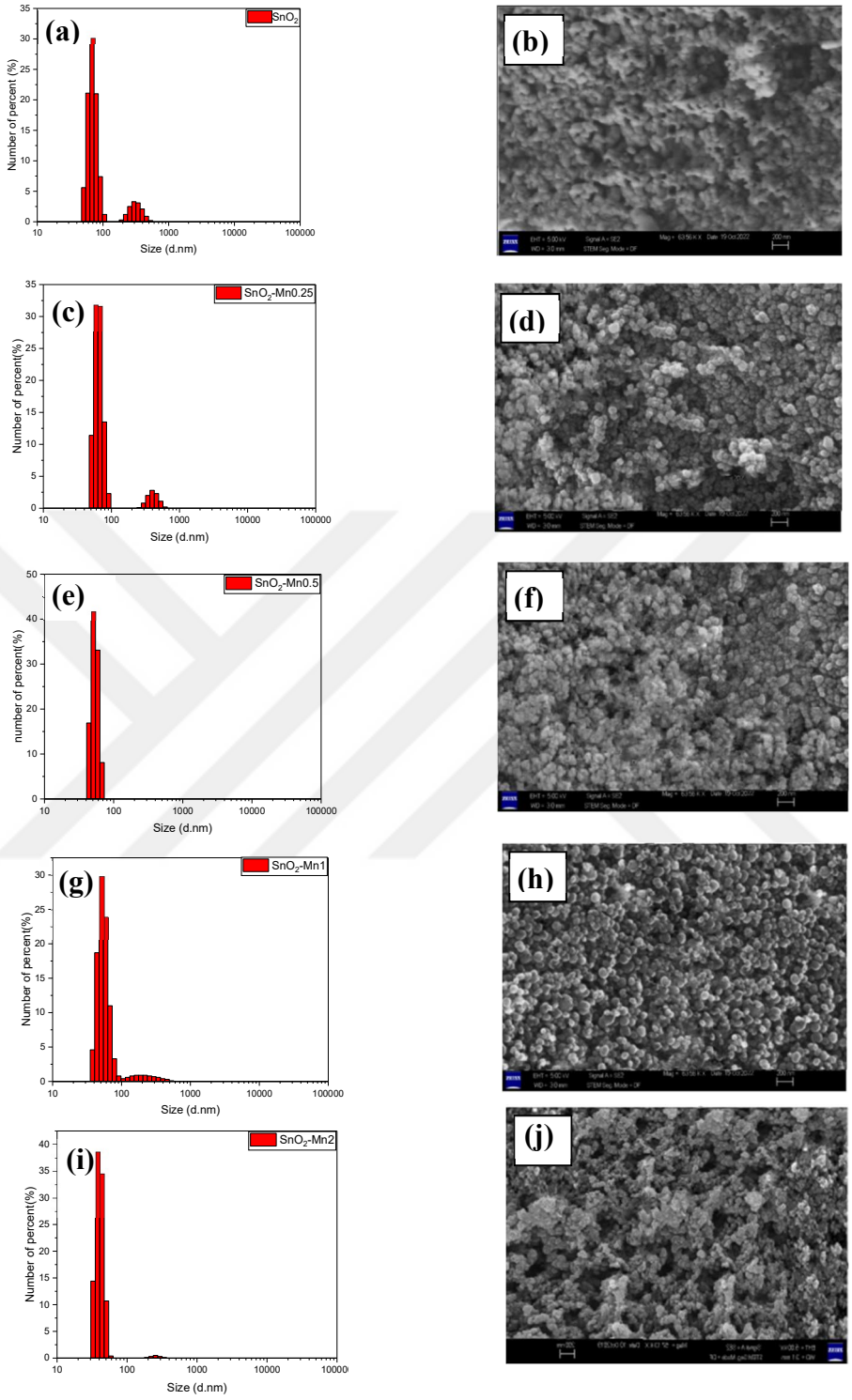

Figure 4.27 Particle size distribution histograms and SEM images (a), (b) undoped SnO_2 and (c), (d) 0.25%, (e), (f) 0. 5%, (g), (h) 1%, (i), (j) 2% Mn doped SnO_2 nanoparticles.

The weak peaks in the 2200 cm^{-1} range are due to the in situ recording of the spectra and the absorption of water or CO_2 from the ambient atmosphere. The presence of hydrogen bonds implicated in O-H oscillations is indicated by the weak vibrations at around 3750 cm^{-1}, which might be caused by Sn-OH groups and adsorbed water (Sambasivam et al., 2010).

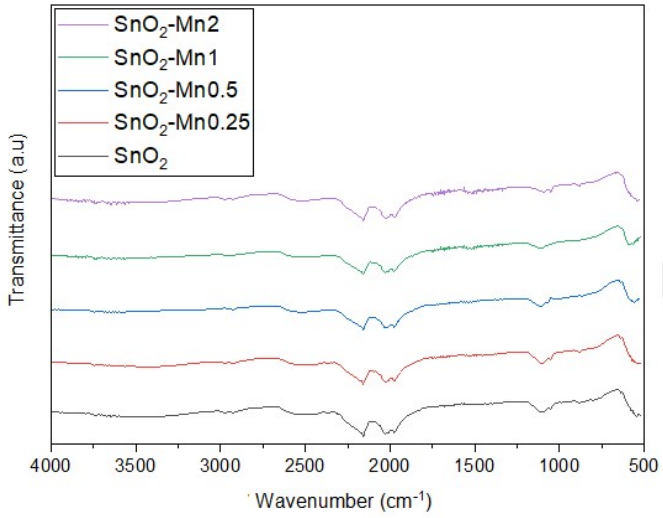

Figure 4.28 FTIR spectra of the undoped and Mn doped SnO_2 nanoparticles

XPS analysis was performed to determine the binding energy and oxidation states of the synthesized SnO-Mn2 nanoparticles. Sn, Mn, and O elements in the broad scan spectra shown in Figure 4.29(a) verified the synthesized samples' purity. The high-resolution XPS spectrum of Sn3d in Figure 4.29 (b) indicates the binding energies of $Sn3d_{5/2}$ and $Sn3d_{3/2}$ with double peak signals at 485.79 eV and 494.15 eV. The energy separation of 8.36 eV between these pairs is consistent with the +4 oxidation state of Sn (Vindhya and Kavitha, 2023b). The Mn2p spectrum in Figure 4.29 (c) represents the $Mn2p_{3/2}$ and $Mn2p_{1/2}$ oxidation states with peaks of 642.08 eV and 653.57 eV binding energies. The effective integration of Mn^{2+} ions into the SnO_2 lattice is shown by the spin orbit interaction energy of 11.49 eV between these peaks. High-resolution analysis of O1s spectra presented in Figure 4.29 (d) reveals a binding energy peak of 529.74 eV, indicating the presence of Sn–O or Mn–O bonds with OH ions adsorbed on the surface. Mn-doped SnO_2 nanoparticles showed a slight change in the binding energies of the Sn $3d_{5/2}$ and Sn $3d_{3/2}$ states, as determined by XPS analysis. This shift reveals the successful incorporation of Mn into the SnO_2 lattice structure and the doping effect of Mn at the oxygen sites (Güldüren et al., 2021; Gupta et al., 2023).

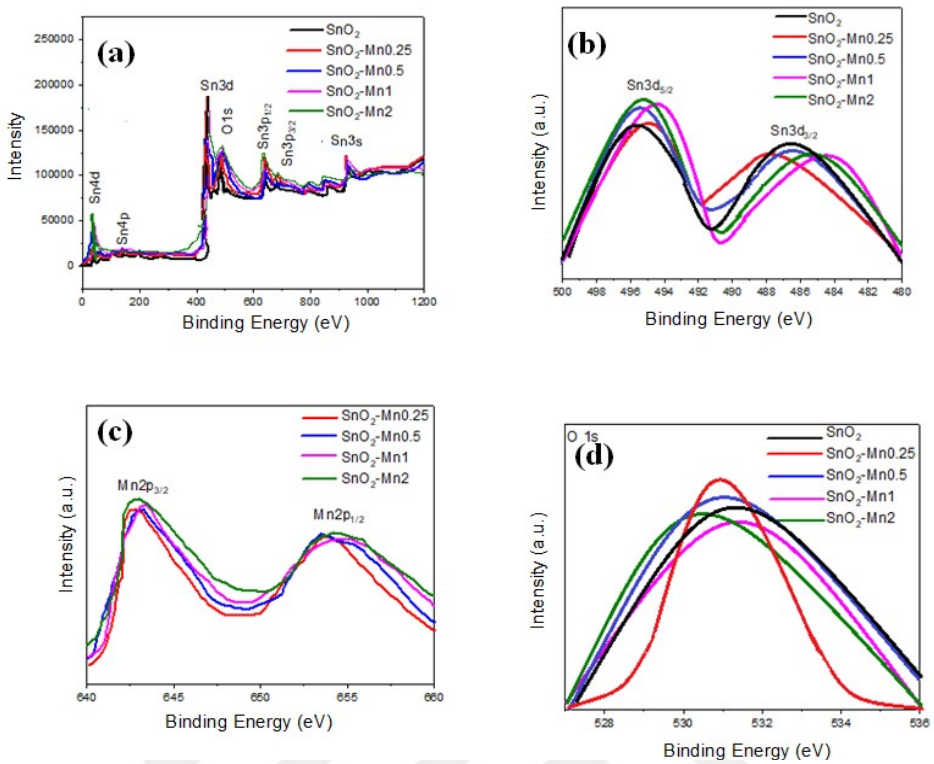

Figure 4.29 X-ray photoelectron spectroscopy of Mn doped SnO_2 nanoparticles (a) survey spectra, (b) core level spectra of tin, (c) core level spectra of magnesium, (d) core level spectra of oxygen

The rightward shifts observed in the SnO_2 structure with Mn doping are due to changes in the electronic and chemical structure of the material caused by Mn doping. When Mn atoms are incorporated into the SnO_2 structure, the local electron density and bond energy of Sn-O bonds are affected. Mn is usually present in the +2 or +3 oxidation states, resulting in a different electronic structure compared to Sn^{4+} (Agrahari et al. 2015). Mn doping increases the binding energy around the oxygen atoms in the SnO_2 structure, manifested by a rightward shift in the XPS spectrum. This shift is associated with factors such as stretching in the crystal structure, changes in bond lengths, and rearrangements in the local chemical environment that occur upon incorporation of Mn into SnO_2. In addition, Mn doping often alters the surface adsorption properties, which may result in rearrangements of OH^- or other ions on the surface and changes in binding energy. As a result, doping of Mn into SnO_2 leads to rightward shifts in the bond structure with these effects (Güldüren et al., 2021; Gupta et al., 2023; Lavanya et al., 2017).

Figure 4.30 depicts the undoped and Ce doped X-ray diffraction (XRD) spectra of produced SnO_2 nanoparticles. The X-ray diffraction patterns of undoped and doped SnO_2 nanoparticles with different Ce amounts (0 to 2%) show distinct peaks in the (110), (101), (200), (211), (221), (301) and (321) planes corresponding to 2θ angles of 26.61°, 33.89°, 37.95°, 51.78°, 69.23°, 71.77° and 78.71°. All diffraction peaks depict the tin oxide phase has a rutile (tetragonal) structure, which is appropriate with JCPDS File No 41-1445 (McCarthy & Welton, 1989).

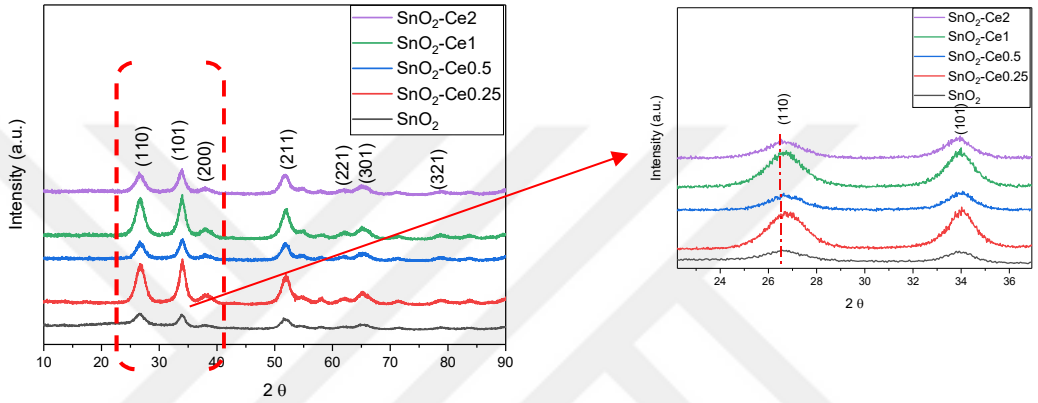

Figure 4.30 XRD pattern of undoped and Ce doped SnO_2 nanoparticles

XRD measurements indicated that both undoped and doped nanoparticles had the same crystal structure, indicating that doping did not lead to a phase change in the structure. Figure 4.30 shows an increase in peak intensity in the XRD patterns of SnO_2 with increasing Ce incorporation, and the peaks shift to larger 2θ values. Li et al. also reported a similar situation, and it was emphasized that the crystallinity of SnO_2 increased with increasing Ce addition (C. Li et al., 2009). This is attributed to Ce ions, which stabilize the crystal structure by integrating into the SnO_2 lattice and forming a more ordered structure. Integrating Ce ions into the crystal structure reduces crystal defects and creates a structure with better crystallinity, leading to sharper and more intense XRD peaks. Changes in the lattice parameters are connected to the shift of the peaks to higher 2θ values. Ce doping occurs when Ce^{4+} (0.092 nm) or Ce^{3+} (0.103 nm) ions replace Sn^{4+} (0.071 nm) ions with smaller ionic radius in the SnO_2 lattice. This substitution causes a narrowing of the lattice and, thus, an increase in the diffraction angles (2θ) in XRD patterns. Silun Zhu et al. reported that the larger ionic radius of Ce ions leads to a change in the host lattice parameters, explaining the shift of the peaks in XRD patterns to larger 2θ values (S. Zhu et al., 2022).These shifts are related to

additional stress levels and imperfections in the crystal structure. According to Ali Baig et al., introducing Ce into the crystal structure creates defects that hinder crystal growth, decreasing crystallite size. While this is seen in XRD patterns with peak broadening, the shift of peak positions to larger 2θ values also indicates these structural changes (Ali Baig et al., 2021). Crystallite sizes have been calculated from XRD data using the Scherrer formula. The typical crystallite size of SnO_2 nanoparticles with varying Ce doping levels, SnO_2, SnO_2-Ce0.25, SnO_2-Ce0.5, SnO_2-Ce1, and SnO_2-Ce2, were6.24, 5.83, 5.94, 5.78, and 5.36 nm, respectively. As a result, the increase in peak intensity observed in the SnO_2 structure with Ce doping indicates the improvement of the crystal structure. In contrast, the peak shift to larger 2θ values can be explained by the lattice parameter changes and the crystal structure's stress. These results emphasize the significant impact of Ce doping on the structural characteristics of SnO_2 and are consistent with research reported in the literature.

A comprehensive investigation was conducted utilizing SEM and DLS methods to assess the impact of Ce doping on the morphological characteristics of SnO_2 nanoparticles (Figure 4.31). SEM analysis demonstrated that both undoped and Ce doped SnO_2 nanoparticles have a spherical shape and display a uniform distribution. Particle size analysis using the Dynamic Light Scattering (DLS) technique indicates that there is a significant decrease in particle size with increasing Ce content.

In particular, while the particle size of SnO_2 nanoparticles produced without Ce doping was 66.42 nm, the particle sizes of SnO_2 nanoparticles with Ce0.25, Ce0.5, Ce1, and Ce2 doping were measured as 66.42 nm, 59.02 nm, 41.41 nm and 45.34 nm, respectively. This is because Ce doping slows down crystal growth, increases the number of dislocations and structural vacancies, and changes the surface energy to form smaller and homogeneous nanoparticles. These findings show that SnO_2 nanoparticles obtained by Ce doping can provide performance improvement in advanced applications requiring high surface area, especially in catalysis and sensor Technologies (Asaithambi et al., 2021; N. Chen et al., 2021; Veerabhadrayya et al., 2020).

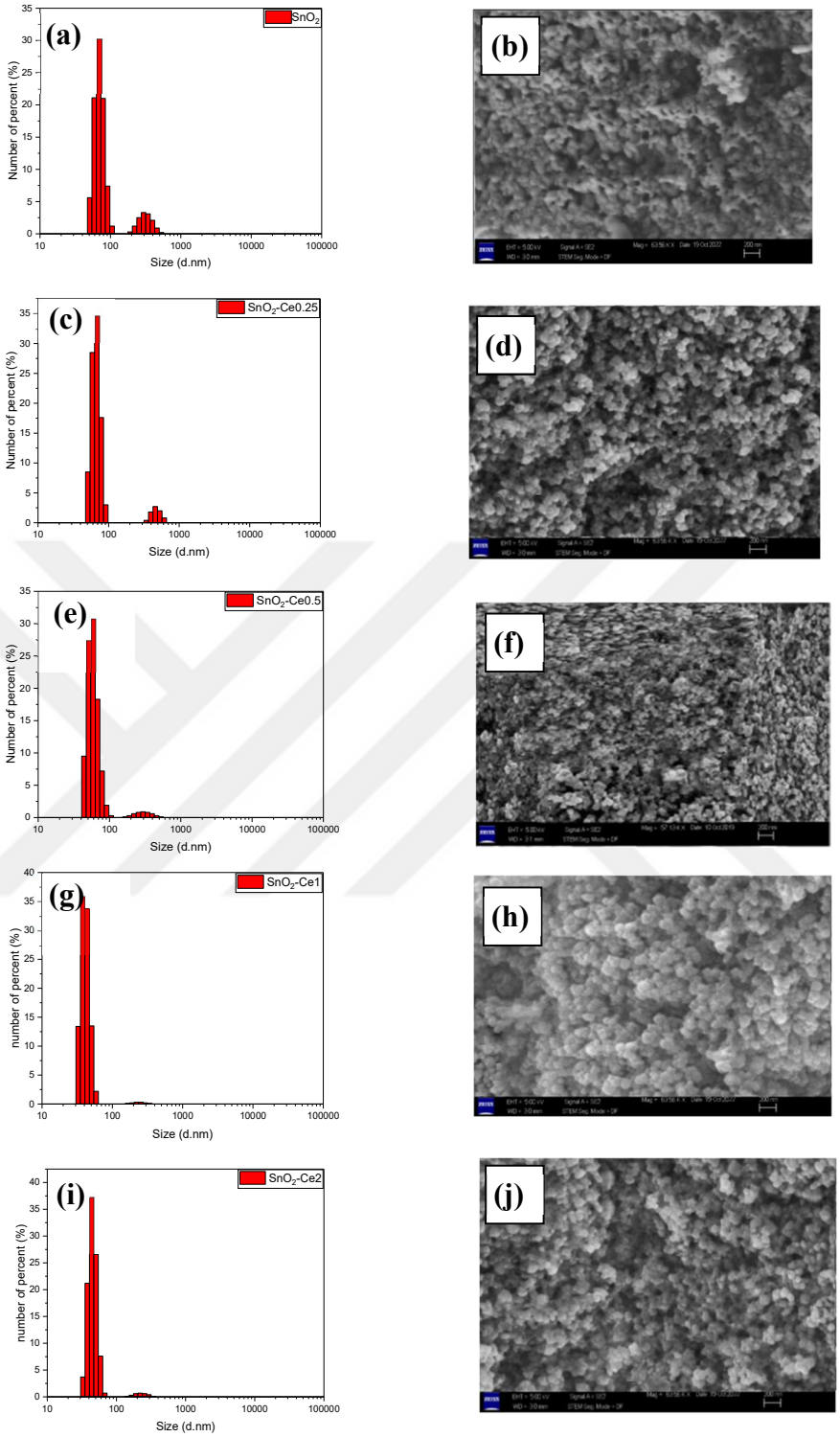

Figure 4.31 Particle size distribution histograms and SEM images (a), (b) undoped SnO_2 and (c), (d) 0.25%, (e), (f) 0. 5%, (g), (h) 1%, (i), (j) 2% Ce doped SnO_2 nanoparticles

Figure 4.32 presents the findings of FTIR spectroscopy, which was used to identify the distinctive molecular vibrations of the obtained samples. In the FTIR spectra, a wide absorption peak was observed in the range of approximately 3310-3500 cm^{-1},

which is indicative of water (H_2O) molecules. This peak corresponds to the O–H stretching vibration modes of hydroxyl (-OH) groups adsorbed on the surface (Mani et al., 2017).A peak at 2358 cm^{-1} assigns the existence of CO_2 molecules in the air (Agrahari et al., 2016).

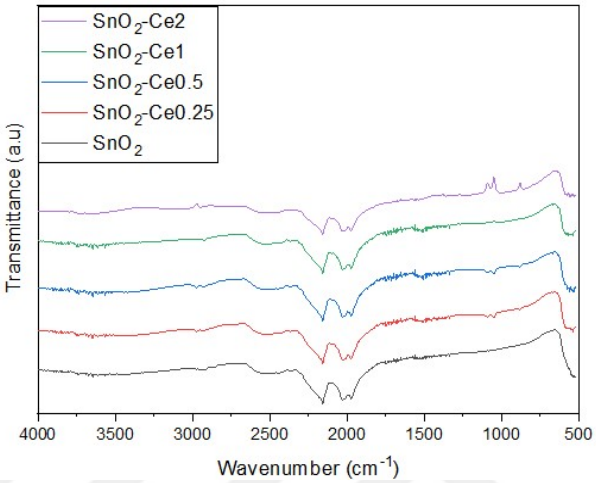

Figure 4.32 FTIR spectra of undoped and Ce doped SnO_2 nanoparticles.

The asymmetric stretching vibration of tin-hydroxyl (Sn-OH) seen at 1655 cm^{-1} in Sn-O-Sn and Ce-O modes or influential bridge groups of SnO_2 is correlated with molecular stretching vibrations at 560-730 cm^{-1}. Ce doping affects the SnO_2 host lattice, causing modest variations in band intensities in the spectra (Selleswari et al., 2019). No further absorption bands were seen, although the Ce-O bond in the SnO_2 crystal phase successfully demonstrated the substitution of Ce by Sn (Singh et al., 2019). Particle size, local defects, and nanoparticle form are the main causes of variations in the placements, shapes, and widths of the peaks in the FTIR spectrum. In this study, it was found that FTIR bands broadened and peak intensity decreased when Ce doping ratio increased. These changes indicate the integration of Ce ions into the matrix structure and thus local distortions in the structure (Ahmed et al., 2019; Bhawna et al., 2020; Selleswari et al., 2019).

Figure 4.33 represents the findings of the XPS analyses carried out to examine the sample's chemical structure. Binding energy corrections were done by referencing the C1s peak at 284.6 eV. At 881.5 eV, 885.4 eV, 900.3 eV, and 904.1 eV, distinct binding energies were observed in the deconvolved spectra of Ce 3d, as seen in Figure 4.33 (b).

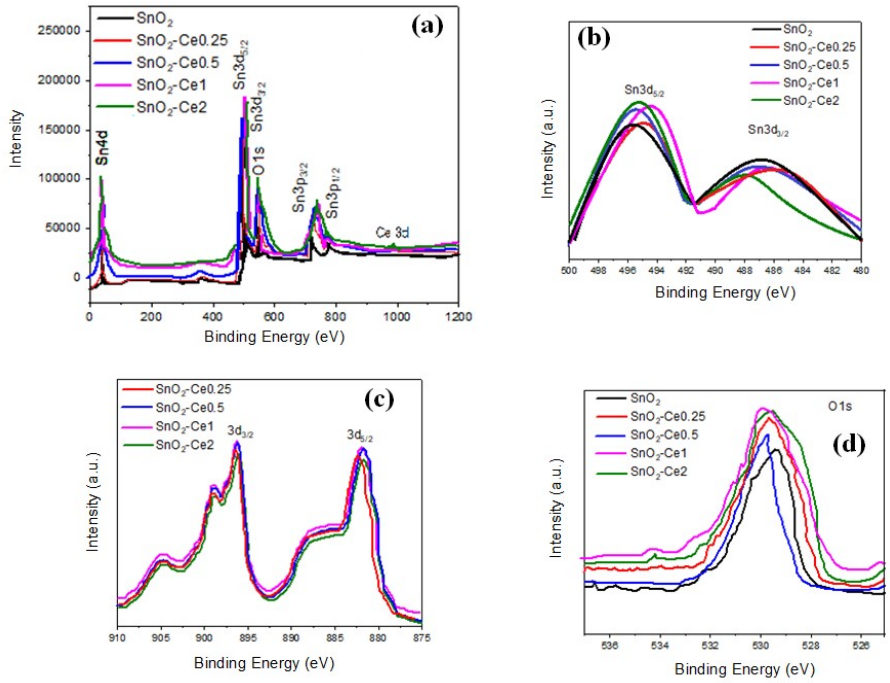

Figure 4.33 X-ray photoelectron spectroscopy of the Ce doped SnO_2 nanoparticles (a) survey spectra (b) core level spectra of tin, (c) core level spectra of cerium, (d) core level spectra of oxygen

These binding energies match Ce $3d_{3/2}$ and Ce $3d_{5/2}$, in that order. The $Sn3d_{5/2}$ and $Sn3d_{3/2}$ peaks are at binding energies of 486.2 eV and 494.6 eV, respectively, according to the Sn spectra in Figure 4.33 (c) (Deivasegamani et al., 2017). Concerning the O1 spectra shown in Figure 4.33 (d), the lattice oxygen atom's binding energy is 529.5 eV (Singh et al., 2020b). Furthermore, a slight shift toward higher binding energy values was observed in the Ce peaks, which suggests a minor rightward change due to the presence of Ce in the sample. This shift could indicate changes in the oxidation state or local electronic environment surrounding Ce atoms (Kumar et al., 2018).

4.4 Electrochemical Detection of Salbutamol with Metal Oxide Nanoparticles Modified Carbon Paste Electrode

The utilization of nanoparticles, with their exceptional surface area, excellent conductivity, and catalytic properties, affects the sensor capabilities of the electrodes. Furthermore, in analytical applications, these structures offer great sensitivity and selectivity while improving the electrode surface's efficiency. Detectionof salbutamol

(SAL), a drug used to treat asthma, in blood and urine samples is critical for pharmaceutical and toxicological analyses. Accurate and reliable determination of SAL is very important for drug dosage control and patient safety. Carbon paste electrodes modified with metal oxide nanoparticles allow sensitive and rapid determination of SAL by electrochemical measurements. Such alterations are crucial for improving the sensitivity and selectivity of the sensors used in SAL detection, which leads to more reliable and accurate findings. Metal oxide nanoparticles were used to modify carbon paste electrodes and the type and amount of doping elements added to the metal oxide particles were investigated from an electrochemical perspective to investigate the sensor sensitivity and analytical performance in the determination of SAL analyte as an electrochemical sensor application. In this context, the developed sensor is designed to provide rapid and easy detection in clinical settings and is intended to offer a straightforward application approach.

4.4.1 Electrochemical Detection of Salbutamol with Undoped CuO Nanoparticles Modified Carbon Paste Electrode

Cyclic voltammetry (CV) was applied to study the oxidation behavior of salbutamol (SAL) following a suitable deposition procedure, using both CuO nanoparticles modified and bare carbon paste electrode (CPE). CV curves of SAL at 8.5 x 10^{-5} M concentration in 0.1 M pH 7.5 PBS containing 0.1 M KNO_3 are presented in Figure 4.34. These measurements were carried out at a scan rate of 40 mV s^{-1} in the potential range of -1.0 to 1.0 V. In the presence of SAL, a pronounced anodic peak was observed in the CPE modified with CuO nanoparticles at approximately 0.64 V versus the Ag/AgCl reference electrode. The oxidation peak current obtained in the modified CPE was significantly higher than that observed in the bare CPE. It could be hypothesized that the modified CPE significantly contributes to SAL oxidation electrocatalytically and provides an environment suitable for SAL to transfer electrons. The CuO nanoparticles modified CPE 's exceptional electrocatalytic activity may be ascribed to its distinctive characteristics, which include a notable specific surface area, superiorelectrical properties, superb conductivity, and stability. The outstanding electrocatalytic activity of carbon paste electrode (CPE) modified with CuO nanoparticles can be attributed to the distinctive properties of the nanoparticles, such

as large specific surface area, superior electrical properties, high conductivity, and long-term stability (Lu et al., 2024; Santos et al., 2018; Shanbhag et al., 2022; Terbouche et al., 2016; Svancara et al., 2012).

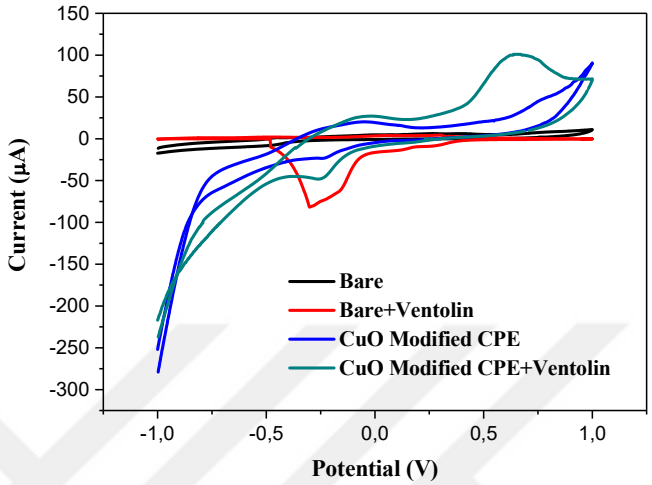

Figure 4.34 CV curves at a bare CPE and 10 wt% CuO nanoparticles modified CPE in the absence and the presence of 8.5 x 10^{-5} M SAL 0.1 M pH 7.5 PBS containing 0.1 M (KNO_3). Scan rate: 40 $mV.s^{-1}$

In the absence of SAL, the modified electrode did not exhibit any electrochemical reaction, indicating that the peak at 0.64 V was caused by SAL oxidation. The results showed that CuO nanoparticle modification could significantly improve the surface activity of current electrodes.

4.4.2 Optimization of Experimental Conditions

Optimization studies should be carried out to maximize the performance of the modified electrochemical sensor. This section of the thesis thoroughly examined several influencing parameters, including pH level, support electrolyte impact, accumulation potential and duration, and nanoparticle concentration, to achieve an ideal electrode and raise the sensitivity and selectivity of the modified electrochemical sensor.

4.4.2.1 Effect of Nanoparticles Amount

The higher amount of CuO nanoparticles in the modified electrodes substantially affects the sensitivity of electrochemical sensors. Therefore, the composition of the

CuO-modified CPE must be adjusted by varying the quantity of incorporated CuO nanoparticles to boost sensor sensitivity. Differential pulse (DP) measurements were used to examine the performance of modified electrodes produced with varied amounts (2 to 20 wt%) of CuO nanoparticles. DP measurements were performed using the modified CPE in a pH 7.5 PBS that included 5 x10^{-5} M Ventolin and 0.1 M (KNO_3). Accumulation took place at -0.3 V for 240 s while stirring continuously, and it stabilized for 15 s after that. Data were recorded with a scan rate of 40 mV.s^{-1} within the potential range of 0.0 V to 0.9 V. As seen in Figure 4.35, the responses obtained extend up to the 10 wt% quantity level. The current responsiveness drops when the modified CPE electrode's CuO nanoparticle incorporation exceeds 10 wt%. Consequently, a lower signal capture is caused by a higher particle load in the redesigned CPE electrode.

An increase in the percentage of the additional particles causes an increase in the number of nanoparticles per unit volume, which in turn causes a drop in the electrolyte contact surface area and a reduction in the accessible detection zones. In addition, an excess of catalyst impedes simple electron transport, leading to a loss of catalytic properties and conductivity, resulting in reduced peak current.

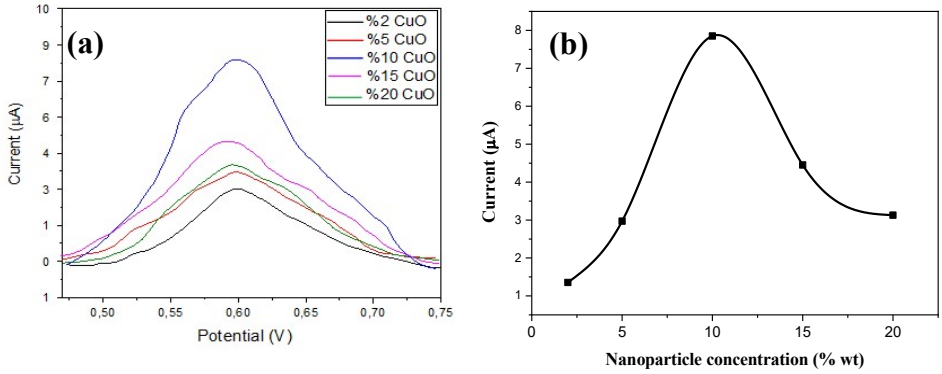

Figure 4.35 Change of current values obtained from differential pulse measurement using different amounts (2 to 20 wt%) of CuO nanoparticles modified CPE in 0.1 M pH 7.5 PBS containing 0.1 M (KNO_3) in the presence of 5 x 10^{-5} M Ventolin.

Furthermore, in the presence of additional nanoparticles, the lower catalytic capabilities and, consequently, conductivity impede easy electron transport, which is what causes the peak current reduction (Shabani et al., 2018; Shetti et al., 2017). In

light of the findings, 10 wt% CuO nanoparticles were added to the CPE electrode in the investigation.

4.4.2.2 Effect of Accumulation Time and Accumulation Potential

The impact of the deposition potential on the peak current magnitude was examined by using differential pulse voltammetry (DPV) throughout a 240 s deposition period in a 0.1 M KNO_3 solution containing 5 x 10^{-5} M Ventolin. The measurements were performed between 0.00 V and 0.9 V at a scan rate of 40 $mV.s^{-1}$. Reducing the accumulation potential from -0.5 V to 0.2 V increased the peak current value. The potential for improvement decreased as it shifted towards a more positive direction (Figure 4.36(a)). It was concluded from the experiment that the acceptable accumulation potential is -0.3 V. Under the same experimental conditions, the effect of deposition time on salbutamol (SAL) oxidation peak current at -0.3 V was also investigated.

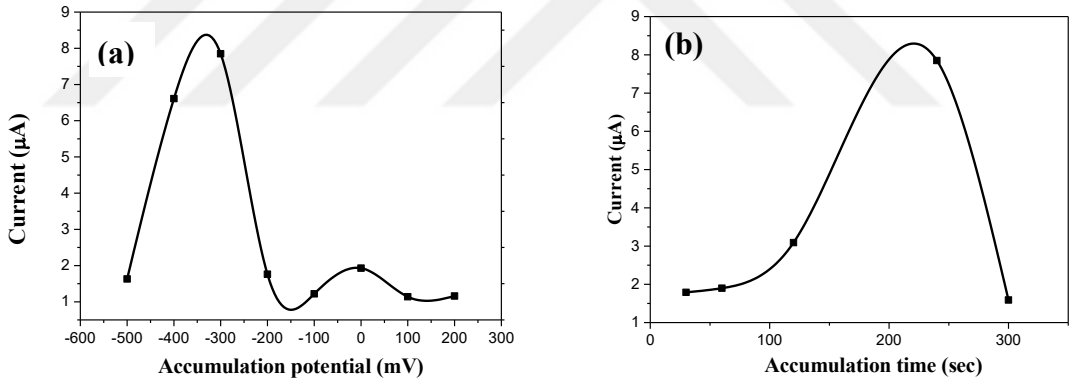

Figure 4.36 (a) The impact of accumulation potential and (b) Accumulating time on the peak current of 5 x 10^{-5} M SAL in 0.1 M pH 7.5 PBS including 0.1 M (KNO_3) on the 10 wt% CuO nanoparticles modified CPE at a scan rate of 40 $mV.s^{-1}$

When the accumulation time was raised, the SAL peak current also steadily increased. Peak currents showed a significant decline after 240 s, as demonstrated in Figure 4.36 (b). In this regard, the most effective accumulation time, taking into consideration both sensitivity and analytical speed, was 240 s.

4.4.2.3 Scan Rate Effect

The peak current of the developed sensors was determined by voltammetrically measuring the effect of 1.0 x 10^{-5} M salbutamol at different scanning rates. Experiments using a wide range of scan rates, from 10 to 1000 $mV.s^{-1}$, revealed a significant correlation between peak current and scan rate (Figure 4.37).

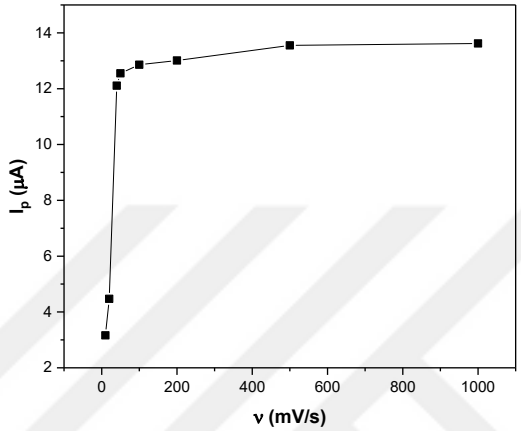

Figure 4.37 Current variations at different scan speeds for CPE modified with 10 wt% CuO nanoparticles

Peak current increases at a faster scanning rate due to both an acceleration of the electrochemical activity of salbutamol and the improvement in the sensitivity of the sensor. However, a decrease in peak current increases was noted at very high scan rates, which may be connected to diffusion control at the electrode surface. The results showed that the maximum sensitivity was obtained at a scan rate of 40 $mV.s^{-1}$.

4.4.2.4 Effect of Support Electrolite and pH

Ion conductivity and the stability of the electrolyte are two variables that affect whether or not electrochemical cells work. Low oxygen mobility of ions at the electrode/electrolyte interface and the rate of interfacial redox reactions limit the effectiveness of electrochemical sensors. It follows that using electrolytes with robust oxygen ion conductivity is essential. Buffer solutions are usually preferred over traditional electrolytes when working with transition metal oxides. Because buffer solutions keep their pH constant, they yield consistent results at different pH levels. Additionally, buffer solutions maintain the characteristics of transition metal oxides

and stop improper reactions by reducing the impact of external variables like acidity or alkalinity. While working with buffer solutions, it is essential to achieve more reliable and consistent results (Islam et al., 2022; Westbroek, 2005).Experiments were conducted to assess the effects of several supporting electrolytes, including KCl, NaCl, $NaNO_3$, and KNO_3 solution (concentration 0.1 M) (Table 4.1). The amount used for the measurements in the DP method was determined as 10 wt% CuO nanoparticles modified CPE. The maximum oxidation peak current of SAL in the KNO_3 solution is shown in Table 4.1.

The oxidation peak of SAL analyt was examined in an electrolyte with a pH range of 4 to 9 and 0.1 M KNO_3 support (Figure 4.38 (a)).From the outset, it is clear that the current responses decrease with increasing pH. As shown, the reaction peak at pH 5.0 and, after that, increased in the direction of a neutral environment. It is observed that the current values reach the maximum value at pH 7.5 (Ghanei-Motlagh & Baghayeri, 2020; Sadeghi et al., 2020).

Table 4.1 Detailed data of DP values of supporting electrolyte solution

Supporting electrolyte solution	**Peak current**	**Peak potential**
NaCl	3.47	0.61
$NaNO_3$	4.05	0.60
KCl	5.55	0.59
KNO_3	7.85	0.55

Consequently, the current investigation employed a pH 7.5 0.1 M KNO_3 solution. The oxidative potential alters negatively with increasing pH, indicating simultaneous proton transport. The reason for the decrease in peak height from pH 4 to pH 5 is the presence of hydrous Cu (II) oxide and hydroxide at pH 4, where the SAL current response reads as around 0.8 V. Moreover, the peak response of around 0.6 V in the case of a pH increase from pH 5 to 7.5 may be explained by the existence of the Cu (II) O form. The SAL reaction was evaluated at 0.4 V, and the decline after pH 7.5

was driven by CuOH generation (Figure 4.38(b)) (Burke et al., 1990; W. Xu et al., 2013).

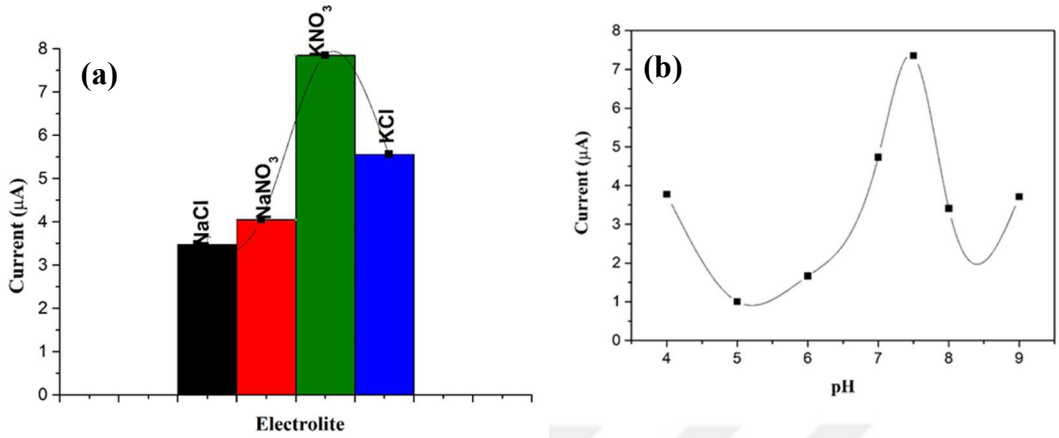

Figure 4.38 Effects of (a) supporting electrolyte solution type and (b) solution pH on the values of the DP peak current (The concentration of SAL solution is 5 x 10^{-5}M)

4.4.2.5 Calibration Curve and Limit of Detection

Differential pulse measurement (DP) was employed in ideal circumstances to quantify SAL. Figure 4.39 illustrates the correlation between anodic peak current and SAL concentration within a concentration range of 0.05 to 500 µM. It has been demonstrated that the oxidation peak current increases with SAL concentration. The calibration graph for CPE modified with 10 weight percent CuO nanoparticles was created under measurement conditions with a scan rate of 40 $mV.s^{-1}$ at various SAL concentrations in 0.1 M pH 7.5 PBS containing 0.1 M KNO_3. Furthermore, the inset displays a similar calibration curve for measuring SAL.

It was discovered that the SAL concentration calibration range was 50 nM to 100 µM, with a correlation value (R^2) of 0.9971. The detection limit (LOD) was calculated using the formula 3 S/m, where S is the standard deviation of the peak current of the lowest concentration over the relevant linearity range (3 runs), and the m value is the slope of the calibration plot. The LOD was determined as 50 nM.

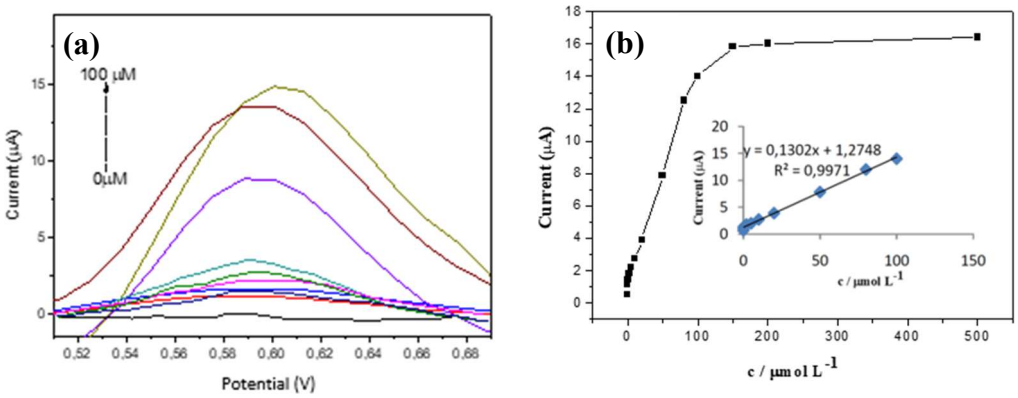

Figure 4.39 (a) DP responses of CuO nanoparticles modified CPE to different, (b) calibration plot used to quantify SAL

4.4.2.6 Selectivity, Repeatability, Reproducibility, and Stability

Under ideal circumstances, DP assessed the repeatability of CPE electrode, stability, and selectivity. The repeatability of the eight parallel sensors was evaluated by comparing the 5 x 10^{-5} M SAL oxidation peak current under identical circumstances. After assessing the repeatability of biosensor, the RSD values were computed to be 3% ($n = 8,\ \bar{x} = 47.06\ \mu M, SD = 0.22$). The DP current response is evaluated for two weeks to monitor the storage stability of the CuO-modified CPE.

The electrode was kept in a dry atmosphere while not in use. After two weeks, it may hold onto 80% of the original signal. The experiment's findings show that the modified electrode exhibits high repeatability and stability. As a last step to confirm the selectivity of the CuO modified CPE sensor, several possible interferents were examined to ascertain their impact on the SAL determination. Research was done on dopamine, glucose, starch, ascorbic acid, epinefrine, Na^{+}, and Fe^{3+} to see how these alien species interfered. Except for dopamine, Figure 4.40 displays the test findings, which indicate that an interference concentration of 8.5 x 10^{-5} M has no discernible effect on SAL signals with deviations less than 10 wt%. The acquired data demonstrated the strong selectivity of this approach for SAL measurement. Current research indicates that undoped CuO nanostructures, including sensors, supercapacitors, photocatalysts, and other devices, cannot meet all requirements. For this reason, additional materials are added to the nanoparticles to create nanocomposites. Researchers have made these kinds of changes to the system to

improve its conductivity and add more components. A process known as doping allows many components to be incorporated into the nanoparticle matrix and nanocomposites to be developed with relatively few element additions.

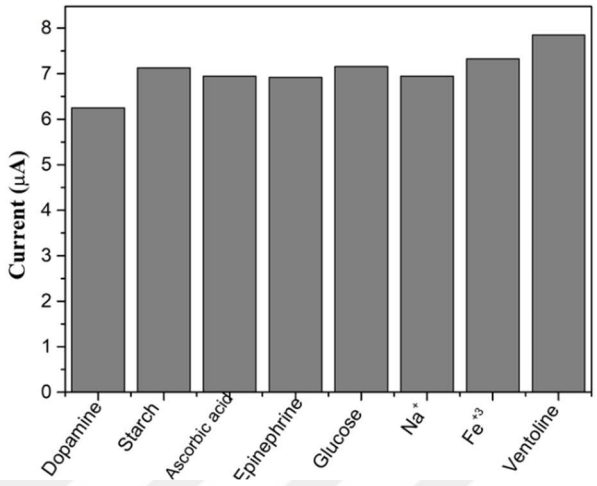

Figure 4.40 DP responses of CPE modified with CuO nanoparticles toward 8.5 x 10^{-5} M SAL 0.1 M pH 7.5 PBS including 0.1 M KNO_3 and other interference compounds

It is commonly recognized that doped nanoparticles with certain elements increase conductivity by creating vacancies and defects. Alkaline atoms, transition metals, noble metals, and inert impurities might all be used as dopants. These dopants can affect the catalytic activity, stabilize the catalytic reduction, promote the active phase's development, or speed up the metal oxide nanoparticles electron exchange rate. They can also modify the concentration of charge carriers, physicochemical properties, surface potential and phase composition, and crystallite size of metal oxide nanoparticles.

The doping of metal oxide nanoparticles may also affect the electronic and physical-chemical characteristics of the nanoparticle surface, such as the sticking coefficients, adsorption and desorption energies, and electronic spectra of surface states. Alkali and alkaline earth elements are well known for promoting electron exchange because of the high charge on the subsequent oxygen atom; transition elements, on the other hand, play a very influential role as dopants to create active sites in metal oxide nanoparticles. Doping with transition metals and rare earth elements improves the electrochemical properties of metal oxides, improving the sensitivity, response time,

and limit of detection of biosensors. In addition, doping increases the electrochemical stability of metal oxides, extending the lifetime of the sensors and providing more reliable measurements. These properties of doped metal oxides allow biosensors to be used more widely and effectively in areas such as health, environmental monitoring, food safety, and biological warfare agent detection (M. Rahman et al., 2014; Rehani et al., 2022; Tripathy & Kim, 2018).

Doping affects a material oxide's beneficial structural features, which can be used for various purposes. For example, dopants may induce strain and defects in the crystal structure, increasing the conductivity of the metal oxide nanoparticles. The maximal alteration in the properties of metal oxide nanoparticles can be achieved with the correct quantity of dopant. Doping may result in synthesizing novel compounds with essentially distinct physicochemical characteristics. The dopant can modify the host metal oxide nanoparticle matrixs structural, optical, electrical, and magnetic properties. One efficient way to manage the materials electrical, structural, and optical characteristics is to dope the parent material with an appropriate element. This gives the material remarkable flexibility. Therefore, it is essential to identify and use the proper dopant to increase the performance of CuObased devices.

Upon reviewing the literature, it becomes evident that a range of transition metal ions (Zn, Pb, Fe, etc.) and alkali metals (Li, Na, etc.) are intentionally integrated into the copper oxide lattice structure to serve diverse purposes (Arun et al., 2018; Ponnarasan et al., 2014; Siddiqui et al., 2018; Vinothkumar et al., 2023).

4.5 Electrochemical Detection of Salbutamol with doped CuO Nanoparticles Modified Carbon Paste Electrode

In this part of the study, electrochemical sensor performance optimization parameters were examined in the electrochemical detection of SAL analyte by introducing (Mn; Ce) into CuO nanoparticles used in CPE modification.

4.5.1 Electrochemical Detection of Salbutamol with Mn doped CuO Nanoparticles Modified Carbon Paste Electrode

The comparison between the electrochemical activity of SAL on the bare CPE surface and the Mn doped CuO nanoparticles modified CPE sensors was evaluated using the cyclic voltammogram technique. The investigations were conducted at a scan rate of 40 $mV.s^{-1}$ with a supporting electrolyte solution of 8.5 x 10^{-5} M SAL (pH = 7.5) in a 0.1 M phosphate buffer. Before performing the cyclic voltammogram measurement, a -300 mV accumulating potential was applied for 240 seconds. The findings showed that no reduction peak was seen on the surfaces of either electrode during the cyclic scan; an oxidation peak was seen at 0.6 V for the CuO nanoparticle-modified CPE and an oxidation peak at 0.2 V for the Mn doped CuO modified CPE (Figure 4.41). The anodic peak current of 8.5 x 10^{-5} M SAL rising on the Mn doped CuO-NP/CPE electrode compared to the CPE electrode indicated that more SAL species were oxidized on the surface of the modified electrode. This implies that the electrocatalytic activity of the modified electrode was enhanced by SAL oxidation. The oxidation behavior of SAL experienced notable enhancement when comparing the bare CPE electrode to the modified CPEs.

This is probably because the modifier CuO is in a nanostructure, which enhances the electrodes' sensing qualities because of its large specific surface area, superior electrical characteristics, high conductivity, and stable structure. Additionally, the peak intensity increased with the Mn contribution.

Zhang and Tsa observed comparable findings with Mn addition leading to a substantial increase in peak intensity (Thiagarajan et al., 2011; L. Zhang, 2020). For example, the study by Guţoiu et al. shows that Mn-doped copper oxide (CuO) nanostructures improve the sensitivity for electrochemical detection of dopamine. Electrooxidation of dopamines is accelerated when Mn is doped to CuO because it raises the electrochemical surface area and enhances the rate of electron transport (Guţoiu et al., 2023).

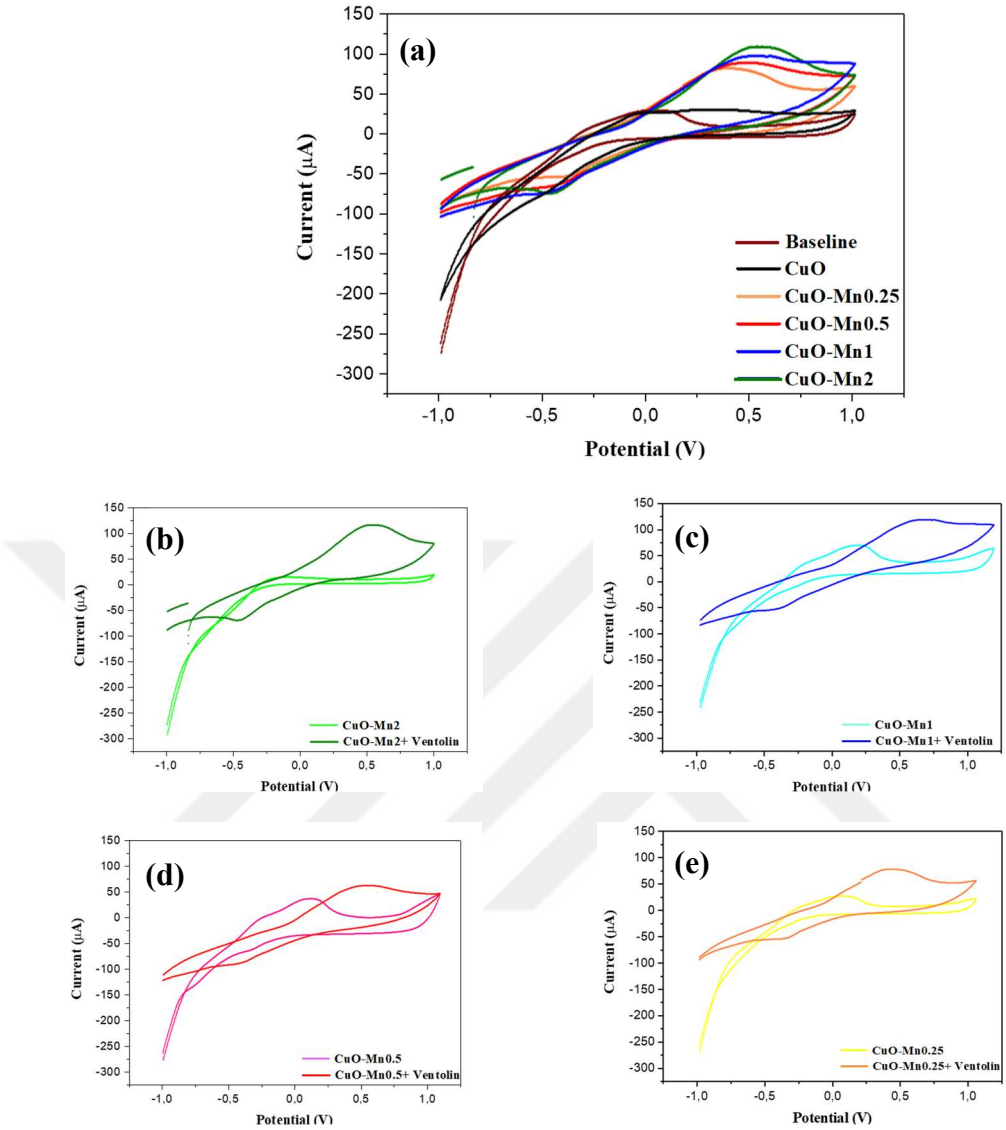

Figure 4.41 (a) CV curves at a bare CPE, 10 wt% CuO and Mn doped CuO nanoparticles modified CPE in the absence and the presence of 8.5 x 10^{-5} M Salbutamol 0.1 M pH 7.5 PBS containing 0.1 M (KNO_3), CV curves of nanoparticles modified CPE with (b) CuO-Mn2 nanoparticles, (c) CuO-Mn1 nanoparticles, (d) CuO-Mn0.5 nanoparticles, (e) CuO-Mn0.25 nanoparticles. Scan rate: 40 $mV.s^{-1}$

Similarly, Haque et al. demonstrated the use of zinc oxide doped with Mn nanostructures for the electrochemical detection of myoglobin, a biomarker of myocardial infarction. Mn doping improves the electrochemical properties of ZnO, enabling myoglobin to bind more effectively to the sensor surface and making its detection more sensitive (Haque et al., 2020). Priyadharshini et al. demonstrated that Mn doped metal oxide nanostructures can offer an environmentally friendly alternative in biosensor applications.

It is seen that Mn doping improves the electrochemical characteristics of metal oxide nanostructures, improves the performance of biosensors, and at the same time, reduces their environmental impact (Priyadharshini et al., 2021). These studies show that Mndoped metal oxide nanostructures can improve biosensors' sensitivity, selectivity, and electrochemical stability, thereby expanding the applications of this technology in areas such as health, environmental monitoring, and food safety. This also clarifies the enhancement of the SAL oxidation peak in the CV plot caused by Mn doping into CuO nanoparticles.

The mechanism by which Mn doping affects the band gap of CuO can be explained as follows: Mn doping creates a broadening impurity band due to the overlap of the wave functions of the dopant electrons adjacent to the band structure of CuO. When the dopant concentration is high enough, this impurity band merges with the lower part of the conduction band, narrowing the band gap. Thus, Mn doping can reduce the band gap by changing the electronic properties of CuO. Recent studies have shown that such arguments are also relevant for 3 wt% Mn-doped CuO (Albert Manoharanet al., 2018; M. Iqbal et al., 2017). The band gap narrowing may also be facilitated by charge transfer between the electrons of Mn^{2+} ions and the CuO conduction or valence band electrons. In Mn-doped CuO nanostructures, this charge transfer can result in trapping levels, which reduce the band gap of CuO (Jiang et al., 2016).

According to the previously indicated explanation, the SAL oxidation peak in CuO-modified electrodes is around 0.64 V; however, Mn doping facilitates the oxidation process, causing the peak to move to the left. Furthermore, the electrochemical properties of CuO nanoparticles improve as the amount of Mn additive increases. In Figure 4.41, the electrochemical behavior of Mn-doped CuO nanoparticles modified and CuO nanoparticle-modified CPEs in the presence of SAL was investigated in detail. As shown in the figure, adding 2% Mn increased the activity of CuO nanoparticles. Consequently, 2% Mn doped CuO nanoparticles will be utilized in the study's next phase to modify the CPE.

4.5.2 Optimization of Experimental Conditions

4.5.2.1 Effect of Nanoparticles Amount

The amount of CuO and CuO-Mn2 nanoparticles in the modified electrodes significantly impacts the electrochemical sensor's sensitivity. The effectiveness of the modified electrodes was evaluated using differential pulse (DP) measurements, which also helped to determine the impact of different Mn amounts (2 to 20 wt% by weight) on CuO nanoparticles. A pH 7.5 PBS containing 0.1 M (KNO_3) and 5 x 10^{-5} M Ventolin was used for the studies. Before the measurement, an accumulating potential of -300 mV was applied for 240 s with continual stirring, followed by 15 s to allow the solution to stabilize. Data were accumulated over the potential range of 0.0 to 0.9 Vat a scan rate of 40 $mV.s^{-1}$. As depicted in Figure 4.42, adding 15 wt% yielded better results than other amounts.

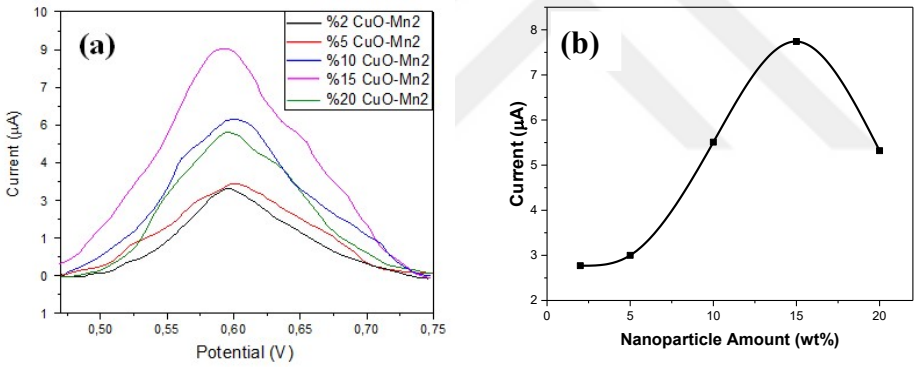

Figure 4.42 (a) DP response, (b) Current values obtained from differential pulse measurement using different amounts (2 to 20 wt%) of Mn doped CuO nanoparticles modified CPE in 0.1 M pH 7.5 PBS containing 0.1 M (KNO_3) in the presence of 5 x 10^{-5} M Ventolin

However, increasing nanoparticles amount above 15% decreased the current responsiveness. The idea that the signal intensity in electrochemical sensors directly correlates with the active surface area the analyte interacts with helps explain this. The overall surface area grows as the number of nanoparticles does, but their interaction with the electrolyte decreases when they come into contact. This reduces the active surface area and produces a lower signal (Shabani et al., 2018; Shetti et al., 2017). For optimal performance, this study used a 15% Mn doped CuO nanoparticles modified

electrode. These findings imply that the quantity of nanoparticles is an essential component in improving the efficiency of electrochemical sensors.

4.5.2.2 Effect of Accumulation Time and Accumulation Potential

By increasing the quantity of SAL adsorbed on the electrode surface, the accumulation process can reduce the detection limit and boost detection sensitivity. In this work, several values of the accumulation potential were set within the range of -0.5 V to 0.2 V by setting the quantity of Mn doped CuO nanoparticles at 15wt % and choosing 240 seconds as the accumulation duration. The impact of accumulating potential on electrochemical oxidation behavior of SAL was examined. The relationship diagram of the experimental data measured by differential pulse voltammetry (DPV) is shown in Figure 4.43(a). When the accumulation potential is less than -0.2 V, the SAL oxidation response peak in the CPE sensor modified by Mn doped CuO nanoparticles is at its maximum. The peak intensities of the oxidation current decreased at higher potentials due to hydrogen reduction on the modified electrode surface (Baghayeri et al., 2019b). Another possible explanation is that higher currents cause structures to cluster together, leading to structures with higher density but smaller surface area. As a result, the best accumulation potential was determined to be -0.2 V. Furthermore, it was investigated how the deposition time affects the voltammetric behavior of SAL on the CPE surface modified with Mn doped CuO (accumulation potential was set to -0.2 V). Figure 4.43(b) shows a plot of the SAL oxidation peak current signal proportional to accumulation time. Notably, after 60 seconds of accumulation, the peak intensity first increases and decreases as the accumulation time increases. The saturation of SAL adsorption on the electrode surface explains this outcome. In subsequent experiments, the ideal accumulation time of 60 seconds was used, considering both sensitivity and work efficiency (Amare and Menkir 2017; Li et al., 2013). Therefore, the accumulation time was set to 60 seconds to obtain a better sensitivity for SAL detection. The sensor modified with CuOMn2 nanoparticles works with a potential of 200 mV and a holding time of 60 seconds, while the sensor modified with CuO nanoparticles uses a potential of 300 mV and a holding time of 240 seconds. Significant changes were observed in the electrochemical properties of CuO nanoparticles with Mn doping. The CuO-Mn2 nanoparticle

modified sensor can respond faster using lower potential (200 mV) and shorter dwell time (60 seconds) compared to the sensor modified with CuO nanoparticles. Mn modified CuO's crystal structure and electronic properties, enhancing the electrical conductivity and catalytic activity.

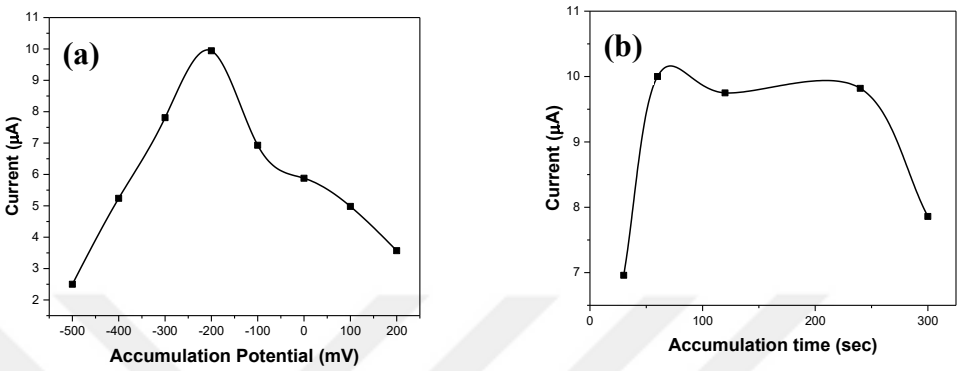

Figure 4.43 (a) The effect of accumulation potential and (b) Accumulation time on the peak current of 5 x 10^{-5} M SAL in 0.1 M pH 7.5 PBS containing 0.1 M (KNO_3) on the 15 wt% Mn doped CuO nanoparticles modified CPE at a scan rate of 40 $mV.s^{-1}$

This shows that Mn doping improves the electrochemical performance of CuO nanoparticles and enables effective measurements in a shorter time with lower potential. Furthermore, the electrochemical characteristics of CuO are altered by the presence of Mn, which makes it possible to conduct quick and effective studies with reduced retention times.

4.5.2.3 Effect of Support Electrolite and pH

The impact of pH on peak current was examined utilizing CPE enhanced with Mn-doped CuO nanoparticles in 0.1M PBS. The study was conducted at pH values ranging from 4.0 to 9.0 with 1 unit increments. According to Figure 4.44(a), the peak current increases to pH 7.5, remains constant in the pH 7-7.5 range, and then decreases when pH increases above 7.5. This can be explained by increased copper (II) complex formation with the ligand on the electrode surface as the pH risesto 7.5. Additionally, at higher pH values, copper (II) can also be expected to precipitate as $Cu(OH)_2$ (Ensafi et al., 2001). The study's ideal pH was determined to be 7.5, and the phosphate buffer was used to get the best results. The CuO-Mn2 nanoparticles modified sensor and the CuO nanoparticles modified sensor exhibit the strongest signals at pH 7.5. However,

the presence of Mn doping in the CuO-Mn2 nanoparticles modified sensor increases the signal strength significantly. While the CuO nanoparticles modified sensor provides a signal strength of roughly 8 µA, the CuO-Mn2 nanoparticles modified sensor reaches a signal strength of 12 µA. This increase indicates that Mn doping improves the electrochemical performance of the sensor and amplifies the signal. The presence of Mn probably alters the electronic and catalytic properties of CuO, enabling the sensor to produce a higher signal and, hence, more sensitive measurements. To correctly understand the electrochemical behavior of the analyte on the electrode in voltammetric experiments, it is essential to choose the supporting electrolyte composition and pH value with great care. Phosphate buffer is preferred in these studies because it offers a wide operating range. Various supporting electrolytes such as NaCl, $NaNO_3$, KCl, and KNO_3 solutions were used to determine the effect of supporting electrolytes. Measurements made using CPE modified with 15 wt% Mn-doped CuO nanoparticles by weight were confirmed by differential pulse voltammetry (DPV) technique. Figure 4.44(b) shows that the SAL oxidation peak current values in KNO_3 solution are the highest. In both CuO nanoparticles modified sensor and CuO-Mn2 nanoparticles modified sensor measurements, salbutamol (SAL) oxidation peak current values were observed at the highest level in the KNO_3 solution used as a support electrolyte solution. The CuO nanoparticles modified sensor detected a positive impact of Mn doping on performance, with the highest Mn amount resulting in a stronger signal.

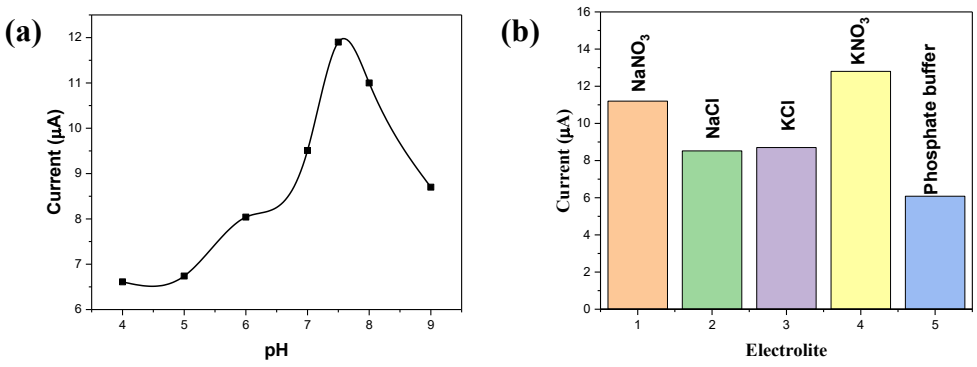

Figure 4.44 Effects of electrodeposition (a) solution pH values and (b) supporting electrolyte solution on DP peak current values (The concentration of SAL solution is 5 x 10^{-5}M)

4.5.2.4 Calibration Curve and Limit of Detection

Under ideal circumstances, SAL was qualitatively analyzed using differential pulse voltammetry (DPV). Figure 4.45 plots the anodic peak current versus the SAL area in the 0.05 µM to 500 µM range. It has been observed that the oxidation of SAL gas increases the peak current. The SAL volume expansion range has been reported to be from 2 µM to 200 µM, with a clearance value (R^2) of 0.9945. The data obtained from the analytical curves were used to calculate the lowest detection limits (LOD). As a result of the calculations, LOQ = 194.17 $nmol.L^{-1}$ and LOD = 58.25 $nmol.L^{-1}$.Comparing the calibration curve and detection limits of CuO and CuO-Mn2 nanoparticles modified sensors, the CuO modified sensor can detect SAL concentrations between 50 nM and 100 µM and provides high accuracy with a correlation value of 0.9971. The LOD of this sensor was determined as 50 nM, indicating its capacity to detect low concentrations. On the other hand, the CuO-Mn2 nanoparticles modified sensor can measure SAL concentrations between 2 µM and 200 µM and provides about the same accuracy with a correlation value of 0.9945. Compared to the CuO nanoparticles modified sensor, this one has a somewhat detection limit (LOD) at 58.25 nM. The CuO-Mn2 nanoparticles modified sensor provides an extensive calibration range, while the CuO sensor delivers superior detection limits.

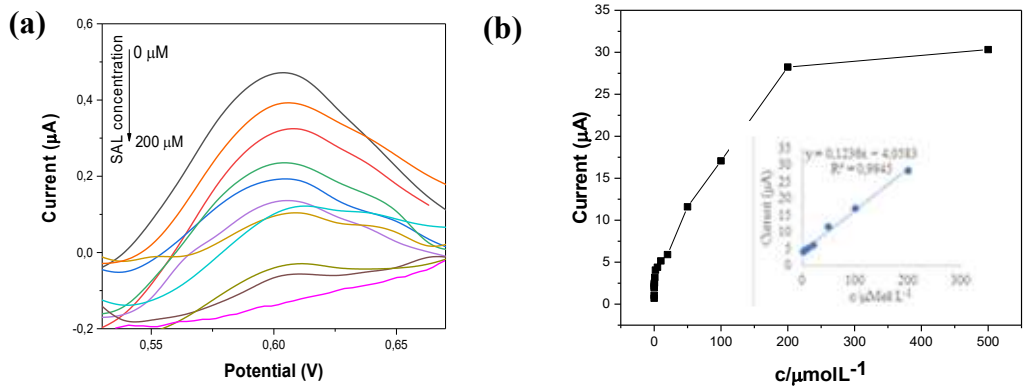

Figure 4.45 (a) DP responses of Mn doped CuO nanoparticles modified CPE to different SAL concentrations. SAL concentration range covered 0.05 to 500 µM. Inset: DPV of Modified CPE in pH 7.5 PBS containing different concentrations of SAL,(b) depicts a corresponding calibration plot for the quantitation of SAL

4.5.2.5 Selectivity, Repeatability, Reproducibility, and Stability

The repeatability of the sensor was investigated by differential pulse voltammetry (DPV) for determination of 5 x 10^{-5} M SAL in a buffer solution containing 0.1 M pH 7.5 PBS and 0.1 M KNO_3, using Mn-doped CuO nanoparticles modified CPE. Additionally, repeatability was evaluated using ten different modified electrodes prepared in ten samples for each analyte. The peak currents showed remarkable repeatability with a RSD of 1.89% for SAL ($n = 8, \bar{x} = 61.74\ \mu M, SD = 0.41$). For two weeks, the DPV current responses were measured every other day to assess the storage stability of the modified CPE. The electrode was kept in a dry atmosphere while not in use. After two weeks, the electrode retained 98.24% of the initial signal. Experimental findings show that the modified electrode exhibits high repeatability and stability.

Many potential interfering substances were tested to evaluate selectivity, such as glucose, Na^+ and Fe^{3+}, ascorbic acid, dopamine, starch, and epinephrine. As shown in Figure 4.46, at a concentration of 8.5 x 10^{-5} M, these substances showed no noticeable effect on SAL signals. However, some interference was observed with Fe^{3+}. Overall, this technique exhibits high selectivity in determining SAL. Comparing the performance of CuO and CuO-Mn2 nanoparticles modified sensors, it is observed that Mn doping significantly improves the catalytic properties of CuO nanoparticles. The CuO nanoparticles modified sensor and CuOMn2 nanoparticles modified sensor exhibited high selectivity towards various potential interferants during SAL detection. In terms of reproducibility, the CuO nanoparticles modified sensor exhibited high consistency with a RSD of 3%. In comparison, the CuO-Mn2 nanoparticles modified sensor exhibited superior reproducibility with a deviation of 1.89% due to the catalytic improvements provided by Mn doping. Regarding reproducibility, it is understood that Mn doping improves the manufacturing consistency of the sensors and provides lower drift.

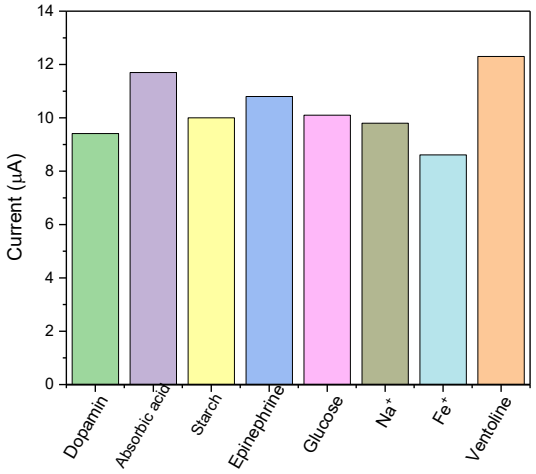

Figure 4.46 DP responses of Mn doped CuO nanoparticles modified CPE toward 8.5 x 10^{-5} M SAL 0.1 M pH 7.5 PBS containing 0.1 M (KNO_3) and other interference compounds.

Regarding storage stability, the CuO nanoparticles modified sensor retains 80% of its initial signal, while the CuO-Mn2 nanoparticles modified sensor shows a significant improvement by retaining 98.24 % of its initial signal after two weeks. It can be concluded that Mn doping improves the catalytic properties of CuO nanoparticles and significantly enhances the sensors' selectivity, reproducibility, and stability performance.

4.5.3 Electrochemical Detection of Salbutamol with Ce doped CuO Nanoparticles Modified Carbon Paste Electrode

Cyclic voltammograms have been used to compare the electrochemical activity of SAL on the CuO/Ce doped CuO-NP/CPE sensors with the bare CPE surface. The studies were conducted with a supporting electrolyte solution of 8.5 x 10^{-5} M SAL (pH = 7.5) in a 0.1 M phosphate buffer, scanning at a rate of 40 $mV.s^{-1}$. 240 seconds of a -300 mV accumulation potential were applied before the CV measurement (Figure 4.47).

Comparing the SAL oxidation processes on bare and modified CPEs, the Ce (III) doped CuO modified sensor showed a higher anodic peak current than the unmodified CPEs. This is possible because of the increased electroactive areas and synergistic electrocatalytic influence of Ce and CuO, which improved the SAL oxidation (Akbari Javar et al., 2022).

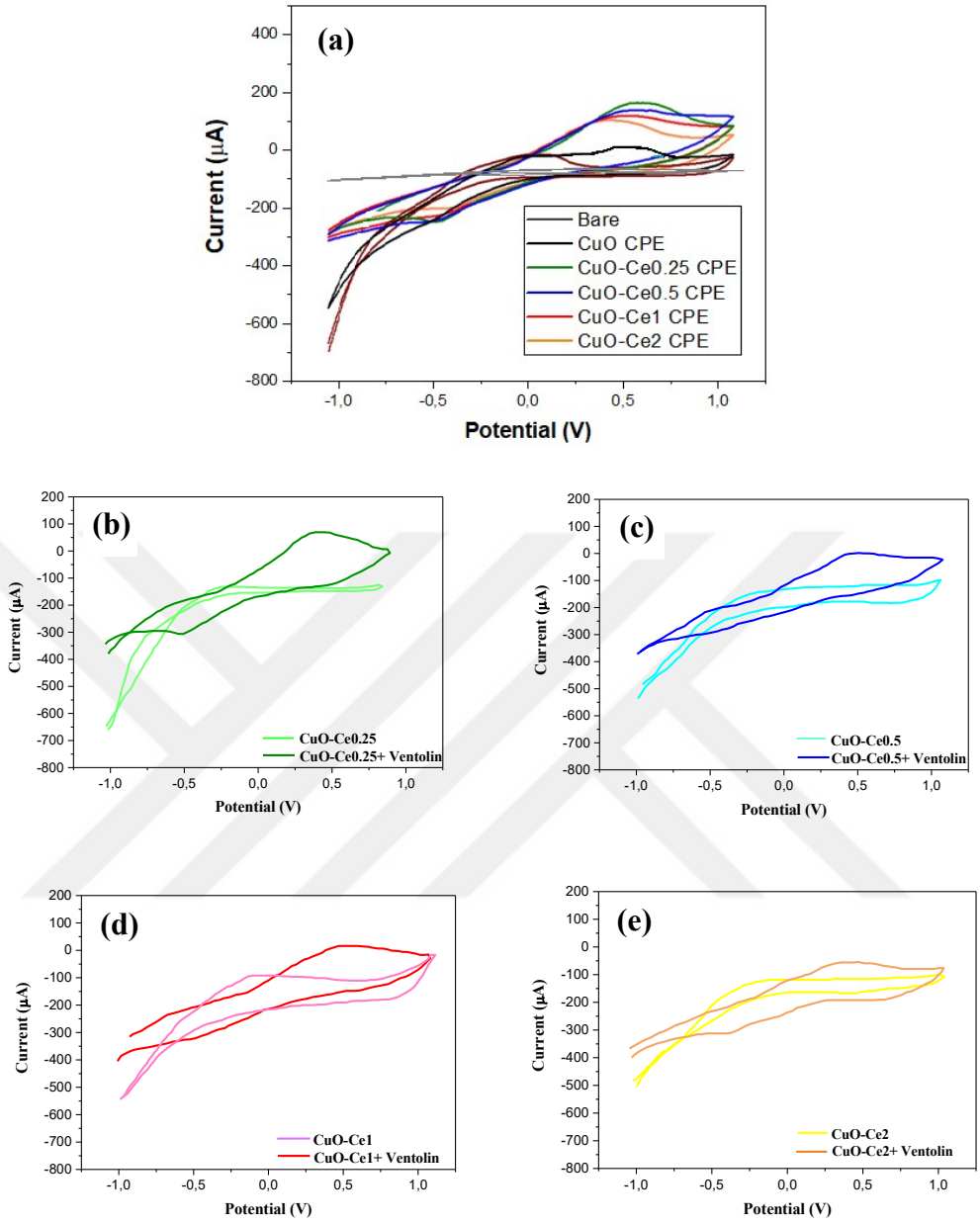

Figure 4.47 (a) CV curves at a bare CPE, 10 wt% CuO and Ce doped CuO nanoparticles modified CPE in the absence and the presence of 8.5 x 10^{-5} M Salbutamol 0.1 M pH 7.5 PBS containing 0.1 M (KNO_3), CV curves of nanoparticles modified CPE with (b) CuO-Ce0.25 nanoparticles, (c) CuO-Ce0.5 nanoparticle, (d) CuO-Ce1 nanoparticles, (e) CuO-Ce2 nanoparticles. Scan rate: 40 $mV.s^{-1}$

This phenomenon may be explained as follows: Cerium is a candidate dopant material for metal oxides due to vacant 4f orbitals, various +3 and +4 valences, electrocatalytic qualities, and redox characteristics. The CuO-Ce complex may result in a change in the crystal structure due to oxygen vacancies that can stabilize CuO and produce features such as highly ionic conductivity, a higher surface to volume ratio, a

high surface charge, and an improved affinity for binding to different analytes and biomolecules (Foroughi et al., 2019). Shanbhag et al. investigated the improvement of the electrochemical properties of tungsten oxide nanorods through hafnium doping despite the lack of research in the literature on determining Ce-doped metal oxides' significance for SAL. This study discovered that Hf doping increased the efficiency of salbutamol and paracetamol oxidation. Doping made the electrode surface's active sites more numerous, which enhanced the sensor's sensitivity and reaction time (Shanbhag et al., 2021). In the study where zirconia nanoparticles with cerium doping were used for electrostatic detection, Ce doping was found to perform the oxidation of dopamine more sensitively and selectively. Doping enhanced sensor performance by increasing electrical conductivity and improving reaction kinetics (Bullapura Matt et al., 2019). These studies show that doping rare earth elements into metal oxides increases the efficiency of oxidation reactions and significantly improves the performance of electrochemical sensors.

Figure 4.47 (b) shows a detailed investigation of the electrochemical behavior of bare, CuO nanoparticle-modified, and Ce-doped CuO nanoparticles modified CPE with SAL. The introduction of 0.25% Ce enhanced the activity of CuO nanoparticles, as shown in the figure. The following thesis section will employ CuO nanoparticles doped with 0.25% Ce for CPE design.

4.5.4 Optimization of Experimental Conditions

4.5.4.1 Effect of Nanoparticles Amount

The sensitivity of electrochemical sensors varies significantly depending on the amount of pure and Ce-doped CuO nanoparticles used for the modification of electrodes. This study evaluated the effect of different amounts of Ce-doped CuO nanoparticles (2 wt% to 20 wt% by weight) on electrode performance using DPV. Modified carbon paste electrodes were subjected to DPV measurements in a 0.1 M pH 7.5 PBS that included 5×10^{-5} M Ventolin and 0.1 M KNO_3. The solution was continuously stirred for 240 seconds at an accumulating potential of -300 mV before being allowed to settle for 15 seconds. Over the potential range of 0.0 to 0.9 V, data were gathered at a scan rate of 40 $mV.s^{-1}$. It was discovered that 5 wt% Ce doped CuO

nanoparticles modified CPE performed better than other amounts, as the bar graphs illustrated in Figure 4.48. However, nanoparticle amounts above 5 wt% reduced the responsiveness of the electrodes. This is explained by the fact that as the number of nanoparticles per volume increases, fewer of the nanoparticles come into contact with the electrolyte, reducing the available sensing surface area.

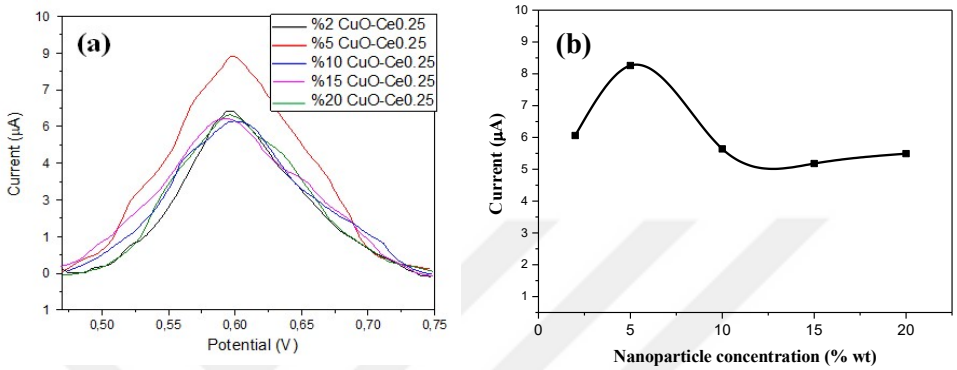

Figure 4.48 (a) DP response, (b) Current values obtained from differential pulse measurement using different amounts(2 to 20 wt%) of Ce doped CuO nanoparticles modified CPE in 0.1 M pH 7.5 PBS containing 0.1 M (KNO_3) in the presence of 5 x 10^{-5} M Ventolin

As the particle amount increases, the detection region becomes less accessible, reducing signal reception. As a result, in this research, electrodes modified with 5wt% Ce doped CuO nanoparticles gave the best results. These findings indicate that nanoparticle amount must be carefully optimized in electrochemical sensor design and that 5 wt% Ce doped CuO nanoparticles are the optimal amount in this context. While the best performance in CuO-modified sensors was achieved with 10 wt% nanoparticles doping, the optimal result in Ce-doped CuO-modified sensors was reached with 5 wt% nanoparticle doping. This indicates that Ce doping increases the catalytic efficiency and surface activity of CuO, enabling high performance with lower nanoparticles amounts. Ce doping has been found to improve the electrochemical properties of CuO and provide more effective sensor performance with less amount of nanoparticles used in CPE modification.

4.5.4.2 Effect of Accumulation Time and Accumulation Potential

The sensitivity of electrochemical sensors can vary significantly depending on the amounts of different additives in the electrodes. In this study, the proportion of Ce-doped CuO nanoparticles was determined to be 5 wt%, and a deposition time of 240 s was applied using various deposition potentials ranging from -0.5 V to 0.2 V. These potentials' impact on SAL's electrochemical oxidation was investigated. The SAL oxidation reaction on the carbon paste electrode (CPE) reinforced with Ce-doped CuO nanoparticles has reached its peak in the accumulation potential, as shown in Figure 4.49 (a), which illustrates the deposition potential effect on the SAL oxidation peak current, - 0.3 V, according to experimental data obtained by differential pulse voltammetry (DPV). The maximum peak current recorded at this potential decreased with increasing potential due to hydrogen depletion, increased structural density, and reduced surface area (Baghayeri et al., 2019b). The ideal deposition potential was determined to be -0.3 V. Additionally, tests were conducted at a deposition potential of -0.3 V to study the effect of deposition time on the voltammetric properties of SAL. Figure 4.49 (b) shows that the peak current of SAL oxidation increases to an accumulation time of 120 s but then decreases as the accumulation time increases. This is the limitation of SAL adsorption at the saturation point of the electrode surface. In subsequent studies, the ideal deposition time was chosen as 120 s, considering both sensitivity and process efficiency (Amare, 2019; Li et al., 2013). Therefore, the accumulation time was set to 120 seconds to achieve maximum sensitivity for SAL detection.

SAL detection was carried out using the sensor modified with CuO nanoparticles under 300 mV holding potential and 240 s holding time. This sensor's peak current of SAL oxidation can reach the saturation point after a long holding time. It was found that the peak current of SAL oxidation in the Ce-doped CuO nanoparticles modified sensor was reduced up to 120 s in the studies carried out at a holding potential of -0.3 V. While no change in sensor current strength was observed, Ce doping improved the electrochemical properties of CuO, increasing their adsorption capacity and optimizingthe ideal holding time to 120 s. This proves that Ce doping improves the processing efficiency of the sensor and contributes to obtaining maximum signal in a

shorter time. In this context, it was observed that while high performance can be achieved with shorter retention times in Cedoped Ce sensors, longer timesand higher potentials are required in CuO sensors.

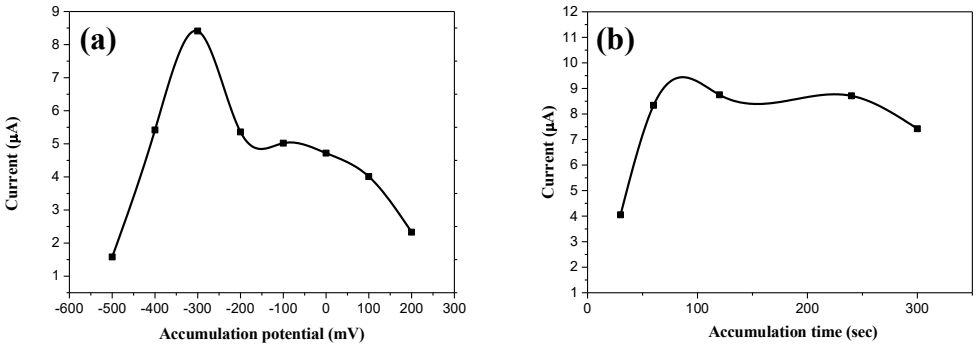

Figure 4.49 (a) The effect of accumulation potential and (b) accumulation time on the peak current of 5 x 10^{-5} M SAL in 0.1 M pH 7.5 PBS containing 0.1 M (KNO_3) on the 5 wt% Ce doped CuO nanoparticles modified CPE at a scan rate of 40 mV.s-[1]

4.5.4.3 Effect of Support Electrolite and pH

The effects of pH on electrochemical behavior were examined by analyzing the results of studies utilizing CPEs enhanced with Ce doped CuO nanoparticles (Figure 4.47). This study examined how different pH values, ranging from 4.0 to 9.0 at 1-unit intervals, affected the peak current. The findings show that the peak current increases to pH 7.5, remains constant in the pH 7-7.5 range, and decreases at higher pH values. This indicates that as the pH increases to 7.5, complex formation on the electrode surface increases as the amount of liganded copper(II) increases. Additionally, at higher pH values, copper(II) can be expected to precipitate as $Cu(OH)_2$. To achieve optimal results, the pH of the phosphate buffer for the study was determined to be 7.5 (Figure 4.50(a)).

It is emphasized that it is crucial to choose the correct supporting electrolyte composition and pH value to interpret the analyte compound in electrochemical studies correctly. In this context, it is stated that phosphate buffer is a frequently preferred buffer system due to its wide operating range. It is noted that various electrolytes were used in studies conducted to determine the effect of supporting electrolytes. Measurements performed using CPEs modified with 5 wt% Ce doped CuO nanoparticles were confirmed by the DP technique. In this context, it is stated that the

highest SAL oxidation peak current values obtained in KNO_3 solution are shown in Figure 4.50(b).

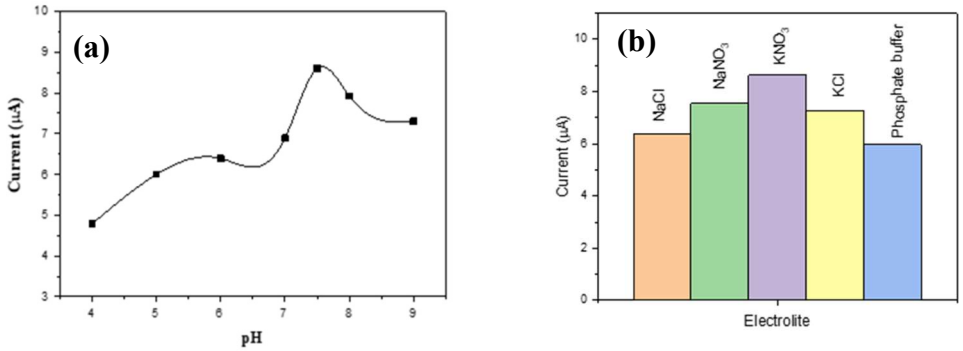

Figure 4.50 (a) Effects of solution pH values and (b) supporting electrolyte solution on DP peak current values. (The concentration of SAL solution is 5 x 10^{-5} M

When the modified sensor and Ce-doped CuO modified sensor were compared, both sensors obtained similar results; CuO modified sensor and Ce-doped CuO modified sensor showed the highest SAL oxidation peak current at pH 7.5. KNO_3 solution was determined as the optimal support electrolyte for both sensors, with maximum performance at pH 7.5. These results confirm that both sensors demonstrate consistent and high performance when exposed to similar pH and KNO_3solutions.

4.5.4.4 Calibration Curve and Limit of Detection

Qualitative analysis of SAL was performed using differential pulse (DP) measurement at ideal conditions. The results displayed in Figure 4.51 indicated positive correlation between the rise in SAL concentration and the oxidation peak current. The data obtained in this analysis show a high correlation value between SAL concentration and anode peak current (R^2 = 0.9929) and a calibration range between 10 µM and 100 µM.

Additionally, analytical curves were created to determine the lowest LOD and LOQ using the collected data. As a result of these calculations, it was determined that the LOD value was 34.18 nM, and the LOQ value was 113.95 nM. CuO modified sensors offer a similar calibration range (50 nM - 100 µM) with a detection limit of 50 nM and a high correlation value (R^2 = 0.9971). Ce doping enables the sensor to provide more

sensitive results at low concentrations by improving its surface activity and catalytic effect and accelerating electron and ion transfer. In general, Ce doped CuO sensors provide higher sensitivity and accuracy by offering lower LOD values and can efficiently detect lower concentrations. These findings reveal that CPEs modified with Ce doped CuO nanoparticles provide high sensitivity and accuracy for the electrochemical analysis of SAL. It seems that these electrodes can effectively detect a wide range of SAL concentrations.

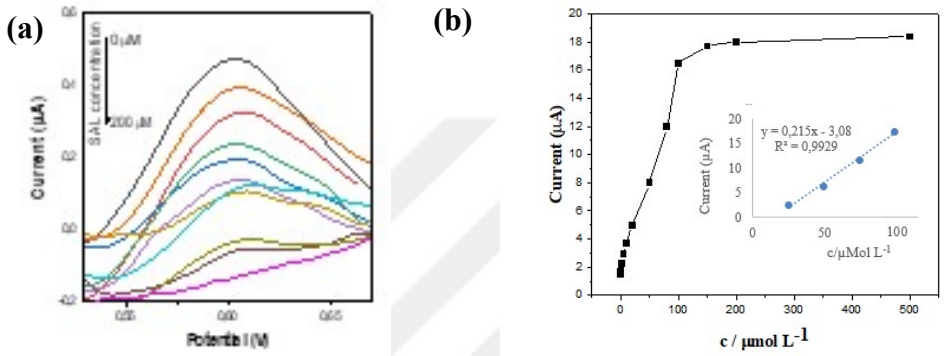

Figure 4.51 (a) DP responses of Ce doped CuO nanoparticles modified CPE to different SAL concentrations. SAL concentration range covered 0.05 to 500 µM. inset: DPV of modified CPEs in pH 7.5 PBS containing different concentrations of SAL,(b) depicts a corresponding calibration plot for the quantitation of SAL

4.5.4.5 Selectivity, Repeatability, Reproducibility, and Stability

The electrochemical analysis of Ce doped CuO nanoparticles modified CPE examined its effect on the repeatability, stability, and selectivity of the sensor (Figure 4.52). This research examined the repeatability of the sensor for detecting 5 x 10^{-5} M SAL using differential pulse voltammetry (DPV) in 0.1 M pH 7.5 PBS. In repeatability tests using ten independent electrodes for each analyte, the calculated RSD for SAL detection was 1.57%, $(n = 8, \bar{x} = 53.97\ \mu M, SD = 0.44)$. indicating high repeatability. By monitoring the DP current responses every other day for two weeks, the storage stability of the modified CPEs was assessed, and it was found that the electrode kept 92% of the initial signal. These findings demonstrate that the modified electrode exhibits high repeatability and stability. The selectivity of the sensor was evaluated by examining various potential interactions, and it was found that CPEs modified with Ce doped CuO nanoparticles showed no noticeable effect on SAL

signals at a concentration of 8.5 x 10^{-5} M. These compelling results demonstrate the sensor's exceptional selectivity in detecting SAL. Selectivity was assessed by testing various potential interferers, including glucose, Na^{+} and Fe^{3+}, ascorbic acid, dopamine, starch, and epinephrine. As shown in Figure 4.52, these compounds had no noticeable effect on SAL signals at a concentration of 8.5 x 10^{-5} M.

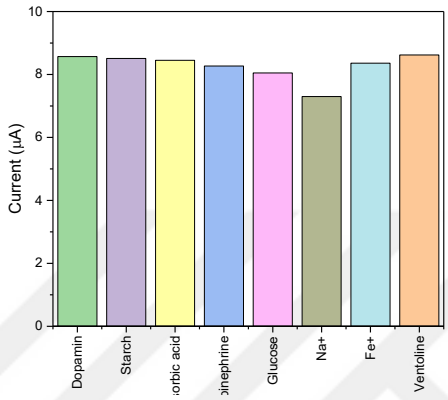

Figure 4.52 DP responses of Ce doped CuO nanoparticles modified CPE toward 8.5 x 10^{-5} M SAL 0.1 M pH 7.5 PBS containing 0.1 M (KNO_3) and other interference compounds.

The results show that Ce doped CuO nanoparticles modified CPE offers superior long-term stability, high repeatability, sensitivity, and selectivity for SAL detection. These characteristics improve the stability of sensor as dependable instruments for analytical applications.

In tests of repeatability for 5 x 10^{-5} M SAL detection, the Ce doped CuO modified sensors demonstrate strong repeatability with a RSD of 1.57%. In contrast, they preserve 92% of the initial signal in storage stability tests. Furthermore, the developed Ce doped CuO modified sensor offers high selectivity and is not affected by potential interferences at 8.5 x 10^{-5} M concentration. In contrast, the CuO modified sensors have a storage stability of 80% and an RSD value of 3%. Ce doped CuO sensors offer lower RSD, higher selectivity, and better long-term stability due to the contribution of Ce, making these materials a more reliable option for analytical applications.

4.5.5 Electrochemical Detection of Salbutamol with SnO_2 Nanoparticles Modified Carbon Paste Electrode

SnO_2 is a well-known n-type semiconductor with a wide bandgap (3.5-4.0 eV), low cost, good chemical stability, and a tetragonal crystal structure. It is extensively utilized in many industries, including photocatalysis, solar cells, lithium-ion batteries, electrode materials, and gas sensors. Regarding inter-lattice oxygen and oxygen vacancies, SnO_2 has a robust initial resistance. Its detection method is based on semiconductor oxides' interfacial response. The detecting mediums oxygen molecules are adsorbedon the semiconductor SnO_2's surface due to its many active site centers, collecting electrons to create chemically adsorbed oxygen ions (G. Liu et al., 2022).CuO nanoparticles are p-type semiconductors, whereas SnO_2 nanoparticles are n-type semiconductors, and their conduction methods differ. N-type semiconductors have excess electron carriers thanks to the donor dopants used in their production, and these electrons move freely and provide high electrical conductivity. This increases the signal transmission speed of the sensors and enables more precise measurements. In addition, the large surface area of n-type semiconductors supports faster and more efficient electrochemical reactions. Their high chemical and thermal stability ensures the long-lasting and reliable performance of the sensors. As a result, n-type semiconductors show high performance even under low operating voltages, improving the sensitivity, speed, and reliability of electrochemical sensors.

The thesis examined the electrochemical performance of CPEs enhanced with n-type semiconductor SnO_2 nanoparticles to detect SAL, leveraging the advantages of SnO_2 nanomaterials. Cyclic voltammetry (CV) was utilized to examine the oxidation behavior of SAL on CPEs that had been treated with SnO_2 nanoparticles and those that were bare. There was no oxidative peak current in CPE augmented with SnO_2 nanoparticles, according to an analysis of the CV curves of 8.5 x 10^{-5} M SAL in 0.1 M pH 7.5 PBS (Figure 4.53). These findings demonstrate that the modified CPEs do not support electrocatalytic SAL oxidation or offer a conducive environment for electron transport. Although pure SnO_2 has great sensitivity, its main disadvantage is its poor selectivity, which precludes it from achieving all practical critical requirements for realistic sensor applications, like high sensitivity, shorter response/recovery time,

stability, and low power consumption (Bouzigues et al., 2011; H. Wang et al., 2023). Therefore, despite the significant research on sensing materials, there is still a scope for research to achieve higher sensitivity and better selectivity in electrochemical biosensor applications. As a result, metal ion doping in the SnO_2 lattice could be an effective way to improve SnO_2 sensing characteristics. In the case of doped SnO_2, substitution and intermediate point defects may exist due to the rearrangement of internal defects in the SnO_2 lattice (Wang et al., 2016). Furthermore, semiconductor behavior can be predicted based on the type of dopant used in the host material (donor or acceptor) to adjust the lattice structure distortion and orientations that determine the amount of SAL detection enhancement. Our results indicate that CPE modified with SnO_2 nanoparticles is insufficient for determining SAL, and more optimization studies are required to alter SnO_2 nanoparticles to improve electrocatalytic efficiency. In this respect, it has been determined that advanced modification processes are needed for n-type semiconductors to function efficiently in electrochemical sensors. In this context, the goal was to improve the electrochemical properties of SnO_2 nanoparticles through modification. The modification in question was accomplished through transition metal/rare earth element doping. Consequently, the effect of element doping on the electrochemical sensing performance of SnO_2 for detecting SAL was investigated.

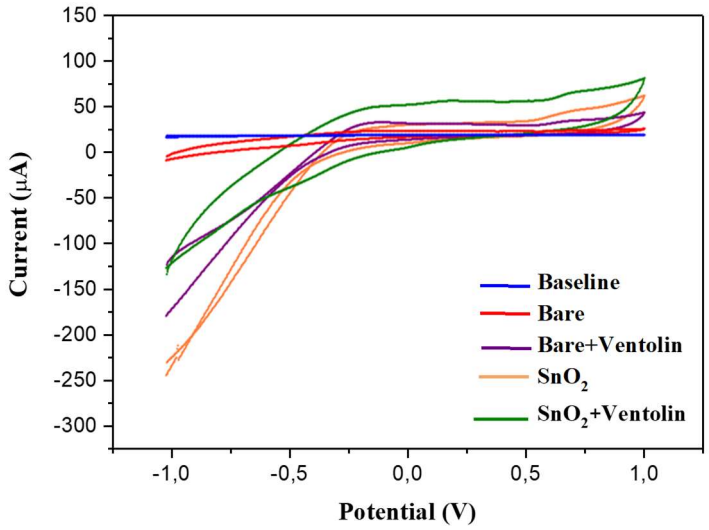

Figure 4.53 CV curves at a bare CPE and 10 wt% SnO_2 nanoparticles modified CPE in the absence and the presence of 8.5×10^{-5} M Salbutamol 0.1 M pH 7.5 PBS containing 0.1 M (KNO_3). Scan rate: 40 $mV.s^{-1}$ electrochemical detection of salbutamol with doped SnO_2 nanoparticlesmodified CPE.

In this part of the study, electrochemical sensor performance optimization parameters were examined in the electrochemical detection of SAL analyte by introducing Mn and Ce into SnO_2 nanoparticles used in CPEs modification.

4.5.6 Electrochemical Detection of Salbutamol with Mn doped SnO_2 Nanoparticles Modified Carbon Paste Electrode

The electrochemical activity of SAL on bare CPE, undoped SnO_2 and Mn doped SnO_2 nanoparticles modified CPE sensors were compared using cyclic voltammograms. A supporting electrolyte solution of 8.5 x 10^{-5} M SAL (pH = 7.5) in 0.1 M PBS (scan rate = 40 $mV.s^{-1}$) was used for the experimental study. Before performing cyclic voltammetry, an accumulating potential of -300 mV was applied for 240 s. Figure 4.54 shows the CVs of bare and SnO_2 sensors and Mn doped SnO_2 sensors with different Mn rates. In the CVs in Figure 4.54, peaks defined in both anodic and cathodic directions were observed with the Mn doped SnO_2 nanosensor. A peak current of 1.1 mA at approximately 0.6 V in the anode direction was observed in the CV curve of the Mn doped SnO_2 modified CPEs electrode, while no peak current was observed in the SnO_2 modified CPE electrode.

CV curve showed that Mn doped SnO_2 nanoparticles modified CPE electrode showed a peak current of 1.2 mA in the cathodic direction, at about -0.4V.Compared to the CPEs electrode, the Mn doped SnO_2 nanoparticles modified CPE s electrode showed an increase in anodic peak current of 8.5 x 10^{-5} M SAL, suggesting that more SAL species were oxidized on the modified electrode's surface. These results imply that the changed electrode's electrocatalytic activity impacted the SAL oxidation. The oxidation behavior of SAL was significantly improved when the modified CPEs and the bare CPE electrode were compared. This situation is caused by the SnO_2 nanostructure used as a modifier. Sensors modified with Mndoped SnO_2 nanoparticles provide significant advantages in determining salbutamol, and these advantages are based on several fundamental mechanisms.

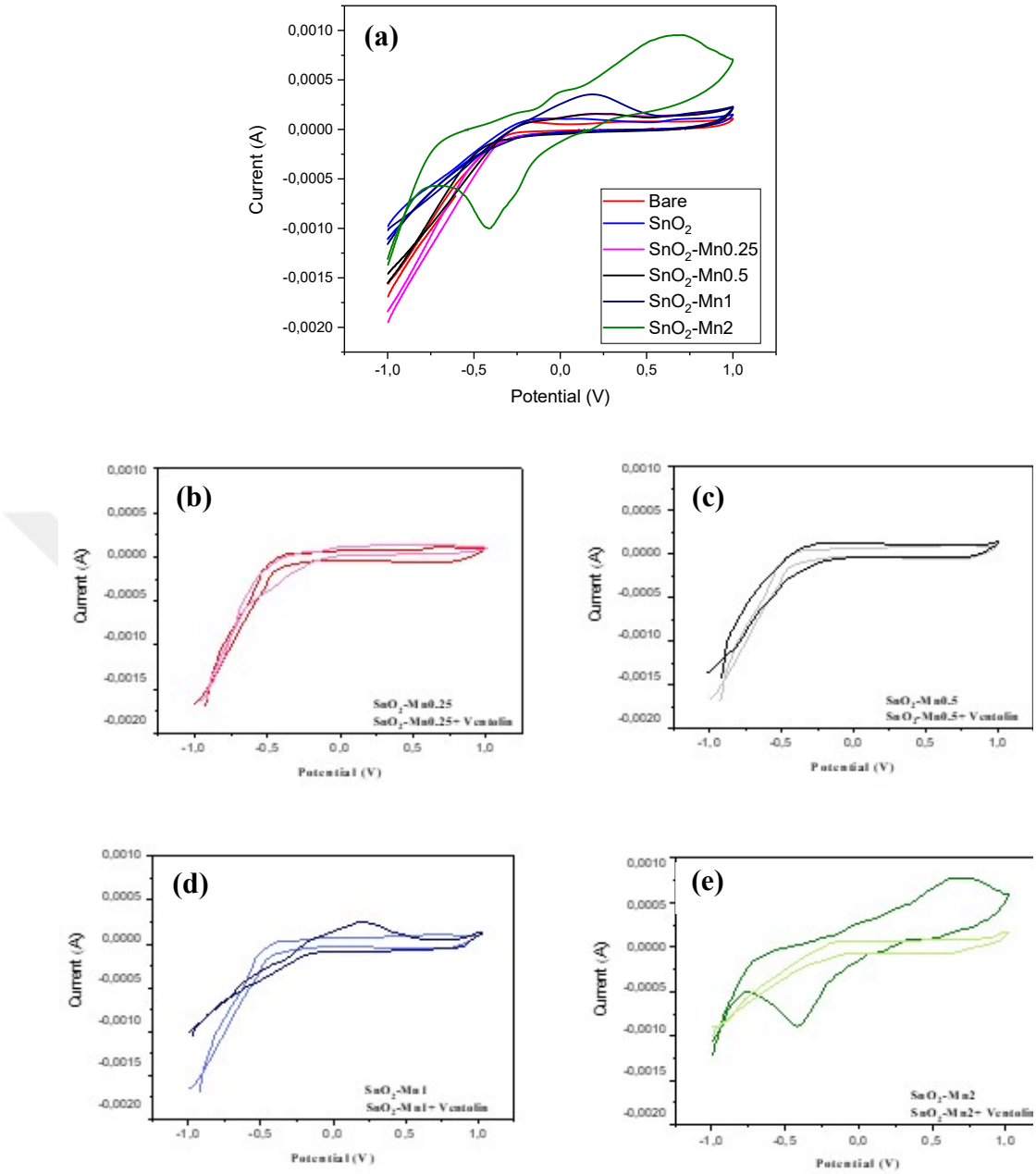

Figure 4.54 (a) CV curves at a bare CPE, 10 wt% SnO_2 and Mn doped SnO_2 nanoparticles modified CPE in the absence and the presence of 8.5 x 10^{-5} M Salbutamol 0.1 M pH 7.5 PBS containing 0.1 M (KNO_3), CV curves of nanoparticles modified CPE s with (b) SnO_2-Mn0.25 nanoparticles, (c) SnO_2-Mn0.5 nanoparticles, (d) SnO_2-Mn1 nanoparticles, (e) SnO_2-Mn2 nanoparticles. Scan rate: 40 $mV.s^{-1}$

Firstly, it has been observed that manganese (Mn) doping significantly improves the electronic and catalytic properties of SnO_2. By integrating into the crystal structure of SnO_2, Mn alters the energy levels of the semiconductor and thus increases the mobility of free electrons. This promotes the sensor's electrical conductivity and

creates a more favorable environment for redox reactions. Mn has the effect of increasing the surface area and number of active sites on the SnO_2 surface. This enlarged surface area allows salbutamol molecules to adsorb more effectively on the sensor surface. The doping of Mn changes the surface properties of SnO_2 and opens more active sites, facilitating the electrochemical reactions of salbutamol. Furthermore, Mn doping provides catalytic centers that accelerate the oxidation of salbutamol. These centers allow salbutamol to be oxidized at lower potentials and thus enable the sensor to give higher current responses.

The presence of Mn increases the electroactivity of SnO_2, which causes the sensor to operate with higher sensitivity and selectivity. As a result, Mn doping increases electron mobility, expands the surface area, and accelerates oxidation reactions, enabling the sensors to perform more sensitive, efficient, and reliable measurements (Choudhari & Jagtap, 2021; Koventhan et al., 2022; Lavanya et al., 2016). This result also clarifies why Mn doping elevates the SAL oxidation peak in the CV graph of SnO_2 nanoparticles.

Mn doping improves the electrochemical detection of analytes through several main mechanisms. Firstly, new active centers are formed on the surface of SnO_2 by the effect of Mn doping. These provide catalytic properties capable of oxidizing analytes at lower potentials. Mn atoms, integrated into the lattice structure of SnO_2, favor oxidation-reduction (redox) reactions and cause acceleration in these processes. This makes the sensor more sensitive to analytes because the reactions take place with lower energy requirements. Secondly, the increased electron mobility provided by Mn doping optimizes the effects of SnO_2 on charge carriers. Mn modifies the band structure of SnO_2, increasing the mobility of electrons. This allows charge transfer to take place more quickly and efficiently. In electrochemical sensors, this means that response times are shortened, and the response speed of the sensor is increased. Thirdly, the surface contacts and adsorption characteristics of SnO_2 are enhanced due to Mn doping. Mn enables analytes to adsorb more effectively by integrating into the surface of SnO_2. This allows analytes to remain on the sensor surface longer and oxidation reactions more efficiently. Improved surface interactions increase the sensitivity and selectivity of the sensor (Choudhari & Jagtap, 2021; Koventhan et al.,

2022; Lavanya et al., 2016). As expected from the above explanation, Mn doping increased the anodic peak current value from 200 µA to 1000 µA at 0.6 V and the cathodic peak current value to 1000 µA at 0.5 V. The electrochemical characteristics of SnO_2 nanoparticles get better as more Mn is introduced. As the figure illustrates (Figure 4.54), the introduction of 2 wt% Mn enhanced the electrochemical activity of the SnO_2 nanoparticles. With these findings, it was decided to utilize 2 wt% Mn doped SnO_2 nanoparticles as a modifier for CPEs to meticulously asses the electrochemical sensor parameters for SAL detection.

4.5.7 Optimization of Experimental Conditions

4.5.7.1 Effect of Nanoparticles Amount

The sensitivity of the electrochemical sensor is mainly determined by the quantity of undoped SnO_2 and Mn doped SnO_2 nanoparticles present in the CPEs. Initially, the sensitivity of DP measurements was assessed using modified electrodes, including Mn doped SnO_2 nanoparticles at different amounts (2 to 20 wt%). Differential pulse (DP) measurements were performed on the modified CPEs at pH 7.5, in 0.1 M PBS containing 0.1 M (KNO_3), and in the presence of 5 x 10^{-5} M Ventolin. The solution was constantly agitated for 240 seconds with an accumulated potential of -300 mV applied before the measurement started. Data were acquiredat a scan rate of 40 $mV.s^{-1}$ between 0.0 and 0.9 V.

The data reveal that the 10 wt% amount performed better than the other amounts (Figure 4.55). Their responsiveness was decreased when more particles were added than the 10 wt% by weight. The reasons why 10 wt% Mn doped SnO_2 nanoparticles outperform higher amount ratios are based on several key factors. Firstly, 10 wt% Mn doping represents an optimal amount that enhances the electrical and catalytic properties of SnO_2 nanoparticles. At this level, Mn ions effectively provide charge carriers and improve catalytic activity. Higher doping levels can lead to agglomeration between nanoparticles and the formation of large particle aggregates, leading to reduced surface area and weakened charge transfer. Furthermore, excess Mn doping can affect the electrical conductivity of SnO_2 and create insulating properties, which degrades sensor performance.

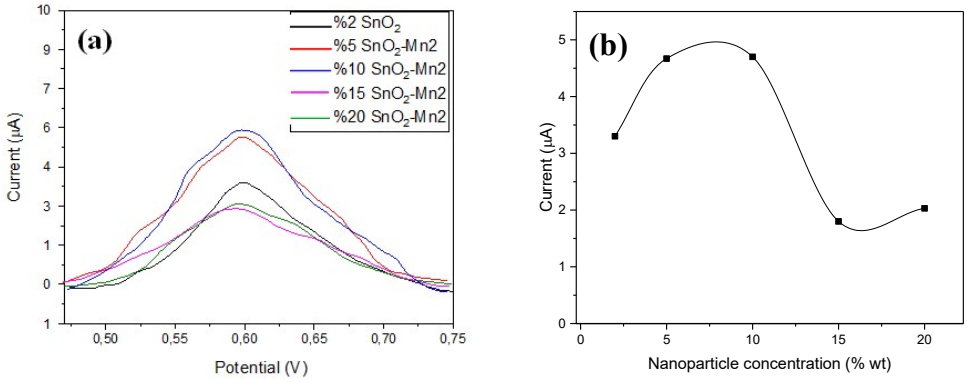

Figure 4.55 (a) DP response, (b) Current values obtained from differential pulse measurement using different amount (2 to 20 wt%) of SnO_2-Mn2 nanoparticles modified CPE in 0.1 M pH 7.5 PBS contains 0.1 M (KNO_3) in the presence of 5 x 10^{-5} M Ventolin

High doping rates can reduce reaction efficiency as excessive Mn weakens the electroactive sites and hinders electrochemical processes. For these reasons, 10 wt% Mn doping optimally balances the electrokinetic and catalytic properties of the nanoparticles, while higher doping levels disrupt this balance and adversely affect sensor performance (Shabani et al., 2018; Shetti et al., 2017). For this reason, the electrode that evolved with 10 wt% Mn doped SnO_2 nanoparticles was utilized in the study.

Undoped SnO_2 nanoparticles modified CPE showed no significant response to the electrochemical oxidation of salbutamol, while CPEs modified with Mn doped SnO_2 nanoparticles catalysed the electrochemical oxidation of salbutamol most effectively at 10 wt% amount.

4.5.7.2 Effect of Accumulation Time and Accumulation Potential

The amount of SAL absorbed on the electrode surface rises with accumulation. As a result, the detection limit decreases, and the sensitivity of the measurement increases. We investigated the impact of deposition potential on the electrochemical oxidation behavior of SAL using a range of deposition potential values between -0.5 V and 0.2 V. The deposition time was 240 s for CPE containing 10 wt% Mn doped SnO_2 nanoparticles. Figure 4.56 (a) shows the correlation diagram of the experimental data acquired by DPV. The oxidation response peak of SAL on the Mn doped SnO_2

nanoparticles modified CPE sensor is maximum at an accumulation potential of -0.2 V.

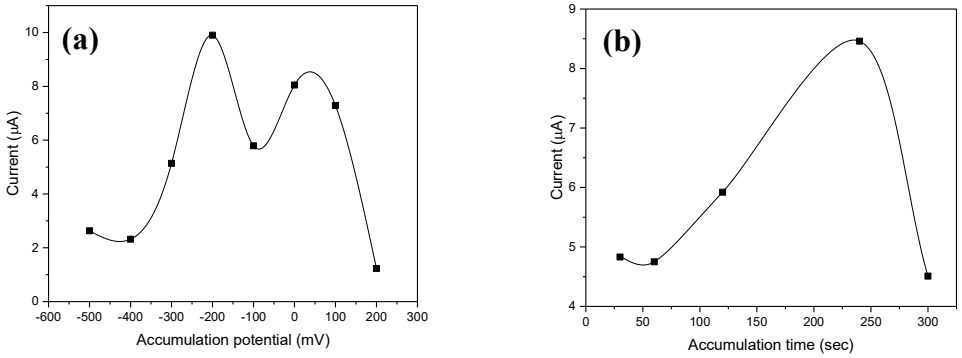

Figure 4.56 The DP peak current values of 5 x 10^{-5} M SAL in 0.1 M pH 7.5 PBS contains 0.1 M (KNO_3) on the 10 wt% Mn doped SnO_2 nanoparticles modified CPE (scan rate:40 $mV.s^{-1}$) (a) accumulation potential effect and (b) accumulation time effect

The peak intensities of the oxidation current come down at higher potentials produced by the reduction of hydrogen on the modified electrode surface (Baghayeri et al., 2019). Another plausible explanation could be nanostructures aggregate at larger current values, producing structures with lower surface areas. Furthermore, the impact of the accumulation time on the voltammetric behavior of SAL on the Mn doped SnO_2 nanoparticles modified CPE surface was investigated while maintaining an accumulation potential fixed at -0.2 V. Figure 4.56 (b) plots the SAL oxidation peak current signal against accumulation time. It is evident that when the accumulation duration is extended, the peak intensity first decreases and then gradually increases after 240 s of accumulation time. This result could be explained by saturation SAL adsorption on the electrode surface. In order to account for efficiency and sensitivity, the following experiment determined that 240 s was the appropriate accumulation time. CPEs modified with undoped SnO_2 nanoparticles showed no significant response to the electrochemical oxidation of salbutamol, whereas CPEs modified with Mn doped SnO_2 nanoparticles reached the highest electrochemical signal level at a deposition potential of -200 mV and deposition time of 240 s.

4.5.7.3 Effect of Support Electrolite and pH

By measuring DP at different pH values between 4 and 9, 0.1 M PBS was used to examine the impact of pH on the CPE's response. According to the oxidation of phenolic hydroxy groups, the peak current was also pH-dependent (Figure 4.57(a)).

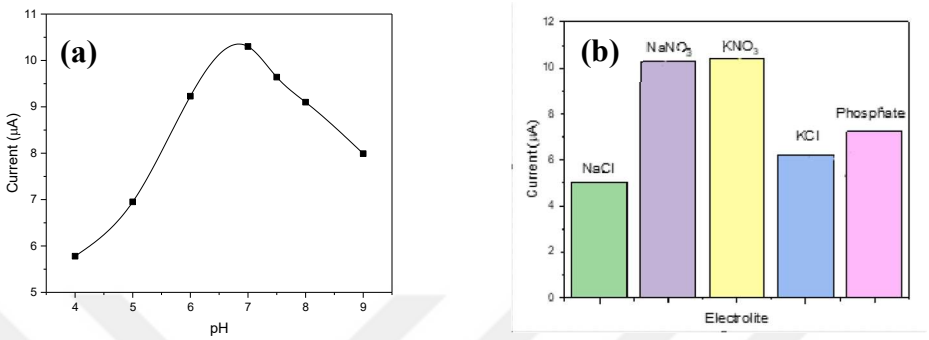

Figure 4.57 The DP peak current values (a) solution pH values and (b) supporting electrolyte solution. (The concentration of SAL solution is 5 x 10^{-5} M)

The peak elevation increased significantly when the pH was raised from 4 to 7 and decreased at pH 8. This is also consistent with other research that has been published (Islam et al., 2022; Westbroek, 2005). Some of this tendency may be explained by the Coulomb force of attraction and repulsion between the SAL and the electrode modifier at different pH settings (Amare and Menkir, 2017). The determined pH for the experiment to yield the best results was a pH 7 phosphate buffer. Choosing the suitable supporting electrolyte composition and pH is imperative to correctly interpret the electrochemical behavior of the analyte material on the electrode used in a voltammetric inquiry. For these investigations, phosphate buffer is the recommended mixed buffer solution due to its extensive operating range. The effects of supporting electrolytes were investigated using various supporting electrolytes, including 0.1 M NaCl, $NaNO_3$, KCl, and KNO_3 solutions. The DP approach measurements were validated using CPEs doped with 10 wt% Mn and modified with SnO_2 nanoparticles. The SAL oxidation peak current values, which are highest in the KNO_3 solution, are shown in Figure 4.57(b). The CPEs modified with undoped SnO_2 nanoparticles gave no visible signal against the electrochemical oxidation of salbutamol, but the CPEs modified with Mn doped SnO_2 nanoparticles reached the highest electrochemical signal level with KNO_3 supported electrolytes in phosphate buffer solution at pH 7.5.

4.5.7.4 Calibration Curve and Limit of Detection

For SAL qualitative analysis, differential pulse measurement has been applied under ideal circumstances (Figure 4.58 (a)). Figure 4.58(b) reveals anodic peak current vs. SAL concentrations in the 0.01–500 µM range. An upward tendency in the anodic peak current was seen with increasing SAL content.

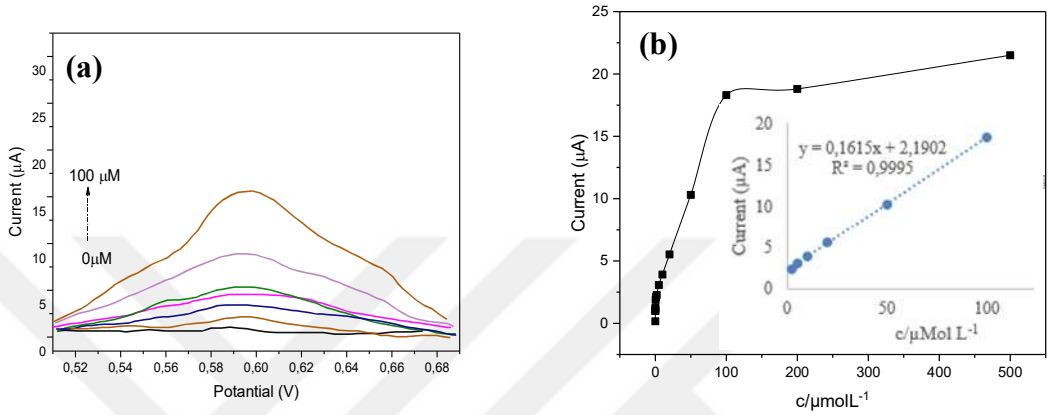

Figure 4.58 (a) DP responses of Mn doped SnO_2 nanoparticles modified CPE to different SAL concentrations, (b) represents the appropriate calibration plot used to quantify SAL. (measurement conditions: different concentrations of SAL in 0.1 M pH 7.5 PBS contains 0.1 M (KNO_3) on the 10 wt% Mn doped SnO_2 nanoparticles modified CPE (scan rate:100 $mV.s^{-1}$)

The calibration range for SAL concentration was found to be 5 µM to 100 µM, with a correlation coefficient (R^2) of 0.9995 (Figure 4.58). These values were derived from the data obtained from the analytical curves and represent the limit of quantification (LOQ) of 10 s/m and the lowest LOD of 3 s/m. Following data entry into the computation, LOQ=189.47 nM and LOD=56.84 nM were discovered.

While electrodes modified with SnO_2 nanoparticles could not be used for salbutamol detection, electrodes modified with Mn doped SnO_2 nanoparticles showed high sensitivity for salbutamol detection, LOQ value was 189.47 nM and LOD value was 56.84 nM.

4.5.7.5 Selectivity, Repeatability, Reproducibility, and Stability

The repeatability of the sensor was examined by utilizing the DPV technique to determine the 5×10^{-5} M SAL in pH 7.5 PBS with 0.1 M (KNO_3) and CPE modified with Mn doped SnO_2 nanoparticles. Each analyte was validated using ten different

electrodes. High repeatability was shown by the RSD of 2.05% for SAL ($n = 10, \overline{x} = 50.09\ \mu M, SD = 0.48$). The DP current responses were measured every other day for a week to evaluate the modified CPE's storage stability. The electrode was kept dry when it was not in use. Even after two weeks, it retained up to 94.92% of the initial signal. According to test findings, the redesigned electrode shows excellent repeatability and stability. To illustrate the selectivity of the Mn doped SnO_2 nanoparticle modified CPE, a variety of potential interferents were examined, such as dopamine, starch, ascorbic acid, epinephrine, glucose, Na^+, and Fe^{3+} (Figure 4.59).

The test findings suggest that the SAL signals are not significantly affected by the interference concentration of 8.5 x 10^{-5} M. It was discovered that this method has a high degree of selectivity for determining SAL. Consequently, with a measurement time of around 20 seconds, the Mn doped SnO_2 nanoparticles modified CPE utilized in this work is a quick and accurate sensor.

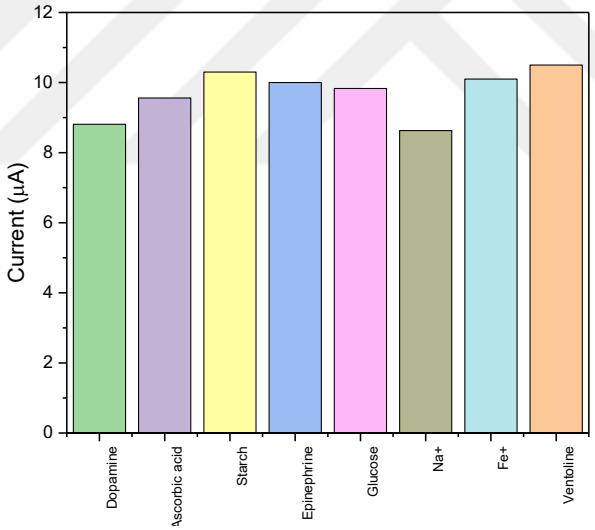

Figure 4.59 Peak current values in case of interference

The electrodes modified with pure SnO_2 nanoparticles did not produce reliable results for detecting salbutamol. However, electrodes modified with Mn doped SnO_2 nanoparticles demonstrated excellent selectivity in detecting salbutamol, even in other substances such as dopamine, starch, ascorbic acid, epinephrine, glucose, Na^+, and Fe^{3+}. This makes it an ideal method for practical applications. Furthermore, this sensor demonstrated high reproducibility (2.05% RSD) and signal stability of 94.92% after two weeks of use, making it a reliable and stable device.

4.5.8 Electrochemical Detection of Salbutamol with Ce doped SnO_2 Nanoparticles Modified Carbon Paste Electrode

The electrochemical activity of SAL on bare CPE, SnO_2 nanoparticles modified CPE, and Ce doped SnO_2 nanoparticles modified CPE sensors were compared using cyclic voltammograms (Figure 4.60). Cyclic voltammograms (CVs) were obtained for electrodes modified with undoped and Ce doped SnO_2 nanoparticles CPE and bare CPE in the presence of 8.5 x 10^{-5} M SAL in 0.1 M PBS (pH = 7.5) at a scan rate of 40 $mV.s^{-1}$. Before conducting cyclic voltammetry, an accumulating potential of -300 mV was applied for 240 s. A notable rise in peak intensity, approximately 300 µA around 0.6 V, was noted in the anodic direction in the Ce doped SnO_2 modified CPE electrode when SAL was present.

This implies that more oxidized SAL species are on the modified electrode's surface. These results suggest that SAL oxidation increased as a result of due to the modified electrode's enhanced electrocatalytic activity. Furthermore, the peak current density in SnO_2-Ce0.25 nanoparticles modified CPE increased by 2-3 times more than that in bare CPE; this suggests that Sn doping has improved its electrochemical performance. Moreover, a converse rise in peak intensity was noted with Ce doping. The idea that the oxygen vacancy brought on by doping plays a significant part in the charge-carrying behavior of SnO_2 nanoparticles is supported by the observed enhancement in the charge-carrying property of Ce doped SnO_2 nanoparticles modified CPE.

The results indicate that 0.25% cerium (Ce) doping in the SnO_2 structure reaches the saturation point, facilitating charge transfer between the modified electrode surface and the redox couple (M. Ibrahim et al., 2017; Lian et al., 2017). The accelerated electron transfer kinetics and greater electroactive surface area of Ce doped SnO_2 nanoparticles can be attributed to the observed reduction in ΔE_P and related improvement in the redox peak current values.

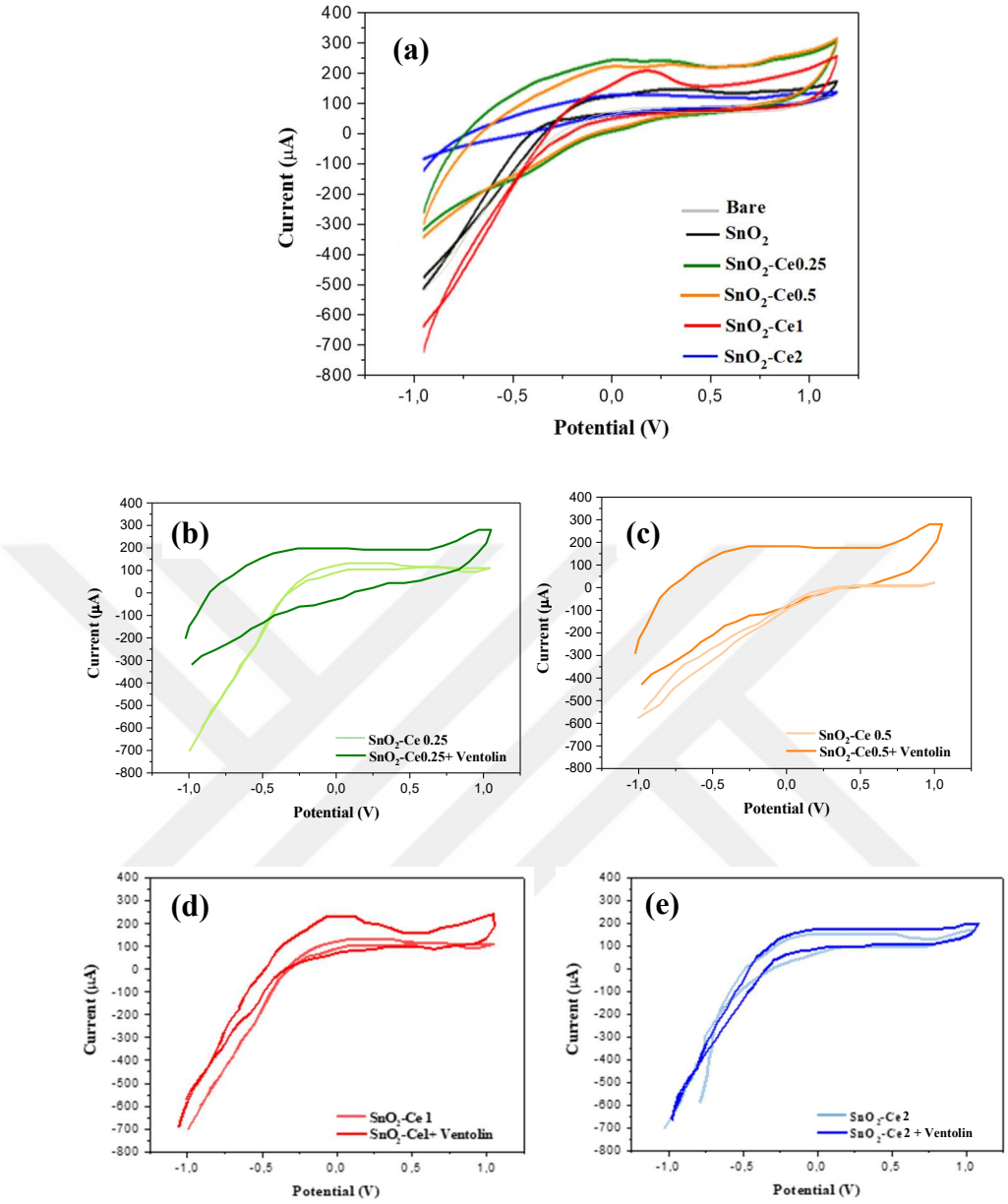

Figure 4.60 (a) CV curves at a bare CPE, 10 wt% SnO_2 and Ce doped SnO_2 nanoparticles modified CPE in the absence and the presence of 8.5 x 10^{-5} M Salbutamol 0.1 M pH 7.5 PBS containing 0.1 M (KNO_3), CV curves of nanoparticles modified CPE with (b) SnO_2-Ce0.25 nanoparticles, (c) SnO_2-Ce0.5 nanoparticles, (d) SnO_2-Ce1 nanoparticles, (e) SnO_2-Ce2 nanoparticles. Scan rate: 40 $mV.s^{-1}$

4.5.9 Optimization of Experimental Conditions

4.5.9.1 Effect of Nanoparticles Amount

The present study examined the effects of different amounts of SnO_2 and Ce doped SnO_2 nanoparticles in modified CPE on the electrochemical sensor performance. In

differential pulse (DP) tests, the modified carbon paste electrodes (CPE) were assessed based on the quantities of Ce-doped SnO_2 nanoparticles. These nanoparticles were employed at varying weight amounts, ranging from 2% to 20 wt%. DP measurements were performed in 5 x 10^{-5} M Ventolin and 0.1 M PBS with 0.1 M KNO_3 at pH 7.5, The electrode surface was subjected to an accumulating potential of -300 mV before the experiment, and this potential was sustained for 240 seconds by vigorously agitating the liquid. After that, the mixture was given fifteen seconds to After that, the mixture was given fifteen seconds to acclimatise. Using a potential range of 0.0 and 0.9 V, data were collected at a scan rate of 40 $mV.s^{-1}$. The results of Figure 4.61 demonstrate that the amount of 15 wt% Ce-doped SnO_2 nanoparticles is superior to other amounts.

The results revealed that the 15 wt% Ce-doped SnO_2 nanoparticles used in the sensor performed better than the different ratios. There are several possible reasons for this situation. Firstly, it can be considered that 15 wt% provides a sufficient amount of Cedoped SnO_2 in the sensor and creates an adequate quantity of active centers for the oxidation of salbutamol. Using a higher amount of Ce-doped SnO_2 may lead to excessive coverage of the sample surface, preventing access and oxidation of salbutamol to the electrode surface. 15 wt% Ce doped SnO_2 is likely to provide the electronic properties of material more favorable for the oxidation of salbutamol. Higher amounts of Ce doping may slow down the oxidation of salbutamol by adversely affecting electron transfer (Shabani et al., 2018; Shetti et al., 2017).

It was found that the amount at the electrode surface produced the strongest electrochemical reaction. Under conditions where more than 15 wt% of nanoparticles were included, the sensor performance degraded, and current responses decreased. As a result, the modified electrode showing optimum performance for this research was determined to be the electrode containing 15 wt% by weight Ce doped SnO_2 nanoparticles.

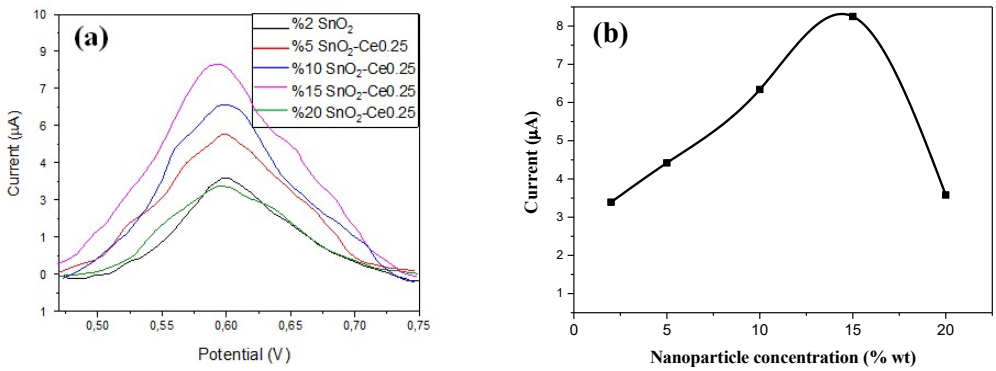

Figure 4.61 (a) DP response, (b) Current values obtained from differential pulse measurement using different amount (2 to 20 wt%) of SnO_2 Ce0.25 nanoparticles modified CPE in 0.1 M pH 7.5 PBS contains 0.1 M (KNO_3) in the presence of 5 x 10^{-5} M Ventolin

4.5.9.2 Effect of Accumulation Time and Accumulation Potential

The quantity of SAL absorbed on the electrode surface increases due to accumulation, which lowers the detection limit and increases measuring sensitivity. Different deposition potential values between -0.5 V and 0.2 V were used, with the amount of Ce doped SnO_2 nanoparticles set at 15 wt% and 240 s as the deposition period, to examine the impact of the deposition potential on the electrochemical oxidation behavior of SAL. Figure 4.62 (a) shows the correlation diagram for the experimental data acquired by DPV. The oxidation response peak of SAL on the Ce doped SnO_2 nanoparticles modified CPE sensor is maximum at an accumulation potential of -0.3 V. Because of the hydrogen reduction at the changed electrode surface, the peak intensities of the oxidation current reduced at higher potentials (Baghayeri et al., 2019). It was discovered that the ideal accumulating potential was -0.3 V. Furthermore, the accumulation time effect on the voltammetric behavior of SAL on the Ce doped SnO_2 modified CPE surface was investigated (with the accumulation potential set at -0.3 V).

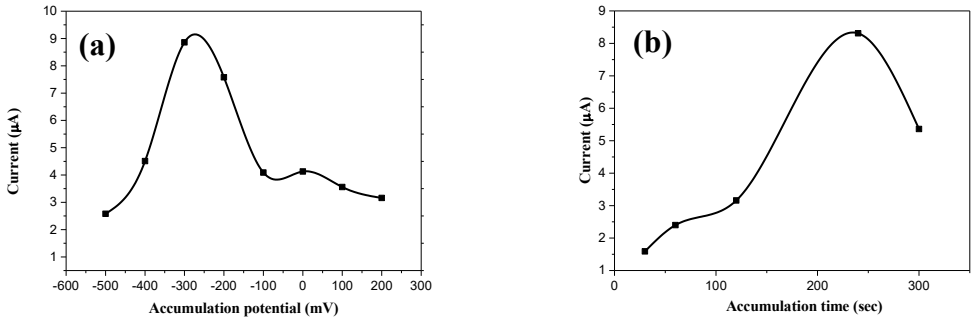

Figure 4.62 15 wt% Ce doped SnO_2 nanoparticles modified CPE (scan rate:40 $mV.s^{-1}$) (a) accumulation potential effect, and (b) accumulation time effect

Figure 4.62 (b) shows the SAL oxidation peak current signal versus accumulation time. It is evident that when the accumulation duration is extended, the peak intensity initially decreases and then gradually increases after 240 seconds of accumulation. This finding might be explained by saturation SAL adsorption on the electrode surface. Therefore, the ideal accumulation time used in the research was 240 seconds, taking into account both efficiency and sensitivity.

The electrodes modified with SnO_2 nanoparticles did not respond sufficiently to salbutamol's electrochemical oxidation. In contrast, the electrodes modified with Ce doped SnO_2 nanoparticles reached the highest electrochemical signal level at a deposition potential of -300 mV and deposition time of 240 s.

4.5.9.3 Effect of Support Electrolite and pH

By measuring DP at different pH values between 4 and 9, 0.1 M PBS was used to examine the impact of pH on the CPE's response. A pH-dependent peak current was also produced by this oxidation of phenolic hydroxy groups (Figure 4.63(a)). Additionally, this is in line with earlier research. Toghan and colleagues introduced a new electrochemical sensor that uses glassy carbon electrodes modified with graphene oxide and poly(o-nitrobenzoic acid) to detect salbutamol in human urine and pharmaceutical formulations (Toghan, Abo-Bakr, et al., 2019). Salbutamol in aqueous solutions is determined electrochemically by Nhi et al. using modified UiO-66/rGO electrodes (Thi Thanh Nhi et al., 2024). Both studies examined the pH value in detail in the sensor optimization stage, and the results are in parallel with the findings obtained in this thesis. Increasing the pH from 4 to 7 resulted in a notable increase in

the peak height, which decreased at pH 8. This trend may be partially explained by the Coulomb repulsion and attraction forces between the SAL and the electrode exchanger, depending on the pH range(Amare and Menkir, 2017). It was found that the optimal pH for the experiment to yield the best results was a pH 7 phosphate buffer.

In a voltammetric investigation, choosing the appropriate supporting electrolyte composition and pH is critical to accurately interpret the electrochemical act of the analyte component on the electrode used. Because of its broad working range, phosphate buffer is the recommended mixed buffer system for these investigations.

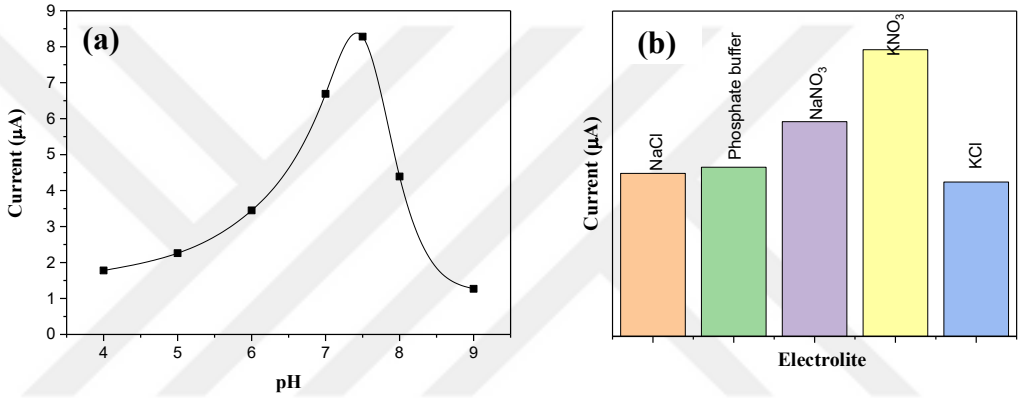

Figure 4.63 The DP peak current values (a) solution pH values, and (b) supporting electrolyte solution

To ascertain the impact of supporting electrolytes, several supporting electrolytes, including 0.1 M solutions of NaCl, $NaNO_3$, KCl, and KNO_3, were employed in the investigations. The DP approach was used to validate the data using CPE doped with 15 %wt Ce doped SnO_2 nanoparticles. Figure 4.63 (b) displays the SAL oxidation peak peak current values, which are greatest in the KNO_3 solution. The electrodes modified with SnO_2 nanoparticles gave no visible signal against the electrochemical oxidation of salbutamol. However, the electrodes modified with Ce-doped SnO_2 nanoparticles reached the highest electrochemical signal level using KNO_3-supported electrolytes in a phosphate buffer solution at pH 7.5.

4.5.9.4 Calibration Curve and Limit of Detection

Qualitative examination of SAL has been performed under ideal circumstances using differential pulse measurement (Figure 4.64 (a)). The association between anodic peak current and SAL concentrations in the 0.01–500 µM range is seen in

Figure 4.64 (b). An upward tendency in the anodic peak current was seen with increasing SAL concentration.

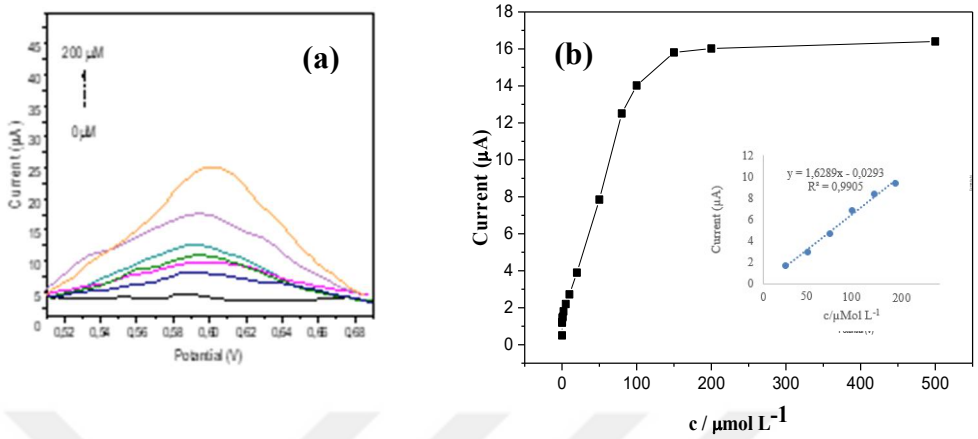

Figure 4.64 (a) DP responses of Ce doped SnO_2 nanoparticles modified CPE to different SAL concentrations. SAL concentration range covered 0.01 to 500 µM. (b) represents the appropriate calibration plot used to quantify SAL

In Figure 4.64 (b: inset), the SAL concentration calibration range was shown to have a correlation value (R^2) of 0.9905. Upon incorporating the data into the calculation, we found that the LOQ is 10.61 nM, and the LOD is 3.16 nM. Salbutamol detection was not possible with electrodes evolved with SnO_2 nanoparticles; however, electrodes modified with Ce doped SnO_2 nanoparticles demonstrated great sensitivity for salbutamol detection. This sensor achieved a limit of detectability (LOQ) of 10.61 nM and a limit of identification (LOD) of 3.16 nM, making it an effective sensor for SAL determination.

4.5.9.5 Selectivity, Repeatability, Reproducibility, and Stability

To determine 5 x 10^{-5} M SAL utilizing DPV in 0.1 M pH 7.5 PBS containing 0.1 M (KNO_3) pH 7.5, the repeatability of the sensor was tested using the Ce doped SnO_2 nanoparticles modified CPE. Ten samples of each analyte were run through ten modified electrodes to test repeatability. The relative standard deviations, which came out to be 1.73%, demonstrated the excellent reproducibility of the peak current of SAL $(n = 10, \bar{x} = 50.37\ \mu M, SD = 0.19)$ DP current responses were monitored every other day over two weeks to evaluate the modified storage stability of CPEs. The electrode was kept in a dry environment when not in use. After two weeks, it could

still maintain 70% of the initial signal. The results of the tests show that compared to other modified electrodes, the modified electrode has reduced repeatability and stability. This situation is thought to be due to the unstable electron states of the Ce element. A variety of potential interferents, including glucose, Na^{+}, Fe^{3+}, ascorbic acid, dopamine, starch, and ascorbic acid, were investigated to illustrate the selectivity of the Ce doped SnO_2 nanoparticles modified CPE (Figure 4.65).

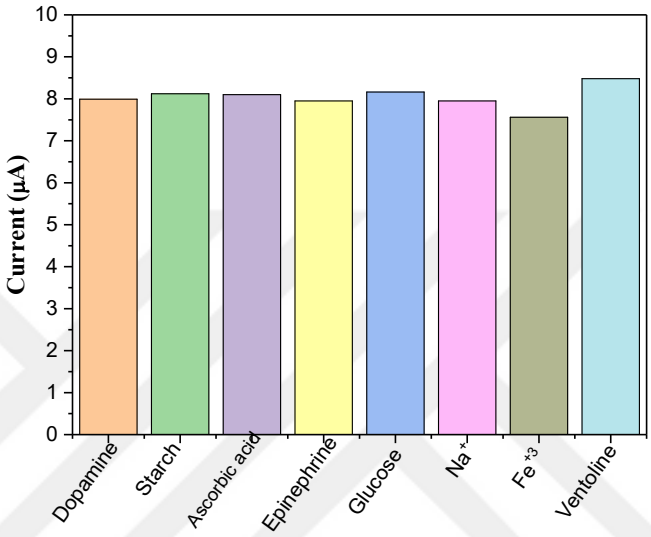

Figure 4.65 Peak current values in case of interference

Based on test results, the 8.5 x 10^{-5} M interference concentration had no discernible effect on the SAL signals. It was found that the selectivity of this approach for figuring out SAL is rather good. While electrodes modified with SnO_2 nanoparticles do not perform well enough to determine salbutamol, electrodes modified with Ce doped SnO_2 nanoparticles allow for the highly selective detection of salbutamol even when other substances like dopamine, starch, ascorbic acid, epinephrine, glucose, Na^{+}, and Fe^{3+} are present. As a result, these electrodes provide an ideal method for practical applications. Furthermore, this sensor demonstrates a reliable and relatively stable performance, showing high reproducibility (1.73% RSD) and 70% signal stability over two weeks of use.

Similar studies on the determination of salbutamol (SAL) in the literature have been thoroughly reviewed, and the findings obtained using various methods are summarized in Table 4.2. These studies are compared in terms of the electrode materials, employed analytical techniques, and sensor performance. Nanomaterials modified sensors have

garnered significant attention due to their enhanced electrode surface area and improved electron transfer capabilities. However, a major limitation is the reliance on costly modifiers and complex electrode modification processes.

Table 4.2 Some electrochemical sensor applications for SAL determination

Method/Electrode	***Method***	***Linear Range (µM)***	***Detection Limit (µM)***	***Reproductibility (RSD%)***	***Reference***
Cathodically pretreated boron-doped diamond	Cyclic and adsorptive stripping voltammetry	17.3-34.7	5.06 µM	4.85	Pınar et al., 2018
Modified glassy carbon electrode	Differential pulse voltammetry	0.2-8.0	0.6 pM	3.8	Amare et al., 2017
3D RGO/Ni foam	Electrochemical-facial deposition	0.042-1.16	23 nM	-	Wang et al., 2018
Indium tin oxide electrode	Squareawave voltammetry	0.15-6.0	0.225 µM		Goyal et al., 2007
SMWCNTa -NF	Differential pulse voltammetry	0.10–0.30	0.10	5.3	Lin et al. 2013
GP-PEDOT:PSS/SPCE modified CPE	inkjet-printing technique	5–550	0.36 nM	7.5	Karuwan et al., 2012

The findings obtained within the scope of the thesis are presented in Table 4.3. These results were evaluated in detail to assess the effectiveness of the method used in the study and the performance of the sensors developed using metal oxide nanoparticles in comparison with the literature. The obtained data reveal that the sensor properties are improved in terms of analytical parameters by nanoparticle modification. Therefore, the results in Table 4.3 support the main performance criteria of the sensor such as detection range, repeatability and stability with electrochemical data.

Table 4.3 Electrochemical results of the developed sensors

Sensor Type	***LOD (nM)***	***Calibration Range***	***RSD (%)***	***Stability (%)***
CuO nanoparticles Modified CPE	50	50 nM-100 µM	3	80
Mn doped CuO nanoparticles modified CPE	58.25	2-200 µM	1.89	98.24
Ce doped CuO nanoparticles modified CPE	34.18	10-100 µM	1.57	92
SnO_2 nanoparticles Modified CPE	-	-	-	-
Mn doped SnO_2 nanoparticles modified CPE	56.84	5-100 µM	2.05	94.92
Ce doped SnO_2 nanoparticles modified CPE	3.16	2-200 µM	1.73	70

CHAPTER FIVE
CONCLUSION

In this thesis, a potential candidate electrochemical sensor material for the detection of salbutamol anlide was investigated. The synthesis of undoped and (Mn; Ce) doped metal oxide (CuO and SnO_2) nanoparticles as electrochemical candidate sensor material was carried out by sol-gel method. Solution pH and calcination temperature, which are important sol-gel parameters in the production of metal oxide structures, were discussed and in addition, the type and amount of transition and rare earth element doping were also discussed. The characterization processes of the produced candidate materials were carried out and the sensor properties were investigated using electrochemical methods. The results obtained in the thesis are given below:

The optimum conditions for producing pure CuO nanoparticles were found to be pH 7 and calcination temperature 500°C. The nanoparticles obtained under these conditions have a spherical morphology and their average size was measured as 73.87 nm. Because more OH- ions were in the solution at high pH levels, nucleation, and crystal formation were encouraged, increasing grain size. In addition, high calcination temperatures accelerated the diffusion mechanism and facilitated grain growth. It was concluded that the Mn doping to CuO nanoparticles caused the stress and defects in the crystal lattice due to the ionic radius of the Mn element being larger than that of the Cu element, causing a decrease in particle size to 68.27 nm. The changes caused by Mn doping in the crystal structure of CuO nanoparticles were confirmed by XRD and FTIR analyses, and the structure was found to be of high purity. The particle size of Ce-doped CuO nanoparticles dropped to 59 nm as the quantity of Ce increased. This indicates that Ce doping has a controlling effect on crystal growth.

Similarly, the effects of dopant elements, pH, and calcination temperature on the production of SnO_2 nanoparticles were thoroughly examined. The ideal synthesis parameters for SnO_2 nanoparticles were found to be pH 2 and a calcination temperature of 400°C. Under these circumstances, SnO_2 nanoparticles were produced with a consistent, spherical shape, with an average size of 66.42 nm. Smaller grain sizes formed at low pH levels because the high concentration of H^+ ions in the solution accelerated the nucleation rate. Grain growth was accelerated by high calcination

temperatures, which also accelerated diffusion processes. Because Mn^{2+} has a greater ion radius than Sn^{2+}, defects in the crystal structure developed during the production of SnO_2 nanoparticles with Mn^{2+} doping, preventing grain size expansion. Through XRD and FTIR investigations, the effects of Mn doping on the crystal structure of SnO_2 were verified, and it was noted that the structure was very pure. The changes caused by Mn doping in the crystal structure of SnO_2 led to a noticeable decrease in grain size (40.66 nm). Particle size dramatically decreased when Ce concentration increased throughout the SnO_2 synthesis process. The average grain size of Ce doped SnO_2 nanoparticles was measured as 66.42, 59.02 nm, 41.41 nm, and 45.34 nm with increasing Ce doping, respectively. This indicates that Ce doping has an inhibitory effect on crystal growth and results in smaller grain sizes. It was found that Ce doping improves the morphological properties of SnO_2 nanoparticles and shows high electrochemical performance.

As a result of evaluations on electroanalytical sensors, pure CuO sensors were found to offer a LOD (limit of detection) of 50 nM for SAL (salbutamol) detection and a calibration range between 50 nM and 100 μM. Mn^{2+}-doped CuO nanoparticles modified sensors provided a slightly higher LOD (58.25 nM) and offered a wide calibration range from 2 μM to 200 μM. The highest performance was obtained with Ce doped CuO nanoparticles. These sensors showed high sensitivity and accuracy with an LOD of 34.18 nM and LOQ (limit of quantification) of 113.95 nM. The sensor was reported to have excellent repeatability and stability, and it could sustain its functionality for two weeks with an RSD of 1.57%. SnO_2 nanoparticles generally did not perform sufficiently for SAL (salbutamol) detection. However, Mn^{2+}-doped SnO_2 nanoparticles significantly solved this problem. Mn doped SnO_2 nanoparticles offered an improved detection sensitivity with LOD values of 56.84 nM and LOQ values of 189.47 nM. The changes caused by Mn doping in the crystal structure of SnO_2 improved the electrochemical performance of the sensors and created a more sensitive platform for the detection of SAL. It was observed that Mn doping improved the electrochemical properties of SnO_2 nanoparticles and provided high selectivity for SAL detection. The effect of Mn addition made the sensor effective even at low concentrations and showed high performance against potential interferences. Ce^{3+} doped SnO_2 nanoparticles presented a high detection sensitivity with a LOD (limit of

detection) of 1.72 nM and LOQ of 3.16 nM. The changes caused by Ce doping in the crystal structure of SnO_2 significantly improved the electrochemical performance of the sensors and created a more sensitive platform for the detection of SAL. Ce doping enhanced electrochemical characteristics of SnO_2 nanoparticles and offer excellent selectivity for SAL detection. The effect of Ce enabled the sensor to be effective even at low concentrations and showed high performance against potential interferences.

The findings obtained in our study reveal that CuO and SnO_2 nanoparticles show high performance in electrochemical sensor applications for the detection of salbutamol (SAL) analyte. However, these results offer significant opportunities for a more comprehensive application potential. Our suggestions for further studies are as follows: Firstly, the adaptation of the sensors to the detection of different biomolecules, critical analytes such as glucose, dopamine and uric acid, could expand the range of applications. Furthermore, the ability to detect more than one analyte simultaneously would be a step that would increase the practical use of the sensors. The effects of different nanostructures, especially nanowires and nanorods, on the performance should be investigated to increase the surface area and reactivity. In addition, testing the obtained modified electrodes in real biological and chemical matrices, such as blood serum and human urine, will reveal the suitability of the sensors for practical applications. The long-term stability and resistance to environmental conditions of the developed sensors should also be evaluated, thus enabling their transition to industrial use. Finally, the use of artificial intelligence and machine learning techniques to analyse sensor data will increase detection accuracy and speed up data processing processes. Studies to be carried out in line with all these suggestions will contribute to the development of commercially viable electrochemical sensors with wide application areas by further improving the performance of nanoparticles.

REFERENCES

Aashima, Uppal, S., Arora, A., Gautam, S., Singh, S., Choudhary, R. J., & Mehta, S. K. (2019). Magnetically retrievable Ce-doped Fe_3O_4 nanoparticles as scaffolds for the removal of azo dyes. *RSC Advances*, *9*(40), 23129-23141. https://doi.org/10.1039/c9ra03252e

Abutaleb, A., & Imran, M. (2021). Thermal conductivity enhancement for CuO nanoflakes in oil-based and oil blend-based nanofluids. *Journal of the Chinese Chemical Society*, *68*(8), 1400-1404. https://doi.org/10.1002/jccs.202100005

Agrahari, V., Mathpal, M. C., Kumar, S., & Agarwal, A. (2016). Low field room temperature magnetism and band gap modifications in Sm doped SnO_2. *Journal of Materials Science: Materials in Electronics*, *27*(3), 3053-3064. https://doi.org/10.1007/s10854-015-4129-2

Agrahari, V., Tripathi, A. K., Mathpal, M. C., Pandey, A. C., Mishra, S. K., Shukla, R. K., & Agarwal, A. (2015). Effect of Mn doping on structural, optical and magnetic properties of SnO2 nanoparticles. Journal of Materials Science: Materials in Electronics, 26(12), 9571–9582. https://doi.org/10.1007/s10854-015-3620-0.

Ahmed, A., Siddique, M. N., Ali, T., & Tripathi, P. (2019). Defect assisted improved room temperature ferromagnetism in Ce doped SnO_2 nanoparticles. *Applied Surface Science*, *483*, 463–471. https://doi.org/10.1016/j.apsusc.2019.03.209

Akbari Javar, H., Rajabizadeh, A., Dehghannoudeh, G., & Mahmoudi-Moghaddam, H. (2022). Electrochemical determination of sulfamethoxazole in biological and drug samples using Ce (III)-doped CuO modified electrode. *Measurement*, *203*, 111936. https://doi.org/10.1016/j.measurement.2022.111936

Al Fatease, A., Haque, M., Umar, A., Ansari, S. G., Alhamhoom, Y., Muhsinah, A. Bin, Mahnashi, M. H., Guo, W., & Ansari, Z. A. (2021). Label-free electrochemical sensor based on manganese doped titanium dioxide nanoparticles for myoglobin detection: Biomarker for acute myocardial infarction. *Molecules*, *26*(14). https://doi.org/10.3390/molecules26144252

Albarakati, A. J., & Matter, I. A. (2023). N-Type Metal Oxide Semiconductor: Materials and Their Environmental Applications. *Biointerface Research in Applied Chemistry*, *13*(6), 1–23. https://doi.org/10.33263/brıac136.519

Albert manoharan, A., Chandramohan, R., David prabu, R., Valanarasu, S., Ganesh, V., Shkir, M., Kathalingam, A., & AlFaify, S. (2018). Facile synthesis and characterization of undoped, Mn doped and Nd co-doped CuO nanoparticles for optoelectronic and magnetic applications. *Journal of Molecular Structure*, *1171*, 388–395. https://doi.org/10.1016/j.molstruc.2018.06.018

Albrecht, T. R., Crootof, A., Scott, C. A., Gevorgyan, S. A., Heckler, I. M., Bundgaard, E., Sainbhi, A. S., Marquez, I., & Gomez, A. (2022). An overview of voltammetric techniques to the present era. *Electrochemical Sensors Based on Carbon Composite Materials*, 1-1-1–24. https://doi.org/10.1088/978-0-7503-5127-0ch1

Ali Baig, A. B., Rathinam, V., & Palaninathan, J. (2021). Facile synthesis of Ce-doped SnO2 nanoparticles with enhanced performance for photocatalytic degradation of organic dye. *Journal of the Iranian Chemical Society*, *18*(1), 13–27. https://doi.org/10.1007/s13738-020-02000-2

Alim, S., Kafi, A. K. M., Rajan, J., & Yusoff, M. M. (2019). Application of polymerized multiporous nanofiber of SnO2 for designing a bienzyme glucose biosensor based on HRP/GOx. *International Journal of Biological Macromolecules*, *123*, 1028–1034. https://doi.org/10.1016/j.ıjbıomac.2018.11.171

Altammar, K. A. (2023). A review on nanoparticles: characteristics, synthesis, applications, and challenges. *Frontiers in Microbiology*, *14*. https://doi.org/10.3389/fmicb.2023.1155622/full

Alvin, E. A., de Moraes, N. C., de Oliveira, Y. M., da Silva, D. G. P., Barbosa, A. I. dos S., Ribeiro, W. S. M., Vermelho, M. V. D., de Freitas, J. M. D., de Freitas, J. D., Dantas, N. O., Meneses, D., Lucca, B. G., de Abreu, F. C., & Silva, A. C. A. (2024). A novel paper-based electrochemical device modified with Ni-doped TiO2 nanocrystals-decorated graphene oxide for ascorbic acid detection. Materials Chemistry and Physics, 314, 128786.

https://doi.org/10.1016/j.matchemphys.2023.128786

Amare, M., & Menkir, G. (2017). Differential pulse voltammetric determination of salbutamol sulfate in syrup pharmaceutical formulation using poly(4-amino-3-hydroxynaphthalene sulfonic acid) modified glassy carbon electrode. *Heliyon*, *3*, e00417. https://doi.org/10.1016/j.heliyon.2017

Arun, L., Karthikeyan, C., Philip, D., Dhayanithi, D., Giridharan, N. V., & Unni, C. (2018). Influence of transition metal ion Ni^{2+} on optical, electrical, magnetic and antibacterial properties of phyto-synthesized CuO nanostructure. *Optical and Quantum Electronics*, *50*(12). https://doi.org/10.1007/s11082-018-1684-9

Asaithambi, S., Sakthivel, P., Karuppaiah, M., Yuvakkumar, R., Velauthapillai, D., Ahamad, T., Khan, M. A. M., Mohammed, M. K. A., Vijayaprabhu, N., & Ravi, G. (2021). The bifunctional performance analysis of synthesized Ce doped SnO_2/g-C_3N_4 composites for asymmetric supercapacitor and visible light photocatalytic applications. *Journal of Alloys and Compounds*, *866*, 158807. https://doi.org/10.1016/j.jallcom.2021.158807

Attou, L., Jaber, B., & Ez-Zahraouy, H. (2018). Effect of annealing temperature on structural, optical and photocatalytic properties of CuO nanoparticles. *Mediterranean Journal of Chemistry*, *7*(5), 308–316. https://doi.org/10.13171/mjc751911261230la

Autolab Application Note EC08. (2011). Basic overview of the working principle of a potentiostat/galvanostat (PGSTAT)-Electrochemical cell setup. *Metrohm Autolab.B.V*, 1-3. https://ceramrtr.ceramika.agh.edu.pl/~szyszkin/eis/Autolab_Application_Note_EC08_(Basic overview of the working principle of a potentiostat-galvanostat (PGSTAT) %96 Electrochemical cell setup).pdf

Baig, N., Kammakakam, I., Falath, W., & Kammakakam, I. (2021). Nanomaterials: a review of synthesis methods, properties, recent progress, and challenges. *Materials Advances*, *2*(6), 1821–1871. https://doi.org/10.1039/d0ma00807a

Bakker, E., & Pretsch, E. (2008). Nanoscale potentiometry. *TrAC - Trends in*

Analytical Chemistry, *27*(7), 612–618. https://doi.org/10.1016/j.trac.2008.04.007

Baldwin, R. P., & Thomsen, K. N. (1991). Chemically modified electrodes in liquid chromatography detection: A review. *Talanta*, *38*(1), 1–16. https://doi.org/10.1016/0039-9140(91)80004-J

Banerjee, A., Maity, S., & Mastrangelo, C. H. (2021). Nanotechnology for Biosensors: A Review. https://doi.org/10.20944/preprints202101.0152.v1

Bănică, F. G. (2012). *Chemical Sensors and Biosensors: Fundamentals and Applications*. Chemical Sensors and Biosensors: Fundamentals and Applications. https://doi.org/10.1002/9781118354162

Baranwal, J., Barse, B., Gatto, G., Broncova, G., Chemosensors, A. K.-, & 2022, undefined. (2022). Electrochemical sensors and their applications: A review. *Mdpi.ComJ Baranwal, B Barse, G Gatto, G Broncova, A KumarChemosensors, 2022•mdpi.Com*. https://doi.org/10.3390/chemosensors10090363

Barbezat, G. (1955). New Instrumental Methods in Electrochemistry. In *Analytica Chimica Acta* (Vol. 12). https://doi.org/10.1016/s0003-2670(00)87868-x

Basavaiah, K., Somashekar, B. C., & Ramakrishna, V. (2007). Rapid titrimetric and spectrophotometric methods for salbutamol sulphate in pharmaceuticals using N-bromosuccinimide. *Acta Pharmaceutica*, *57*(1), 87-98. https://doi.org/10.2478/v10007-007-0007-7

Behera, A. (2022). Advanced Semiconductor/Conductor Materials. *Advanced Materials*, 557–596. https://doi.org/10.1007/978-3-030-80359-9_16

Bekmezci, M., Bayat, R., Erduran, V., & Sen, F. (2022). Biofunctionalization of functionalized nanomaterials for electrochemical sensors. Functionalized Nanomaterial-Based Electrochemical Sensors, 55–69. https://doi.org/10.1016/b978-0-12-823788-5.00003-x

Ben Brahim, K. A., Bendany, M., El Hamdouni, Y., Abbi, K., Bakkouche, C., Fattoumi, H., Hermouche, L., Labjar, N., Dalimi, M., & El Hajjaji, S. (2023). Electrochemical Detection of Sulfadiazine by Sensors based on Chemically

Modified Carbon Electrodes: A Review. *Current Topics in Medicinal Chemistry*, *23*(15), 1464–1476. https://doi.org/10.2174/1568026623666230210115740

Bernal, J. L., Del Nozal, M. J., Velasco, H., & Toribio, L. (2006). HPLC Versus SFC for the Determination of Salbutamol Sulphate and Its Impurities in Pharmaceuticals., *19*(10), 1579-1589. https://doi.org/10.1080/10826079608005493

Bhalla, N., Jolly, P., Formisano, N., & Estrela, P. (2016). Introduction to biosensors. *Essays in Biochemistry*, 60–61. https://doi.org/10.1042/ebc20150001

Bharat, T. C., Shubham, Mondal, S., Gupta, H. S., Singh, P. K., & Das, A. K. (2019). Synthesis of Doped Zinc Oxide Nanoparticles: A Review. *Materials Today: Proceedings*, *11*, 767-775. https://doi.org/10.1016/j.matpr.2019.03.041

Bhawna, Choudhary, A. K., Gupta, A., Kumar, S., Kumar, P., Singh, R. P., Singh, P., & Kumar, V. (2020). Synthesis, Antimicrobial Activity, and Photocatalytic Performance of Ce Doped SnO_2 Nanoparticles. *Frontiers in Nanotechnology*, *2*. https://doi.org/10.3389/fnano.2020.595352

Blanca, J., Muñoz, P., Morgado, M., Méndez, N., Aranda, A., Reuvers, T., & Hooghuis, H. (2005). Determination of clenbuterol, ractopamine and zilpaterol in liver and urine by liquid chromatography tandem mass spectrometry. *Analytica Chimica Acta*, *529*(1-2 SPEC. ISS.), 199-205. https://doi.org/10.1016/j.aca.2004.09.061

Bokov, D., Jalil, A. T., Chupradit, S., Suksatan, W., Ansari, M. J., Shewael, I. H., Valiev, G. H., & Kianfar, E. (2021). Nanomaterial by sol-gel method: synthesis and application. *Wiley Online Library*, *2021*. https://doi.org/10.1155/2021/5102014

Boshta, N. M., El-Essawy, F. A., Alshammari, M. B., Noreldein, S. G., & Darwesh, O. M. (2022). Discovery of Quinazoline-2,4(1H,3H)-Dione Derivatives as Potential Antibacterial Agent: Design, Synthesis, and Their Antibacterial Activity. *Molecules*, *27*(12). https://doi.org/10.3390/molecules27123853

Bourdillon, P. D. V, Dawson, J. R., Foale, R. A., Timmis, A. D., Poole-Wilson, P. A., & Sutton, G. C. (1980). Salbutamol in treatment of heart failure. *Br HeartJ*, *43*,

206–210. https://doi.org/10.1136/hrt.43.2.206

Bouzigues, C., Gacoin, T., & Alexandrou, A. (2011). Biological applications of rare-earth based nanoparticles. *ACS Nano*, *5*(11), 8488–8505. https://doi.org/10.1021/nn202378b

Brett, C. M. A., Oliveira Brett, A. M., & Serrano, S. H. P. (1994). On the adsorption and electrochemical oxidation of DNA at glassy carbon electrodes. *Journal of Electroanalytical Chemistry*, *366*(1–2), 225–231. https://doi.org/10.1016/0022-0728(93)02994-s

Bullapura Matt, S., Manjunatha, S., Manjunatha, S., Sidlingappa, D. M., & Sidlingappa, M. (2019). Synthesis of Cerium-Doped Zirconia Nanoparticles for the Electrochemical Detection of Dopamine by Modified Carbon Paste Electrode. *Wiley Online LibrarySB Matt, S Manjunatha, S Manjunatha, DM Sidlingappa, M SidlingappaChemistrySelect, 2019•Wiley Online Library*, *4*(19), 5839–5844. https://doi.org/10.1002/slct.201900642

Burke, L. D., Ahern, M. J. G., & Ryan, T. G. (1990). An Investigation of the Anodic Behavior of Copper and Its Anodically Produced Oxides in Aqueous Solutions of High pH. *Journal of The Electrochemical Society*, *137*(2), 553–561. https://doi.org/10.1149/1.2086496/xml

Carneiro, P., Morais, S., & Pereira, M. C. (2019). Nanomaterials towards biosensing of Alzheimer's disease biomarkers. *Nanomaterials*, *9*(12), 1–23. https://doi.org/10.3390/nano9121663

Cervantes-López, J. L., Rangel, R., Espino, J., Martínez, E., García-Gutiérrez, R., Bartolo-Pérez, P., Alvarado-Gil, J. J., & Contreras, O. E. (2017). Photoluminescence on cerium-doped ZnO nanorods produced under sequential atomic layer deposition–hydrothermal processes. *Applied Physics A: Materials Science and Processing*, *123*(1), 1–14. https://doi.org/10.1007/s00339-016-0722-3

Chen, C., Li, H., & Fan, Y. (2011). Determination of salbutamol sulfate in medicaments by capillary electrophoresis with contactless conductivity detection. *Chinese Journal of Chromatography*, *29*(2), 137–140.

https://doi.org/10.3724/sp.j.1123.2011.00137

Chen, D., Yang, M., Zheng, N., Xie, N., Liu, D., Xie, C., & Yao, D. (2016). A novel aptasensor for electrochemical detection of ractopamine, clenbuterol, salbutamol, phenylethanolamine and procaterol. *Biosensors and Bioelectronics*, *80*, 525–531. https://doi.org/10.1016/j.bios.2016.01.025

Chen, N., Liu, B., Zhang, P., Wang, C., Du, Y., Chang, W., & Hong, W. (2021). Enhanced photocatalytic performance of Ce-doped SnO_2 hollow spheres by a one-pot hydrothermal method. *Inorganic Chemistry Communications*, *132*, 108848. https://doi.org/10.1016/j.ınoche.2021.108848

Cheng, Y., Chen, K. S., Meyer, N. L., Yuan, J., Hirst, L. S., Chase, P. B., & Xiong, P. (2011). Functionalized SnO_2 nanobelt field-effect transistor sensors for label-free detection of cardiac troponin. *Biosensors and Bioelectronics*, *26*(11), 4538–4544. https://doi.org/10.1016/j.bios.2011.05.019

Chithra, M. J., Sathya, M., & Pushpanathan, K. (2015a). Effect of pH on crystal size and photoluminescence property of ZnO nanoparticles prepared by chemical precipitation method. *Acta Metallurgica Sinica (English Letters)*, *28*(3), 394–404. https://doi.org/10.1007/s40195-015-0218-8

Chithra, M. J., Sathya, M., & Pushpanathan, K. (2015b). Effect of pH on crystal size and photoluminescence property of ZnO nanoparticles prepared by chemical precipitation method. *Acta Metallurgica Sinica (English Letters)*, *28*(3), 394–404. https://doi.org/10.1007/s40195-015-0218-8

Choi, W., Termin, A., & Hoffmann, M. R. (1994). The Role of Metal Ion Dopants in Quantum-Sized TiC: Correlation between Photoreactivity and Charge Carrier Recombination Dynamics. In *J. Phys. Chem* (Vol. 98). https://pubs.acs.org/sharingguidelines

Choudhari, U., & Jagtap, S. (2021). Electrochemical studies on doped SnO2 nanocomposite for selective detection of lung cancer biomarkers. *AIP Advances*, *11*(12). https://doi.org/10.1063/5.0072691/993401

Chu, M. N., Nguyen, L. T. H., Truong, M. X., Do, T. H., Duong, T. T. A., Nguyen, L. T. T., Pham, M. A., Tran, T. K. N., Ngo, T. C. Q., & Pham, V. H. (2022). Ce^{3+}/Ce^{4+}-Doped ZrO_2/CuO Nanocomposite for Enhanced Photocatalytic Degradation of Methylene Blue under Visible Light. *Toxics 2022, Vol. 10, Page 463*, *10*(8), 463. https://doi.org/10.3390/toxics10080463

Collins, G., Blömker, M., Osiak, M., Holmes, J. D., Bredol, M., & O'Dwyer, C. (2013). Three-dimensionally ordered hierarchically porous tin dioxide inverse opals and immobilization of palladium nanoparticles for catalytic applications. *Chemistry of Materials*, *25*(21), 4312–4320. https://doi.org/10.1021/cm402458v

Dangi, R., Basnet, B., Pandey, M., Bhusal, S., Budhathoki, B., Parajuli, K., Tiwari, S. K., & Kafle, B. P. (2023). Effect of Oxygen Vacancy on the Crystallinity and Optical Band Gap in Tin Oxide Thin Film. *Energies 2023, Vol. 16, Page 2653*, *16*(6), 2653. https://doi.org/10.3390/en16062653

Danks, A. E., Hall, S. R., & Schnepp, Z. (2016). The evolution of 'sol–gel' chemistry as a technique for materials synthesis. *Materials Horizons*, *3*(2), 91–112. https://doi.org/10.1039/c5mh00260e

Dar, G. N., Umar, A., Zaidi, S. A., Ibrahim, A. A., Abaker, M., Baskoutas, S., & Al-Assiri, M. S. (2012). Ce-doped ZnO nanorods for the detection of hazardous chemical. *Sensors and Actuators, B: Chemical*, *173*, 72–78. https://doi.org/10.1016/j.snb.2012.06.001

de Rooij, D. M. R. (2003). Electrochemical Methods: Fundamentals and Applications. *Anti-Corrosion Methods and Materials*, *50*(5). https://doi.org/10.1108/acmm.2003.12850eae.001

Dechtrirat, D., Sookcharoenpinyo, B., Prajongtat, P., Sriprachuabwong, C., Sanguankiat, A., Tuantranont, A., & Hannongbua, S. (2018). An electrochemical MIP sensor for selective detection of salbutamol based on a graphene/PEDOT:PSS modified screen printed carbon electrode. *RSC Advances*, *8*(1), 206–212. https://doi.org/10.1039/c7ra09601a

Deivasegamani, R., Karunanidhi, G., Santhosh, C., Gopal, T., Saravana achari, D.,

Neogi, A., Nivetha, R., Pradeep, N., Venkatraman, U., Bhatnagar, A., Jeong, S. K., & Grace, A. N. (2017). Chemoresistive sensor for hydrogen using thin films of tin dioxide doped with cerium and palladium. *Microchimica Acta*, *184*(12), 4765–4773. https://doi.org/10.1007/s00604-017-2514-7

Delahay, P., & Mattax, C. C. (1954). Theory of Electrolysis at Constant Current in Unstirred Solution. III. Experimental Study of Potential-Time Curves. *Journal of the American Chemical Society*, *76*(3), 874–878. https://doi.org/10.1021/ja01632a071

Delice, T. K., & Azem, N. F. A. (2022). Influence of Sol-Gel Process Parameters on Structural Properties of CuO Nanoparticles. *Euroasia Journal of Mathematics, Engineering, Natural & Medical Sciences*, *9*(23), 73–81. https://doi.org/10.5281/zenodo.7130723

Desimoni, E., & Brunetti, B. (2015). About estimating the limit of detection by the signal to noise approach. *Pharmaceutıca Analytica Acta*, *6*(3), 1–4. https://doi.org/10.4172/2153-2435.1000355

Dinda, B. (2019). Classification of Iridoids. *Pharmacology and Applications of Naturally Occurring Iridoids*, 1–15. https://doi.org/10.1007/978-3-030-05575-2_1

Dicpinigaitis, P. V., Morice, A. H., Birring, S. S., McGarvey, L., Smith, J. A., Canning, B. J., & Page, C. P. (2014). Antitussive Drugs—Past, Present, and Future. Pharmacological Reviews, 66(2), 468–512. https://doi.org/10.1124/pr.111.005116.

Dixon, S. C., Scanlon, D. O., Carmalt, C. J., & Parkin, I. P. (2016). n-Type doped transparent conducting binary oxides: an overview. *Journal of Materials Chemistry C*, *4*(29), 6946–6961. https://doi.org/10.1039/c6tc01881e

Dol, I., & Knochen, M. (2004). Flow-injection spectrophotometric determination of salbutamol with 4-aminoantipyrine. *Talanta*, *64*(5 SPEC. ISS.), 1233–1236. https://doi.org/10.1016/j.talanta.2004.04.040

Dong, Y., & Zheng, J. (2014). A nonenzymatic l-cysteine sensor based on SnO2-MWCNTs nanocomposites. *Journal of Molecular Liquids*, *196*, 280–284.

https://doi.org/10.1016/j.molliq.2014.03.046

Durst, R. A., Bäumner, A. J., Murray, R. W., Buck, R. P., & Andrieux, C. P. (1997). Chemically modified electrodes: Recommended terminology and definitions. *Pure and Applied Chemistry*, *69*(6), 1317–1323. https://doi.org/10.1351/pac199769061317

Ealias, A. M., & Saravanakumar, M. P. (2017). A review on the classification, characterisation, synthesis of nanoparticles and their application. *IOP Conference Series: Materials Science and Engineering*, *263*(3). https://doi.org/10.1088/1757-899x/263/3/032019

Eggins B.R. Chemical Sensors and Biosensors. Wiley, 2002. 273 pp., ISBN: ISBN 0-471-89914-3 £34.95. Sensor Review, 22(4), 364–364. https://doi.org/10.1108/sr.2002.22.4.364.3

Elci, A., Demirtas, O., Ozturk, I. M., Bek, A., & Nalbant Esenturk, E. (2018). Synthesis of tin oxide-coated gold nanostars and evaluation of their surface-enhanced Raman scattering activities. *Journal of Materials Science*, *53*(24), 16345–16356. https://doi.org/10.1007/s10853-018-2792-4

Electrochemistry, A. (2001). Analytical electrochemistry. In *Choice Reviews Online* (Vol. 38, Issue 10). https://doi.org/10.5860/choice.38-5590

Ensafi, A. A., Abbasi, S., Rahimi Mansour, H., & Mohammadpour Baltork, I. (2001). Differential Pulse Adsorption Stripping Voltammetric Determination of Copper(II) with 2-Mercaptobenzimidazol at a Hanging Mercury-Drop Electrode. *Analytical Sciences*, *17*(5), 609–612. https://doi.org/10.2116/analsci.17.609

Piñón-Espitia, M., Torres-Ochoa, J. A., Córtazar-Martínez, O., Herrera-Gomez, A., Herrera-Perez, G., & Ochoa-Lara, M. T. (2020). Charge Transfer Effects in CuO Nanofibers, Observed by EELS and XPS. Microscopy and Microanalysis, 26(S2), 1424–1425. https://doi.org/10.1017/s143192762001805x

Erwin, S. C., Zu, L., Haftel, M. I., Efros, A. L., Kennedy, T. A., & Norris, D. J. (2005). Doping semiconductor nanocrystals. *Nature*, *436*(7047), 91–94.

https://doi.org/10.1038/nature03832

Fang, F., Kennedy, J., Futter, J., Markwitz, A., & Manikandan, E. (2013). Transition metal doped metal oxide nanostructures synthesized by arc discharge method. *2013 International Conference on Manipulation, Manufacturing and Measurement on the Nanoscale, 3M-NANO 2013 - Conference Proceedings*, 220–223. https://doi.org/10.1109/3m-nano.2013.6737418

Ferrari, A. G. M., Foster, C. W., Kelly, P. J., Brownson, D. A. C., & Banks, C. E. (2018). Determination of the electrochemical area of screen-printed electrochemical sensing platforms. *Biosensors*, *8*(2), 1–10. https://doi.org/10.3390/bios8020053

Findik, F. (2021). Nanomaterials and their applications. *Periodicals of Engineering and Natural Sciences*, *9*(3), 62–75. https://doi.org/10.21533/pen.v9ı3.1837.g857

Foroughi, M. M., Jahani, S., & Hassani Nadiki, H. (2019). Lanthanum doped fern-like CuO nanoleaves/MWCNTs modified glassy carbon electrode for simultaneous determination of tramadol and acetaminophen. *Sensors and Actuators B: Chemical*, *285*, 562–570. https://doi.org/10.1016/j.snb.2019.01.069

Gaber, A., Abdel- Rahim, M. A., Abdel-Latief, A. Y., & Abdel-Salam, M. N. (2014). Influence of Calcination Temperature on the Structure and Porosity of Nanocrystalline SnO2 Synthesized by a Conventional Precipitation method. *International Journal of Electrochemical Science*, *9*(1), 81–95. https://doi.org/10.1016/s1452-3981(23)07699-x

Ganesan, K., Jothi, V. K., Natarajan, A., Rajaram, A., Ravichandran, S., & Ramalingam, S. (2020). Green synthesis of Copper oxide nanoparticles decorated with graphene oxide for anticancer activity and catalytic applications. *Arabian Journal of Chemistry*, *13*(8), 6802–6814. https://doi.org/10.1016/j.arabjc.2020.06.033

Gao, X., Guo, H., Xia, Y., Yin, J., & Liu, Z. (2010). Unipolar resistive switching characteristics in Co3O4 films. *Thin Solid Films*, *519*(1), 450–452. https://doi.org/10.1016/j.tsf.2010.07.075

García Suárez, M., Aroussi, S., Dahamni, M. A., Ghamnia, M., Tonneau, D., & Fauquet, C. (2022). Characterization of Some Physical and Photocatalytic Properties of CuO Nanofilms Synthesized by a Gentle Chemical Technique. *Mdpi.ComS Aroussi, MA Dahamni, M Ghamnia, D Tonneau, C FauquetCondensed Matter, 2022•mdpi.Com*. https://doi.org/10.3390/condmat7020037

Ghanei-Motlagh, M., & Baghayeri, M. (2020). Determination of Trace Tl(I) by Differential Pulse Anodic Stripping Voltammetry Using a Novel Modified Carbon Paste Electrode. *Journal of The Electrochemical Society*, *167*(6), 066508. https://doi.org/10.1149/1945-7111/ab823c

Gooding, J. J. (2008). Advances in interfacial design for electrochemical biosensors and sensors: Aryl diazonium salts for modifying carbon and metal electrodes. *Electroanalysis*, *20*(6), 573–582. https://doi.org/10.1002/elan.200704124

Goyal, R. N., Oyama, M., & Singh, S. P. (2007). Fast determination of salbutamol, abused by athletes for doping, in pharmaceuticals and human biological fluids by square wave voltammetry. Journal of Electroanalytical Chemistry, 611(1–2), 140–148. https://doi.org/10.1016/j.jelechem.2007.08.014

Greczynski, G., & Hultman, L. (2020). X-ray photoelectron spectroscopy: Towards reliable binding energy referencing. In *Progress in Materials Science* (Vol. 107). Elsevier Ltd. https://doi.org/10.1016/j.pmatsci.2019.100591

Grieshaber, D., MacKenzie, R., Vörös, J., Sensors, E. R.-, & 2008, undefined. (2008). Electrochemical biosensors-sensor principles and architectures. *Mdpi.ComD Grieshaber, R MacKenzie, J Vörös, E ReimhultSensors, 2008•mdpi.Com*, *8*, 1400–1458. https://www.mdpi.com/1424-8220/8/3/1400

Gu, F., Wang, H., Han, D., & Wang, Z. (2017). Enhancing the sensing performance of SnO_2 inverse opal thin films by In and Au doping. *Sensors and Actuators B: Chemical*, *245*, 1023–1031. https://doi.org/10.1016/j.snb.2017.02.031

Güldüren, M. E., İskenderoğlu, D., Güney, H., Gür, E., Acar, M., & Morkoç Karadeniz, S. (2023). Investigating the influence of Ni doping on the CuO thin films deposited via ultrasonic spray pyrolysis: Structural, optical and H2 gas sensing

analyses. *International Journal of Hydrogen Energy*, *48*(2), 828–839. https://doi.org/10.1016/j.ijhydene.2022.09.283

Güldüren, M. E., Taşer, A., & Güney, H. (2021). Mn-doping-induced tunable bandgap and luminescence properties of SnO_2 nanoparticles grown by SILAR method. *Optical Materials*, *121*, 111606. https://doi.org/10.1016/j.optmat.2021.111606

Guo, X.-C., Wang, H.-H., Chen, X.-J., Xia, Z.-Y., Kang, W.-Y., & Zhou, W.-H. (2017). One Step Electrodeposition of Graphene-Au Nanocomposites for Highly Sensitive Electrochemical Detection of Salbutamol. *Int. J. Electrochem. Sci*, *12*, 861–875. https://doi.org/10.20964/2017.02.29

Gupta, P., Rathore, V., Sahoo, S., & Majumder, S. (2023). Investigation of electronic properties of Mn doped SnO_2 thin film. *Vacuum*, *211*, 111914. https://doi.org/10.1016/j.vacuum.2023.111914

Gurylev, V. (2021). Extrinsic Defects in Nanostructured Semiconductors. Nanostructured Photocatalyst via Defect Engineering, 319–348. https://doi.org/10.1007/978-3-030-81911-8_10

Guţoiu, S., Pogăcean, F., Măgeruşan, L., Miclăuş, M. O., Grad, O., Pană, I. O., & Pruneanu, S. (2023). Enhancement of Dopamine Electrochemical Detection with Manganese Doped Crystalline Copper Oxide. *Coatings*, *13*(6), 1014. https://doi.org/10.3390/COATINGS13061014/S1

Haider, S., & Haider, A. (Eds.). (2021). Transition Metal Compounds - Synthesis, Properties, and Application. https://doi.org/10.5772/intechopen.91598

Han, X. (2020). Development of electrochemical immunosensor for detecting salbutamol by competitive immune strategy. *International Journal of Electrochemical Science*, *15*, 7337–7346. https://doi.org/10.20964/2020.08.93

Haque, M., Fouad, H., Seo, H. K., Othman, A. Y., Kulkarni, A., & Ansari, Z. A. (2020). Investigation of Mn doped ZnO nanoparticles towards ascertaining myocardial infarction through an electrochemical detection of myoglobin. *IEEE Access*, *8*, 164678–164692. https://doi.org/10.1109/access.2020.3021458

He, H., Zhang, Y., Pan, Q., Wu, G., Dong, G., & Qiu, J. (2015). Controllable synthesis of Zn_2GeO_4 :Eu nanocrystals with multi-color emission for white light-emitting diodes †. *J. Mater. Chem. C*, *3*, 5419. https://doi.org/10.1039/c5tc00844a

Hilary, I. Z., Chowdhury, L. N., Gafur, A. M. S., Khan, M. A., & Khan, N. (2015). Preparation and Characterization of Copper Oxide Nanoparticles Synthesized via Chemical Precipitation Method. *Open Access Library Journal*, *2*, 1409. https://doi.org/10.4236/oalib.1101409

Holzwarth, U., & Gibson, N. (2011). *The Scherrer equation versus the "Debye-Scherrer equation."* https://doi.org/10.1038/nnano.2011.145

Horti, N. C., Kamatagi, M. D., Patil, N. R., Wari, M. N., & Inamdar, S. R. (2018). Photoluminescence properties of SnO2 nanoparticles: Effect of solvents. *Optik*, *169*, 314–320. https://doi.org/10.1016/j.ijleo.2018.05.085

Hu, K., & McClements, D. J. (2014). Fabrication of surfactant-stabilized zein nanoparticles: A pH modulated antisolvent precipitation method. *Food Research International*, *64*, 329-335. https://doi.org/10.1016/j.foodres.2014.07.004

Huang, X., Zhu, Y., & Kianfar, E. (2021). Nano Biosensors: Properties, applications and electrochemical techniques. *Journal of Materials Research and Technology*, *12*, 1649–1672. https://doi.org/10.1016/j.jmrt.2021.03.048

Hussen, M. K., Dejene, F. B., & Tsega, M. (2019). Effect of pH on material properties of ZnAl2O4:Cr3+ nano particles prepared by sol–gel method. *Journal of Materials Science: Materials in Electronics*, *30*(11), 10191–10201. https://doi.org/10.1007/s10854-019-01355-4

Ibrahim, M., Temerk, Y., & Ibrahim, H. (2017). Fabrication of a new biosensor based on a Sn doped ceria nanoparticle modified glassy carbon paste electrode for the selective determination of the anticancer drug dacarbazine in pharmaceuticals. *RSC Advances*, *7*(51), 32357-32366. https://doi.org/10.1039/c7ra04331g

Ibrahim, S. A., & Sreekantan, S. (2011). Effect of pH on TiO2 Nanoparticles via Sol-Gel Method. *Advanced Materials Research*, *173*, 184–189.

https://doi.org/10.4028/www.scıentific.net/amr.173.184

Iqbal, M., Thebo, A. A., Shah, A. H., Iqbal, A., Thebo, K. H., Phulpoto, S., & Mohsin, M. A. (2017). Influence of Mn-doping on the photocatalytic and solar cell efficiency of CuO nanowires. *Inorganic Chemistry Communications*, *76*, 71–76. https://doi.org/10.1016/j.inoche.2016.11.023

Iqbal, T., Masood, A., Khalid, N. R., Tahir, M. B., Asiri, A. M., & Alrobei, H. (2022). Green synthesis of novel lanthanum doped copper oxide nanoparticles for photocatalytic application: Correlation between experiment and COMSOL simulation. *Ceramics International*, *48*(10), 13420–13430. https://doi.org/10.1016/j.ceramint.2022.01.160

Islam, M. S., Bhardwaj, A., Mathur, L., Kim, I. H., Park, J. Y., & Song, S. J. (2022). Effects of electrolyte variation on ammonia sensing temperature for BiVO4 sensing electrode in mixed potential gas sensor. *Sensors and Actuators B: Chemical*, *371*, 132504. https://doi.org/10.1016/j.snb.2022.132504

Jan, T., Iqbal, J., Mansoor, Q., Ismail, M., Sajjad Haider Naqvi, M., Gul, A., Faizan-Ul-Hassan Naqvi, S., & Abbas, F. (2014). Synthesis, physical properties and antibacterial activity of Ce doped CuO: a novel nanomaterial. *Journal of Physics D: Applied Physics*, *47*(35), 355301. https://doi.org/10.1088/0022-3727/47/35/355301

Jang, J., Chung, S., Kang, H., & Subramanian, V. (2016). P-type CuO and Cu2O transistors derived from a sol–gel copper (II) acetate monohydrate precursor. *Thin Solid Films*, *600*, 157–161. https://doi.org/10.1016/j.tsf.2016.01.036

Jara-Ulloa, P., Salgado-Figueroa, P., Moscoso, R., -, al, Sivakumar, M., Pandi, K., Chen, S.-M., Chikere, C., Faisal, N. H., T Lin, P. K., & Fernandez, C. (2019). Zinc oxide nanoparticles modified-carbon paste electrode used for the electrochemical determination of Gallic acid. *Journal of Physics: Conference Series*, *1310*(1), 012008. https://doi.org/10.1088/1742-6596/1310/1/012008

Jiang, T., Kong, J., Wang, Y., Meng, D., Wang, D., & Yu, M. (2016). Optical and Photocatalytic properties of Mn-doped CuO nanosheets prepared by hydrothermal

method. *Crystal Research and Technology*, *51*(1), 58–64. https://doi.org/10.1002/crat.201500152

Justino, C. I. L., Duarte, A. C., & Rocha-Santos, T. A. P. (2016). Critical overview on the application of sensors and biosensors for clinical analysis. *TrAC - Trends in Analytical Chemistry*, *85*, 36–60. https://doi.org/10.1016/j.trac.2016.04.004

Kailasa, S., Rani, B. G., Bhargava Reddy, M. S., Jayarambabu, N., Munindra, P., Sharma, S., & Venkateswara Rao, K. (2020). NiO nanoparticles -decorated conductive polyaniline nanosheets for amperometric glucose biosensor. *Materials Chemistry and Physics*, *242*, 122524. https://doi.org/10.1016/j.matchemphys.2019.122524

Kalantar-Zadeh, K. (2013). Sensors: An introductory course. *Sensors: An Introductory Course*, *9781461450528*, 1–196. https://doi.org/10.1007/978-1-4614-5052-8/cover

Kara, S. (Ed.). (2012). A Roadmap of Biomedical Engineers and Milestones. https://doi.org/10.5772/2494

Karan, K., Chandrasekar, B., Bruno Chandrasekar, L., Chandramohan, R., Karunakaran, M., & Vijayalakshmi, R. (2016). Synthesis and characterization of Copper oxide and Zinc Oxide nanomaterials. *Nature of Scientific Materials*, *1*, 18–22.https://doi.org/10.24909/nosm2016111.4

Karuwan, C., Wisitsoraat, A., Maturos, T., Phokharatkul, D., Sappat, A., Jaruwongrungsee, K., Lomas, T., & Tuantranont, A. (2009). Flow injection based microfluidic device with carbon nanotube electrode for rapid salbutamol detection. *Talanta*, *79*(4), 995–1000. https://doi.org/10.1016/j.talanta.2009.02.015

Karuwan, C., Sriprachuabwong, C., Wisitsoraat, A., Phokharatkul, D., Sritongkham, P., & Tuantranont, A. (2012). Inkjet-printed graphene-poly(3,4-ethylenedioxythiophene):poly(styrene-sulfonate) modified on screen printed carbon electrode for electrochemical sensing of salbutamol. Sensors and Actuators B: Chemical, 161(1), 549–555. https://doi.org/10.1016/j.snb.2011.10.074.

Kayani, Z. N., Abbas, E., Saddiqe, Z., Riaz, S., & Naseem, S. (2018). Photocatalytic,

antibacterial, optical and magnetic properties of Fe-doped ZnO nano-particles prepared by sol-gel. *Materials Science in Semiconductor Processing*, *88*, 109–119. https://doi.org/10.1016/j.mssp.2018.08.003

Keles, G., Sifa Ataman, E., Betul Taskin, S., Ilker Polatoglu, ˙, & Kurbanoglu, S. (2024). Nanostructured Metal Oxide-Based Electrochemical Biosensors in Medical Diagnosis. *Mdpi.ComG Keles, E Sifa Ataman, SB Taskin, İ Polatoglu, S KurbanogluBiosensors, 2024•mdpi.Com*. https://doi.org/10.3390/bios14050238

Khaliq, N., Rasheed, M. A., Khan, M., Maqbool, M., Ahmad, M., Karim, S., Nisar, A., Schmuki, P., Cho, S. O., & Ali, G. (2021). Voltage-Switchable Biosensor with Gold Nanoparticles on TiO_2 Nanotubes Decorated with CdS Quantum Dots for the Detection of Cholesterol and H_2O_2. *ACS Publications*, *13*(3), 3668. https://doi.org/10.1021/acsami.0c19979

Khan, I., Khan, S., Ahmed, H., & Nongjai, R. (2013). Structural and dielectric properties of Mn doped copper oxide (CuO) nanostructure. *AIP Conference Proceedings*, *1536*(1), 241–242. https://doi.org/10.1063/1.4810190

Khashan, K. S., Jabir, M. S., & Abdulameer, F. A. (2018). Preparation and characterization of copper oxide nanoparticles decorated carbon nanoparticles using laser ablation in liquid. *Journal of Physics: Conference Series*, *1003*(1). https://doi.org/10.1088/1742-6596/1003/1/012100

Khlifi, N., Mnif, S., Nasr, F. Ben, Fourati, N., Zerrouki, C., Chehimi, M. M., Guermazi, H., Aifa, S., & Guermazi, S. (2022). Non-doped and transition metal-doped CuO nano-powders: structure-physical properties and anti-adhesion activity relationship. *Pubs.Rsc.OrgN Khlifi, S Mnif, FB Nasr, N Fourati, C Zerrouki, MM Chehimi, H Guermazi, S AifaRSC Advances, 2022 pubs.Rsc.Org*. https://doi.org/10.1039/d2ra02433k

Kim, S. H., Umar, A., & Hwang, S. W. (2015). Rose-like CuO nanostructures for highly sensitive glucose chemical sensor application. *Ceramics International*, *41*(8), 9468–9475. https://doi.org/10.1016/j.ceramint.2015.04.003

Kissinger, P. T., & Heineman, W. R. (1983). Cyclic voltammetry. *Journal of Chemical*

Education, *60*(9), 702–706. https://doi.org/10.1021/ed060p702

Koc Delice, T., Ak Azem, F., Ozdemir, K., & Alpat, S. (2024). Development of CuO nanoparticles modified electrochemical sensor for detection of salbutamol. Materials Research Express, 11(4), 045005. https://doi.org/10.1088/2053-1591/ad3baf.

Koç, F., Çok, S., Gizli, N., & Sert Çok, S. (2020). Tuning the properties of silica aerogels through pH controlled sol-gel processes. *Res. Eng. Struct. Mat*, *6*(3), 257–269. https://doi.org/10.17515/resm2019.166ma1203

Koshkin, V. M., & Slezov, V. V. (2004). Doping nanoparticles. Technical Physics Letters, 30(5), 367–369. https://doi.org/10.1134/1.1760857

Koventhan, C., Vinothkumar, V., & Chen, S. M. (2022). Rational design of manganese oxide/tin oxide hybrid nanocomposite based electrochemical sensor for detection of prochlorperazine (Antipsychotic drug). *Microchemical Journal*, *175*, 107082. https://doi.org/10.1016/j.microc.2021.107082

Krishnakumar, T., Jayaprakash, R., Parthibavarman, M., Phani, A. R., Singh, V. N., & Mehta, B. R. (2009). Microwave-assisted synthesis and investigation of SnO_2 nanoparticles. *Materials Letters*, *63*(11), 896–898. https://doi.org/10.1016/j.matlet.2009.01.032

Kuchmenko, T. A., & Lvova, L. B. (2019). A perspective on recent advances in piezoelectric chemical sensors for environmental monitoring and foodstuffs analysis. *Chemosensors*, *7*(3), 14–17. https://doi.org/10.3390/chemosensors7030039

Kumar, M., Bhatt, V., Abhyankar, A. C., Kim, J., Kumar, A., Patil, S. H., & Yun, J.-H. (2018). New insights towards strikingly improved room temperature ethanol sensing properties of p-type Ce-doped SnO_2 sensors. Scientific Reports, 8(1). https://doi.org/10.1038/s41598-018-26504-3

Kumar, A., Kumar, N., Chitkara, M., & Dhillon, G. (2022). Physicochemical investigations of structurally enriched Sm^{3+} substituted SnO_2 nanocrystals. *Journal*

of Materials Science: Materials in Electronics, *33*(8), 5283–5296. https://doi.org/10.1007/s10854-022-07716-w

Kumar, B., Chand Soni, T., & Sinha, S. K. (2022). Fabrication of TiO_2 nanotubes on Ti6Al4V thin plate for non-enzymatic cholesterol biosensor. *Materials Today: Proceedings*, *66*, 562–565. https://doi.org/10.1016/j.matpr.2022.06.165

Kumar, P., Inwati, G. K., Mathpal, M. C., Ghosh, S., Roos, W. D., & Swart, H. C. (2021). Defects induced enhancement of antifungal activities of Zn doped CuO nanostructures. *Applied Surface Science*, *560*, 150026. https://doi.org/10.1016/j.apsusc.2021.150026

Kumar, P., Rajan, R., Upadhyaya, K., Behl, G., Xiang, X. X., Huo, P., & Liu, B. (2024). Metal oxide nanomaterials based electrochemical and optical biosensors for biomedical applications: Recent advances and future prospectives. *Environmental Research*, *247*, 118002. https://doi.org/10.1016/j.envres.2023.118002

Lavanya, N., Fazio, E., Neri, F., Bonavita, A., Leonardi, S. G., Neri, G., & Sekar, C. (2016). Electrochemical sensor for simultaneous determination of ascorbic acid, uric acid and folic acid based on Mn-SnO_2 nanoparticles modified glassy carbon electrode. *Journal of Electroanalytical Chemistry*, *770*, 23–32. https://doi.org/10.1016/j.jelechem.2016.03.017

Lavanya, N., Radhakrishnan, S., & Sekar, C. (2012). Fabrication of hydrogen peroxide biosensor based on Ni doped SnO_2 nanoparticles. *Biosensors and Bioelectronics*, *36*(1), 41–47. https://doi.org/10.1016/j.bios.2012.03.035

Lavanya, N., Sekar, C., Fazio, E., Neri, F., Leonardi, S. G., & Neri, G. (2017). Development of a selective hydrogen leak sensor based on chemically doped SnO_2 for automotive applications. International Journal of Hydrogen Energy, 42(15), 10645-10655.

Lee, S., Oh, J., Kim, D., & Piao, Y. (2016). A sensitive electrochemical sensor using an iron oxide/graphene composite for the simultaneous detection of heavy metal ions. *Talanta*, *160*, 528–536. https://doi.org/10.1016/j.talanta.2016.07.034

Li, C., Yu, Z., Fang, S., Wu, S., Gui, Y., & Chen, R. (2009). Synthesis and gas-sensing properties of Ce-doped SnO_2 materials. *Journal of Physics: Conference Series*, *152*. https://doi.org/10.1088/1742-6596/152/1/012033

Li, L., Huang, J., Wang, T., Zhang, H., Liu, Y., & Li, J. (2010). An excellent enzyme biosensor based on Sb-doped SnO2 nanowires. *Biosensors and Bioelectronics*, *25*(11), 2436–2441. https://doi.org/10.1016/j.bios.2010.03.037

Li, L., Wang, T., Zhong, Y., Li, R., Deng, W., Xiao, X., Xu, Y., Zhang, J., Hu, X., &Wang, Y. (2024). A review of nanomaterials for biosensing applications. *Journal of Materials Chemistry B*, *12*(5), 1168–1193. https://doi.org/10.1039/d3tb02648e

Li, P., Zhang, D., Jiang, C., Zong, X., & Cao, Y. (2017). Ultra-sensitive suspended atomically thin-layered black phosphorus mercury sensors. *Biosensors and Bioelectronics*, *98*, 68–75. https://doi.org/10.1016/j.bios.2017.06.027

Li, Y., Wei, Y., Shi, G., Xian, Y., Electroanalysis, L. J.-, & 2011, undefined. (2011). Facile synthesis of leaf-like CuO nanoparticles and their application on glucose biosensor. *Wiley Online LibraryY Li, Y Wei, G Shi, Y Xian, L JinElectroanalysis, 2011•Wiley Online Library*, *23*(2), 497–502. https://doi.org/10.1002/elan.201000343

Li, Y., Xu, J., & Sun, C. (2015). *Chemical sensors and biosensors for the detection of melamine*. https://doi.org/10.1039/c4ra13080d

Li, Y., Ye, Z., Luo, P., Li, Y., & Ye, B. (2014). *A sensitive voltammetric sensor for salbutamol based on MWNTs composite nano-Au film modified electrode*. https://doi.org/10.1039/c3ay41758a

Li, Z., Hou, B., Xu, Y., Wu, D., & Sun, Y. (2005). Studies of Fe-doped SiO_2/TiO_2 composite nanoparticles prepared by sol-gel-hydrothermal method. *Journal of Materials Science*, *40*(15), 3939–3943. https://doi.org/10.1007/s10853-005-0521-2

Lian, X., Li, Y., Tong, X., Zou, Y., Liu, X., An, D., & Wang, Q. (2017). Synthesis of Ce-doped SnO_2 nanoparticles and their acetone gas sensing properties. *Applied Surface Science*, *407*, 447–455. https://doi.org/10.1016/j.apsusc.2017.02.228

Lin, K.-C., Hong, C.-P., & Chen, S.-M. (2013). Simultaneous determination for toxic ractopamine and salbutamol in pork sample using hybrid carbon nanotubes. Sensors and Actuators B: Chemical, 177, 428–436. https://doi.org/10.1016/j.snb.2012.11.052.

Liu, G., Xia, T., Liang, X., Hou, S., & Hou, S. (2022). Enzymatic Electrochemical Biosensor from Eu-Doped SnO_2 Embedded in MXene for High Performance Sensing Lactate. *ChemElectroChem*, *9*(22). https://doi.org/10.1002/celc.202200848

Liu, R., Zhang, Y., Liu, M., Ni, Y., Yue, Y., Wu, S., & Li, S. (2023). Electrochemical sensor based on Fe_3O_4/α-Fe_2O_3@Au magnetic nanocomposites for sensitive determination of the TP53 gene. *Bioelectrochemistry*, *152*, 108429. https://doi.org/10.1016/j.bioelechem.2023.108429

Lomae, A., Chaiyo, S., Chailapakul, O., Siangproh, W., & Panchompoo, J. (2022). Fully integrated colorimetric sensor based on transparency substrate for salbutamol determination. *MethodsX*, *9*, 101913. https://doi.org/10.1016/j.mex.2022.101913

Lorenzo, E., Pariente, F., Hernàndez, L., Tobalina, F., Darder, M., Wu, Q., Maskus, M., & Abruña, H. D. (1998). Analytical strategies for amperometric biosensors based on chemically modified electrodes. *Biosensors and Bioelectronics*, *13*(3–4), 319–332. https://doi.org/10.1016/s0956-5663(97)00138-3

Lu, W., Xue, S., Liu, X., Bao, C., & Shi, H. (2024). An ultrasensitive photoelectrochemical immunosensor for carcinoembryonic antigen detection based on cobalt borate nanosheet array and Mn_2O_3 @Au nanocube. *Microchemical Journal*, *196*. https://doi.org/10.1016/j.microc.2023.109606

Lv, Y., Li, L., Yin, P., & Lei, T. (2020). Synthesis and evaluation of the structural and antibacterial properties of doped copper oxide. *Dalton Transactions*, *49*(15), 4699–4709. https://doi.org/10.1039/d0dt00201a

Lwin, N., Othman, R., Noor, A. F. M., Sreekantan, S., Yong, T. C., Singh, R., & Tin, C. C. (2015). Influence of pH on the physical and electromagnetic properties of Mg–Mn ferrite synthesized by a solution combustion method. *Materials*

Characterization, *110*, 109–115. https://doi.org/10.1016/j.matchar.2015.10.020

Ma, L., Wang, Q., Islam, S. M., Liu, Y., Ma, S., & Kanatzidis, M. G. (2016). Highly Selective and Efficient Removal of Heavy Metals by Layered Double Hydroxide Intercalated with the MoS 4 2− Ion. *J. Am. Chem. Soc*, *138*. https://doi.org/10.1021/jacs.6b00110

Malhotra, B. D., & Turner, A. P. F. (2003). Preface. Perspectives in Biosensors, ix–x. https://doi.org/10.1016/s1061-8945(03)80002-8

Malik, S., Singh, J., Goyat, R., Saharan, Y., Chaudhry, V., Umar, A., Ibrahim, A. A., Akbar, S., Ameen, S., & Baskoutas, S. (2023). Nanomaterials-based biosensor and their applications: A review. *Heliyon*, *9*(9), e19929. https://doi.org/10.1016/j.heliyon.2023.e19929

Mani, R., Vivekanandan, K., & Subiramaniyam, N. P. (2017). Photocatalytic activity of different organic dyes by using pure and Fe doped SnO_2 nanopowders catalyst under UV light irradiation. *Journal of Materials Science: Materials in Electronics*, *28*(18), 13846–13852. https://doi.org/10.1007/s10854-017-7231-9

Manikandan, D., Boukhvalov, D. W., Amirthapandian, S., Zhidkov, I. S., Kukharenko, A. I., Cholakh, S. O., Kurmaev, E. Z., & Murugan, R. (2018). An insight into the origin of room-temperature ferromagnetism in SnO2 and Mn-doped SnO_2 quantum dots: an experimental and DFT approach. *Physical Chemistry Chemical Physics*, *20*(9), 6500–6514. https://doi.org/10.1039/c7cp07182e

Mariammal, R. N., Ramachandran, K., Kalaiselvan, G., Arumugam, S., Renganathan, B., & Sastikumar, D. (2013). Effect of magnetism on the ethanol sensitivity of undoped and Mn-doped CuO nanoflakes. *Applied Surface Science*, *270*, 545–552. https://doi.org/10.1016/j.apsusc.2013.01.084

Matthews, C. J., Andrews, E. S. V., & Patrick, W. M. (2021). Enzyme-based amperometric biosensors for malic acid – A review. *Analytica Chimica Acta*, *1156*, 338218. https://doi.org/10.1016/j.aca.2021.338218

McCarthy, G. J., & Welton, J. M. (1989). X-Ray Diffraction Data for SnO_2. An

Illustration of the New Powder Data Evaluation Methods. *Powder Diffraction*, *4*(3), 156–159. https://doi.org/10.1017/s0885715600016638

Mehtab, A., Ahmed, J., Alshehri, S. M., Mao, Y., & Ahmad, T. (2022). Rare earth doped metal oxide nanoparticles for photocatalysis: A perspective. *Nanotechnology*, *33*(14). https://doi.org/10.1088/1361-6528/ac43e7

Meng, F., Miao, H., Shi, J., Hu, Z., Li, G., & Ding, Y. (2017). The synthesis of carbon/cerium oxide composites clusters with the assistance of the glucaminium-based surfactant and their electrochemical performance in the glucose monitoring. *Journal of Alloys and Compounds*, *713*, 125–131. https://doi.org/10.1016/j.jallcom.2017.04.203

Meng, Z., Stolz, R. M., Mendecki, L., & Mirica, K. A. (2019). Electrically-transduced chemical sensors based on two-dimensional nanomaterials. *Chemical Reviews*, *119*(1), 478–598. https://doi.org/10.1021/acs.chemrev.8b00311

Meyer, B. K., Polity, A., Reppin, D., Becker, M., Hering, P., Klar, P. J., Sander, T., Reindl, C., Benz, J., Eickhoff, M., Heiliger, C., Heinemann, M., Bläsing, J., Krost, A., Shokovets, S., Müller, C., & Ronning, C. (2012). Binary copper oxide semiconductors: From materials towards devices. *Physica Status Solidi (B) Basic Research*, *249*(8), 1487–1509. https://doi.org/10.1002/pssb.201248128

Meyer, W., Hock, D., Biedermann, K., Gubo, M., Müller, S., Hammer, L., & Heinz, K. (2008). Coexistence of rocksalt and wurtzite structure in nanosized CoO films. *Physical Review Letters*, *101*(1), 016103. https://doi.org/10.1103/physrevlett.101.016103

Mijajlovi´c, A. M., Ognjanovi´cognjanovi´c, M., Manojlovi´c, D. M., Vlahovi´c, F. V., Dana Đur ¯ Di´cdi´c, S. ¯, Stankovi´c, V. S., & Stankovi´c, D. S. (2023). Eu2O3@Cr2O3 Nanoparticles-Modified Carbon Paste Electrode for Efficient Electrochemical Sensing of Neurotransmitters Precursor L-DOPA. *Mdpi.ComA Mijajlović, M Ognjanović, D Manojlović, F Vlahović, S Đurđić, V Stanković, D StankovićBiosensors, 2023 mdpi.Com*. https://doi.org/10.3390/bios13020201

Miranda-Castro, R., de los Santos Álvarez, N., & Lobo-Castañón, M. J. (2020).

Amperometric detection of NADH using carbon-based electrodes. *Laboratory Methods in Dynamic Electroanalysis*, 67–74. https://doi.org/10.1016/b978-0-12-815932-3.00007-3

Mohammadzadeh Jahani, P., Akbari Javar, H., & Mahmoudi-Moghaddam, H. (2021). A new electrochemical sensor based on Europium-doped NiO nanocomposite for detection of venlafaxine. *Measurement*, *173*, 108616. https://doi.org/10.1016/j.measurement.2020.108616

Mohammed, W. M., Mubark, T. H., & Al-Haddad, R. M. S. (2018). Effect of CuO Nanoparticles on Antimicrobial Activity Prepared by Sol-Gel Method. *International Journal of Applied Engineering Research*, *13*, 10559–10562.

Momeni, M. M., Nazari, Z., Kazempour, A., Hakimiyan, M., & Mirhoseini, S. M. (2014). Preparation of CuO nanostructures coating on copper as supercapacitor materials. *Https://Doi.Org/10.1179/1743294414Y.0000000318*, *30*(11), 775–778. https://doi.org/10.1179/1743294414Y.0000000318

More, P., Kadam, S. A., Ma, Y., Chen, Y., Tarwal, N., Navale, Y., Salunkhe, A., & Patil, V. (2022). Spray Synthesized Mn-doped CuO Electrodes for High Performance Supercapacitor. ChemistrySelect, 7(37). Portico. https://doi.org/10.1002/slct.202202504.

Mülazımoğlu, İ. E. (2008). *Camsı karbon elektrot yüzeyine çeşitli flavonoid türevlerinin modifikasyonu, yüzey karakterizasyonu, elektrokimyasal ve spektroskopik özelliklerinin incelenmesi*. Selçuk Üniversitesi Fen Bilimleri Enstitüsü. https://hdl.handle.net/20.500.12395/625

Murray, R. W. (1983). Electroanalytical Chemistry. *Accts. Chem. Res*, *13*, 135–141.

Murray, R. W., Ewing, A. G., & Durst, R. A. (1987). Chemically Modified Electrodes: Molecular Design for Electroanalysis. *Analytical Chemistry*, *59*(5). https://doi.org/10.1021/AC00132A001

Muthukumaran, M., Venkateswara Raju, C., Sumathi, C., Ravi, G., Solairaj, D., Rameshthangam, P., Wilson, J., Rajendran, S., & Alwarappan, S. (2016). Cerium

doped nickel-oxide nanostructures for riboflavin biosensing and antibacterial applications. *New Journal of Chemistry*, *40*(3), 2741–2748. https://doi.org/10.1039/c5nj03539b

Nagajyothi, P. C., Muthuraman, P., Sreekanth, T. V. M., Kim, D. H., & Shim, J. (2017). Green synthesis: In-vitro anticancer activity of copper oxide nanoparticles against human cervical carcinoma cells. *Arabian Journal of Chemistry*, *10*(2), 215–225. https://doi.org/10.1016/j.arabjc.2016.01.011

Nagaveni, K., Hegde, M. S., Ravishankar, N., Subbanna, G. N., & Madras, G. (2004). Synthesis and structure of nanocrystalline TiO_2 with lower band gap showing high photocatalytic activity. *Langmuir*, *20*(7), 2900–2907. https://doi.org/10.1021/la035777v

Nagle, L. C., Wahl, A., Ogourstov, V., Seymour, I., Barry, F., Rohan, J. F., & Loughlin, R. Mac. (2021). Electrochemical discrimination of salbutamol from its excipients in ventolintm at nanoporous gold microdisc arrays. *Sensors*, *21*(12). https://doi.org/10.3390/s21123975

Naktiyok, J., & Özer, A. K. (2019). SYNTHESIS OF COPPER OXIDE (CuO) FROM THERMAL DECOMPOSITION OF COPPER ACETATE MONOHYDRATE ($Cu(CH_3COO)_2.H_2O$). *Niğde Ömer Halisdemir Üniversitesi Mühendislik Bilimleri Dergisi*, *8*(2), 1292–1298. https://doi.org/10.28948/ngumuh.598177

Nam, N. H., & Luong, N. H. (2019). Nanoparticles: synthesis and applications. Materials for Biomedical Engineering, 211–240. https://doi.org/10.1016/b978-0-08-102814-8.00008-1.

Namakka, M., Rahman, M. R., Said, K. A. M. Bin, Abdul Mannan, M., & Patwary, A. M. (2023). A review of nanoparticle synthesis methods, classifications, applications, and characterization. *Environmental Nanotechnology, Monitoring &Management*, *20*, 100900. https://doi.org/10.1016/j.enmm.2023.100900

Narayanan, R., & El-Sayed, M. A. (2005). *Catalysis with Transition Metal Nanoparticles in Colloidal Solution: Nanoparticle Shape Dependence and Stability*. https://doi.org/10.1021/jp051066p

Navrátilová, Z., & Kula, P. (2003). Clay modified electrodes: Present applications and prospects. *Electroanalysis*, *15*(10), 837–846. https://doi.org/10.1002/elan.200390103

Negrescu, A., Killian, M., … S. R.-J. of F., & 2022, undefined. (n.d.). Metal oxide nanoparticles: review of synthesis, characterization and biological effects. *Mdpi.ComAM Negrescu, MS Killian, SNV Raghu, P Schmuki, A Mazare, A CimpeanJournal of Functional Biomaterials, 2022•mdpi.Com*. Retrieved August 3, 2024, from https://www.mdpi.com/2079-4983/13/4/274

Nicholson, R. S. (1965). Theory and Application of Cyclic Voltammetry for Measurement of Electrode Reaction Kinetics. *Analytical Chemistry*, *37*(11), 1351–1355. https://doi.org/10.1021/ac60230a016

Norris, D. J., Efros, A. L., & Erwin, S. C. (2008). Doped Nanocrystals. *Science*, *319*(5871), 1776–1779. https://doi.org/10.1126/science.1143802

Nunes, D., Pimentel, A., Goncalves, A., Pereira, S., Branquinho, R., Barquinha, P., Fortunato, E., & Martins, R. (2019). Metal oxide nanostructures for sensor applications. *Semiconductor Science and Technology*, *34*(4), 043001. https://doi.org/10.1088/1361-6641/ab011e

O'Regan, B., & Grätzel, M. (1991). A low-cost, high-efficiency solar cell based on dye-sensitized colloidal TiO_2 films. *Nature 1991 353:6346*, *353*(6346), 737–740. https://doi.org/10.1038/353737a0

Parashar, M., Shukla, V. K., & Singh, R. (2020). Metal oxides nanoparticles via sol–gel method: a review on synthesis, characterization and applications. *Journal of Materials Science: Materials in Electronics*, *31*(5), 3729–3749. https://doi.org/10.1007/S10854-020-02994-8/metrics

Phromma, S., Wutikhun, T., Kasamechonchung, P., Eksangsri, T., & Sapcharoenkun, C. (2020). Effect of Calcination Temperature on Photocatalytic Activity of Synthesized TiO_2 Nanoparticles via Wet Ball Milling Sol-Gel Method. *Applied Sciences 2020, Vol. 10, Page 993*, *10*(3), 993. https://doi.org/10.3390/app10030993

Pike, J., Chan, S. W., Zhang, F., Wang, X., & Hanson, J. (2006). Formation of stable Cu_2O from reduction of CuO nanoparticles. *Applied Catalysis A-General*, *303*(2), 273–277. https://doi.org/10.1016/j.apcata.2006.02.008

Pinto, A. H., Nogueira, A. E., Dalmaschio, C. J., Frigini, I. N., de Almeida, J. C., Ferrer, M. M., Berengue, O. M., Gonçalves, R. A., & de Mendonça, V. R. (2022a). Doped Tin Dioxide (d-SnO2) and Its Nanostructures: Review of the Theoretical Aspects, Photocatalytic and Biomedical Applications. *Solids 2022, Vol. 3, Pages 327-360*, *3*(2), 327–360. https://doi.org/10.3390/solids3020024

Pohanka, M., & Leuchter, J. (2017). Biosensors Based on Semiconductors, a Review. *International Journal of Electrochemical Science*, *12*(7), 6611–6621. https://doi.org/10.20964/2017.07.52

Ponnar, M., Thangamani, C., Monisha, P., Gomathi, S. S., & Pushpanathan, K. (2018a). Influence of Ce doping on CuO nanoparticles synthesized by microwave irradiation method. *Applied Surface Science*, *449*, 132–143. https://doi.org/10.1016/j.apsusc.2018.01.126

Ponnarasan, V., Physics, A. K.-A. S. in T., & 2014, undefined. (2014). Studies on pure and divalent metal doped copper oxide nanoparticles. *CiteseerV Ponnarasan, A KrishnanAdvanced Studies in Theoretical Physics, 2014 Citeseer*, *8*(6), 251–258. https://doi.org/10.12988/astp.2014.312147

Pradhan, N., Das Adhikari, S., Nag, A., & Sarma, D. D. (2017). Luminescence, Plasmonic, and Magnetic Properties of Doped Semiconductor Nanocrystals. *Angewandte Chemie - International Edition*, *56*(25), 7038–7054. https://doi.org/10.1002/anie.201611526

Priyadharshini, M., Rajesh, P., Illiyas, S., Maqbool, S., Hariharan, V., & Inban, M. E. (2021). Synthesis of Environment-friendly Manganese-doped Metal Oxide Nanoparticles for the Biosensor Applications. *Journal of Environmental Research Article Nanotechnology J. Environ. Nanotechnol*, *10*(3), 9–15. https://doi.org/10.13074/jent.2021.09.213440

Püntener, M., Vigassy, T., Baier, E., Ceresa, A., & Pretsch, E. (2004). Improving the

lower detection limit of potentiometric sensors by covalently binding the ionophore to a polymer backbone. *Analytica Chimica Acta*, *503*(2), 187-194. https://doi.org/10.1016/j.aca.2003.10.030

Qu, X., Li, Y., Li, L., Wang, Y., Liang, J., & Liang, J. (2015). *Review Article Fluorescent Gold Nanoclusters: Synthesis and Recent Biological Application*. https://doi.org/10.1155/2015/784097

Ragupathy, S., Ramasundaram, S., Thennarasu, G., Harishsenthil, P., Krishnakumar, M., & Hwan Oh, T. (2023). Effect of Mn doping on structural, optical and photocatalytic properties of SnO_2 nanoparticles. *Ceramics International*, *49*(11), 17776–17783. https://doi.org/10.1016/j.ceramint.2023.02.143

Rahman, M. A. (2014). A Review on Semiconductors Including Applications and Temperature Effects in Semiconductors. *American Scientific Journal for Engineering, Technology, and Sciences*, *7*(1), 50–70. http://asrjetsjournal.org/

Rahman, M., Khan, S., One, A. A.-Pl., & 2014, undefined. (2014). Fabrication of smart chemical sensors based on transition-doped-semiconductor nanostructure materials with μ-chips. *Journals.Plos.OrgMM Rahman, SB Khan, AM AsiriPLoS One, 2014journals.Plos.Org*, *9*(1), 85036. https://doi.org/10.1371/journal.pone.0085036

Rai, V. K. (2007). Temperature sensors and optical sensors. *Applied Physics B: Lasers and Optics*, *88*(2), 297–303. https://doi.org/10.1007/s00340-007-2717-4

Rajesh, N., Kannan, J. C., Krishnakumar, T., Leonardi, S. G., & Neri, G. (2014). Sensing behavior to ethanol of tin oxide nanoparticles prepared by microwave synthesis with different irradiation time. *Sensors and Actuators B: Chemical*, *194*, 96–104. https://doi.org/10.1016/j.snb.2013.12.060

Rajeshwaran, P., & Sivarajan, A. (2015). Influence of Mn doping on structural, optical and acetone gas sensing properties of SnO2 nanoparticles by a novel microwave technique. *Journal of Materials Science: Materials in Electronics*, *26*(1), 539–546. https://doi.org/10.1007/s10854-014-2432-y

Randviir, E. P., & Banks, C. E. (2013). Electrochemical impedance spectroscopy: An overview of bioanalytical applications. In *Analytical Methods* (Vol. 5, Issue 5). https://doi.org/10.1039/c3ay26476a

Rao Bitra, H. C., Rao, A. V., Kumar, A. G. S., & Rao, G. N. (2021). Investigation of low temperature dielectric properties of manganese doped-copper oxide nanoparticles by coprecipitation method. *Digest Journal of Nanomaterials and Biostructures*, *16*(3), 1173–1183. https://doi.org/10.15251/djnb.2021.163.1173

Ravichandran, K., & Baldwin, R. P. (1981). Chemically modified carbon paste electrodes. *Journal of Electroanalytical Chemistry and Interfacial Electrochemistry*, *126*(1-3), 293–300. https://doi.org/10.1016/S0022-0728(81)80438-X

Rehani, D., Saxena, M., Solanki, P. R., & Sharma, S. N. (2022). Transition Metal and Rare-Earth Metal Doping in SnO_2 Nanoparticles. *Journal of Superconductivity and Novel Magnetism*, *35*(9), 2573–2581. https://doi.org/10.1007/S10948-022-06283-9

Richa, Tyagi, A. K., & Ahlawat, D. S. (2017). Influence of pH variation on structural and magnetic properties of Ni-Zn ferrite nanoparticles synthesized by auto combustion method. *Oriental Journal of Chemistry*, *33*(1), 296–303. https://doi.org/10.13005/ojc/330135

Roduner, E. (2006). Size matters: Why nanomaterials are different. *Chemical Society Reviews*, *35*(7), 583–592. https://doi.org/10.1039/b502142c

Rumyantseva, M., Labeau, M., Delabouglise, G., Ryabova, L., Kutsenok, I., & Gaskov, A. (1997). Copper and nickel doping effect on interaction of SnO2 films with H2S. *Journal of Materials Chemistry*, *7*(9), 1785–1790. https://doi.org/10.1039/a701896g

Sabbaghan, M., Ghalkhani, M., Hosseini, M., & Ghanbari, M. (2021). Mn-doped ZnS synthesis in DABCO based ionic liquid: Morphology and electrochemical sensing performance for isoprenaline analysis. *Journal of Industrial and Engineering Chemistry*, *95*, 367–375. https://doi.org/10.1016/j.jıec.2021.01.012

Sadeghi, M., Jahanshahi, M., & Javadian, H. (2020). Highly sensitive biosensor for detection of DNA nucleobases: Enhanced electrochemical sensing based on polyaniline/single-layer MoS_2 nanosheets nanocomposite modified carbon paste electrode. *Microchemical Journal*, *152*, 104315. https://doi.org/10.1016/j.microc.2019.104315

Sahin, B., & Kaya, T. (2019). Electrochemical amperometric biosensor applications of nanostructured metal oxides: a review. *Materials Research Express*, *6*(4), 042003. https://doi.org/10.1088/2053-1591/aafa95

Sahu, K. K., Raj, B., Basu, S., & Mohapatra, M. (2021). Calcination Strategy for Scalable Synthesis of Pithecellobium-Type Hierarchical Dual-Phase Nanostructured CuxO to Columnar Self-Assembled CuO and Its Electrochemical Performances. *ACS Omega*, *6*(2), 1108–1118. https://doi.org/10.1021/acsomega.0c03899

Said, N. M. (2014). *Electrochemical biosensor based on microfabricated electrode arrays for life sciences applications*. https://cora.ucc.ie/handle/10468/1759

Sajid, M., Imran, M., Salahuddin, & Iqbal, J. (2018). Tailoring structural, surface, optical, and dielectric properties of CuO nanosheets for applications in high-frequency devices. *Applied Physics A: Materials Science and Processing*, *124*(11). https://doi.org/10.1007/s00339-018-2179-z

Salah, N., Habib, S., & Azam, A. (2016). Magnetic properties of microwave-synthesized Mn-doped SnO_2 nanoparticles. *Applied Physics A: Materials Science and Processing*, *122*(11), 1–9. https://doi.org/10.1007/S00339-016-0519-4

Salah, N., Habib, S., Azam, A., Ansari, M. S., & Al-Shawafi, W. M. (2016). Formation of Mn-doped SnO_2 nanoparticles via the microwave technique: Structural, optical and electrical properties. *Nanomaterials and Nanotechnology*, *6*(1). https://doi.org/10.5772/62520

Sambasivam, S., Kim, S. B., Jeong, J. H., Choi, B. C., Lim, K. T., Kim, S. S., & Song, T. K. (2010). Effect of Er^{3+} doping in SnO_2 semiconductor nanoparticles synthesized by solgel technique. *Current Applied Physics*, *10*(6), 1383–1386.

https://doi.org/10.1016/j.cap.2010.05.001

Santos, A. M., Wong, A., & Fatibello-Filho, O. (2018). Simultaneous determination of salbutamol and propranolol in biological fluid samples using an electrochemical sensor based on functionalized-graphene, ionic liquid and silver nanoparticles. *Journal of Electroanalytical Chemistry*, *824*, 1-8. https://doi.org/10.1016/j.jelechem.2018.07.018

Saranya, P. E., & Selladurai, S. (2018). Facile synthesis of $NiSnO_3$/graphene nanocomposite for high-performance electrode towards asymmetric supercapacitor device. *Journal of Materials Science*, *53*(23), 16022–16046. https://doi.org/10.1007/S10853-018-2742-1

Sawkar, R. R., Shanbhag, M. M., Tuwar, S. M., Veerapur, R. S., & Shetti, N. P. (2022). Glucose Incorporated Graphite Matrix for Electroanalysis of Trimethoprim. *Biosensors*, *12*(10), 909. https://doi.org/10.3390/bios12100909

Scholz, F. (2010). Electroanalytical methods: Guide to experiments and applications. *Electroanalytical Methods: Guide to Experiments and Applications*, 1–359. https://doi.org/10.1007/978-3-642-02915-8/cover

Selleswari, D., Meena, P., & Mangalaraj, D. (2019). Design of CuO/SnO_2 heterojunction photocatalyst with enhanced UV light-driven photocatalytic activity on congo-red and malachite green dyes. *Journal of the Iranian Chemical Society*, *16*(6), 1291–1300. https://doi.org/10.1007/S13738-019-01606-5

Şerban, I., & Enesca, A. (2020). Metal Oxides-Based Semiconductors for Biosensors Applications. *Frontiers in Chemistry*, *8*, 532523. https://doi.org/10.3389/Fchem.2020.00354/bıbtex

Shaalan, N. M., Hamad, D., Abdel-Latief, A. Y., & Abdel-Rahim, M. A. (2016). Preparation of quantum size of tin oxide: Structural and physical characterization. *Progress in Natural Science: Materials International*, *26*(2), 145–151. https://doi.org/10.1016/j.pnsc.2016.03.002

Shabani, R., Rizi, Z. L., & Moosavi, R. (2018). Selective Potentiometric Sensor for

Isoniazid Ultra-Trace Determination Based on Fe_3O_4 Nanoparticles Modified Carbon Paste Electrode (Fe3O4/CPE). *International Journal of Nanoscience and Nanotechnology*, *14*(3), 241–249. https://www.ijnnonline.net/article_32222.html

Shah, A. H., & Rather, M. A. (2021). Effect of calcination temperature on the crystallite size, particle size and zeta potential of TiO_2nanoparticles synthesized via polyol-mediated method. *Materials Today: Proceedings*, *44*, 482–488. https://doi.org/10.1016/j.matpr.2020.10.199

Shanbhag, M. M., Shetti, N. P., Kalanur, S. S., Pollet, B. G., Upadhyaya, K. P., Ayachit, N. H., & Aminabhavi, T. M. (2021). Hf-doped tungsten oxide nanorods as electrode materials for electrochemical detection of paracetamol and salbutamol. *Applied Nano Materials, 2021•ACS Publications*, *2022*(1), 1263–1275. https://doi.org/10.1021/acsanm.1c03853

Shanbhag, M. M., Shetti, N. P., Kalanur, S. S., Pollet, B. G., Upadhyaya, K. P., Ayachit, N. H., & Aminabhavi, T. M. (2022). Hf-Doped Tungsten Oxide Nanorods as Electrode Materials for Electrochemical Detection of Paracetamol and Salbutamol. *ACS Applied Nano Materials*, *5*(1), 1263–1275. https://doi.org/10.1021/acsanm.1c03853

Sharma, A., Ahmed, A., Singh, A., Oruganti, S. K., Khosla, A., & Arya, S. (2021). Review—Recent Advances in Tin Oxide Nanomaterials as Electrochemical/Chemiresistive Sensors. *Journal of The Electrochemical Society*, *168*(2), 027505. https://doi.org/10.1149/1945-7111/abdee8

Sharma, A., Dutta, R. K., Roychowdhury, A., Das, D., Goyal, A., & Kapoor, A. (2017). Cobalt doped CuO nanoparticles as a highly efficient heterogeneous catalyst for reduction of 4-nitrophenol to 4-aminophenol. *Applied Catalysis A: General*, *543*, 257–265. https://doi.org/10.1016/j.apcata.2017.06.037

Sharma, A. K., & Mahajan, A. (2023). Potential applications of chemiresistive gas sensors. *Carbon Nanomaterials and Their Nanocomposite-Based Chemiresistive Gas Sensors: Applications, Fabrication and Commercialization*, 223–245. https://doi.org/10.1016/b978-0-12-822837-1.00002-2

Shenoy, R. U. K., Rama, A., Govindan, I., & Naha, A. (2022). The purview of doped nanoparticles: Insights into their biomedical applications. *OpenNano*, *8*, 100070. https://doi.org/10.1016/j.onano.2022.100070

Shetti, N. P., Nayak, D. S., Malode, S. J., & Kulkarni, R. M. (2017). An electrochemical sensor for clozapine at ruthenium doped TiO_2 nanoparticles modified electrode. *Sensors and Actuators B: Chemical*, *247*, 858–867. https://doi.org/10.1016/j.snb.2017.03.102

Shukla, M., Pramila, Agrawal, J., Dixit, T., Palani, I. A., & Singh, V. (2018). Facile hydrothermal synthesis of mn doped ZnO nanopencils for development of amperometric glucose biosensors. *Materials Research Express*, *5*(5). https://doi.org/10.1088/2053-1591/aac339

Siddiqui, H., Parra, M. R., Qureshi, M. S., Malik, M. M., & Haque, F. Z. (2018). Studies of structural, optical, and electrical properties associated with defects in sodium-doped copper oxide (CuO/Na) nanostructures. *Journal of Materials Science*, *53*(12), 8826–8843. https://doi.org/10.1007/s10853-018-2179-6

Singh, B. P., Chaudhary, M., Kumar, A., Singh, A. K., Gautam, Y. K., Rani, S., & Walia, R. (2020). Effect of Co and Mn doping on the morphological, optical and magnetic properties of CuO nanostructures. *Solid State Sciences*, *106*, 106296. https://doi.org/10.1016/j.solidstatesciences.2020.106296

Singh, I., Dey, S., Santra, S., Landfester, K., Muñoz-Espí, R., & Chandra, A. (2018). Cerium-Doped Copper(II) Oxide Hollow Nanostructures as Efficient and Tunable Sensors for Volatile Organic Compounds. *ACS Omega*, *3*(5), 5029–5037. https://doi.org/10.1021/acsomega.8b00203

Singh, P. K., Kumar, P., Hussain, M., Das, A. K., & Nayak, G. C. (2016). Synthesis and characterization of CuO nanoparticles using strong base electrolyte through electrochemical discharge process. *Bulletin of Materials Science*, *39*(2), 469–478. https://doi.org/10.1007/s12034-016-1159-1

Singh, S. J., Lim, Y. Y., Hmar, J. J. L., & Chinnamuthu, P. (2022). Temperature dependency on Ce-doped CuO nanoparticles: a comparative study via XRD line

broadening analysis. *Applied Physics A: Materials Science and Processing*, *128*(3). https://doi.org/10.1007/s00339-022-05334-1

Sivakumar, K., Senthil Kumar, V., Muthukumarasamy, N., Thambidurai, M., & Senthil, T. S. (2012). Influence of pH on ZnO nanocrystalline thin films prepared by sol-gel dip coating method. *Bulletin of Materials Science*, *35*(3), 327–331. https://doi.org/10.1007/s12034-012-0305-7

Joshi, N., Alwarappan, S., Pillai, ShreekumarR., Singh, ShreeR., Ram, M. K., & Kumar, A. (2012). Gold Nanoparticles Modified Glassy Carbon Electrodes as Electrochemical Biosensors. Advanced Science Letters, 5(1), 131–134. https://doi.org/10.1166/asl.2012.1967

Smith, T. J., & Stevenson, K. J. (2007). Reference electrodes. *Handbook of Electrochemistry*, 73–110. https://doi.org/10.1016/b978-044451958-0.50005-7

Smith Timothy J., S. K. J. (2013). *Handbook of electrochemistry -Reference electrodes*. 1–2.

Song, X., Liu, D., Zhang, Y., Ding, Y., Li, M., Wang, S., He, X., & Qu, Y. (2010). Grain growth kinetics of SnO2 nanocrystals synthesized by precipitation method. *Journal Wuhan University of Technology, Materials Science Edition*, *25*(6), 929–934. https://doi.org/10.1007/s11595-010-0122-z/metrics

Srinivasan, L. V., & Rana, S. S. (2024). A critical review of various synthesis methods of nanoparticles and their applications in biomedical, regenerative medicine, food packaging, and environment. *Discover Applied Sciences*, *6*(7). https://doi.org/10.1007/S42452-024-06040-8

Stetter, J. R., Penrose, W. R., & Yao, S. (2003). Sensors, Chemical Sensors, Electrochemical Sensors, and ECS. *Journal of The Electrochemical Society*, *150*(2), S11. https://doi.org/10.1149/1.1539051

Stojanović, Z. S., Đurović, A. D., Kravić, S., Ashrafi, A. M., & Richtera, L. (2023). Electrochemical sensing platform based on the use of ZnONPs and MWCNTs as CPE modifiers for a selective and sensitive determination of polyamine spermine

in the urine sample. *Electroanalysis*, *35*(6), e202200446. https://doi.org/10.1002/elan.202200446

Stradiotto, N. R., Yamanaka, H., & Zanoni, M. V. B. (2003). Electrochemical sensors: a powerful tool in analytical chemistry. Journal of the Brazilian Chemical Society, 14(2), 159–173. https://doi.org/10.1590/s0103-50532003000200003

Subramaniam, M. P., Arunachalam, G., Kandasamy, R., Veluswamy, P., & Hiroya, I. (2018). Effect of pH and annealing temperature on the properties of tin oxide nanoparticles prepared by sol–gel method. *Journal of Materials Science: Materials in Electronics*, *29*(1), 658–666. https://doi.org/10.1007/s10854-017-7959-2

Sun, J., Lin, H., & Zhang, D. (2019). YAG:Ce-Al_2O_3 composite/spinel dual-layer ceramic phosphor for high luminous density light converting application. Materials Research Express, 6(11), 116212. https://doi.org/10.1088/2053-1591/ab4b0b

Svancara, I., Vytras, K., Barek, J., & Zima, J. (2001). Carbon paste electrodes in modern electroanalysis. *Critical Reviews in Analytical Chemistry*, *31*(4), 311–345. https://doi.org/10.1080/20014091076785

Švancara, I., Vytřas, K., Kalcher, K., Walcarius, A., & Wang, J. (2009). Carbon paste electrodes in facts, numbers, and notes: A review on the occasion of the 50-years jubilee of carbon paste in electrochemistry and electroanalysis. *Electroanalysis*, *21*(1), 7–28. https://doi.org/10.1002/elan.200804340

Svancara, I., Kalcher, K., Walcarius, A., & Vytras, K. (2012). Electroanalysis with Carbon Paste Electrodes. https://doi.org/10.1201/b11478

Szalay, B., Tátrai, E., Nyíro, G., Vezér, T., & Dura, G. (2012). Potential toxic effects of iron oxide nanoparticles in in vivo and in vitro experiments. *Journal of Applied Toxicology*, *32*(6), 446–453. https://doi.org/10.1002/jat.1779

Tahira, A., Baloach, Q., Chacha, G. S., Sirajuddin, Willander, M., & Ibupoto, Z. H. (2016). Fe-doped cobalt oxide nanostructures for the development of sensitive dopamine biosensor. *Sensor Letters*, *14*(8), 764–768. https://doi.org/10.1166/sl.2016.3693

Talay Pınar, P., Ali, H. S., Abdullah, A. A., Yardım, Y., & Şentürk, Z. (2018). Electroanalytical determination of Salbutamol in pharmaceutical formulations using cathodically pretreated boron-doped diamond electrode. Journal of Research in Pharmacy, 22(1), 144–152. https://doi.org/10.12991/jrp.2018.88

Terbouche, A., Lameche, S., Ait-Ramdane-Terbouche, C., Guerniche, D., Lerari, D., Bachari, K., Hauchard, D., Terbouche, A., Lameche, S., Ait-Ramdane-Terbouche, C., Guerniche, D., Lerari, D., & Bachari, K. (2016). A new electrochemical sensor based on carbon paste electrode/Ru(III) complex for determination of nitrite: Electrochemical impedance and cyclic voltammetry measurements. *Measurement - Journal of the International Measurement Confederation (IMEKO)*, *92*, 524-533. https://doi.org/10.1016/j.measurement.2016.06.034

Thanh Nhi, L. T., Hoa, L. T., Uyen, D. T., Sinh, L. H., Nguyen, D. M., Bach, T. N., Tam Toan, T. T., & Quang Khieu, D. (2024). Electrochemical determination of salbutamol in aqueous solutions with UiO-66/rGO-modified electrodes. *Vietnam Journal of Chemistry*, *62*(1), 103–113. https://doi.org/10.1002/vjch.202300189

Thévenot, D. R., Toth, K., Durst, R. A., & Wilson, G. S. (2001). Electrochemical biosensors: Recommended definitions and classification. *Biosensors and Bioelectronics*, *16*(1–2), 121–131. https://doi.org/10.1016/S0956-5663(01)00115-4

T Thanh Nhi, L. T., Hoa, L. T., Uyen, D. T., Sinh, L. H., Nguyen, D. M., Bach, T. N., Tam Toan, T. T., & Quang Khieu, D. (2024). Electrochemical determination of salbutamol in aqueous solutions with UiO-66/rGO-modified electrodes. Vietnam Journal of Chemistry, 62(1), 103–113. Portico. https://doi.org/10.1002/vjch.202300189

Thiagarajan, S., Sanmugam, A., & Vikraman, D. (2017). Facile Methodology of Sol-Gel Synthesis for Metal Oxide Nanostructures. *Recent Applications in Sol-Gel Synthesis*. https://doi.org/10.5772/intechopen.68708

Thiagarajan, S., Tsai, T. H., & Chen, S. M. (2011). Electrochemical fabrication of nano manganese oxide modified electrode for the Detection of H_2O_2. *International*

Journal of Electrochemical Science, *6*(6), 2235–2245. https://doi.org/10.1016/s1452-3981(23)18180-6

Tiwari, J. N., Tiwari, R. N., & Kim, K. S. (2012). Zero-dimensional, one-dimensional, two-dimensional and three-dimensional nanostructured materials for advanced electrochemical energy devices. *Progress in Materials Science*, *57*(4), 724–803. https://doi.org/10.1016/j.pmatscı.2011.08.003

Toghan, A., Abo-bakr, A. M., Rageh, H. M., & Abd-Elsabour, M. (2019). A novel electrochemical sensor for determination of salbutamol based on graphene oxide/poly (O-nitrobenzoic acid) modified glassy carbon electrode and its analytical application in pharmaceutical formulation and human urine. J. Biosens. Bioelectron, 10(270), 2.

Tran, T. H., & Nguyen, V. T. (2014). Copper Oxide Nanomaterials Prepared by Solution Methods, Some Properties, and Potential Applications: A Brief Review. *International Scholarly Research Notices*, *2014*, 1–14. https://doi.org/10.1155/2014/856592

Tripathy, N., & Kim, D.-H. (2018). *Metal oxide modified ZnO nanomaterials for biosensor applications*. *5*, 27. https://doi.org/10.1186/s40580-018-0159-9

Tseng, T. K., Lin, Y. S., Chen, Y. J., & Chu, H. (2010). A Review of Photocatalysts Prepared by Sol-Gel Method for VOCs Removal. *International Journal of Molecular Sciences 2010, Vol. 11, Pages 2336-2361*, *11*(6), 2336–2361. https://doi.org/10.3390/IJMS11062336

Uslu, B., & Ozkan, S. A. (2007). Solid Electrodes in Electroanalytical Chemistry: Present Applications and Prospects for High Throughput Screening of Drug Compounds. *Combinatorial Chemistry & High Throughput Screening*, *10*(7), 495–513. https://doi.org/10.2174/138620707782152425

Varughese, A., Kaur, R., & Singh, P. (2020). Green Synthesis and Characterization of Copper Oxide Nanoparticles Using Psidium guajava Leaf Extract. IOP Conference Series: Materials Science and Engineering, 961(1), 012011. https://doi.org/10.1088/1757-899x/961/1/012011

Ventura, R., Ramírez, R., Monfort, N., & Segura, J. (2009). Ultraperformance liquid chromatography tandem mass spectrometric method for direct quantification of salbutamol in urine samples in doping control. *Journal of Pharmaceutical and Biomedical Analysis*, *50*(5), 886–890. https://doi.org/10.1016/j.jpba.2009.06.009

Venugopal, B., Nandan, B., Ayyachamy, A., Balaji, V., Amirthapandian, S., Panigrahi, B. K., & Paramasivam, T. (2014). Influence of manganese ions in the band gap of tin oxide nanoparticles: structure, microstructure and optical studies. *Pubs.Rsc.OrgB Venugopal, B Nandan, A Ayyachamy, V Balaji, S Amirthapandian, BK PanigrahiRSC Advances, 2014 pubs.Rsc.Org*. https://doi.org/10.1039/c3ra46378h

Veerabhadrayya, M., Kumari, R. A., Nagaraju, G., Ravikiran, Y. T., & Chethan, B. (2020). Structural, optical and electrical properties of Ce doped SnO_2 nanoparticles prepared by surfactant assisted gel combustion method.Journal of Nano- and Electronic Physics; Sumy Ukraine Vol. 12, Iss. 4, (2020). https://doi.org/10.21272/jnep.12(4).04017

Verma, K., Goel, S., & Sharma, R. (2022). Influence of calcination and sintering temperature on the microstructure, dielectric, ferroelectric and piezoelectric properties of the lead-free KNN ceramics. *Journal of Materials Science: Materials in Electronics*, *33*(35), 26067–26085. https://doi.org/10.1007/S10854-022-09295-2

Vindhya, P. S., & Kavitha, V. T. (2023). A comprehensive study on photocatalytic, antimicrobial, antioxidant and cytotoxicity effects of biosynthesized pure and Ni doped CuO nanoparticles. *Inorganic Chemistry Communications*, *150*, 110472. https://doi.org/10.1016/j.ınoche.2023.110472

Vinothkumar, V., Prasad, G. V., Chen, S. M., Sangili, A., Jang, S. J., Lim, H. C., & Kim, T. H. (2023). One-step synthesis of calcium-doped copper oxide nanoparticles as an efficient bifunctional electrocatalyst for sensor and supercapacitor applications.*journal of energy storage*, *59*, 106415. https://doi.org/10.1016/j.est.2022.106415

Wang, C. Y., Bahnemann, D. W., & Dohrmann, J. K. (2000). A novel preparation of iron-doped TiO2 nanoparticles with enhanced photocatalytic activity. *Chemical Communications*, *16*, 1539–1540. https://doi.org/10.1039/b002988m

Wang, H., & Lu, J. (2020). A review on particle size effect in metal-catalyzed heterogeneous reactions. Chinese Journal of Chemistry,38(11), 1422-1444. https://doi.org/10.1002/cjoc.202000205

Wang, H., Xiong, R., Cui, Z., Wan, J., Sa, B., Wu, X., Song, W., Wang, X., & Zeng, D. (2023). Ultrasensitive Detection for Lithium-Ion Battery Electrolyte Leakage by Rare-Earth Nd-Doped SnO_2 Nanofibers. *ACS Sensors*, *8*(4), 1700–1709. https://doi.org/10.1021/acssensors.2c02862

Wang, M. Y., Zhu, W., Ma, L., Ma, J. J., Zhang, D. E., Tong, Z. W., & Chen, J. (2016). Enhanced simultaneous detection of ractopamine and salbutamol - Via electrochemical-facial deposition of MnO_2 nanoflowers onto 3D RGO/Ni foam templates. *Biosensors and Bioelectronics*, *78*. https://doi.org/10.1016/j.bios.2015.11.062

Wang, X., Hu, C., Liu, H., Du, G., He, X., & Xi, Y. (2010). Synthesis of CuO nanostructures and their application for nonenzymatic glucose sensing. *Sensors and Actuators B: Chemical*, *144*(1), 220–225. https://doi.org/10.1016/j.snb.2009.09.067

Wang, Y., Fan, D., Zhao, G., Feng, J., Wei, D., Zhang, N., Cao, W., Du, B., & Wei, Q. (2018). Ultrasensitive photoelectrochemical immunosensor for the detection of amyloid β-protein based on $SnO_2/SnS_2/Ag_2S$ nanocomposites. *Biosensors and Bioelectronics*, *120*, 1–7. https://doi.org/10.1016/j.bios.2018.08.026

Wang, Y., Xu, H., Zhang, J., & Li, G. (2008). Electrochemical Sensors for Clinic Analysis. *Sensors*, *8*, 2043–2081.https://doi.org/10.3390/s8042043

Westbroek, P. (2005). Fundamentals of electrochemistry. *Analytical Electrochemistry in Textiles*, 3–36. https://doi.org/10.1533/9781845690878.1.1

J. Williams, S. Bekam, & C. Daglesh. (2021). Morphological studies of p-type Mn-

doped SnO_2 nanostructure. Experimental and Theoretical Nanotechnology, 13–19. https://doi.org/10.56053/5.1.13.

Wu, Y., He, Y., Wu, T., Chen, T., Weng, W., & Wan, H. (2007). Influence of some parameters on the synthesis of nanosized NiO material by modified sol-gel method. *Materials Letters*, *61*(14-15), 3174-3178. https://doi.org/10.1016/J.matlet.2006.11.018

Xin, Y., Wang, N., Wang, C., Gao, W., Chen, M., Liu, N., Duan, J., & Hou, B. (2020). Electrochemical detection of hydroquinone and catechol with covalent organic framework modified carbon paste electrode. *Journal of Electroanalytical Chemistry*, *877*, 114530. https://doi.org/10.1016/j.jelechem.2020.114530

Xu, H., Li, J., Li, P., Shi, J., & Gao, X. (2022). Effect of rare earth doping on electronic and gas-sensing properties of SnO_2 nanostructures. *Journal of Alloys and Compounds*, *909*, 164687. https://doi.org/10.1016/j.jallcom.2022.164687

Xu, W., Lei, R., Cao, W., Guo, C., Zhang, X., & Wang, S. (2013). Voltammetric Method Using Multi-Walled Carbon Nanotubes Modified Glassy Carbon Electrode for the Determination of Terbutaline Sulfate in Pork Sample. *Journal of Analytical Sciences, Methods and Instrumentation*, *2013*(02), 75–79. https://doi.org/10.4236/jasmi.2013.32009

Yang, L., Zhou, Q., Wang, G., & Yang, Y. (2013). Acetylcholinesterase biosensor based on SnO_2 nanoparticles–carboxylic graphene–nafion modified electrode for detection of pesticides. *Biosensors and Bioelectronics*, *49*, 25–31. https://doi.org/10.1016/j.bios.2013.04.037

Yao, Y. (2019). Facile synthesis of au nanoparticles@reduced graphene oxide nanocomposition-modified electrode for simultaneous determination of copper and mercury ions. *International Journal of Electrochemical Science*, *14*(4), 3844–3855. https://doi.org/10.20964/2019.04.06

Yıldız, D. E., Unal, F., & Taşaltın, N. (2024). Non-enzymatic electrochemical voltammetric sensors based on thulium:zinc oxide for dopamine detection. *Journal of Materials Science: Materials in Electronics*, *35*(7), 475.

https://doi.org/10.1007/s10854-024-12155-w

Yuan, M., & Minteer, S. D. (2019). Redox polymers in electrochemical systems: From methods of mediation to energy storage. *Current Opinion in Electrochemistry*, *15*, 1–6. https://doi.org/10.1016/j.coelec.2019.03.003

Zayyoun, N., Bahmad, L., Laânab, L., & Jaber, B. (2016). The effect of pH on the synthesis of stable Cu_2O/CuO nanoparticles by sol–gel method in a glycolic medium. *Applied Physics A: Materials Science and Processing*, *122*(5). https://doi.org/10.1007/s00339-016-0024-9

Zhang, G., & Liu, M. (1999). Preparation of nanostructured tin oxide using a sol-gel process based on tin tetrachloride and ethylene glycol. *Journal of Materials Science*, *34*(13), 3213–3219. https://doi.org/10.1023/a:1004685907751/metrics

Zhang, L. (2020). Electrochemical Detection of Ascorbic Acid in Citrus Juices using Mn-doped ZnO nanorods modified graphene oxide. *Int. J. Electrochem. Sci*, *15*, 5049–5057. https://doi.org/10.20964/2020.06.79

Zhao, S., Shen, Y., Li, A., Chen, Y., Gao, S., Liu, W., & Wei, D. (2021). Effects of rare earth elements doping on gas sensing properties of ZnO nanowires. *Ceramics International*, *47*(17), 24218–24226. https://doi.org/10.1016/j.ceramint.2021.05.133

Zhao, Y., Xu, L., Guo, M., Li, Z., Xu, Z., Ye, J., Li, W., & Wei, S. (2022). Effects of calcination temperature on grain growth and phase transformation of nano-zirconia with different crystal forms prepared by hydrothermal method. *Journal of Materials Research and Technology*, *19*, 4003-4017. https://doi.org/10.1016/j.jmrt.2022.06.137

Zheng, B., Fan, J., Chen, B., Qin, X., Wang, J., Wang, F., Deng, R., & Liu, X. (2022). Rare-Earth Doping in Nanostructured Inorganic Materials. *Chemical Reviews*, *122*(6), 5519–5603. https://doi.org/10.1021/acs.chemrev.1c00644

Zhu, D., Li, Q., Pang, X., Liu, Y., Wang, X., & Chen, G. (2016). A sensitive electrochemical impedance immunosensor for determination of malachite green

and leucomalachite green in the aqueous environment. *Analytical and Bioanalytical Chemistry*, *408*(20), 5593–5600. https://doi.org/10.1007/s00216-016-9660-3

Zhu, S., Shi, S., Zheng, X., Wang, X., Yu, G., Jiang, Y., Feng, J., Zhu, L., & Zhang, G. (2022). Enhanced Oxygen Vacancies in Ce-Doped SnO_2 Nanofibers for Highly Efficient Soot Catalytic Combustion. *Mdpi.ComS Zhu, S Shi, X Zheng, X Wang, G Yu, Y Jiang, J Feng, L Zhu, G ZhangCatalysts, 2022•mdpi.Com*. https://doi.org/10.3390/catal12060596